UNIVERSITÉ LAVAL

Fibres optiques amplificatrices pompées par la gaine pour les réseaux de communication

Thèse

Charles Matte-Breton

Doctorat en génie électrique
Philosophiæ doctor (Ph. D.)

Québec, Canada

Fibres optiques amplificatrices pompées par la gaine pour les réseaux de communication

Thèse

Charles Matte-Breton

Sous la direction de:

Sophie LaRochelle, directrice de recherche
Younès Messaddeq, codirecteur de recherche

Résumé

Avec la demande croissante en matière de consommation Internet, une nouvelle génération de systèmes de communication est présentement en cours de développement. L'une des caractéristiques de cette nouvelle génération est qu'elle exploite le multiplexage spatial afin d'augmenter la capacité et le niveau d'intégration des réseaux. Dans ce contexte, il est judicieux de s'intéresser à la place que pourrait occuper le multiplexage spatial dans la technologie de fibres amplificatrices.

À court terme, le multiplexage spatial pourrait être utilisé conjointement avec le pompage par la gaine afin de diminuer la complexité et le nombre de composants dans les noeuds des réseaux de communication ayant de nombreux ports d'entrée et de sortie à amplifier à un même endroit, en permettant l'amplification simultanée des signaux présents dans plusieurs coeurs d'une même fibre optique et à partir d'une seule source de pompage. Cependant, avec le pompage par la gaine, la puissance pompe est répartie sur l'entièreté de la gaine, menant ainsi à une faible intensité lumineuse de la pompe, ce qui a pour effet d'accentuer les effets de saturation de l'amplification, les rendant ainsi moins compatibles avec les réseaux reconfigurables.

Une application alternative pour le pompage par la gaine est l'amplification de signaux dans la bande L. En effet, il s'agit d'une application où les niveaux d'inversion de population d'ions d'erbium requis sont plus bas, ce qui est compatible avec la forte saturation propre au pompage par la gaine.

Dans ce contexte, cette thèse vise à explorer l'intérêt du développement de fibres amplificatrices pompées par la gaine pour les réseaux de communication et à proposer des améliorations concrètes relatives à cette technologie.

D'abord, le chapitre 1 vise à déterminer si, et sous quelles conditions, le co-dopage à l'erbium-ytterbium est préférable au dopage à l'erbium seul dans les fibres amplificatrices pompées par la gaine qui amplifient la bande C dans les réseaux de communication. Ce chapitre permet de conclure que le co-dopage à l'erbium-ytterbium est généralement uniquement préférable à l'erbium seul lorsque l'amplificateur doit être opéré en régime de forte saturation ou lorsque la région spectrale couverte par l'amplificateur ne s'étend pas en bas de 1535 nm.

Ensuite, le chapitre 2 étudie l'impact de la géométrie de distribution des ions d'erbium sur

le gain et la compression du gain dans une fibre amplificatrice pompée par la gaine. Plus spécifiquement, le dopage en anneau autour du coeur est comparé au dopage uniforme dans le coeur et à un profil de dopant qui couvrirait à la fois le coeur et une région périphérique du coeur afin de couvrir presque entièrement le mode fondamental. Ce chapitre permet de conclure que, parmi ces géométries, le dopage en anneau autour du coeur est celui qui permet de minimiser les effets de saturation.

Puis, le chapitre 3 présente une nouvelle méthode de couplage latéral de la pompe dans la gaine, sans fusion et sans altération du signal, qui permet d'augmenter l'efficacité de couplage de la pompe significativement par rapport aux méthodes alternatives sans fusion.

Les chapitres 4 à 6 présentent un processus d'optimisation ayant pour but d'utiliser les analyses et développements des chapitres 1 à 3 pour concevoir un amplificateur à fibre à coeurs multiples répondant de façon optimale aux spécifications requises pour un amplificateur s'insérant dans un noeud de réseau reconfigurable et couvrant la bande C. Le chapitre 4 présente la fabrication et la caractérisation de la première fibre amplificatrice à coeurs multiples utilisant une géométrie de distribution des ions actifs en anneau autour de chacun des coeurs. Ses performances s'avèrent être décevantes dû au taux élevé d'agrégats d'ions d'erbium et à la présence d'ASE dans la gaine. Dans le chapitre 5, un nouveau design de coeur est testé, en fabriquant une fibre amplificatrice à coeur unique, afin de corriger les deux principales lacunes de la fibre précédente. Dans le chapitre 6, le design présenté au chapitre 5 est réutilisé dans une seconde itération de fibre amplificatrice à coeurs multiples. Cette fibre est caractérisée en injectant de la puissance pompe dans la gaine et de la puissance signal simultanément dans tous les coeurs à l'aide d'un fan-in/fan-out pour mesurer le gain, le facteur de bruit ainsi que les variations de gain entre les coeurs.

Le chapitre 7 explore une application alternative du pompage par la gaine en investiguant l'utilisation de couches concentriques hétérogènes de dopage à l'erbium seul et de co-dopage à l'erbium-ytterbium afin de maximiser l'efficacité de conversion de puissance dans les fibres amplificatrices pompées par la gaine et couvrant la bande L.

Le chapitre 8 démontre qu'il est possible de recycler la puissance pompe résiduelle à la sortie d'une fibre amplificatrice multicoeur pompée par la gaine en y inscrivant un réseau de Bragg intra-gaine. Cette méthode a l'avantage de ne pas nécessiter l'ajout de composants additionnels, à l'entrée et à la sortie, qui peuvent induire des pertes d'insertion.

Finalement, le chapitre 9 est une discussion générale sur les progrès effectués dans le cadre de cette thèse ainsi que les défis qui restent à surmonter par rapport à l'utilisation des fibres amplificatrices pompées par la gaine dans les réseaux de communication.

Table des matières

Liste des tableaux

Liste des figures

Liste des acronymes, abréviations et symboles

Liste des acronymes et abréviations

CP *Cladding-pumped* en anglais, ou pompé par la gaine en français

DFUT *Doped fiber under test* en anglais, ou fibre dopée à l'étude en français

DWDM *Dense wavelength division multiplexing* en anglais, ou multiplexage en longueur d'onde dense en français

EDFA *Erbium doped fiber amplifier* en anglais, ou fibre optique amplificatrice dopée à l'erbium en français

EDFUT *Erbium-doped fiber under test* en anglais, ou fibre dopée à l'erbium à l'étude en français

EDF *Erbium doped fiber* en anglais, ou fibre optique dopée à l'erbium en français

EONs *Elastic optical networks* en anglais, ou réseaux optiques élastiques en français

EYDFA *Erbium-ytterbium doped fiber amplifier* en anglais, ou amplificateur à fibre optique dopée à l'erbium-ytterbium en français

FL *Fiber length* en anglais, ou longueur de fibre en français

FUT *Fiber under test* en anglais, ou fibre à l'étude en français

GFF *Gain flattening filter* en anglais, ou filtre d'égalisation du gain en français

G *Gain* en anglais et en français

ICBG *Inner-cladding Bragg grating* en anglais, ou réseau de Bragg intra-gaine en français

LD *Laser diode* en anglais, ou diode laser en français

MCVD *Modified chemical vapor deposition* en anglais, ou dépôt chimique en phase vapeur modifié en français

MC *Multicore* en anglais, ou multicoeur en français

MFD *Mode field diameter* en anglais, ou diamètre du champ modal en français

MMF *Multimode fiber* en anglais, ou fibre multimode en français

NF *Noise figure* en anglais, ou facteur de bruit en français

OSA *Optical spectrum analyzer* en anglais, ou analyseur de spectre optique en français

OTDR *Optical time domain reflectometer* en anglais, ou réflectomètre optique temporel en français

PCE *Power conversion efficiency* en anglais, ou efficacité de conversion de puissance

PS *Power splitter* en anglais, ou répartiteur de puissance en français

RMSE *Root mean square error* en anglais, ou racine de l'erreur quadratique moyenne en français

ROADM *Reconfigurable optical add drop multiplexer* en anglais, ou multiplexeur optique d'insertion-extraction reconfigurable en français

SDM *Space-division multiplexing* en anglais, ou multiplexage spatial en français

SMF *Single mode fiber* en anglais, ou fibre à mode unique en français

UB *Ultraviolet* en anglais et en français

VOA *Variable optical attenuator* en anglais, ou atténuateur optique variable en français

WSS *Wavelength selective switch* en anglais, ou commutateur sélectif de longueur d'onde en français

Symboles et constantes physiques

α_{ASE} Perte de fond de l'ASE, m^{-1}

α_p Perte de fond de la pompe, m^{-1}

α_s Perte de fond du signal, m^{-1}

η Efficacité de couplage, %

Γ_{ASE} Recouvrement entre la puissance de l'ASE et l'élément de résolution radiale, %

γ_{Er} Pourcentage d'ions appariés, %

Γ_p Recouvrement entre la puissance de la pompe et l'élément de résolution radiale, %

Γ_s Recouvrement entre la puissance du signal et l'élément de résolution radiale, %

λ_{ASE} Longueur d'onde de l'ASE, nm

λ_p	Longueur d'onde de la pompe, nm
λ_s	Longueur d'onde du signal, nm
ν_{ASE}	Fréquence optique de l'ASE, Hz
ν_p	Fréquence optique de la pompe, Hz
ν_s	Fréquence optique du signal, Hz
ρ_{Er}	Concentration d'ions d'erbium, ions/m^3
ρ_{Yb}	Concentration d'ions d'ytterbium, ions/m^3
$\sigma_{abs,ASE}$	Section efficace d'absorption de l'ASE, m^2
$\sigma_{abs,p}$	Section efficace d'absorption de la pompe, m^2
$\sigma_{abs,s}$	Section efficace d'absorption du signal, m^2
$\sigma_{ems,ASE}$	Section efficace d'émission de l'ASE, m^2
$\sigma_{ems,p}$	Section efficace d'émission de la pompe, m^2
$\sigma_{ems,s}$	Section efficace d'émission du signal, m^2
τ_{Er}	Durée de vie du niveau métastable supérieur de l'erbium, ms
τ_{Yb}	Durée de vie du niveau métastable supérieur de l'ytterbium, ms
A_k	Aire de l'élément de résolution radiale, m^2
A_{clad}	Aire de la gaine, m^2
c	Vitesse de la lumière dans le vide, $299\,792\,458\,m/s$
h	Constante de Planck, $6.626\,070\,04 \times 10^{-34}\,m^2 \cdot kg/s$
k_B	Constante de Boltzman, $1.380\,648\,52 \times 10^{-23}\,m^2 \cdot kg \cdot s^{-2} \cdot K^{-1}$
K_{tr}	Taux de transition de l'énergie des ions d'ytterium vers les ions d'erbium, m^3/s
L	Longueur de fibre, m
n_1	Densité de population de l'état fondamental de l'erbium, ions/m^3
n_2	Densité de population du niveau supérieur de l'erbium, ions/m^3
n_2^p	Densité de population du niveau supérieur des ions d'erbium appariés, ions/m^3
n_2^s	Densité de population du niveau supérieur des ions d'erbium non-appariés, ions/m^3
n_{clad}	Indice de réfraction de la gaine, µm
n_{core}	Indice de réfraction du coeur, µm
n_{doped}	Indice de réfraction de la région dopée, µm

P_p	puissance de la pompe, W
P_s	Puissance du signal, dBm
$P_{ASE}^{\pm}$	Puissance de l'ASE, dBm
R	Réflectivité effective, µ%
r_{bound}	Rayon de la frontière entre deux régions avec des types de dopage différents, µm
r_{clad}	Rayon de la gaine, µm
r_{core}	Rayon du coeur, µm
T	Température, °K

À mes parents, Yves et
Marie-Josée, qui m'ont toujours
soutenu dans ma curiosité

et à mon épouse Paola, une
partenaire de vie extraordinaire.

Remerciements

J'aimerais tout d'abord remercier ma directrice de recherche Sophie LaRochelle qui est, de loin, la personne qui a eu le plus gros impact sur mon parcours académique. Presque sept ans se sont écoulés déjà depuis mon stage en recherche avec toi en 2015 et je ne serai jamais assez reconnaissant pour toutes les opportunités que tu m'as offertes depuis, notamment un stage chez CorActive, un stage aux Bell Labs au New Jersey, de nombreuses conférences et plusieurs écoles d'été. En plus de m'offrir toutes ces opportunités, tu as toujours été disponible et très généreuse de ton temps. Bref, je te remercie pour tes précieux conseils, pour avoir vu du potentiel en moi et pour avoir consacré autant de ressources dans mon développement académique et professionnel. Si c'était à refaire, je recommencerais sans hésiter mes études graduées avec toi.

J'aimerais aussi remercier René-Jean Essiambre, Colin Kelly et, encore une fois, Sophie LaRochelle, pour la définition d'un projet de recherche passionnant et concret.

Merci aussi à René-Jean pour avoir travaillé d'arrache-pied pour me permettre de faire un stage dans les mythiques Bell Labs. Je n'oublierai jamais les soupers en ta compagnie et tout ce que tu as fait pour moi.

Je tiens également à remercier Nicolas Fontaine et Roland Ryf pour leur mentorat pendant mon stage au New Jersey et pour les nombreuses bières qu'on a partagées. J'ai beaucoup apprécié toutes les discussions que nous avons eues ensemble.

Mon doctorat n'aurait jamais été possible sans l'aide inestimable de Nelson Landry, Simon Levasseur, Nicolas Grégoire, Steeve Morency et Patrick Larochelle. Votre expertise est un catalyseur exceptionnel pour la science et, sans vous, le COPL ne serait définitivement pas ce qu'il est aujourd'hui. J'ai énormément de respect pour votre travail et j'ai adoré travailler avec vous au cours des dernières années.

J'aimerais aussi remercier toutes les personnes avec qui j'ai eu la chance de partager des discussions enrichissantes au COPL ou lors de conférences internationales. Notamment, Gabriel Lachance, Omid Jafari, Rizan Homayoun Nejad et Antoine Gervais.

Je tiens également à remercier mes parents, Pupu et Mumu, ainsi que mes soeurs, les Bubu.

Mon parcours académique a été exigeant et éprouvant par moments mais, grâce à ma famille, j'ai toujours pu recharger mes batteries autour d'un bon souper ou d'un feu de camp chaleureux, entouré de personnes que j'aime, qui me font rire, et avec qui j'adore échanger des idées.

Finalement, je souhaite offrir un merci tout particulier à ma partenaire de vie et épouse Paola, qui me complète à merveille et qui m'impressionnera toujours par son originalité, son sens de l'humour, son leadership et son intelligence émotionnelle exceptionnelle.

Avant-propos

Dans cette thèse, huit chapitres sont basés sur des articles de journaux ou de conférences, soit les chapitres 1 à 8.

Pour assurer la cohérence et l'uniformité entre les différents chapitres de la thèse, les symboles utilisés dans ces chapitres ont été adaptés à ceux présentés à la table des symboles et constantes physiques du présent document.

Chapitre 1 :

- $\sigma_a \rightarrow \sigma_{abs}$
- $\sigma_e \rightarrow \sigma_{ems}$

Chapitre 2 :

- $\sigma_{ap} \rightarrow \sigma_{abs,p}$
- $\sigma_{a,\lambda} \rightarrow \sigma_{abs,\lambda}$
- $\sigma_{e,\lambda} \rightarrow \sigma_{ems,\lambda}$
- $\rho \rightarrow \rho_{Er}$
- $P_{in} \rightarrow P_{s,in}$

Chapitre 4 :

- $k \rightarrow \gamma_{Er}$

Chapitre 7 :

- $A_{ring} \rightarrow A_k$

De plus, certaines corrections additionnelles, énumérées ci-dessous, ont été apportées suite aux commentaires des membres du jury.

Chapitre 3 :

- n = 1.33 → n = 1.363

Chapitres 5 et 6 : Afin de clarifier que les oxydes ne sont pas ajoutés directement à la solution et qu'ils sont plutôt formés lors de l'étape de frittage :

- Al_2O_3 → aluminium

— P_2O_5 → phosphorus

— Al_2O_3 → aluminium

La phrase ci-dessous a été ajoutée afin de clarifier que la mesure prise au CAMECA néglige la présence d'$AlPO_4$:

— It is worth noting that the CAMECA measurement results neglect the presence of $AlPO_4$, leading to an overestimation of the concentrations of Al_2O_3 and P_2O_5 which are actually indicative of the total concentration of aluminium and phosphorus elements in the glass matrix.

Contribution personnelle aux articles publiés

Le chapitre 1 correspond à l'article "Modeling and characterization of cladding-pumped erbium-ytterbium co-doped fibers for amplification in communication systems" rédigé dans le cadre d'une collaboration avec Nokia Canada et paru en décembre 2019 dans la revue IEEE Journal of Lightwave Technology, Vol. 38, No. 7, pp. 1936-1944. L'article vise à déterminer si, et sous quelles conditions, le co-dopage à l'erbium-ytterbium est préférable au dopage à l'erbium seul dans les fibres amplificatrices pompées par la gaine qui amplifient la bande C dans les réseaux de communication. Pour ce faire, deux fibres ayant un polymère guidant et une gaine en forme de D ont été fabriquées et caractérisées en laboratoire. Les résultats de mesures ont ensuite été comparées à un modèle numérique afin de le valider. Une fois validé, ce modèle numérique a finalement pu être utilisé afin d'estimer les performances de fibres dopées à l'erbium seul ou à l'erbium-ytterbium dans différents scénarios afin de les comparer. Dans le cadre de cet article, mon rôle a été de concevoir les designs de fibres et de les soumettre aux techniciens pour fabrication, de caractériser les deux fibres en laboratoire, d'élaborer et de valider le modèle numérique, d'utiliser ce modèle à des fins d'estimation de performances de fibres dopées sous différents scénarios et, finalement, de rédiger l'article. J'ai aussi assuré la rédaction des réponses aux questions du comité de révision. Je tiens à remercier Roland Ryf, Nicolas K. Fontaine, René-Jean Essiambre, Haoshuo Chen, Colin Kelly, Younès Messaddeq et Sophie LaRochelle pour leurs précieux conseils et commentaires dans le cadre des analyses théoriques, des expériences au laboratoire et du processus de rédaction.

Le chapitre 2 correspond à l'article "Demonstration of an erbium-doped fiber with annular doping for low gain compression in cladding-pumped amplifiers" rédigé dans le cadre d'une collaboration avec Nokia Canada et paru en octobre 2018 dans la revue Optics Express, Vol. 26, No. 20, pp. 26633-26645. L'article étudie l'impact de la géométrie de distribution des ions d'erbium sur le gain et la compression du gain dans une fibre amplificatrice pompée par la gaine. Plus spécifiquement, le dopage en anneau autour du coeur est comparé au dopage uniforme dans le coeur et à un profil de dopant qui couvrirait à la fois le coeur et une région périphérique du coeur afin de couvrir le mode du signal presque entièrement. Dans le cadre de

cet article, un modèle numérique est d'abord utilisé afin de prédire la performance des trois géométries de distribution du dopant. Ensuite, une fibre ayant un profil de dopant en anneau est fabriquée et caractérisée afin de valider l'exactitude du modèle dans le cas particulier de simulations de fibres amplificatrices ayant une géométrie de distribution du dopant en anneau. Pour cet article, mon rôle a été de concevoir le modèle numérique, de l'utiliser pour générer tous les résultats de simulation, de caractériser la fibre en laboratoire et de rédiger l'article. J'ai aussi assuré la rédaction des réponses aux questions du comité de révision. Je tiens à remercier Haoshuo Chen, Nicolas K. Fontaine, Roland Ryf, René-Jean Essiambre, Colin Kelly, Cang Jin, Younès Messaddeq et Sophie LaRochelle pour leurs précieux conseils et commentaires dans le cadre des analyses théoriques, des expériences au laboratoire et du processus de rédaction.

Le chapitre 3 correspond à l'article "Novel fuseless optical fiber side-coupler based on half-taper for cladding-pumped EDFAs" présenté à la "Optical Fiber Communication Conference" en mars 2020. L'article présente une nouvelle méthode de couplage latéral de la pompe dans la gaine, sans fusion et sans altération du signal, qui permet d'augmenter l'efficacité de couplage de la pompe significativement par rapport aux méthodes sans fusion alternatives. En plus d'expliquer en quoi consiste cette nouvelle méthode, l'article présente des résultats de mesure de l'efficacité de couplage pour différentes géométries d'effilage. Pour cet article de conférence, mon rôle a tout d'abord été de proposer cette nouvelle méthode. Il est à noter qu'une demande de brevet est en cours. Ensuite, j'ai assemblé les coupleurs latéraux en laboratoire, mesuré leur efficacité de couplage, rédigé l'article et présenté les résultats à la conférence. Je tiens à remercier Younès Messaddeq et Sophie LaRochelle pour leurs précieux conseils et commentaires dans le cadre des expériences au laboratoire et du processus de rédaction ainsi que Ruohui Wang pour son aide au laboratoire avec la fabrication des fibres côniques.

Le chapitre 4 correspond à l'article "An 8-core erbium-doped fiber with annular doping for low gain compression in cladding-pumped amplifiers" rédigé dans le cadre d'une collaboration avec Nokia Canada et présenté à la "45th European Conference on Optical Communication" en septembre 2019. L'article présente la fabrication et la caractérisation de la première fibre amplificatrice à coeurs multiples ayant une géométrie de distribution des ions d'erbium en anneau dans chacun de ses coeurs. Dans le cadre de cet article, j'ai soumis un design initial de fibre aux techniciens, visant à répondre aux besoins de l'industrie, pour ensuite l'adapter itérativement en fonction de certaines contraintes de fabrication qui ont uniquement pu être identifiées suite à la fabrication de plusieurs préformes. Ensuite, mon rôle a été de caractériser la fibre au laboratoire, de simuler la fibre à l'aide d'un modèle numérique, d'analyser les résultats en comparant les données expérimentales aux simulations, de rédiger l'article et de le présenter à la conférence. Je tiens à remercier Roland Ryf, Nicolas K. Fontaine, René-Jean Essiambre, Haoshuo Chen, Younès Messaddeq, Juan Carlos Alvarado Zacarias, Rodrigo Amezcua Correa, Colin Kelly et Sophie LaRochelle pour leurs précieux conseils et commentaires dans le cadre des analyses théoriques, des expériences au laboratoire et du processus de rédaction.

Le chapitre 5 correspond à l'article "Characterization of an aluminophosphosilicate fiber with annular erbium doping for improved performance of cladding-pumped amplifiers" écrit dans le cadre d'une collaboration avec Nokia Canada et présenté à la "46th European Conference on Optical Communication" en décembre 2020. L'article présente un nouveau design de coeur visant à corriger les deux principales lacunes de la fibre présentée au chapitre 4. Dans le cadre de cet article, mon rôle a consisté à concevoir le nouveau design de fibre et de l'ajuster itérativement en fonction de mesures prises suite à la fabrication de plusieurs préformes afin de considérer les contraintes de fabrication reliées à l'utilisation d'aluminophosphosilicate. J'ai ensuite modifié le modèle numérique afin d'y inclure l'effet des agrégats d'ions d'erbium. J'ai aussi caractérisé la fibre au laboratoire, simulé la fibre à l'aide du nouveau modèle numérique, comparé les résultats expérimentaux avec les résultats de simulations, rédigé l'article et présenté l'article en question lors de la conférence. Je tiens à remercier René-Jean Essiambre, Colin Kelly, Younès Messaddeq et Sophie LaRochelle pour leurs précieux conseils et commentaires dans le cadre des analyses théoriques, des expériences au laboratoire et du processus de rédaction.

Le chapitre 6 correspond à l'article "Multicore Cladding-Pumped Fiber Amplifier with Annular Erbium Doping for Low Gain Compression" paru en janvier 2022 dans la revue IEEE Journal of Lightwave Technology, Vol. 40, No. 6, pp. 1836-1846 et écrit dans le cadre d'une collaboration avec Nokia Canada. Le chapitre présente la fabrication et la caractérisation de la seconde itération de fibre amplificatrice à coeurs multiples ayant une géométrie de distribution des ions d'erbium en anneau autour de chacun de ses coeurs. Dans le cadre de cet article, j'ai soumis un design initial de fibre aux techniciens pour ensuite choisir le ratio d'étirement entre la préforme et la fibre en fonction de simulations basées sur des mesures effectuées sur la préforme. Ensuite, mon rôle a été de caractériser la fibre au laboratoire et de lancer des simulations permettant de déterminer la longueur de fibre requise avec fan-in/fan-out, lorsque tous les coeurs reçoivent de la puissance de signal simultanément. J'ai aussi fait les démarches afin de sous-traiter la fabrication d'un fan-in/fan-out adapté à la fibre avec l'entreprise Chiral Photonics et mesuré les performances de chacun des huit coeurs, au laboratoire, avec fan-in/fan-out, lorsque tous les coeurs sont utilisés. Finalement, j'ai assuré la rédaction de l'article et formulé la réponse destinée au comité de révision. Je tiens à remercier René-Jean Essiambre, Colin Kelly, Younès Messaddeq et Sophie LaRochelle pour leurs précieux conseils et commentaires dans le cadre des analyses théoriques, des expériences au laboratoire et du processus de rédaction.

Le chapitre 7 correspond à l'article "Concentric Layers with Heterogeneous Doping for Cladding-Pumped L-Band Fiber Amplifiers" écrit dans le cadre d'une collaboration avec Huawei Canada et présenté à la conférence "Photonics West 2022" en janvier 2022. Dans le cadre de cet article, qui explore l'intérêt des couches concentriques hétérogènes de dopants afin d'augmenter l'efficacité de conversion de puissance, j'ai conçu le modèle numérique requis pour considérer deux structures de distribution du dopant différentes dans un même coeur. J'ai aussi effectué

les simulations numériques et rédigé l'article. Finalement, j'ai présenté les résultats lors de la conférence. Je tiens à remercier Lixian Wang, Frédéric Maes, Younès Messaddeq et Sophie LaRochelle pour leurs précieux conseils et commentaires dans le cadre des analyses théoriques et du processus de rédaction.

Le chapitre 8 correspond à l'article "Large area Bragg grating for pump recycling in cladding-pumped multicore erbium-doped fiber amplifiers" paru dans la revue Optics Express en mai 2022. Dans le cadre de cet article, qui démontre l'intérêt du recyclage de la puissance pompe résiduelle à la sortie de la fibre à l'aide d'un ICBG afin d'augmenter l'efficacité de conversion de puissance, j'ai conçu le modèle numérique requis pour considérer la puissance pompe réfléchie se propageant dans le sens inverse du signal. J'ai aussi effectué les simulations numériques ainsi que les mesures expérimentales du gain et du facteur de bruit, conduit les analyses ayant permis d'estimer la réflectivité efficace ainsi que la PCE et rédigé toutes les sections de l'article, hormis la seconde qui a principalement été rédigée par Lauris Talbot. Il est à noter que l'inscription du ICBG a aussi été pris en charge par Lauris Talbot. Je tiens finalement à remercier Lauris Talbot, Younès Messaddeq, Martin Bernier et Sophie LaRochelle pour leurs précieux conseils et commentaires dans le cadre des analyses théoriques, des expériences au laboratoire et du processus de rédaction.

Introduction

I.1 Mise en contexte

I.1.1 Réseaux de communications optiques

Pendant l'époque précambrienne, certaines formes de vie ont développé des photorécepteurs biologiques permettant de détecter la présence de lumière ambiante dans leur environnement [18; 19]. Aujourd'hui, la majorité des espèces animales possèdent des organes photosensibles, beaucoup plus complexes qu'un simple photorécepteur [20], qui leur permettent de recevoir davantage d'information en provenance de leur environnement immédiat. Au fil des millénaires, cette caractéristique morphologique a influencé les interactions interspécifiques et intraspécifiques, notamment en permettant aux individus de communiquer des messages visuels entre eux, par l'intermédiaire de pelage coloré, de mouvements expressifs ou de toute autre forme d'information qui se transmet par la lumière [21], contribuant ainsi à la création de réseaux d'individus collaboratifs.

De façon analogue, les réseaux de communications optiques déployés au cours du 20^{e} siècle utilisent aussi des signaux lumineux pour connecter les individus entre eux, en assurant une communication continue et quasi instantanée entre des individus de partout à travers le monde. Autrefois accessibles par une infime partie de la population mondiale, la diminution des coûts économiques reliés au déploiement et à l'entretien de ces réseaux a permis de démocratiser l'information. Aujourd'hui, c'est plus de 65% de la population mondiale qui a accès à Internet [22]. Pendant ce temps, le trafic internet total a augmenté de façon exponentielle, ouvrant ainsi la porte à des applications telles que la diffusion vidéo en temps réel, la domotique ou encore l'infonuagique [23].

Alors que les guides d'ondes creux ont été considérés pour la transmission d'information sur des longues distances vers la fin des années 50 [24], la fibre optique est finalement la technologie qui a été retenue par l'industrie pour déploiement à partir des années 1980 [23]. Ayant un diamètre de quelques dizaines de microns et composées de silice, un matériau peu dispendieux, les fibres optiques peuvent aujourd'hui atteindre des pertes aussi faibles que 0.1419 dB/km [25] et une capacité de 10.66 Pb/s par fibre [26]. La fibre optique est donc aujourd'hui le principal medium utilisé pour acheminer l'information dans les réseaux de communications optiques déployés à

travers le monde.

I.1.2 Fibres amplificatrices

L'étendue planétaire des réseaux actuels implique qu'un signal doit pouvoir être acheminé sur des milliers de kilomètres tout en conservant une qualité de signal suffisante pour minimiser les pertes d'information lors de la détection. Or, malgré les faibles pertes par kilomètre qu'on retrouve dans une fibre optique moderne, il est nécessaire d'amplifier le signal périodiquement pour assurer que l'information puisse être reçue par le destinataire [27]. Pour cela, il est souhaitable d'utiliser un amplificateur optique qui, par définition, permet d'amplifier un signal lumineux directement sans recourir à une conversion électrique, quelle qu'elle soit, afin d'éviter les coûts engendrés par cette complexité additionnelle.

L'une des technologies permettant d'amplifier un signal optique directement est l'amplificateur optique à semi-conducteur. Or, le principal problème avec cette technologie provient du fait que la durée de vie de ses états supérieurs est extrêmement courte, de sorte que les variations instantanées de la puissance du signal dans chacun des canaux amplifiés ont un effet sur le gain des autres canaux amplifiés, causant par le fait même de la diaphonie inter-canaux [28]. Ainsi, vu leur temps de vie largement supérieur, on préfère généralement utiliser des amplificateurs à fibre dopée à l'erbium. Leur temps de vie élevé combiné à leur large bande d'amplification autour de la région spectrale ayant les plus faibles pertes dans une fibre optique de silice standard, communément appelée bande C, permet l'amplification en parallèle de multiples canaux situés à des longueurs d'onde distinctes avec peu d'interférence entre les canaux. De plus, les amplificateurs à fibre dopée à l'erbium offrent un gain élevé, un facteur de bruit faible, une puissance de saturation élevée et sont peu sensibles en polarisation tout en étant peu couteux et facile à connecter sur une fibre passive standard [29].

Typiquement, un amplificateur à fibre dopée à l'erbium est constitué 1) d'une fibre ayant un coeur dopé d'ions d'erbium, 2) d'une source de pompage émettant de la puissance dans l'une des régions spectrales d'absorption de l'erbium, soit autour de 980 nm ou de 1480 nm, et 3) d'un multiplexeur spectral permettant de combiner le signal d'entrée et la pompe dans le coeur de la fibre dopée. Tous ces composants sont assemblés et insérés dans le lien de communication à amplifier à l'aide de fusions tel que présenté à la figure I.1. Des isolateurs sont aussi insérés entre les amplificateurs afin d'éviter l'obtention d'un effet laser et de limiter l'interférence multi-parcours.

Puisque les besoins de l'industrie varient largement selon l'application spécifique pour laquelle un amplificateur est utilisé, les contraintes de conception des amplificateurs sont, elles aussi, très variées selon le type de réseaux de communications optiques considéré.

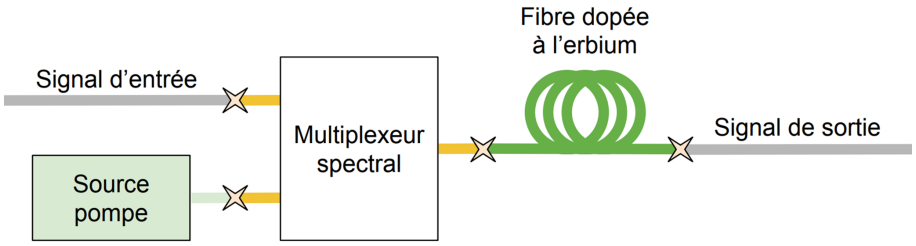

FIGURE I.1 – Schéma d'un amplificateur à fibre dopée à l'erbium pompée par le coeur.

Fibres amplificatrices dans les liens de communication sous-marins

Afin de connecter les réseaux de communications optiques des divers continents entre eux, des centaines de câbles sous-marins ont été déposés au fond des océans [30]. Puisque les signaux doivent être amplifiés à tous les 60 km à 100 km, des amplificateurs optiques sont répartis sur toute la longueur du câble, tel qu'illustré à la figure I.2. Sur les rives, l'équipement d'alimentation électrique fourni une tension pouvant aller jusqu'à ±15000 V, acheminée aux amplificateurs par l'intermédiaire d'un câble de cuivre [1]. Dans un tel contexte, le nombre de fibres optiques contenues dans un câble est contraint par l'alimentation électrique totale disponible. Dans ces liens sous-marins, l'efficacité de conversion de puissance est donc un facteur crucial à considérer lors de la conception d'un amplificateur optique.

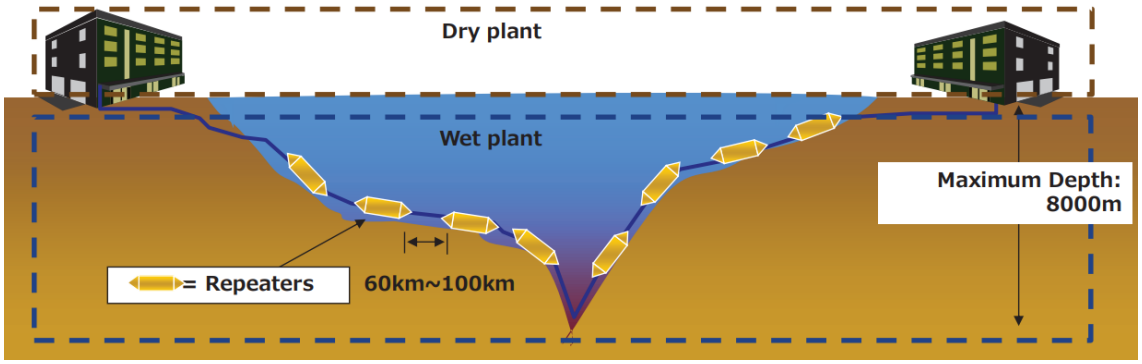

FIGURE I.2 – Schéma des principales parties d'un système sous-marin. Figure tirée de [1].

Fibres amplificatrices dans les multiplexeurs optiques d'insertion-extraction reconfigurables (ROADMs)

Dans les réseaux de communication actuels, des multiplexeurs optiques d'insertion-extraction [31] permettent d'acheminer les différents canaux spectraux d'une même fibre vers plusieurs fibres distinctes, afin de leur faire emprunter des trajectoires différentes et ainsi exploiter la granularité inhérente du multiplexage spectral [32]. Puisque la demande croit et évolue avec le temps, ces multiplexeurs sont aujourd'hui généralement reconfigurables à distance [33], tel que présenté à la figure I.3 afin de permettre une adaptation des réseaux à la demande, sans

devoir recourir à une intervention manuelle de la part d'un technicien.

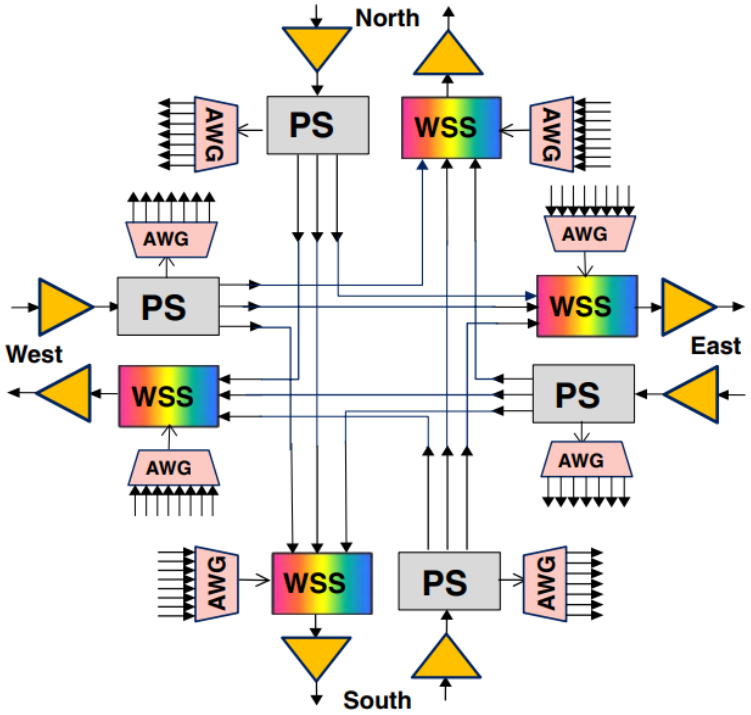

FIGURE I.3 – Schéma d'un ROADM à quatre directions. WSS, wavelength selective switch ou commutateur sélectif de longueur d'onde ; PS, power splitter ou répartiteur de puissance. Figure tirée de [2].

Alors que les réseaux utilisaient auparavant une grille fixe standardisée qui divise la bande C en divisions spectrales de 50 GHz ou 100 GHz de largeur de bande, une grille flexible est aujourd'hui privilégiée afin d'exploiter optimalement la bande C et d'ouvrir la porte aux types de modulation qui occupent plus de 100 GHz de largeur de bande. Le schéma I.4 illustre la différence entre les réseaux à grille fixe et ceux à grille flexible.

Que la grille soit fixe ou flexible, les amplificateurs utilisés dans les ROADMs, représentés par des triangles oranges à la figure I.3, reçoivent un nombre de canaux et une puissance du signal à l'entrée qui peut varier significativement au cours de leur durée de vie. Or, typiquement, les amplificateurs optiques sont opérés en régime de saturation tel qu'illustré par la ligne pointillée bleue à la figure I.5. Un tel régime permet de compenser les pertes dues à la dépréciation des systèmes ou à tout événement incontrôlable en fournissant automatiquement un gain plus élevé lorsque les pertes augmentent au cours de la durée de vie des liens de fibres optiques [34]. De plus, à mesure que la saturation augmente, l'inclinaison de la courbe de gain en fonction de la longueur d'onde varie. L'opération en régime de saturation permet donc de sélectionner la puissance d'entrée pour laquelle le gain est plat sur la région spectrale d'intérêt [35], générant ainsi un gain relativement uniforme sur tous les canaux amplifiés. La puissance est donc relativement uniforme spectralement à l'entrée du GFF, permettant ainsi de maximiser

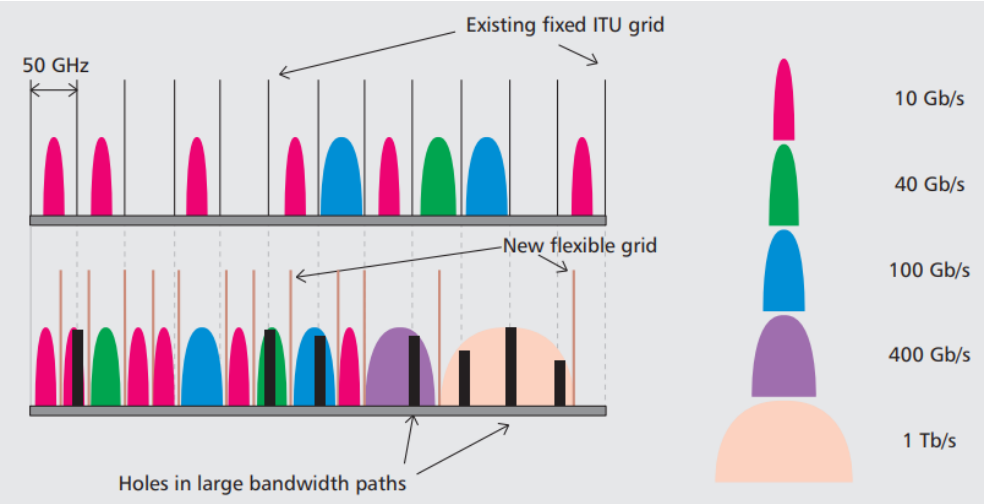

FIGURE I.4 – Représentation schématique de la différence entre les réseaux à grille fixe et ceux à grille flexible. Figure tirée de [3].

l'efficacité énergétique.

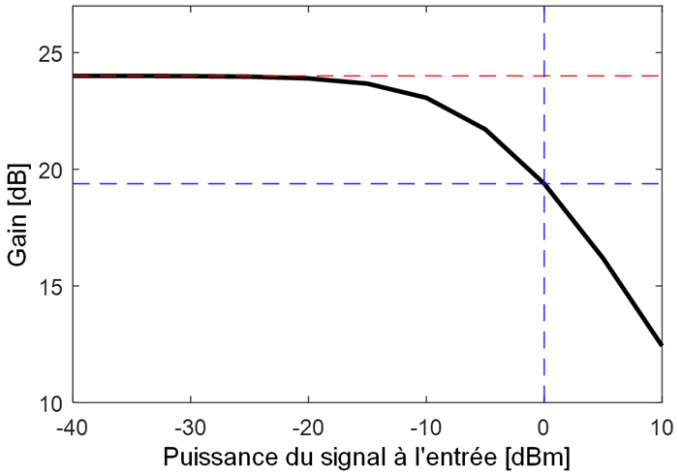

FIGURE I.5 – Gain en fonction de la puissance du signal à l'entrée d'un amplificateur à mode unique pompé par le coeur. La ligne hachurée rouge représente le gain à petit signal tandis que les lignes hachurées bleues représentent le gain lorsque la puissance du signal à l'entrée est de 0 dBm.

Cependant, dans un lien de communication reconfigurable, une telle opération en régime saturé peut causer problème puisque, lorsqu'un canal est ajouté ou retiré, tous les autres canaux présents subissent une variation de puissance [36]. Pour limiter les variations de gain, trois méthodes distinctes sont actuellement utilisées :

1. L'ajustement automatique en temps réel de la puissance de la pompe, qui consiste à ajuster la puissance de la pompe en fonction de la puissance du signal à l'entrée afin de

maintenir le niveau d'inversion des ions actifs constant dans la fibre et, par conséquent, la distribution spectrale du gain [37; 38; 39].

2. L'ajout d'un faux canal ayant une puissance variable, qui consiste à ajuster la puissance du canal lorsque certains canaux sont retirés ou ajoutés afin de maintenir le niveau de saturation constant [40; 41].
3. L'utilisation d'un DGFF (dynamic gain flattening filter) qui consiste à induire des pertes avec une dépendance en longueur d'onde afin que le gain à la sortie soit uniforme spectralement [42; 43; 44; 45]. Cette dernière est cependant peu utilisée aujourd'hui vu son niveau de complexité, ses pertes d'insertion élevées, son inefficacité énergétique, ses temps de réponses élevés et son coût total, par rapport aux méthodes alternatives.

Or, malgré ces ajustements, lorsque les modifications soudaines de gain sont importantes, le régime transitoire peut mener à des instabilités sur le réseau [46; 47]. Dans un tel réseau reconfigurable, il est donc souhaitable que le gain des fibres amplificatrices utilisées reste aussi stable que possible pour une variation de puissance d'entrée donnée.

Fibres amplificatrices pour le multiplexage spatial

Afin de maximiser le débit d'information acheminé entre les utilisateurs et de minimiser le coût par bit transmis, les réseaux de communications optiques actuels utilisent déjà plusieurs dimensions physiques de la lumière : phase, polarisation, temps, longueur d'onde et espace [48]. Tandis que les quatre premières dimensions énumérées ont pu être exploitées au cours des dernières décennies en modifiant uniquement les modulateurs et démodulateurs présents à l'entrée et à la sortie des liens de communication, la dimension spatiale nécessite le remplacement ou l'ajout de plusieurs composants physiques intermédiaires. Alors que la dimension spatiale a d'abord été exploitée en déployant plusieurs fibres à mode unique en parallèle [49], l'intérêt pour le multiplexage spatial à l'intérieur d'une seule et même fibre a connu une forte croissance au cours des dernières années [50]. Un exemple de lien de communication exploitant le multiplexage spatial est illustré à la figure I.6. Dans de tels systèmes, les différents canaux sont insérés dans les différents modes d'une fibre à l'aide d'un multiplexeur spatial. Contrairement aux réseaux traditionnels qui utilisent de la fibre à mode unique, autant pour la fibre passive qui transporte les modes que pour la fibre active qui permet leur amplification de façon ponctuelle dans les amplificateurs optiques, la fibre utilisée doit être multiplexée spatialement. Dans de tels systèmes, des égaliseurs de gain sont souvent nécessaires afin de compenser la différence, entre les modes, de pertes et de gain généré lors de l'amplification. À la sortie du système, un démultiplexeur modal permet de séparer le contenu des modes en différents canaux qui sont par la suite traités à l'aide d'algorithmes permettant de retrouver l'information transmise malgré l'interférence ayant pu avoir lieu entre les différents modes au cours de la transmission.

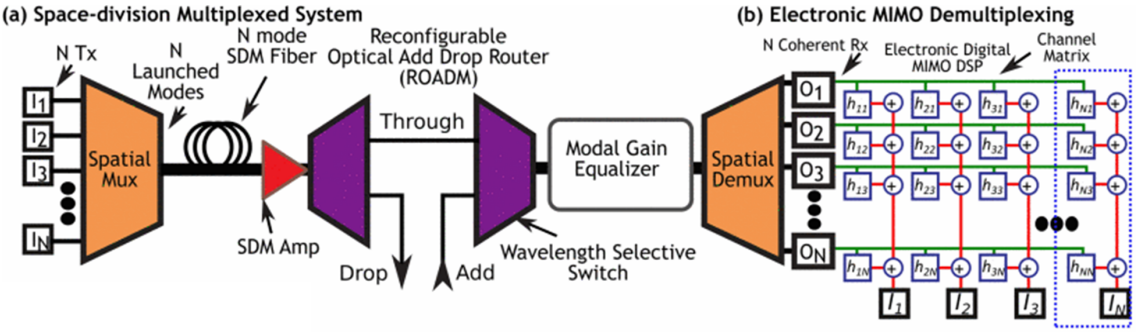

FIGURE I.6 – Exemple d'un lien de communication exploitant le multiplexage spatial avec une fibre à coeur unique et à modes multiples. Figure tirée de [4].

Or, afin de transporter plusieurs modes dans une même fibre, il existe plusieurs types de fibres multiplexées spatialement. Les principaux types sont :

- Les fibres à coeurs multiples, qui contiennent plusieurs coeurs à mode unique dans une même gaine. Ces coeurs sont séparés d'une distance suffisante pour que le couplage et l'interférence entre les canaux qu'ils transportent soient négligeables. Une fibre à coeurs multiples est illustrée à la figure I.7a ;
- Les fibres à coeur unique et à modes multiples, qui contiennent un seul coeur qui est cependant assez large pour guider plusieurs modes. Il est à noter que l'interférence entre les modes d'un même coeur est un défi important dans de telles fibres. Un exemple de fibre à coeur unique et à modes multiples est présenté à la figure I.7b ;
- Les fibres à coeurs et modes multiples (figure I.7c), qui contiennent plusieurs coeurs étant chacun assez large pour guider chacun quelques modes. Encore une fois, la distance entre les coeurs est suffisante pour que l'interaction entre leurs modes respectifs soit négligeable ;
- Les fibres à coeurs couplés (figure I.7d) dont les coeurs sont suffisamment près les uns des autres pour que l'information soit couplée d'un coeur à l'autre au cours de la propagation. De telles fibres nécessitent donc un traitement plus complexe à la sortie du système afin de retrouver l'information initialement envoyée dans les différents canaux. Les principaux avantages de cette méthode sont qu'elle offre une plus grande densité spatiale que les fibres à coeurs découplés et moins de différence entre les vitesses de groupes des canaux spatiaux par rapport aux coeurs à modes multiples, ce qui simplifie le traitement de signal à la réception.

Pour amplifier les différents modes transmis par un lien de fibre optique avec multiplexage spatial, il serait évidemment inefficace de démultiplexer les modes et de les multiplexer à nouveau ensuite dans le seul but d'utiliser des amplificateurs optiques traditionnels pour effectuer l'amplification. Or, il est possible de concevoir des amplificateurs optiques multiplexés spatialement et adaptés à la fibre contenant les modes à amplifier en produisant une fibre ayant un

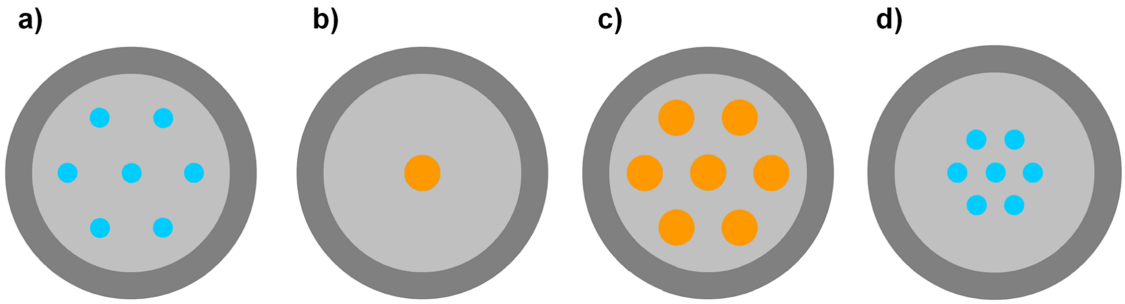

FIGURE I.7 – Schéma des principaux types de multiplexage spatial. Les cercles bleus représentent des coeurs à mode unique tandis que les cercles oranges représentent des coeurs à modes multiples.

profil d'indice similaire, mais contenant des ions actifs recouvrant les régions où les modes se trouvent.

I.1.3 Fibres amplificatrices pompées par la gaine

Afin d'exciter les ions actifs présents dans de telles fibres, il est nécessaire de les faire interagir avec de la lumière de pompage. Or, il existe deux méthodes d'injection de la pompe distinctes dans les fibres amplificatrices [51] :

— Le pompage par le coeur, qui consiste à injecter de la pompe dans les modes guidés par le coeur. Cette méthode est celle utilisée dans les amplificateurs traditionnels et a l'avantage d'offrir une densité de puissance de la pompe supérieure comparativement au pompage par la gaine, pour une puissance de la pompe totale donnée, étant donné que la superficie du coeur est nettement inférieure à celle de la gaine. Puisque la puissance de saturation du signal dépend de l'intensité locale du signal et de la pompe, le pompage par le coeur permet généralement d'obtenir une puissance de saturation supérieure. Il est aussi possible d'utiliser une seule source de pompage pour plusieurs coeurs à condition d'utiliser des diviseurs de puissance pour séparer la puissance d'une même source dans plusieurs coeurs ;

— Le pompage par la gaine, qui consiste à injecter la puissance de la pompe dans la gaine de la fibre afin qu'elle interagisse avec tous les ions actifs présents dans la fibre [51; 52]. Par rapport au pompage par le coeur, la méthode de pompage par la gaine a l'avantage d'être plus simple et moins coûteuse à implémenter lorsque plusieurs coeurs doivent être amplifiés en parallèle. En effet, une seule source peut être utilisée pour injecter la puissance pompe dans la gaine d'une fibre à coeurs multiples en utilisant un seul coupleur de puissance [53]. De plus, contrairement à la méthode de couplage par le coeur, celle-ci permet d'utiliser une diode laser multimode, moins chère et plus efficace pour convertir l'énergie électrique en énergie optique que les sources de pompage utilisées pour le pompage par le coeur. Lorsque la puissance est injectée dans la gaine d'une

fibre, un polymère guidant à bas indice doit être utilisé afin d'assurer le confinement de la pompe dans la fibre [52]. En revanche, le pompage par la gaine implique aussi que la puissance de la pompe est distribuée sur une plus grande surface, menant ainsi à une intensité de puissance plus faible. Une intensité de puissance plus faible peut avoir pour effet de diminuer la puissance de saturation et de diminuer l'efficacité énergétique. Cependant, certains groupes de recherche suggèrent que, lorsqu'on considère l'efficacité énergétique des diodes multimodes et la consommation énergétique des systèmes de refroidissement requis avec les diodes à mode unique, le pompage par la gaine peut permettre d'augmenter l'efficacité énergétique lorsque la densité de coeurs dans la fibre est suffisamment élevée [54; 10].

Dans cette optique, l'utilisation du pompage par la gaine pour les fibres amplificatrices dans les réseaux de communication a été considérée par plusieurs groupes de recherche au cours des dernières années, principalement avec des fibres amplificatrices qui contiennent plusieurs coeurs et/ou plusieurs modes à amplifier.

Fibres amplificatrices pompées par la gaine pour le multiplexage spatial

Le pompage par la gaine a été démontré à plusieurs reprises dans une perspective d'intégration et de diminution du nombre de composants, en utilisant une source de pompage multimode pour amplifier quatre [5], six [55; 6; 13], sept [14; 7; 15; 56; 57], 12 [8; 9; 10], 19 [11; 58] ou 32 [12] coeurs. Des exemples de configuration des coeurs dans la gaine sont présentés à la figure I.8.

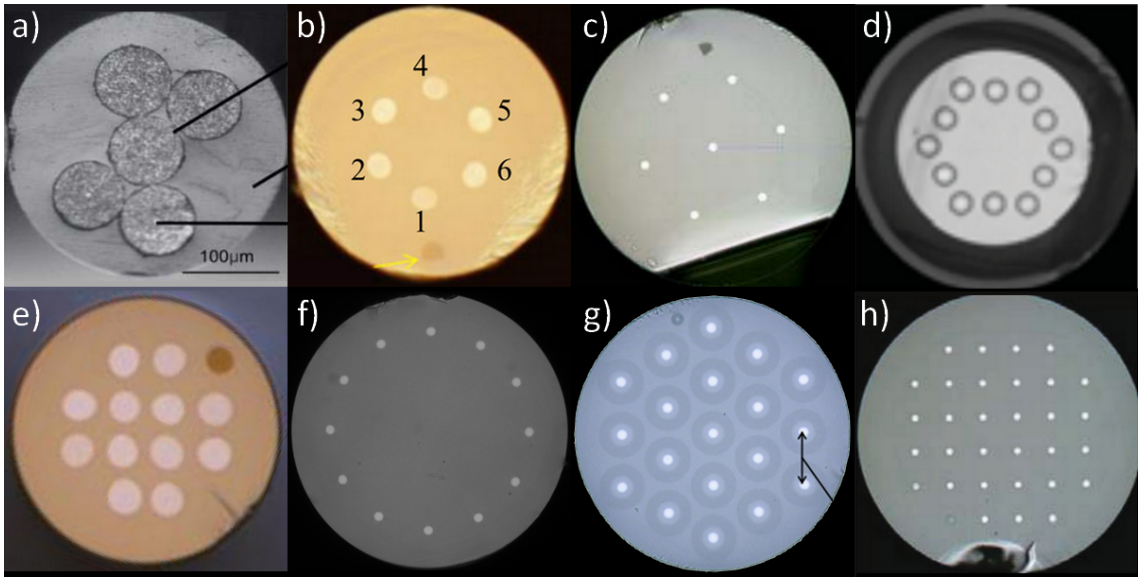

FIGURE I.8 – Exemples de géométries utilisées dans les fibres amplificatrices à coeurs multiples pompées par la gaine. Images tirées de a) [5], b) [6], c) [7], d) [8], e) [9], f) [10], g) [11] et h) [12].

Le pompage par la gaine a aussi été investigué dans les fibres amplificatrices ayant des coeurs multimodes puisqu'une distribution uniforme de la puissance de la pompe sur toute la fibre permet l'obtention d'une amplification uniforme des différents modes présents dans un même coeur de fibre amplificatrice [59; 60; 56; 9; 55; 6].

Pour coupler la puissance de la pompe dans la gaine, plusieurs configurations existent. D'abord, la puissance peut être couplée par les extrémités de la fibre dopée, soit en utilisant un montage en espace libre tel que celui présenté à la figure I.9, soit à l'aide d'un fan-in tel que présenté à la figure I.10. Alors que ces deux méthodes ont le désavantage d'occuper une superficie de la gaine qui pourrait alternativement être utilisée pour augmenter la densité de canaux spatiaux, le couplage latéral, illustré à la figure I.11, ne permet pas d'atteindre une efficacité de couplage supérieure à 70% [61], à moins d'avoir recours à une fusion entre la fibre acheminant la pompe et la fibre amplificatrice, ce qui peut mener à une déformation des coeurs, diminuant ainsi la qualité du signal [62; 63].

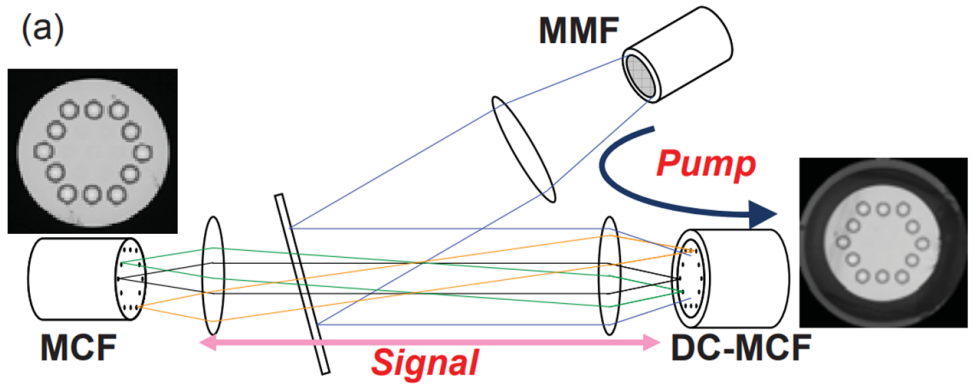

FIGURE I.9 – Montage pour injecter la pompe dans la gaine en espace libre. Tirée de [8].

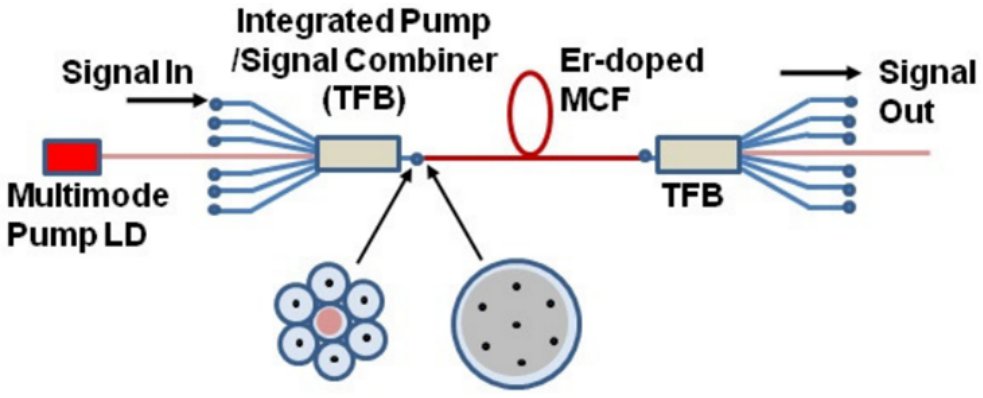

FIGURE I.10 – Montage pour injecter la pompe dans la gaine à l'aide d'un fan-in. Tirée de [13].

À long terme, il serait avantageux de déployer des liens de communications entièrement mul-

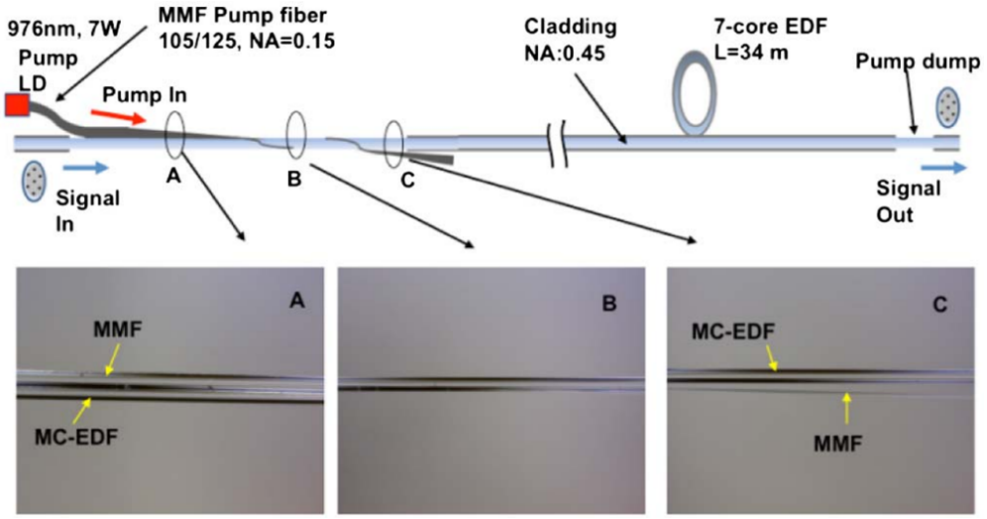

FIGURE I.11 – Montage pour injecter la pompe dans la gaine latéralement. Tirée de [14].

tiplexés spatialement, autant au niveau de la fibre passive que de la fibre amplificatrice. Cependant, les réseaux actuels sont presque entièrement constitués de fibres passives à coeur et mode uniques. Puisqu'il est impossible de remplacer le réseau en entier du jour au lendemain, des interfaces sont requises pour passer des fibres à coeur et mode uniques vers les fibres multiplexées spatialement. Pour cela, des fan-in/fan-out, tel que ceux présentés à la figure I.10, peuvent être utilisés, avec ou sans canal pour la pompe. Pour éviter d'avoir recours à cet intermédiaire, des fibres à éléments multiples, tel que présenté à la figure I.12, ont été proposées. Avec de telles fibres, les éléments de la fibre à coeurs multiples peuvent être séparés, après avoir retiré le polymère à faible indice, pour ensuite être fusionnées aux fibres à coeur unique à l'aide d'une simple épissure.

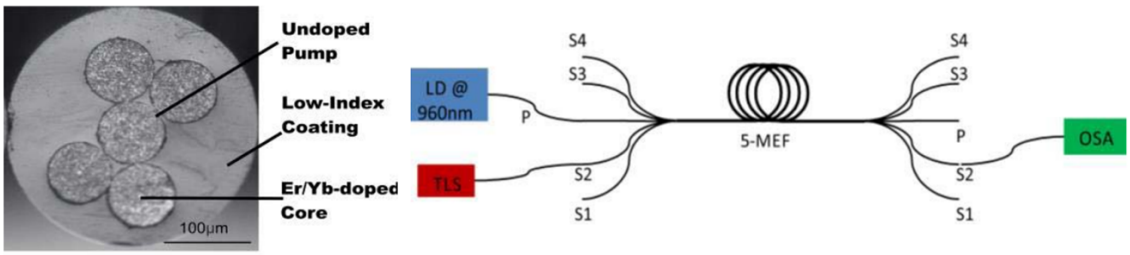

FIGURE I.12 – Montage pour injecter la pompe dans une fibre à éléments multiples. Tirée de [5].

Aussi, comme pour les fibres amplificatrices pompées par le coeur [64], les fibres amplificatrices pompées par la gaine emploient généralement l'erbium à titre de dopant pour amplifier les canaux de la bande C [13; 14; 60; 55; 59; 6; 11; 58; 9; 56; 57] ou de la bande L [6; 58; 9]. Cependant, vu le faible recouvrement entre la puissance pompe guidée par la gaine et le coeur dopé, la puissance totale requise pour atteindre un niveau d'inversion des ions suffisant pour une

amplification de qualité a pour effet de diminuer l'efficacité de conversion de puissance (PCE). Pour améliorer l'efficacité de conversion de puissance, le co-dopage à l'erbium-ytterbium a été proposé, puisqu'il permet l'obtention d'un taux d'absorption plus élevé, grâce à la puissance absorbée par l'ytterbium et redistribuée à l'erbium, permettant ainsi d'obtenir un niveau d'inversion suffisant pour amplifier les signaux avec une puissance totale de pompe plus faible. Lorsque utilisé dans la bande C, avec une longueur de fibre permettant de maximiser l'efficacité de conversion de puissance, le co-dopage à l'erbium-ytterbium produit un gain nettement plus faible dans les longueurs d'ondes inférieures à 1535 nm que sur le reste de la bande C [7; 8]. Pour cette raison, les fibres amplificatrices pompées par la gaine et co-dopées à l'erbium-ytterbium sont généralement opérées uniquement sur la région de la bande C au-delà de 1535 nm [12; 10] ou encore sur la bande L [5].

Outre l'utilisation d'ions d'ytterbium, une méthode ayant été proposée afin d'augmenter l'efficacité de conversion de puissance est le recyclage de la pompe à partir du principe "turbo" [15], qui consiste à acheminer la pompe résiduelle à la sortie de la fibre vers l'entrée de la fibre par l'intermédiaire d'une fibre passive, tel qu'illustré à la figure I.13.

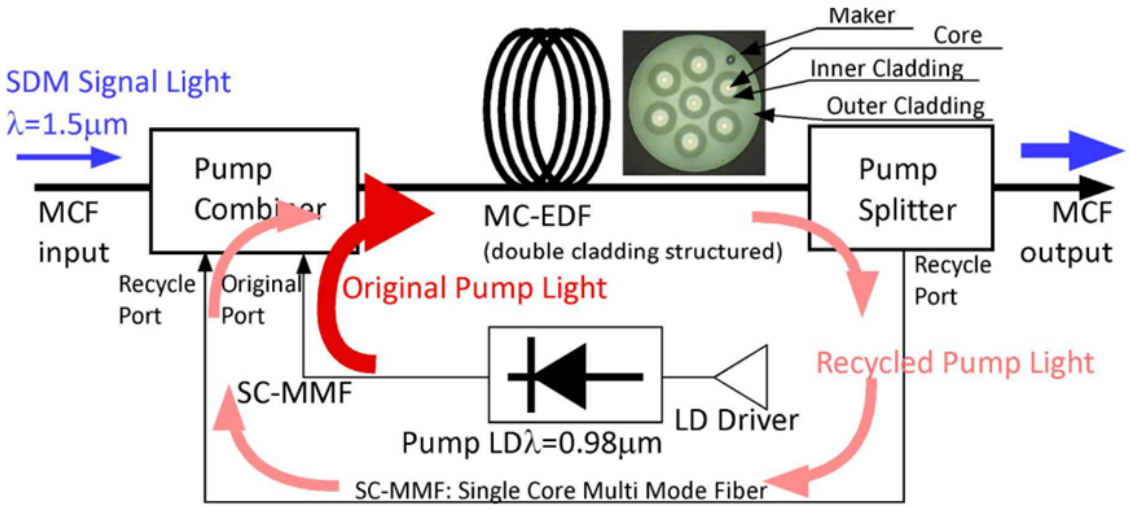

FIGURE I.13 – Montage utilisé pour recycler la pompe à partir du principe "turbo". Tirée de [15].

I.2 Objectifs et structure de la thèse

Dans un contexte où l'intérêt pour les systèmes intégrés et multiplexés spatialement dans les réseaux de communication est grandissant, et considérant les avantages que pourrait apporter l'utilisation de fibres amplificatrices pompées par la gaine dans de tels systèmes, cette thèse vise à explorer l'intérêt du pompage par la gaine pour les réseaux de communications optiques actuels et futurs.

I.2.1 Fibres amplificatrices pompées par la gaine pour les réseaux reconfigurables

Plus précisément, l'une des applications commerciales qui pourrait, à court terme, bénéficier des avantages des fibres amplificatrices pompées par la gaine est celle des réseaux reconfigurables.

En effet, l'une des caractéristiques propres aux réseaux reconfigurables est qu'ils comportent des multiplexeurs optiques d'insertion-extraction reconfigurables [31]. Or, plusieurs fibres distinctes provenant de différents lieux géographiques s'y rencontrent et contiennent des canaux devant être amplifiés. Il s'agit donc d'une opportunité intéressante d'utiliser une même fibre amplificatrice pour amplifier plusieurs coeurs à partir d'une même source de pompage et de profiter des diminutions de coûts que permet le pompage par la gaine dans une fibre à coeurs multiples.

En revanche, tel que mentionné précédemment, il est à noter que l'un des obstacles les plus importants dans l'implémentation du pompage par la gaine réside au niveau de la faible intensité de la pompe lorsque celle-ci est répartie sur toute la surface de la gaine. Cette faible intensité mène à une diminution de la puissance de saturation, qui est particulièrement critique dans les réseaux reconfigurables puisqu'elle augmente les variations de gain lorsque des canaux sont ajoutés ou retirés. Tel qu'illustré à la figure I.14, le fait de retirer des canaux du signal à l'entrée a pour effet de modifier la répartition spectrale de la puissance à la sortie de sorte que certains canaux aient une intensité plus forte que les autres. Ainsi, la compression du gain devra être minimisée et la puissance de saturation augmentée, afin que cette technologie puisse être viable dans ces réseaux reconfigurables.

Bien que les méthodes utilisées actuellement pour l'ajustement du gain soient théoriquement compatibles avec le pompage par la gaine, le fait d'utiliser la méthode d'ajustement automatique en temps réel de la puissance pompe [37; 38; 39] viendrait limiter les avantages engendrés par l'utilisation du pompage par la gaine puisqu'elle nécessiterait d'ajouter une source de pompage individuelle dans chacun des coeurs afin de contrôler la puissance pompe individuellement pour chacun des canaux spatiaux [65], ramenant ainsi la complexité et le nombre de composants au même niveau qu'avec la méthode de pompage par le coeur. La méthode d'ajout d'un faux canal peut cependant être utilisé de la même manière que dans les systèmes actuels [40; 41].

Bref, dans le cadre de ce projet doctoral, en collaboration avec l'entreprise Nokia, on souhaite explorer l'intérêt du multiplexage spatial dans les fibres optiques amplificatrices situées dans les multiplexeurs optiques d'insertion-extraction reconfigurables (ROADMs). Les analyses effectuées assumeront que la technologie doit être compatible avec les réseaux actuels, qui sont eux-mêmes principalement constitués de fibres à coeur et à mode unique. Afin d'aligner l'innovation générée par cette thèse avec les besoins de l'industrie, des spécifications techniques

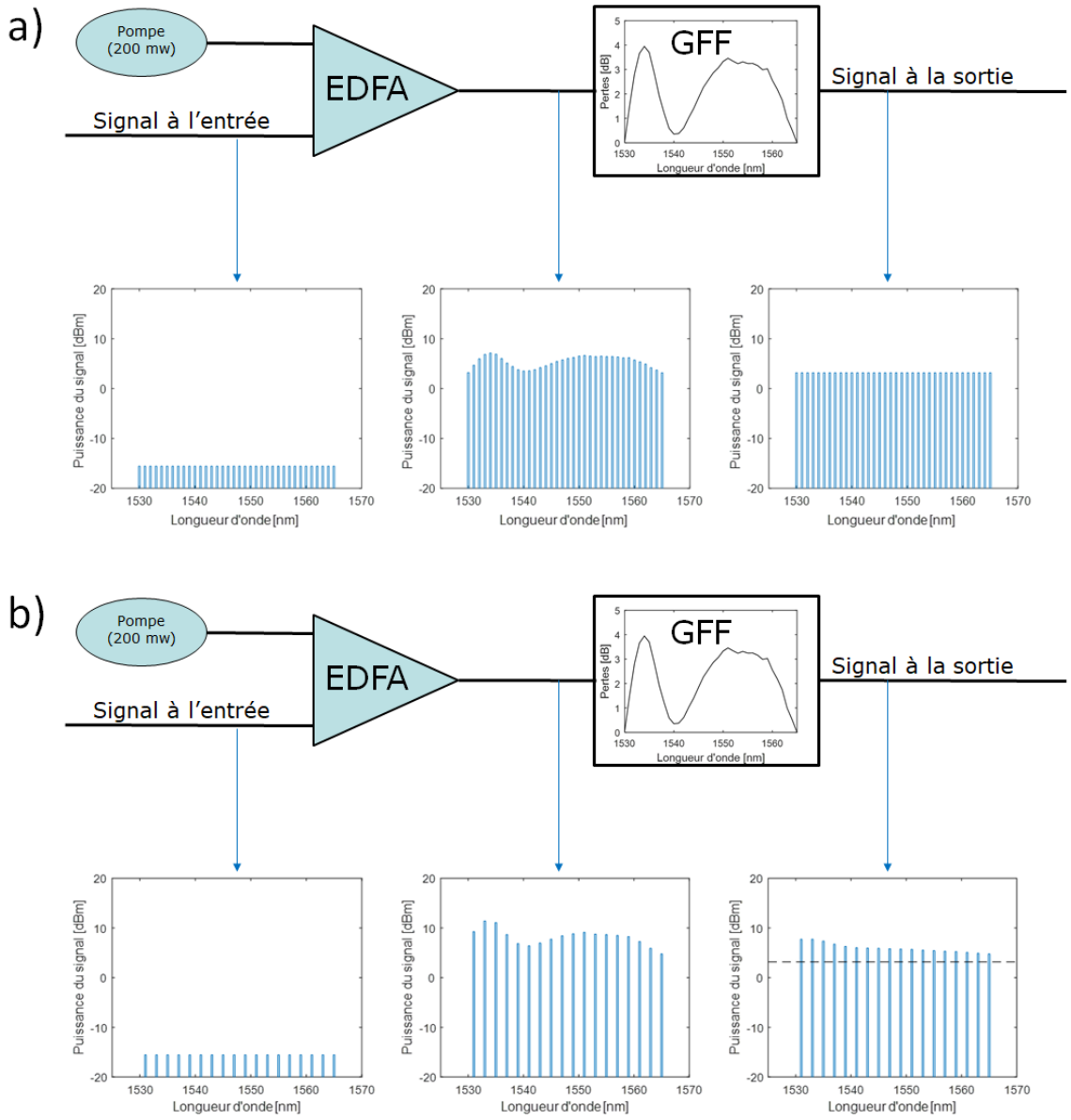

FIGURE I.14 – Puissance du signal à l'entrée de l'amplificateur, après l'EDFA et après le filtre d'égalisation du gain lorsque a) le signal d'entrée contient 36 canaux de -17.7 dBm et b) le signal d'entrée contient 18 canaux de -17.7 dBm.

typiques serviront de référence tout au long du processus de recherche. Celles-ci sont présentées dans le tableau I.1.

Il est à noter que, puisque l'amplificateur viendra s'insérer dans des réseaux terrestres, aucune contrainte n'a été fixée sur l'efficacité énergétique ainsi que sur la puissance de la pompe totale utilisée. Cependant, une puissance de la pompe totale trop élevée, combinée à une efficacité énergétique très basse, peut mener un niveau élevé de pompe résiduelle à diffuser à la sortie de la fibre, augmentant ainsi les risques de surchauffe et de combustion.

Tableau I.1 – Spécifications techniques visées pour l'amplificateur à concevoir

Paramètre	Spécifications
Nombre de coeurs	8
Plage de puissance du signal à l'entrée	-23.1 dBm à 1.4 dBm
Plage spectrale couverte	1529 nm à 1565 nm
Gain	>17 dB sur toute la plage spectrale
Facteur de bruit	<5 dB sur toute la plage spectrale
Compression du gain	<5 dB sur toute la plage spectrale
Méthode de couplage de la pompe	Par la gaine, avec une seule diode laser multimode centrée à 980 nm

I.2.2 Fibres amplificatrices pompées par la gaine pour maximiser l'efficacité de conversion de puissance dans la bande L

L'un des principaux enjeux relatifs aux amplificateurs optiques est l'efficacité de conversion de puissance, qui est particulièrement critique dans les liens de communication sous-marins. Or, lorsque la puissance de la pompe est répartie sur la gaine, une puissance de la pompe totale beaucoup plus élevée est nécessaire pour atteindre la même intensité de pompage sur la région dopée, comparativement au pompage par la gaine.

Plutôt que de lutter contre la saturation dans les amplificateurs qui amplifient la bande C, le pompage par la gaine peut être avantageusement utilisé dans les applications où une plus faible inversion des ions actifs est requise. Par exemple, le pompage par la gaine peut être utilisé pour les amplificateurs pour la bande L, qui sont intrinsèquement plus compatibles avec le pompage de gaine que les amplificateurs pour la bande C.

Bref, dans le cadre de ce projet doctoral, on souhaite aussi explorer l'intérêt des fibres amplificatrices pompées par la gaine pour amplifier la bande L avec une efficacité de conversion de puissance élevée.

I.2.3 Structure de la thèse

Le coeur de la thèse se divise en six sections ayant des objectifs distincts :

1. Analyse de l'impact du co-dopage à l'ytterbium sur les performances d'amplification des EDFAs dans la bande C (chapitre 1)
2. Analyse de l'impact de la géométrie de distribution des ions d'erbium sur les performances d'amplification (chapitre 2)
3. Démonstration d'une nouvelle méthode de couplage latéral de la pompe dans la gaine ne nécessitant pas de fusion (chapitre 3)
4. Optimisation d'un design de fibre amplificatrice à coeurs multiples pompée par la gaine pour les réseaux reconfigurables utilisant une géométrie de distribution de l'erbium en

anneau (chapitres 4, 5 et 6)

5. Optimisation d'un design de fibre amplificatrice pompée par la gaine pour la bande L par l'utilisation de couches concentriques hétérogènes de dopants (chapitre 7)
6. Démonstration d'une méthode de recyclage de la puissance pompe résiduelle à la sortie de la fibre amplificatrice multicoeur en inscrivant un réseau de Bragg intra-gaine (chapitre 8)

Ensuite, le chapitre 9 viendra faire un retour sur les objectifs de la thèse ainsi que sur les applications abordées dans le cadre de celle-ci.

Enfin, les conclusions de la thèse s'ensuivront.

Analyse de l'impact du co-dopage à l'ytterbium sur les performances d'amplification des EDFAs dans la bande C

L'un des principaux désagréments des fibres à coeurs multiples pompées par la gaine est la faible intensité de pompe qui a pour effet de diminuer le taux d'absorption de la pompe par les ions d'erbium. Le fait d'augmenter significativement la puissance de la pompe utilisée pour compenser cet effet mène à une puissance de la pompe résiduelle importante à la sortie, diminuant ainsi l'efficacité de conversion de puissance.

Bien que le dopage d'ions d'erbium soit le plus utilisé en communication vu le gain plat qu'il permet d'obtenir sur toute la bande C [66], le co-dopage erbium-ytterbium, largement utilisé dans les lasers à fibre [67; 68], pourrait s'avérer intéressant pour les fibres à coeurs multiples pompées par la gaine vu la section efficace d'absorption de la pompe plus élevée qu'il permet d'atteindre [69; 70].

Malgré les avantages potentiels du co-dopage à l'erbium-ytterbium, celui-ci a aussi pour effet de modifier les sections efficaces d'absorption et d'émission de l'erbium dans la bande C, affectant ainsi l'uniformité spectrale du gain. Or, pour être considéré comme étant viable dans la bande C, ce type de dopage doit, pour une même puissance de la pompe, permettre d'atteindre un gain égal ou supérieur à celui obtenu avec le dopage à l'erbium seul pour des canaux situés dans cette région spectrale.

Ainsi, le chapitre 1 de la thèse examine le gain que permet d'atteindre le dopage à l'erbium dans la bande C et le compare à celui du co-dopage à l'erbium-ytterbium à l'aide de simulations et de mesures expérimentales effectuées sur deux fibres fabriquées spécifiquement à cette fin de comparaison.

Analyse de l'impact de la géométrie de distribution des ions d'erbium sur les performances d'amplification

Tel que discuté précédemment, il est souhaitable de maximiser la puissance de saturation des amplificateurs utilisés dans les réseaux reconfigurables afin de minimiser les variations de gain lorsque des canaux sont retirés ou ajoutés.

Or, l'insertion d'ions actifs dans le coeur de la fibre est la manière la plus simple de procéder en termes de fabrication et permet un recouvrement relativement élevé avec le ou les modes guidés. Cependant, lorsque la pompe est injectée par la gaine d'une fibre amplificatrice dopée d'ions actifs dans le coeur, on note une diminution significative de la puissance de saturation puisque l'intensité locale de la puissance de la pompe se voit diminuée considérablement sur la région active tandis que l'intensité de la puissance signal reste la même. Pour contrer cet effet, un anneau d'erbium situé à l'extérieur du coeur et à une distance suffisante peut être utilisé afin de permettre aux ions actifs d'interagir avec la région évanescente du mode transporté par le coeur, ayant une faible intensité, puisque c'est l'intensité locale de la puissance optique qui définit le niveau de saturation dans le signal [71; 72]. Vu le faible recouvrement obtenu dans une telle configuration, une longueur de fibre supérieure doit être utilisée.

Dans le chapitre 2 de la thèse, le dopage à l'erbium dans le coeur a été comparé au dopage en anneau ainsi qu'à un dopage qui recouvre à la fois le coeur et la gaine en périphérie du coeur, à l'aide de simulations et de mesures expérimentales, afin de comparer quantitativement les performances, en termes de gain et de compression du gain, de fibres amplificatrices utilisant ces géométries de distribution des ions actifs.

Démonstration d'une nouvelle méthode de couplage latéral de la pompe dans la gaine ne nécessitant pas de fusion

Plusieurs méthodes d'injection latérale de la pompe dans la gaine d'une fibre optique ont été démontrées par le passé. Or, dans le cas d'un amplificateur à fibre à coeurs multiples, il est préférable de ne pas chauffer la gaine de la fibre afin d'éviter toute déformation pouvant engendrer des pertes ou de la diaphonie entre les canaux [62; 63]. Cependant, les méthodes de couplage de pompe actuelles qui n'engendrent absolument aucune altération du signal ne permettent pas d'obtenir une efficacité de couplage supérieure à 70% [61].

Dans le chapitre 3 de la thèse, une nouvelle méthode de couplage latéral ne nécessitant pas de chauffer la fibre réceptrice est présentée. Suite à des résultats expérimentaux convaincants, une demande de brevet a été déposée.

Optimisation d'un design de fibre amplificatrice à coeurs multiples pompée par la gaine pour les réseaux reconfigurables utilisant une géométrie de distribution de l'erbium en anneau

Un processus d'optimisation d'un design de fibre à coeurs multiples visant à atteindre les spécifications techniques présentées au tableau I.1 est discuté aux chapitres 4 à 6. Afin de converger vers un design satisfaisant, trois fibres distinctes ont été fabriquées et caractérisées.

Vu les résultats obtenus aux chapitres 1 à 3, ces fibres utilisent un profil de distribution des ions actifs en anneau avec de l'erbium seul à titre de dopant actif.

Dans le chapitre 4, la première fibre à coeurs multiples utilisant une géométrie de distribution de l'erbium en anneau autour de chacun des coeurs est présentée. Les résultats de caractérisation permettent d'identifier deux problèmes majeurs à considérer dans les fibres utilisant une géométrie de distribution de l'erbium en anneau : l'agrégation des ions d'erbium et la présence d'ASE dans les modes de gaine.

Dans le chapitre 5, un nouveau design de coeur est validé en fabriquant une fibre à coeur unique ayant une géométrie de distribution des ions d'erbium en anneau et en la caractérisant expérimentalement. Ce design vise à corriger les problèmes identifiés lors de la caractérisation de la fibre présentée au chapitre 4 en ajoutant du phosphore dans l'anneau de dopant et en rapprochant légèrement l'anneau du coeur.

Dans le chapitre 6, une fibre à huit coeurs utilisant le design de coeur présenté au chapitre 5 est fabriquée et caractérisée. Pour la première fois, un fan-in/fan-out est utilisé afin d'injecter du signal dans tous les coeurs en parallèle et de mesurer les variations de gain entre les coeurs. Cette démonstration constitue l'aboutissement des travaux des chapitres précédents.

Optimisation d'un design de fibre amplificatrice pompée par la gaine pour la bande L par l'utilisation de couches concentriques hétérogènes de dopants

Bien que le dopage à l'erbium et le co-dopage à l'erbium-ytterbium aient été explorés à maintes reprises avec le pompage par la gaine, il n'existe, dans la littérature scientifique, aucun témoignage d'utilisation de couches de dopage à l'erbium seul en combinaison avec des couches d'erbium-ytterbium interagissant avec un seul et même mode. Or, en pompant la fibre à partir d'une longueur d'onde qui n'excite pas les ions d'erbium directement, mais qui excite les ions d'ytterbium, les anneaux d'erbium seuls peuvent agir à titre de filtre absorbant l'ASE, qui est principalement situé dans la bande C. Pour un amplificateur dans la bande L, la présence d'ASE dans la bande C utilise une partie de la pompe disponible, nuisant ainsi à l'efficacité de conversion de puissance.

Dans le chapitre 7, on cherche à déterminer, par des simulations numériques, si l'utilisation de couches concentriques hétérogènes de dopants dans les fibres amplificatrices pour la bande L

pompées par la gaine permet d'augmenter l'efficacité de conversion de puissance par rapport aux designs qui utilisent uniquement de l'erbium seul ou un co-dopage à l'erbium-ytterbium.

Démonstration d'une méthode de recyclage de la puissance pompe résiduelle à la sortie de la fibre amplificatrice multicoeur en inscrivant un réseau de Bragg intra-gaine

Vue la faible intensité locale de la pompe dans la région où se trouvent les ions de dopant actif, les fibres amplificatrices pompées par la gaine ont généralement une importante puissance pompe résiduelle à la sortie de la fibre afin de maintenir un niveau d'inversion des ions d'erbium suffisant, pour toute position longitudinale, afin d'amplifier le signal. Alors que la méthode turbo [73] a déjà été démontrée efficace pour les fibres amplificatrices multicoeurs, elle a le désavantage de nécessiter l'ajout de composants complexes et qui causent des pertes au signal, afin de récupérer et réinjecter la pompe.

Alternativement, il est possible d'inscrire un réseau de Bragg à l'intérieur de la gaine, près de la sortie de la fibre, afin de réfléchir la pompe pour qu'elle passe à nouveau à travers la fibre. Alors que cette méthode a déjà été démontré efficace pour les lasers à fibre [74], elle n'a encore jamais été investigué avec les fibres amplificatrices à coeurs multiples.

Dans le chapitre 8, on cherche donc à valider l'intérêt du recyclage de la pompe par inscription d'un réseau de Bragg intra-gaine pour les fibres amplificatrices multicoeurs utilisées dans les réseaux de communication.

Chapitre 1

Modeling and characterization of cladding-pumped erbium-ytterbium co-doped fibers for amplification in communication systems

C. Matte-Breton[1], R. Ryf[2], N. K. Fontaine[2], R.-J. Essiambre[2], H. Chen[2], C. Kelly[3], Y. Messaddeq[1] et S. LaRochelle[1]

[1]Dept. of Electrical and Computer Engineering, U. Laval, Québec, QC, G1K 7P4, Canada
[2]Nokia Bell Labs, Holmdel, NJ, 07733, USA
[3]Nokia Canada, Ottawa, ON, K2K 2T6, Canada

Publié dans IEEE Journal of Lightwave Technology, Vol. **38**, no. 7, p. 1936-1944 (2019).

1.1 Résumé

Les amplificateurs à fibre optique pompée par gaine suscitent un intérêt grandissant dans le contexte du multiplexage spatial, mais sont connus pour offrir un faible rendement énergétique. Dans ce contexte, le co-dopage à l'ytterbium (Yb) peut être une solution intéressante afin d'améliorer les performances des amplificateurs à fibre dopée à l'erbium (Er). Nous présentons une comparaison directe détaillée entre le codopage Er/Yb et le dopage Er à l'aide de simulations numériques validées par des résultats expérimentaux. Deux fibres à double gaine, l'une dopée à l'erbium seul et l'autre co-dopée à l'erbium et l'ytterbium, ont été conçues, fabriquées et caractérisées. À l'aide des paramètres extraits expérimentalement, nous simulons des amplificateurs à fibre multicoeur et étudions l'intérêt du codopage Er/Yb. Nous calculons

aussi le gain minimum des amplificateurs sur une fenêtre spectrale de 35 nm en considérant différents scénarios.

1.2 Abstract

Cladding-pumped optical fiber amplifiers are of increased interest in the context of space-division multiplexing but are known to suffer from low power efficiency. In this context, ytterbium (Yb) co-doping can be an attractive solution to improve the performance of erbium (Er) doped fiber amplifiers. We present a detailed direct comparison between Er/Yb-co-doping and Er-doping using numerical simulations validated by experimental results. Two double-cladding fibers, one doped with Er only and the other one co-doped with Er and Yb, were designed, fabricated and characterized. Using the experimentally extracted parameters, we simulate multi-core fiber amplifiers and investigate the interest of Er/Yb-co-doping. We calculate the minimum gain of the amplifiers over a 35-nm spectral window considering various scenarios.

1.3 Introduction

Space-division multiplexing (SDM) in optical communication systems is currently considered to overcome the capacity limit of optical fiber links [76; 77]. Deploying SDM will require novel sub-systems, such as optical amplifiers, that will meet stringent performance requirements over all spatial channels. At this time, cladding-pumped optical fiber amplifiers offer the best solution in terms of simplicity and ease of integration in SDM links. Furthermore, cladding-pumping can be advantageously used to lower mode-dependent gain when using mode-division multiplexing over few mode fibers. In multi-core transmissions, cladding pumping avoids spatial channel demultiplexing/multiplexing at the amplifier input and allows the use of low-cost high-power multi-mode pump lasers. Although many research groups have recently demonstrated cladding-pumped multi-core amplifiers [13; 55; 78; 12; 5; 8; 7], one drawback of this technology remains its low pumping efficiency. How pumping efficiency translates into power efficiency depends on the specific amplifier designs, for example the number of cores in the cladding-pumped amplifier. Similarly, a detailed comparison of the power consumption of multiple single core amplifiers to a multi-core cladding-pumped amplifier will depend on the specific pumping scheme of the single core amplifiers, for example pump sharing among the amplifiers could reduce power cooling requirements. Comparison of power efficiency of the single-core versus multi-core approach is discussed in [79; 80]. In this paper, we focus on the improvement of the pumping efficiency of multi-core cladding-pumped amplifiers.

The low pumping efficiency of the cladding pumping geometry results from a significant decrease in the overlap between pump power and the erbium doped cores. Such decrease in the overlap results in the need to either (i) use very long fiber lengths, leading to important cost efficiency reduction, (ii) increase erbium doping concentration, leading to more clustering, or

(iii) increase core density, leading to more crosstalk between the cores. Another possible solution is to use Er/Yb co-doping instead of only Er-doping in order to increase the absorption and pumping rates [69; 70]. However, an important drawback with Er/Yb co-doping is that the presence of phosphorus in the doped region is required to suppress the back-transfer of energy from erbium to ytterbium by decreasing the non-radiative decay time from the $^4I_{11/2}$ to the $^4I_{13/2}$ energy level [81; 82; 83; 84; 85; 86] and the presence of phosphorus and ytterbium in the glass matrix narrows the erbium absorption and emission cross-sections in the C-band (Fig. 1.6) [87; 88; 89; 90]. An attempt to broaden the cross-sections by varying the aluminum concentration led to negligible change on the cross-sections [88]. Another way to broaden the cross-sections is to use fluoride phosphate glasses [91]. The issue with this method is that fluoride glass is very fragile and hard to handle, making it challenging to use commercially. Because of the narrow cross-sections, different portions of the C-band and L-band are commonly used instead of the typical 1530-1565 nm C-band in order to obtain a flat gain and achieve efficient power consumption in EYDFAs [92; 93]. Indeed, despite the narrow cross-sections, wide band amplification can be achieved in EYDFAs by operating an amplifier in highly saturated conditions, leading to high gain toward the longer wavelengths, while the gain remains insufficient below 1535 nm. Using this principle, multiple MC-CP-EYDFAs have been demonstrated for wideband amplification [12; 5; 8; 7; 94].

In order to make Er/Yb-co-doped fiber amplifiers compatible with current communication networks, it is required to operate them with a flat gain over the entire C-band. By using a gain flattening filter (GFF) with up to 20 dB of depth, the amplifier gain can be flattened but at the expense of power efficiency. The gain after the GFF is limited by the channel with the minimum gain at the output of the doped fiber. The main issue with narrow cross-sections is therefore that the amplification of the channels with the highest gain will consume much of the pump power to generate high gain that will be thrown out by the GFF.

Since the minimum gain over the C-band is increased by a high pump absorption rate but decreased by the inefficient cross-sections shape, no "rule of thumb" exists to determine if and when Er/Yb-co-doping is advantageous compared to Er-doping. For a given pump power, this comparison might be done by determining the required fiber length for a given minimum gain or the minimum gain at the optimal fiber length.

In order to achieve a fair comparison between the two types of doping, ie. Er-doping vs Er/Yb-co-doping, numerical simulations must be executed with different scenarios. In this work, we consider a simple one-stage co-propagating pump amplifier. The residual pump power at the amplifier output is assumed to be discarded. The doped fiber parameters will be the same for the two Er/Yb-co-doped and Er-doped fiber designs except for the Yb ion concentration and the absorption/emission cross-sections that should differ according to the doping type. Our objective is to identify how to select the optimal doping for a C-band amplifier that maximizes the minimum gain at the optimal fiber length under given operating conditions

such as input power, pump power and number of cores conditions. To our knowledge, this is the first detailed direct comparison between Er/Yb-co-doping and Er-doping, using simulations validated with experimental results, that investigates the interest of Er/Yb-co-doping in CP-MC-FAs (cladding-pumped multicore fiber amplifiers) in terms of minimum gain over the 1530-1565 nm C-band. In section 1.4, we introduce the model of the Er-doped and Er/Yb-co-doped amplifiers. In section 1.5, a single-core erbium-ytterbium doped fiber (EYDF) and a single-core erbium doped fiber (EDF) are fabricated and characterized. Then, the gain and noise figure (NF) of the fibers are compared with simulation results to validate the model in section 1.6. Finally, with the experimentally extracted parameters, section 1.7 calculates the performances of cladding-pumped multicore erbium doped fiber amplifiers (CP-MC-EDFAs) and cladding-pumped multicore erbium-ytterbium doped fiber amplifiers (CP-MC-EYDFAs) in order to conclude on the interest of CP-MC-EYDFAs for communication systems.

1.4 Modeling of doped fiber amplifiers

The model is based on the standard set of power propagation and population rate equations of Er/Yb-co-doped fibers, as described in [82; 95; 96; 97], that neglects back-transfer and considers only the Er^{3+} $I_{15/2}$ and $I_{13/2}$ energy levels. This was proven to be a valid assumption in phosphate glass hosts and in silica-based fibers with small amounts of phosphorus in the doped region [81; 82; 83; 84; 85; 86]. Rather than using population average over the transverse cross-section, we introduce radial resolution of the rare-earth ion populations as described in [87; 13]. Since our aim is to design single-mode amplifiers, only the LP_{01} mode is considered in the simulations for the signal. The pump power is assumed to be uniformly distributed in the cladding that is D-shaped and has a diameter across the core of 125 µm (105 µm perpendicular to the flat portion). Consequently, there is no azimuthal dependence and we divide the fiber cross-section in K rings, each with uniform Er^{3+} concentration, and we calculate the inversion of each ring to calculate transition rates and gain. We also neglect background propagation loss. The propagation of the pump power, P_p, the signal, P_s, and the ASE, $P^{\pm}_{ASE}$, in the forward (+) and backward (-) direction are described by

$$\begin{cases} \frac{\mathrm{d}P_p(z)}{\mathrm{d}z} = -\left(\sigma_{abs,p,Er}\left(\sum_{k=1}^{K} n_{1,Er,k}(z)\Gamma_{p,k}\right) + \sigma_{abs,p,Yb}\left(\sum_{k=1}^{K} n_{1,Yb,k}(z)\Gamma_{p,k}\right)\right) P_p(z) \\ \frac{\mathrm{d}P_{s,\lambda}(z)}{\mathrm{d}z} = \left(\sigma_{ems,Er,\lambda}\sum_{k=1}^{K} n_{2,Er,k}(z)\Gamma_{\lambda,k} - \sigma_{abs,Er,\lambda}\sum_{k=1}^{K} n_{1,Er,k}(z)\Gamma_{\lambda,k}\right) P_{s,\lambda}(z) \\ \frac{\mathrm{d}P^{\pm}_{ASE,\lambda}(z)}{\mathrm{d}z} = \left(\sigma_{ems,Er,\lambda}\sum_{k=1}^{K} n_{2,Er,k}(z)\Gamma_{\lambda,k} - \sigma_{abs,Er,\lambda}\sum_{k=1}^{K} n_{1,Er,k}(z)\Gamma_{\lambda,k}\right) P^{\pm}_{ASE,\lambda}(z) \\ \qquad\qquad + \sigma_{ems,Er,\lambda}\left(\sum_{k=1}^{K} n_{2,Er,k}(z)\Gamma_{\lambda,k}\right) 2h\nu_\lambda\Delta\nu_\lambda \end{cases} \tag{1.1}$$

where λ stands for the wavelength channel of the signal or the amplified spontaneous emission (ASE), and k refers to the different rings with area A_k. Also, $\sigma_{abs,p,Er}$ and $\sigma_{abs,p,Yb}$ are the absorption cross-sections at 976 nm for Er^{3+} and Yb^{3+} respectively, $\sigma_{ems,Er,\lambda}$ and $\sigma_{abs,Er,\lambda}$ are the emission and absorption cross-sections at the signal or ASE wavelengths for Er^{3+}. The pump and signal (or ASE) overlaps with each ring are $\Gamma_{p,k}$ and $\Gamma_{\lambda,k}$ respectively. As usual, h is Planck constant, ν_p and ν_λ are the pump and signal (or ASE) frequency. The radially resolved population inversion along the fiber are given by

$$\begin{cases} n_{2,Er,k}(z) = \frac{W_{1,k}(z)+W_{2,k}(z)+A_k K_{tr} n_{2,Yb,k}(z)}{W_{1,k}(z)+W_{2,k}(z)+W_{3,k}(z)+A_k K_{tr} n_{2,Yb,k}(z)+\frac{A_k}{\tau_{Er}}} \rho_{Er,k}(z) \\ n_{2,Yb,k}(z) = \frac{W_{4,k}(z)}{W_{4,k}(z)+A_k K_{tr} n_{2,Yb,k}(z)+\frac{A_k}{\tau_{Yb}}} \rho_{Yb,k}(z) \\ \rho_{Er,k}(z) = n_{1,Er,k}(z) + n_{2,Er,k}(z) \\ \rho_{Yb,k}(z) = n_{1,Yb,k}(z) + n_{2,Yb,k}(z) \end{cases} \tag{1.2}$$

where the lower and upper level population densities of a given ring are $n_{1,Er,k}$ and $n_{2,Er,k}$ for Er^{3+} and $n_{1,Yb,k}$ and $n_{2,Yb,k}$ for Yb^{3+}, while $\rho_{Er,k}$ and $\rho_{Yb,k}$ are the Er^{3+} and Yb^{3+} concentrations of a given doped ring. The lifetime of the Er^{3+} and Yb^{3+} upper metastable levels are τ_{Er} and τ_{Yb}. It can be found in the literature that the lifetime of these upper metastable levels are generally around 10 ms and 1.5 ms for erbium and ytterbium [87]. These lifetimes will not be characterized and we will rather use values found in the literature for our simulations. Also, K_{tr} is the energy-transfer rate from ytterbium to erbium. Finally, the transition rates associated with pump absorption by erbium (W_1), signal and ASE absorption by erbium (W_2), signal and ASE stimulated emission by erbium (W_3) and pump absorption by ytterbium (W_4) are written as

$$\begin{cases} W_{1,k}(z) = \frac{\sigma_{abs,p,Er}\Gamma_{p,k}}{h\nu_p} P_p(z) \\ W_{2,k}(z) = \sum_{\lambda,s} \frac{\sigma_{abs,Er,\lambda}\Gamma_{\lambda,k}}{h\nu_\lambda} P_{s,\lambda}(z) + \sum_{\lambda,ASE} \frac{\sigma_{abs,Er,\lambda}\Gamma_{\lambda,k}}{h\nu_\lambda} P_{ASE,\lambda}(z) \\ W_{3,k}(z) = \sum_{\lambda,s} \frac{\sigma_{ems,Er,\lambda}\Gamma_{\lambda,k}}{h\nu_\lambda} P_{s,\lambda}(z) + \sum_{\lambda,ASE} \frac{\sigma_{ems,Er,\lambda}\Gamma_{\lambda,k}}{h\nu_\lambda} P_{ASE,\lambda}(z) \\ W_{4,k}(z) = \frac{\sigma_{abs,p,Yb}\Gamma_{p,k}}{h\nu_p} P_p(z) \end{cases} \tag{1.3}$$

For the simulations of the Er-doped fiber, $\rho_{Yb,k}$, K_{tr} and $\sigma_{abs,p,Yb}$ is set to 0, whereas for the simulation of the Er/Yb-co-doped fiber the absorption of the Er^{3+} is considered negligible compared to the absorption of ytterbium and $\sigma_{abs,p,Er}$ is thus set to 0.

1.5 Fabrication and parameter characterization of an EYDF and an EDF

An EYDF (fiber A) and an EDF (fiber B) were fabricated using the solution doping method [98] with Al_2O_3, P_2O_5, Er_2O_3 and Yb_2O_3 in the case of fiber A ; and Al_2O_3 with Er_2O_3 in the case of fiber B (Fig. 1.1). The fibers were designed to have the same refractive index profile and the same erbium concentration profile. In the EYDF, the target Yb^{3+} concentration in ions/m^3 was 10 times higher than the Er^{3+} concentration, and the phosphorus concentration was 100 times higher than the Er^{3+} concentration. The Al_2O_3 concentration was used to control the refractive index profile. The preforms were polished in order to obtain D shaped fibers to break the symmetry of the pump modes guided by the cladding and the silica cladding was surrounded by a low refractive index polymer (n=1.37). For both fibers, the silica cladding diameter was 125 µm (105 µm when measured perpendicular to the flat section).

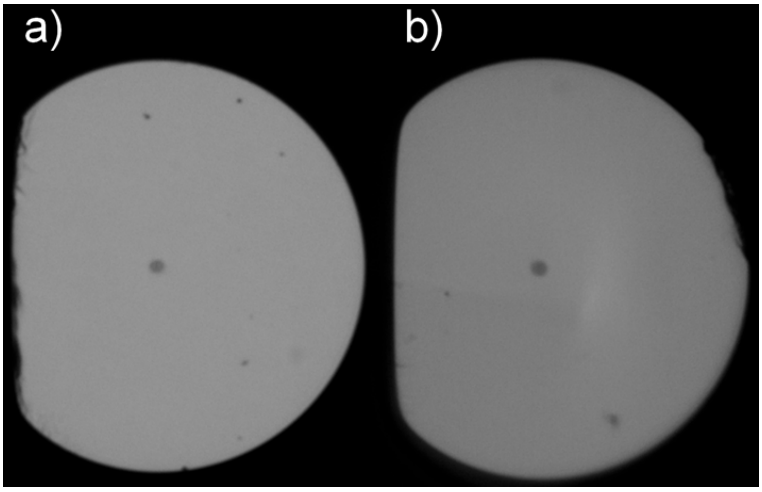

FIGURE 1.1 – Microscope image of a) fiber A and b) fiber B.

The core refractive index profile was measured on the preforms with a NR-9200HR refracted near-field analyzer (EXFO) at 657.6 nm. To apply the measurement results to the C-band, we neglect the dispersion of the refractive index difference between the core and the glass cladding, Δn. Also, we scale the radial position using the diameter ratio of the fabricated fiber and the preform. The resulting refractive index profiles of fiber A and B are shown in Fig. 1.2. The dip at the center of the core in fiber A is caused by evaporation during the MCVD process. The higher evaporation could be caused by the presence of Yb_2O_3 and P_2O_5 in the glass matrix.

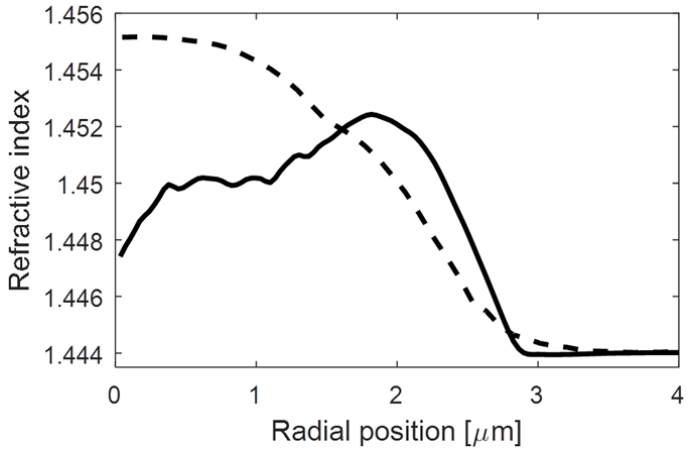

FIGURE 1.2 – Refractive index profile of fiber A (solid) and fiber B (dashed).

With the measured refractive index profiles, we used COMSOL to calculate the LP_{01} mode overlap with 30 rings of 0.1 µm thickness located in the 0-3 µm radial position of the fiber. The calculations were executed for wavelengths between 1420 nm and 1620 nm for fiber A and fiber B and are shown in Fig. 1.3. The pump overlap in each ring was calculated by considering a uniform pump power distribution over the fiber. Considering that both fibers have the same D-shape with a cladding area of 1.003×10^{-8} m^2, the pump overlap with each ring is the same for both fibers and is directly proportional to the area of the ring, i.e., to a first approximation, proportional to the radius of the ring.

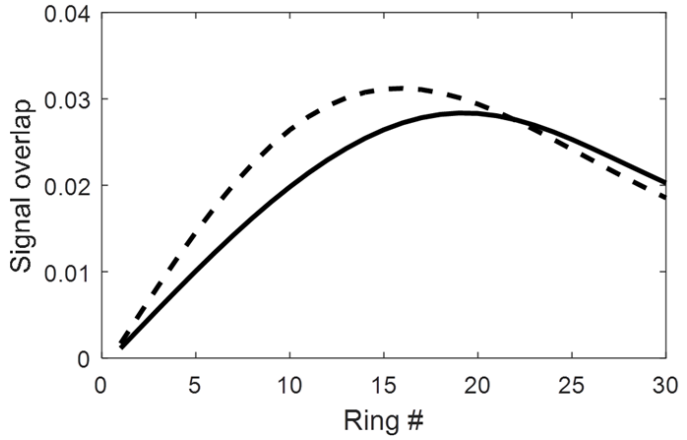

FIGURE 1.3 – Signal overlap with each ring in fiber A (solid) and fiber B (dashed) at 1550 nm.

The doping concentrations of Er^{3+}, Yb^{3+} and P_2O_5 were measured on the preform at different radial positions using an electron micro probe analyzer. As before, the radial position was scaled using the diameter ratio of the fabricated fiber and the preform and the erbium and ytterbium measured concentrations are shown in Fig. 1.4. While not used in the simulations, note that the phosphorus concentration was, on average, 1.2×10^{27} m^{-3} in the core region of

fiber A.

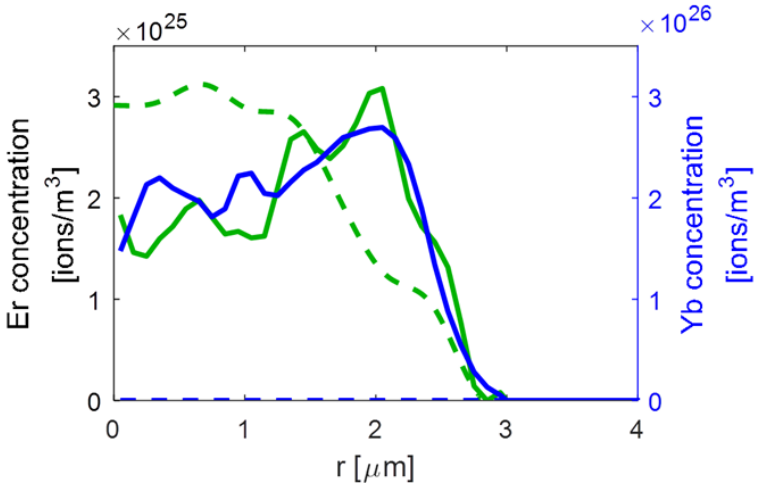

FIGURE 1.4 – Erbium (green) and ytterbium (blue) concentration profile of fiber A (solid) and fiber B (dashed).

Using a supercontinuum laser source with an average of approximately -35 dBm/nm output power over the 1420 nm – 1620 nm region, we injected the light in the core of the EYDF (fiber A) and EDF (fiber B) by splicing the output fiber of the supercontinuum at the input of the fiber under test (FUT) and measuring the output power of the FUT as a function of wavelength on an optical spectrum analyzer (OSA, 1 nm resolution). Then, the difference between the input and output power was calculated and divided by the fiber length used. Fiber lengths of 80 cm for fiber A and 70 cm for fiber B were used. The resulting absorption curves, as a function of wavelength, are shown in Fig. 1.5.

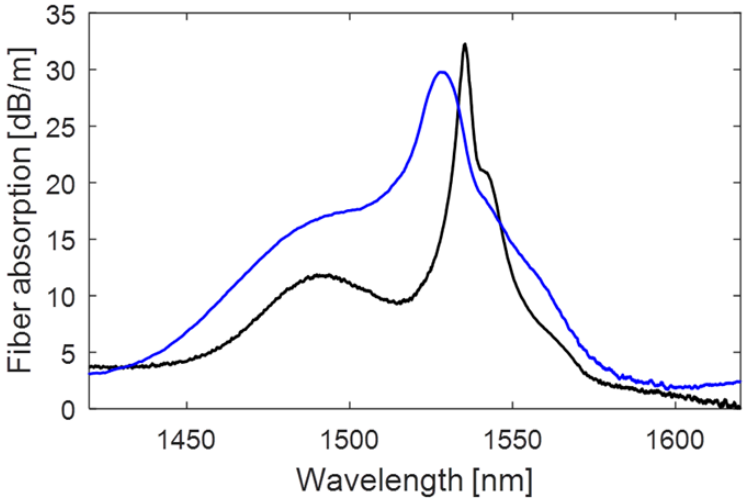

FIGURE 1.5 – Absorption as a function of wavelength from 1420 nm to 1620 nm for fiber A (black) and fiber B (blue).

Knowing the LP_{01} overlap and the Er^{3+} concentration profile of each ring in fibers A and B, the absorption and emission cross-sections were calculated with the McCumber relation, see [99] for example, written as

$$\sigma_{abs}(\nu)[m^2] = \frac{\alpha[dB/m]}{(10\log_{10} e)\sum_k \rho_k[ions/m^3]\Gamma_k} \tag{1.4}$$

$$\sigma_{ems}(\nu) \;=\; \sigma_{abs}(\nu)\cdot e^{(\epsilon - h\nu)/k_B T} \tag{1.5}$$

$$\epsilon = \frac{hc}{\lambda_\epsilon} \tag{1.6}$$

In Eq. 1.4 to 1.6, σ_{abs} is the absorption cross-section, α is the measured absorption, ρ_k is the doping concentration in the ring k, Γ_k is the power confinement in the ring k, σ_{ems} is the emission cross-section, ν is the optical frequency, c is the speed of light, ϵ is the mean transition energy between two manifolds, T is the equilibrium temperature and k_B is the Boltzmann constant. The mean wavelength at which the transition occurs, λ_ϵ, is generally close to the peak absorption value. We set λ_ϵ to 1535 nm for fiber A and 1532 nm for fiber B in order to obtain cross-sections in agreement with the literature [85],[89],[90]. The resulting cross-sections are shown in Fig. 1.6.

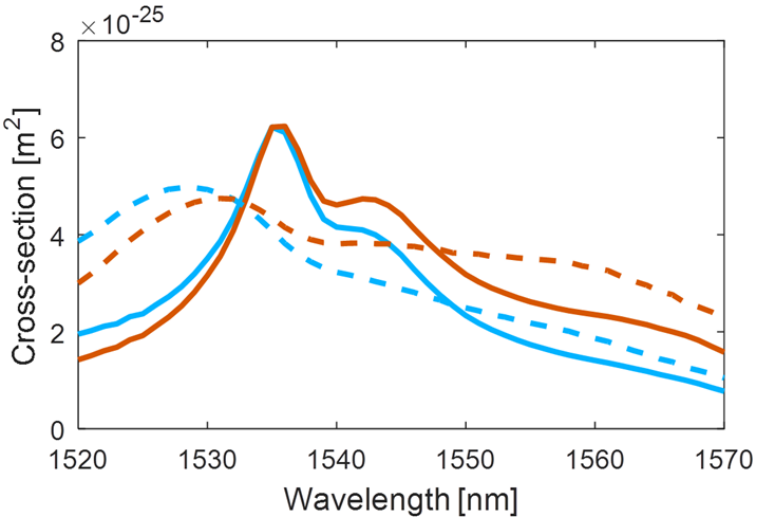

FIGURE 1.6 – Absorption (cyan) and emission (orange) cross-sections as a function of wavelength from 1520 nm to 1570 nm for fiber A (solid lines) and fiber B (dashed lines).

In order to measure the absorption cross-section near 976 nm, we injected the light of a supercontinuum laser source with an average of approximately -42 dBm/nm output power over the 880 nm – 1000 nm region in the cladding of fiber A and a supercontinuum laser source with an average of -36 dBm/nm output power over the 800 nm – 1300 nm region in the cladding of fiber B and measured the output power with an OSA (1 nm resolution). We used 15 m of fiber A and 183 m of fiber B. Absorption was estimated as the loss difference with respect to the measurement at 880 nm in order to substract background loss and the result is shown in Fig. 1.7. Since the pump source that will be used for the gain measurements is centered at 976 nm, we compute the absorption average from 974 nm to 978 nm of both fibers and obtained 0.785 dB/m for fiber A and 0.0394 dB/m for fiber B. Using the measured Yb^{3+} (for fiber A) and the Er^{3+} (for fiber B) concentration in each ring, we calculated the respective absorption cross-sections near 976 nm were calculated and found $\sigma_{abs,p,Yb} = 3.86\times10^{-25}$ m^2 for fiber A and $\sigma_{abs,p,Er} = 2.25\times10^{-25}$ m^2 for fiber B. For fiber B, the absorption peak at 943 nm is caused by the absorption from OH^- impurities over the 183 m of fiber used. Although it cannot be distinguished properly because of the scale of the y axis, the same peak is observed on the absorption curve of fiber A. The transfer rate from Yb^{3+} to Er^{3+} upper metastable levels K_{tr} in fiber A could not be characterized and will be determined by fitting the gain measurements of the EYDF in the section 1.6.

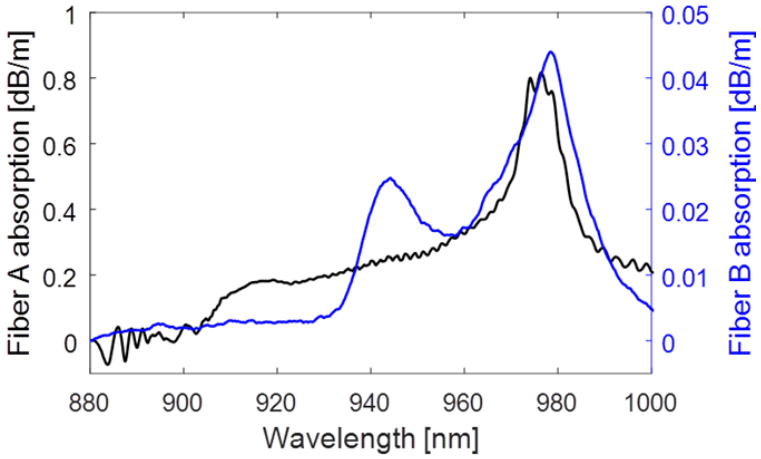

FIGURE 1.7 – Absorption in the cladding as a function of wavelength from 880 nm to 1000 nm for fiber A (black) and fiber B (blue).

The signal background loss was measured at 1700 nm by injecting the light of a supercontinuum laser source with an average of approximately -40 dBm/nm output power in the core of the fiber under test and measured the output power with an OSA (1 nm resolution). We used 100 m of fiber A and 172 m of fiber B and measured a signal background loss of 0.099 dB/m for fiber A and 0.039 dB/m for fiber B. The pump background loss was measured at 880 nm with a supercontinuum laser source with an average of -36 dBm/nm output power over the 800 nm – 1300 nm region and a fiber length of 113 m for fiber A and 183 m for fiber B.

1.6 Gain and NF : model validation

In this section, we perform experimental characterization of the two single core cladding-pumped doped fibers : fiber A (EYDF) and fiber B (EDF). The experimental results served to validate the model and the fiber parameters that will be used to compare MC-CP-EYDFAs with MC-CP-EDFAs through numerical simulations in section 1.7 and section 1.8. We spliced 3.36 m of fiber A and 3.50 m of fiber B to standard single-mode fiber (SMF) pigtails at both ends. We measured a 2.1 dB total loss for the two splices and connectors using a tunable laser set at 1640 nm and -5 dBm. In the calculation of the internal gain and NF, we assume that 1.05 dB loss occurs before the doped fibers and 1.05 dB after. Right after the first splice, the DFUT (doped fiber under test) was stripped over 20 cm. Then, a coreless fiber, spliced on the output fiber of the pump laser diode, is tapered and rolled around the DFUT in order to achieve side-coupling of the pump power in the cladding of the DFUT. Starting about 1 cm from the output splice, a glass etching cream (Armour Etch #15-0150) is applied over four cm in order to make the surface of the fiber irregular which removes the pump through surface scattering. Overall, approximately 10 cm of the DFUT is not pumped significantly, a few centimeters before the pump coupling and a few centimeters after the pump dump. Thus, for the simulations, we consider 3.26 m of fiber length for fiber A and 3.40 m for fiber B.

FIGURE 1.8 – Setup used to measure the gain and NF of fiber A and B.

The setup used for the gain and NF measurements is shown in Fig. 1.8. The 14 channels are distributed uniformly from 1531.2 nm to 1562.2 nm with 300 GHz spacing. The total signal input power is set to -15 dBm (-26.46 dBm/ch), -5 dBm (-16.46 dBm/ch) and 5 dBm (-6.46 dBm/ch). The output power of the pump laser diode is set to 3 W, 5 W and 7 W. The pump power coupling efficiency is measured after the gain and NF measurements are completed by cutting the fiber 40 cm after the input splice to measure the 976 nm power when the pump is set to 5 W. We measured 2.35 W for fiber A and 2.40 W for fiber B, which leads to pump power coupling efficiencies of 47% and 48%. These coupling efficiency values are used for the simulations. Also, for the simulations, the C-band is loaded with 32 channels uniformly distributed between 1531 nm and 1562 nm with 1 nm spacing. As in the experiments, the total signal input power is set to -15 dBm, -5 dBm and 5 dBm. The transition rate from ytterbium to erbium (K_{tr}) was set to $1.0\text{x}10^{-22}$ m^3/s. This value was determined by minimizing the error between gain measurements and simulations with coupled pump power of 3.29 W and input signal power of 5 dBm for fiber A. This value compares well to the literature

[87]. All of the fibers parameters are summarized in Table 1.1.

Tableau 1.1 – Fibers parameters

Parameter	Value		Unit
	Fiber A	Fiber B	
L	3.36	3.50	m
N_{cores}	1	1	-
$\Gamma_{\lambda,k}$	Fig. 1.3	Fig. 1.3	-
$\Gamma_{p,k}$	A_k/A_{clad}		-
$\rho_{Er,k}$	Fig. 1.4	Fig. 1.4	ions/m^3
$\rho_{Yb,k}$	Fig. 1.4	-	ions/m^3
$\sigma_{abs,\lambda}$	Fig. 1.6	Fig. 1.6	m^2
$\sigma_{ems,\lambda}$	Fig. 1.6	Fig. 1.6	m^2
$\sigma_{abs,p,Er}$	-	2.25x10^{-25}	m^2
$\sigma_{abs,p,Yb}$	3.86x10^{-25}	-	m^2
τ_{Er}	10	10	ms
τ_{Yb}	1.5	-	ms
K_{tr}	1x10^{-22}	-	m^3/s

Fig. 1.9 and Fig. 1.10 compare simulations and measurements of gain and NF for fiber A and B respectively. For both the gain and NF measurements, the insertion loss of the components and splices are considered in order to determine the internal gain and the internal NF, which is what is directly obtained with the simulations. A good agreement is observed between measurements and simulations with a maximum gain difference of <2.4 dB for fiber A and <2.7 dB for fiber B, and a maximum NF difference of <2 dB for fibers A and B. When using cladding pumping, because of the small core sizes, the pump overlap with the cores is low and leads to poor gains for both fibers. In the next section, we will use these values to design MC-CP-EYDFA and the core sizes will be adjusted accordingly.

1.7 Interest of MC-CP-EYDFA for communications

In order to investigate the interest of MC-CP-EYDFAs for communications, we use the same model but with seven cores sharing the available pump instead of one. The signal in each core consists of 31 channels, from 1530 nm to 1560 nm. Some of the characterization results obtained in section 1.6 are used for the simulation based comparison of MC-CP-EYDFAs with MC-CP-EDFAs. More specifically, the absorption and emission cross-sections, the lifetime of Er^{3+} and Yb^{3+} upper metastable levels, and the energy-transfer rate from ytterbium to erbium (K_{tr}) of the CP-MC-EYDFAs and the CP-MC-EDFAs are the same as fiber A and fiber B respectively. For these simulations, we assume ideal refractive index and doping profiles. The fiber cores are 6 µm diameter step-index cores with $\Delta n = 0.013$. The Er^{3+} concentration is uniform over the core region and set to 2x10^{25} ions/m^3. The Yb^{3+} concentration is set to 2x10^{26} ions/m^3 in the cores of the CP-MC-EYDFAs and to 0 ions/m^3 for CP-MC-EDFAs.

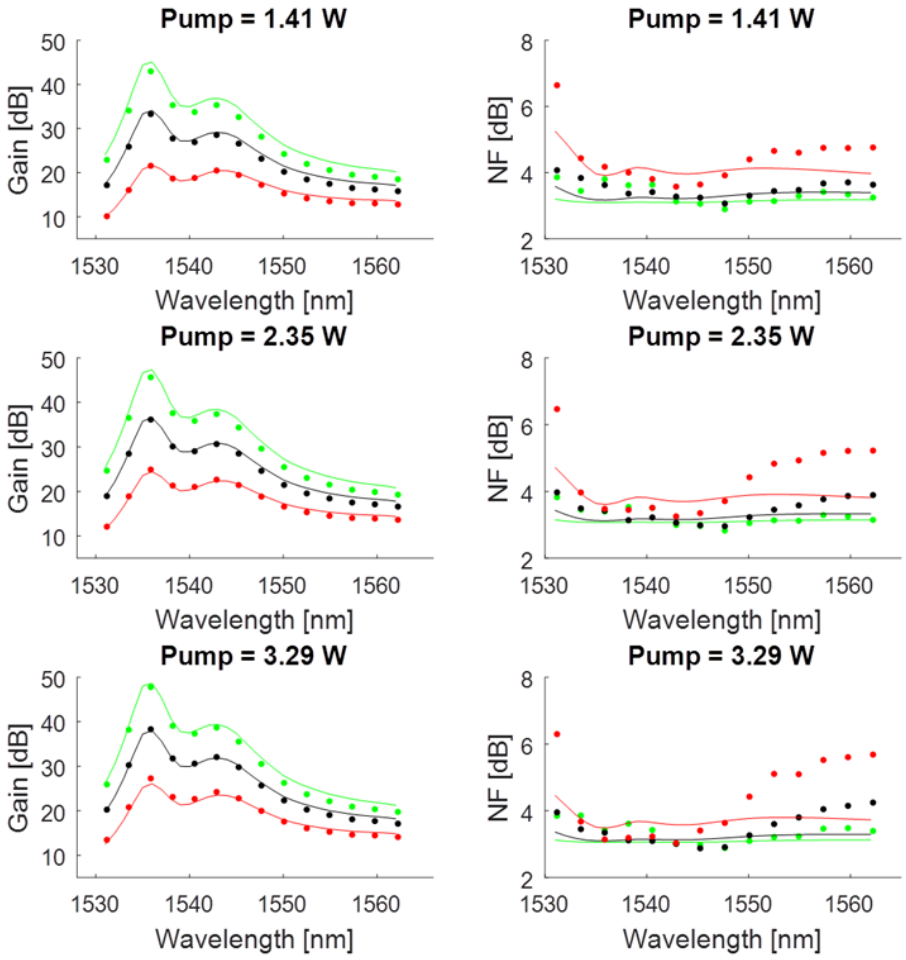

FIGURE 1.9 – Measured (markers) and simulated (solid lines) gain (left) and NF (right) of fiber A for input power of -15 dBm (green), -5 dBm (black) and 5 dBm (red) with coupled pump power of 1.41 W (top), 2.35 W (center) and 3.29 W (bottom).

In order to investigate if Er/Yb-co-doping can lead to a higher minimum gain over 1530 nm to 1560 nm region, we plot the minimum gain as a function of fiber length for different operating conditions of CP-MC-EYDFAs and CP-MC-EDFAs. The results are shown in Fig. 1.11 for different pump input power and different signal input power. From these results, we see that CP-MC-EYDFA will lead to higher minimum gain, compared to CP-MC-EDFA, when there is a higher signal power or a lower pump power, which are the conditions that lead to saturation of CP-MC-EDFA. On Fig. 1.12, the maximum NF over the 1530 nm to 1560 nm region is shown for the same scenarios as Fig. 1.11. For all the scenarios where Er/Yb-codoping allows to reach a higher minimum gain compared to Er-doping, Er/Yb-codoping also allows to keep the NF lower. It thus seems that the use of CP-MC-EYDFAs could be of interest when the available pump power is limited, for example in subsea networks. Although the minimum gain can be very similar, gain variations across the C-band can be very different. For example, for the -5 dBm input signal power and 8 W input pump power scenario, the minimum gain

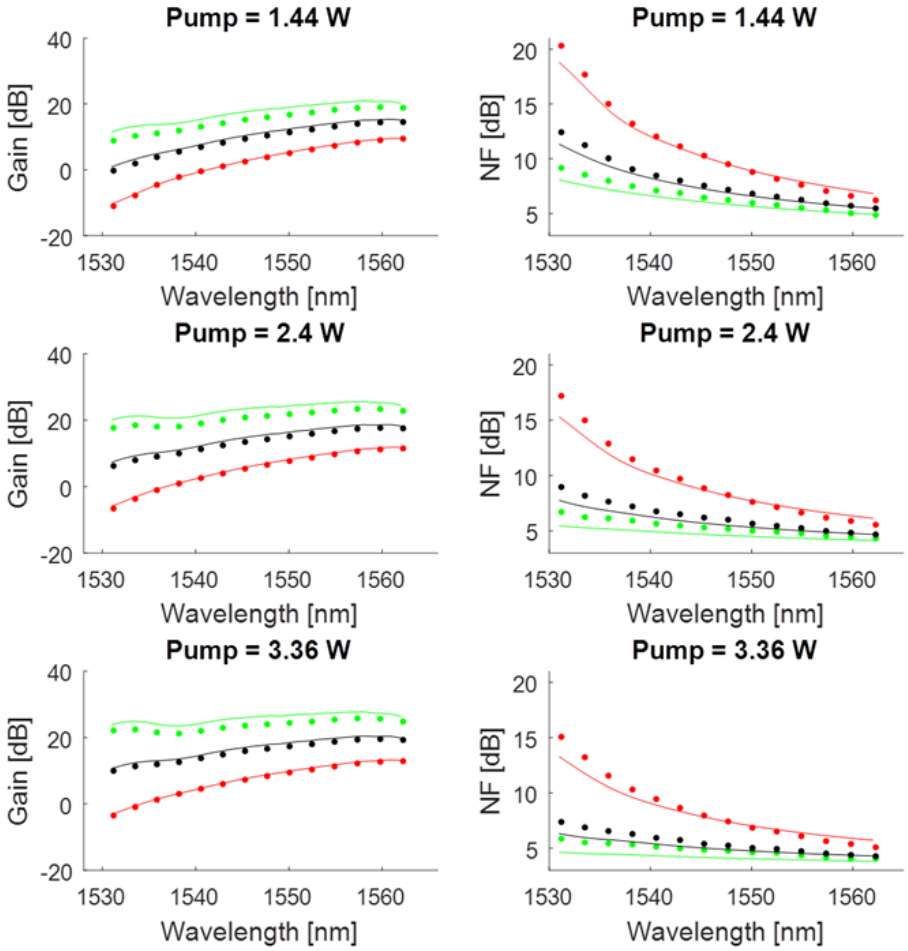

FIGURE 1.10 – Measured (markers) and simulated (solid lines) gain (left) and NF (right) of fiber B for input power of -15 dBm (green), -5 dBm (black) and 5 dBm (red) with coupled pump power of 1.44 W (top), 2.40 W (center) and 3.36 W (bottom).

over the 1530-1560 nm region is almost the same for both fibers (16.6 dB vs 17.3 dB for the CP-MC-EYDFA and the CP-MC-EDFA respectively) and occurs at approximately the same fiber length (1.8 m and 1.9 m for the for the CP-MC-EYDFA and the CP-MC-EDFA). Under these conditions, the average upper state population over the total length of the fiber is 71.6% for the CP-MC-EYDFA and 63.8% for the CP-MC-EDFA. The spectral gain variations in the CP-MC-EYDFA are therefore much larger, as shown in Fig. 1.13, and would require a GFF with >15 dB of depth. However, the maximum NF over this spectral window for fiber A is only 3.4 dB compared to 4.5 dB for fiber B.

1.8 Optimal wavelength range for MC-CP-EYDFAs

In this section, we investigate what is optimum transmissions 30-nm window of CP-MC-EYDFA vs CP-MC-EDFA. We first perform simulations of CP-MC-EYDFA using the same

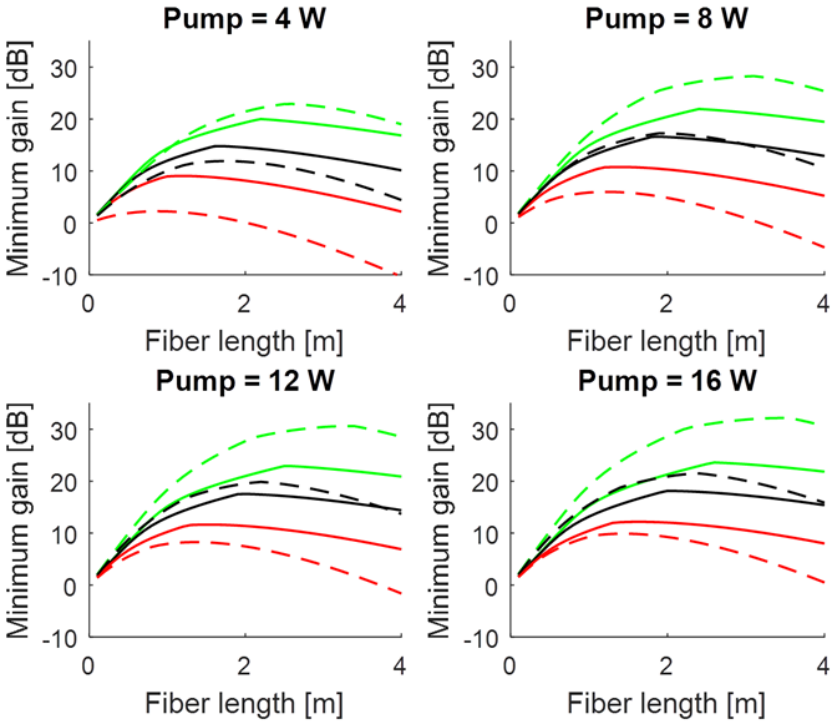

FIGURE 1.11 – Simulated gain of a CP-MC-EYDFA (solid) and a CP-MC-EDFA (dashed) for input signal power of -15 dBm (green), -5 dBm (black) and 5 dBm (red) with coupled pump power of a) 4 W, b) 8 W, c) 12 W and d) 16 W and 7 cores sharing the pump.

fiber parameters as in section 1.7. For each spectral region, two scenarios are considered : a) 8 W input pump power and -5 dBm input signal power, and b) 16 W input pump power and -5 dBm input signal power. For both scenarios, the minimum gain over the spectral region is plotted as a function of fiber length in Fig. 1.14. The results shown in this section are the internal gain and the internal NF. In order to determine the total amplifier gain and NF for a given application, the loss of isolators, splices and other sources of loss should also be considered.

The results indicate that the optimal 30-nm wide wavelength range for CP-MC-EYDFA is 1536 nm – 1566 nm. However, it is worth noticing that the 1535 nm – 1565 nm wavelength range gives a very similar result while being inside the C-band. When compared to the CP-MC-EDFA results shown on Fig. 1.11, the Er/Yb-co-doping results lead to better gain and pump efficiency. Due to the lower emission cross-section at the higher wavelengths, a longer fiber is also required. Note that for 8 W input pump power, the optimal length for the EYDFA is 6.1 m and the minimum gain is 26.2 dB.

At the optimal fiber length, the maximum NF calculated over the wavelength range of the various scenarios shown on Fig. 1.14 was $<$3.5 dB for a pump power of 8 W and $<$3.4 dB for a pump power of 16 W (with variations less than 0.1 dB among the tested wavelength ranges).

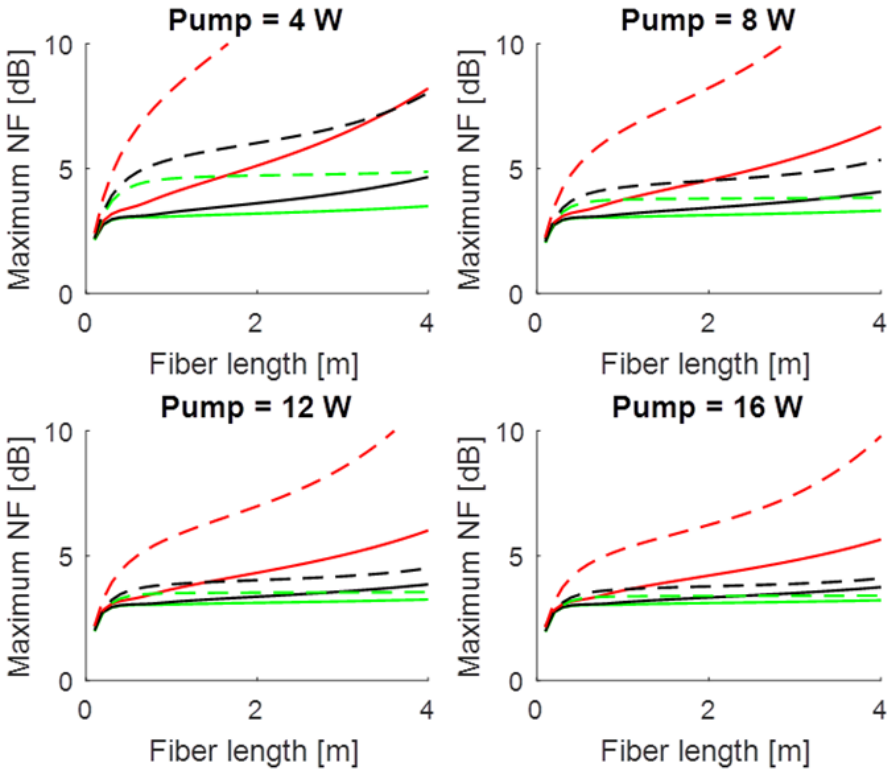

FIGURE 1.12 – Simulated NF of a CP-MC-EYDFA (solid) and a CP-MC-EDFA (dashed) for input signal power of -15 dBm (green), -5 dBm (black) and 5 dBm (red) with coupled pump power of a) 4 W, b) 8 W, c) 12 W and d) 16 W and 7 cores sharing the pump.

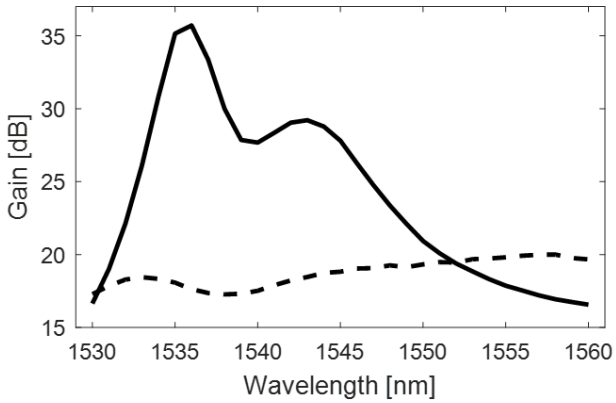

FIGURE 1.13 – Simulated gain of a seven-core CP-MC-EYDFA (solid) and a CP-MC-EDFA (dashed) for input signal power of -5 dBm, input pump power of 8 W.

The only noticeable increase in NF occurred when the fiber length was much longer than the optimal length.

If we repeat the same experiment for MC-CP-EDFAs, we find an optimal wavelength range

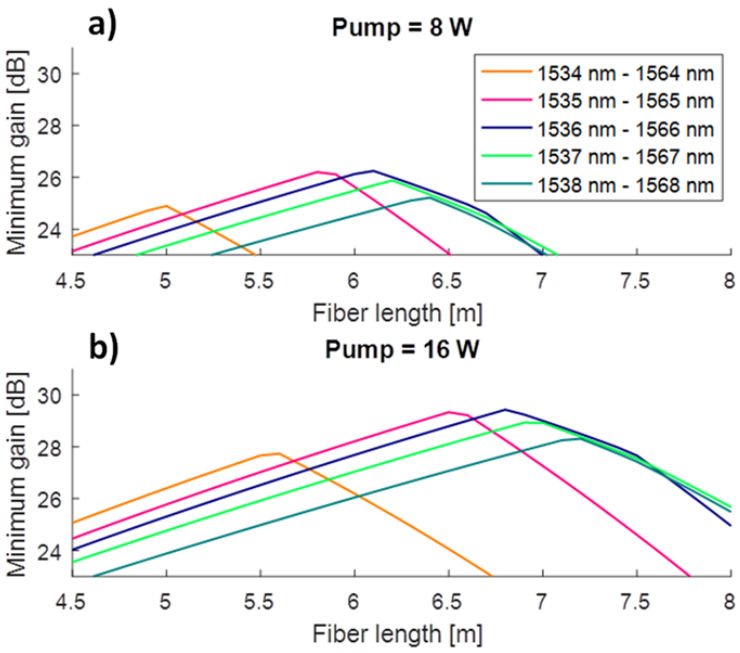

FIGURE 1.14 – Simulated minimum gain of a CP-MC-EYDFA for different 30-nm spectral windows with input signal power of -5 dBm and input pump power of a) 8 W, b) 16 W.

of 1531– 1561 nm, and an optimal minimum gain of 17.6 dB for 2.2 m of fiber length, 8 W of input pump power and -5 dBm of input signal power. The gain curve of the MC-CP-EYDFA and MC-CP-EDFA at their optimal fiber length over their optimal 30-nm wide spectral region is shown on Fig. 1.15.

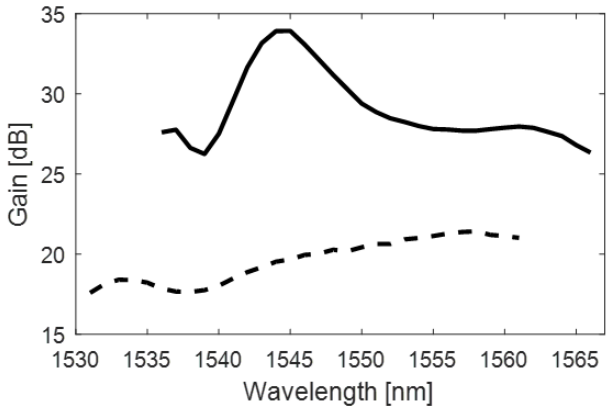

FIGURE 1.15 – Simulated gain of a CP-MC-EYDFA (solid) and a CP-MC-EDFA (dashed) for input signal power of -5 dBm, input pump power of 8 W, and 7 cores. The results were obtained with fiber lengths of 6.1 m for the CP-MC-EYDFA and 2.2 m for the CP-MC-EDFA over the respective 30-nm spectral windows from 1536 – 1566 nm and 1531 – 1561 nm.

Similarly, we found that when a 35-nm transmission window is desired, the optimal wavelength

range is 1535 – 1570 nm for EYDFAs and 1532 – 1567 nm for EDFAs. The calculated gain spectra at 8 W with the optimal fiber lengths are shown in Fig. 1.16 and the resulting minimum gain is 23.1 dB for the EYDFA and 17.7 dB for the EDFA.

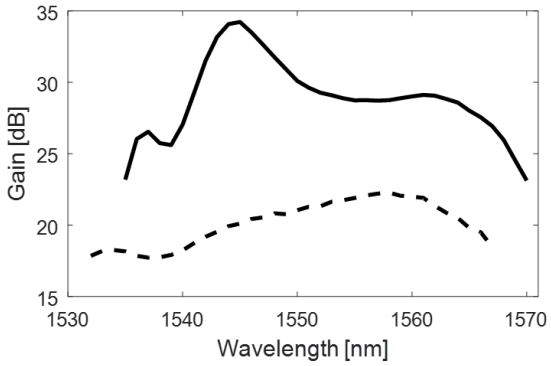

FIGURE 1.16 – Simulated gain of a CP-MC-EYDFA (solid) and a CP-MC-EDFA (dashed) for input signal power of -5 dBm, input pump power of 8 W, and 7 cores. The results were obtained with fiber lengths of 6.6 m for the CP-MC-EYDFA and 2.4 m for the CP-MC-EDFA over the respective 35-nm spectral windows from 1535 – 1570 nm and 1532 – 1567 nm.

The results shown in Fig. 15 and 16 indicate that, when it is possible to select the spectral region, CP-MC-EYDFAs offer a higher minimum gain compared to CP-MC-EDFAs since they use the pump more efficiently. However, the results also indicate that a deeper GFF is required.

1.9 Conclusion

Through numerical simulations with parameters validated by experimental results with a single-core fiber, we investigated the benefits of using Er/Yb co-doping for a multi-core amplifier in order to achieve a higher minimum gain than with erbium ion doping only. All the simulations parameters are in agreement with typical values found in the literature. We first compared cladding-pumped Er and Er/Yb doped amplifiers and found that Er/Yb co-doping could only be beneficial over the 1530-1560 nm spectral region in the specific case of a highly saturated amplifier, for example for low input pump power or high input signal power. Under these conditions Er/Yb co-doping can be advantageous because of its efficient absorption rate that leads to high population inversion levels even when available pump power is low. However, when the remaining output pump is reused [100], the benefits of Er/Yb co-doping might not be advantageous compared to Er-only doping since only a small fraction of pump light reaches the output of the fiber. Also, one of the drawbacks of using Er/Yb co-doping is the need for a deep GFF. However, when the 30-nm spectral window can be shifted to slight longer wavelengths, for example 1535 nm to 1565 nm, we also demonstrate that MC-CP-EYDFAs can reach much higher minimum gain than MC-CP-EDFAs. The results thus demonstrate that, although Er/Yb co-doping does not provide increased performance of MC-CP amplifiers in all

scenarios, there can be important benefits of using co-doping in specific scenarios.

1.10 Acknowledgment

We would like to acknowledge the help of Mr N. Grégoire and Mr. Steeve Morency for the fiber fabrication and characterization.

Chapitre 2

Demonstration of an erbium-doped fiber with annular doping for low gain compression in cladding-pumped amplifiers

C. Matte-Breton[1], H. Chen[2], N. K. Fontaine[2], R. Ryf[2], R.-J. Essiambre[2], C. Kelly[3], C. Jin[1,4], Y. Messaddeq[1] et S. LaRochelle[1]

[1]Centre for Optics, Photonics and Lasers (COPL), U. Laval, Québec, QC, G1V 0A6, Canada
[2]Nokia Bell Labs, 791 Holmdel-Keyport Rd, Holmdel, NJ 07733, USA
[3]Nokia Canada, 600 March Rd, Ottawa, ON, K2K 2T6, Canada
[4]now with OFS, 19 Schoolhouse Rd, Somerset, NJ, 08873, USA

Publié dans Optics Express, Vol. **26**, no. 20, 26633-26645 (2018). [101]

2.1 Résumé

Nous présentons la conception et la caractérisation d'un amplificateur pompé par la gaine ayant un dopage à l'erbium situé dans une région annulaire en périphérie du coeur. Cette géométrie de dopant vise à réduire la saturation du gain, conduisant ainsi à une compression de gain plus faible par rapport à un dopage uniforme dans le coeur. À partir de simulations numériques, nous comparons dans un premier temps les performances de trois fibres avec différents profils de dopant à l'erbium. Lorsque les fibres dopées sont opérées avec une longueur

de fibre optimale, les résultats montrent qu'une plus faible intensité de signal qui chevauche la région dopée à l'erbium permet d'obtenir un gain plus élevé et une saturation plus faible de l'amplificateur. Une fibre à coeur simple dopée à l'erbium avec un profil de dopant annulaire et une gaine en forme de D a été fabriquée. Les mesures expérimentales démontrent moins de 4 dB de compression du gain sur la bande C pour une puissance d'entrée allant de -40 dBm à 3 dBm. Les fibres amplificatrices ayant une faible compression du gain représentent une avenue intéressante pour les applications qui nécessitent de reconfigurer le nombre de canaux à l'entrée des amplificateurs. Un gain et une puissance de saturation plus élevés sont également des enjeux clés pour les fibres amplificatrices à coeurs multiples pompées par la gaine.

2.2 Abstract

We present the design and characterization of a cladding-pumped amplifier with erbium doping located in an annular region near the core. This erbium-doped fiber is proposed to reduce gain saturation, leading to smaller gain compression when compared to uniform core doping. Through numerical simulations, we first compare the performance of three fibers with different erbium doping profiles in the core or the cladding. When the doped fibers are operated at the optimum length, results show that the smaller overlap of the signal mode field with the annular erbium doping region leads to higher gain and lower saturation of the amplifier. A single-core erbium-doped fiber with an annular doping and a D-shaped cladding was fabricated. Measurements demonstrate less than 4 dB of gain compression over the C-band for input power ranging from -40 dBm to 3 dBm. Small gain compression EDFAs are of interest for applications that require input channel reconfiguration. Higher gain and saturation output power are also key issues in cladding-pumped multi-core amplifiers.

2.3 Introduction

Fueled by cloud-based applications, video streaming and supercomputing, data traffic carried by communication networks has grown considerably in the last few decades. Optical fibers are deployed worldwide to form the backbone of high capacity networks that must deliver an ever increasing bandwidth with reduced cost and complexity. In this context, space-division multiplexing (SDM) is currently being investigated as a possible means to scale optical fiber capacity beyond the fundamental limit of single-mode single-core optical fibers [77; 76; 102; 103]. Recent demonstrations of transmissions over few-mode multi-core fibers show that the number of channels could be increased by two orders of magnitude, allowing in excess of 10 Pb/s transmission per optical fiber link [104; 105]. A key technology to the deployment of SDM links is a compatible in-line optical fiber amplifier [61; 106], which should ideally avoid the demultiplexing of spatial channels often done before amplification in laboratory experiments of SDM transmission. A spatially integrated optical amplifier sharing the same

pump is also of interest for applications requiring a compact solution for switching and routing [107].

Although initial work on multi-core erbium-doped fiber amplifiers (MC-EDFAs) used in-core pumping, there is a growing interest in cladding-pumped MC-EDFAs [13; 8; 12; 108; 109; 53; 6; 63; 7]. Erbium-doped fiber amplifiers (EDFAs) with in-core pumping are well-known for their high performance in terms of gain, noise, optical bandwidth and power efficiency. However, in multi-core SDM links, these advantages are offset by the need to introduce demultiplexing and multiplexing stages at the amplifier input in order to insert the pump in each core. In-core pumping therefore leads to a high component count while cladding pumping can decrease system complexity and cost by eliminating the need for components such as pump-signal multiplexers. An additional advantage of cladding pumping that is of particular interest is the use of a single high-power pump source that can be side-coupled to the double-clad fiber. In this configuration, a low cost multimode pump can be used as the pump does not need to be coupled to a single-mode fiber to be injected in the amplifier. Another advantage of cladding pumping arises in SDM links with mode multiplexing. When simultaneously amplifying multiple modes, the more uniform pump power distribution over the optical fiber cross-section can reduce differential modal gain [110]. Numerous cladding-pumped MC-EDFAs have thus been fabricated and characterized with several designs proposing solutions to address the low pumping efficiency. A few examples are a six-core EDFA with more than 20 dB gain over the 1542 nm – 1576 nm wavelength range [13], a 32-core co-doped Er/Yb fiber amplifier with >17 dB gain over the 1544 nm – 1564 nm wavelength range [12] and an EDFA with six cores, each delivering >18 dBm output power with >17 dB gain over the C-band [108]. Few-mode MC-EDFAs were also demonstrated using an annular cladding [109; 53] or slightly coupled cores [6] to increase pump intensity and pumping efficiency.

Cladding pumping presents new opportunities for engineering the erbium doping profile in order to improve the amplifier performance. For instance, ring doping, which consists of including erbium ions in an annular region rather than doping the core uniformly, or a structured erbium concentration profile can be used to reduce differential modal gain [111; 112; 60] or to increase output power [71; 72]. More generally, assuming uniform distribution of the pump in the cladding, annular doping allows to control the signal overlap with the erbium-doped region without modifying the pump overlap. This is illustrated in Fig. 2.1 that compares the mode intensity profiles of an EDFA with in-core pumping and uniform doping in the core [Fig. 2.1(a)], to the mode intensity profiles of an EDFA with cladding pumping having an annular-doped region in the core [Fig. 2.1(b)]. In this particular case, the optical fiber supports two mode groups, LP_{01} and LP_{11}, and the relative gain of the two modes is controlled through the erbium doping profile (see for example [111]). In this work, we consider a double-clad optical fiber with an annular erbium-doped region located in the cladding for amplification of a single mode [Fig. 2.1(c)]. The purpose of this design is to reduce signal overlap with the doped region

in order to reduce saturation and minimize gain compression [71; 72], which is an important advantage for EDFAs used in dynamic and reconfigurable networks. To our knowledge, this is the first direct detailed comparison of simulation and measurement of a cladding-pumped EDFA, with erbium-ion doping located in the cladding, that is designed specifically to lower gain compression.

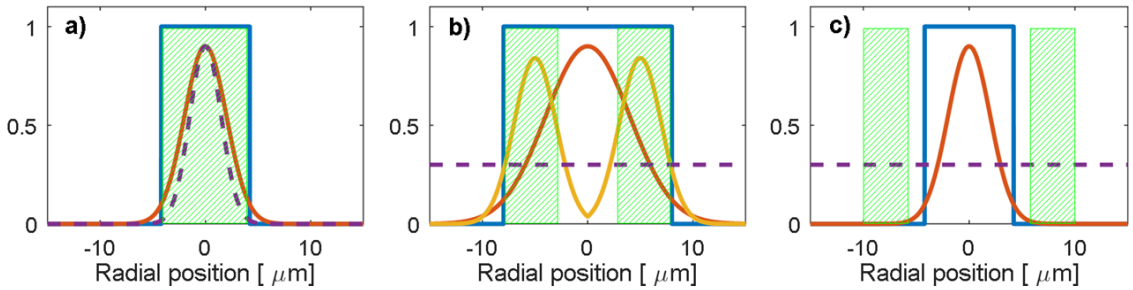

FIGURE 2.1 – Normalized LP_{01} (orange) and LP_{11} (yellow) mode intensity profiles, and normalized pump intensity distribution (purple, dashed) of : a) a core-pumped single-mode fiber, b) a cladding-pumped multi-mode fiber with erbium doping in an annular region of the core, and c) a cladding-pumped single-mode fiber with erbium doping in the cladding close to the core. The blue lines indicate the refractive index profiles and the shaded green areas are the erbium-doped regions.

In this paper, we expand on our initial report in [16] and present here in detail the optimization of the doped fiber design and compare simulation results to experimental measurements. The paper is focused on optimizing the erbium doping profile to reduce gain compression in a single-mode fiber amplifier. While we investigate the simulation and fabrication of a single-core fiber, the results could be straightforwardly extended to MC-EDFA. In section 2.4, we simulate different doped fiber designs and compare their minimum gain over the C-band for a maximum of 4 dB of gain compression. The ideal gain compression of an EDFA used in dynamic and reconfigurable network would be 0 dB to avoid gain excursions when channels are rerouted. However, the lower the gain compression, the harder it is to achieve a high minimum gain over a significant input power range. These simulations are performed using standard values found in the literature for erbium-doped aluminosilicate glass. In section 2.5, we first characterize the parameters of a fabricated fiber with annular doping in the cladding. We then use a tapered fiber to inject the pump in the cladding and measure the amplifier gain and NF. Using the experimentally determined parameters, we compare simulation results to validate the approach. Finally, we conclude, in section 2.6, by a discussion and recommendations for further MC-EDFAs designs.

2.4 Design of the erbium-doped fiber

As optical channels are routed through reconfigurable networks, the input power to an EDFA can vary leading to transients for the remaining channels. A useful measure to quantify the

impact of changing the number of input channels is the static gain compression. Gain compression at a given signal wavelength is defined as the gain difference for two values of total input power. Operation of EDFAs in saturation will therefore lead to high gain compression as the gain changes more rapidly with input power when the amplifier input power is above its saturation power. In this paper, we propose to modify the erbium doping profile of a cladding-pumped fiber to investigate how to achieve sufficient gain and output power, while maintaining low gain compression. By placing the erbium ions (Er^{3+}) in the evanescent tail of the signal mode field, i.e. in an annular region located in the cladding but close to the core, the local signal intensity overlapping with the doped region remains low even as the amplifier gain increases. In this section, we compare three fiber designs to illustrate this behavior. We perform numerical simulations using a standard rate equation model with fiber parameters compatible with common fabrication processes such as modified chemical vapor deposition (MCVD) with solution doping. We examine fiber designs meeting a target of <4 dB of gain compression and contrast their minimum achievable gain and fiber length.

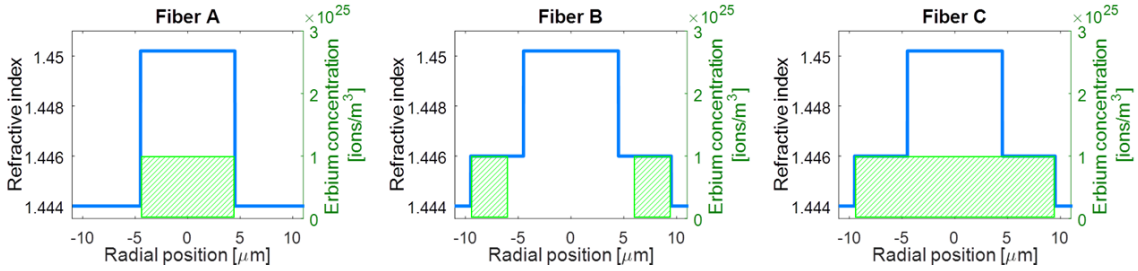

FIGURE 2.2 – Refractive index (blue line) and erbium concentration (green shaded area) profiles of fibers A, B and C.

2.4.1 Erbium doping profiles

To minimize the number of fabrication steps, we simulate radially dependent erbium doping profiles that have only one erbium ion (Er^{3+}) concentration level, namely $\rho_{Er,0} = 1\text{x}10^{25}$ ions/m^3. The three fibers under study are a fiber with uniform doping across the core (Fiber A), a fiber with a uniformly doped annular region in the cladding (Fiber B) and a fiber in which both the core and a portion of the cladding are doped with the same concentration of Er^{3+} (Fiber C). The refractive index profiles and the Er^{3+} concentration profiles of the three fibers are illustrated in Fig. 2.2. All three fibers have a silica cladding with an index of 1.4440 at 1550 nm. Fiber A is a step-index fiber with core radius of 4.5 µm and refractive index of 1.4502. The numerical aperture is 0.134 and the V number is 2.44 at 1550 nm, which mean that the LP_{11} mode is very close to cutoff. In cladding-pumped amplifiers, enlarging the cores to reduce signal intensity helps to reduce saturation [108]. In Fiber B and C, because some Er^{3+} are incorporated in the cladding, silica is replaced by aluminosilicate to increase the solubility of the Er^{3+} in this region. Therefore, the region between r = 4.5 µm and r = 9.5 µm has a refractive index of 1.4460, which is a reasonable value for aluminosilicate to accept an

Er^{3+} concentration of 1x10^{25} ions/m^3. For Fiber B, the erbium doping is only found between r = 6.0 µm and r = 9.5 µm while, for comparison purposes, Fiber C is doped with erbium from r = 0.0 µm to r = 9.5 µm.

2.4.2 Model and simulations

Simulations were performed using the standard EDFA two-level model with the usual set of power propagation and population rate equations in which we introduce radial resolution as described in [13]. Since we aim to design single-mode cores, only the LP_{01} mode is considered in the simulations for the signal (we assume that no higher-order modes are present). The pump power is assumed to be uniformly distributed in the cladding that has a diameter of 140 µm. Consequently, there is not azimuthal dependence and we divide the fiber cross-section in K rings, each with uniform Er^{3+} concentration, and we calculate the average inversion of each ring to calculate transition rates and gain. We write

$$\begin{cases} \frac{\mathrm{d}P_p(z)}{\mathrm{d}z} = -\sigma_{abs,p}\left(\sum_{k=1}^{K} n_{1,k}(z)\Gamma_{p,k}\right)P_p(z) - \alpha_p P_p(z) \\ \frac{\mathrm{d}P_{s,\lambda}(z)}{\mathrm{d}z} = \left(\sigma_{ems,\lambda}\sum_{k=1}^{K} n_{2,k}(z)\Gamma_{\lambda,k} - \sigma_{abs,\lambda}\sum_{k=1}^{K} n_{1,k}(z)\Gamma_{\lambda,k}\right)P_{s,\lambda}(z) - \alpha_s P_{s,\lambda}(z) \\ \frac{\mathrm{d}P^{\pm}_{ASE,\lambda}(z)}{\mathrm{d}z} = \left(\sigma_{ems,\lambda}\sum_{k=1}^{K} n_{2,k}(z)\Gamma_{\lambda,k} - \sigma_{abs,\lambda}\sum_{k=1}^{K} n_{1,k}(z)\Gamma_{\lambda,k}\right)P^{\pm}_{ASE,\lambda}(z) \\ \qquad\qquad +\sigma_{ems,\lambda}\left(\sum_{k=1}^{K} n_{2,k}(z)\Gamma_{\lambda,k}\right)2h\nu_\lambda\Delta\nu_\lambda - \alpha_s P^{\pm}_{ASE,\lambda}(z) \end{cases} \tag{2.1}$$

$$\begin{cases} n_{1,k}(z) = \frac{\frac{A_k}{\tau}+W_{3,k}(z)}{W_{1,k}(z)+W_{2,k}(z)+W_{3,k}(z)+\frac{A_k}{\tau}}\rho_{Er,k}(z) \\ n_{2,k}(z) = \frac{W_{1,k}(z)+W_{2,k}(z)}{W_{1,k}(z)+W_{2,k}(z)+W_{3,k}(z)+\frac{A_k}{\tau}}\rho_{Er,k}(z) \\ \rho_{Er,k}(z) = n_{1,k}(z) + n_{2,k}(z) \end{cases} \tag{2.2}$$

$$\begin{cases} W_{1,k}(z) = \frac{\sigma_{abs,p}\Gamma_{p,k}}{h\nu_p}P_p(z) \\ W_{2,k}(z) = \sum_{\lambda,s}\frac{\sigma_{abs,\lambda}\Gamma_{\lambda,k}}{h\nu_\lambda}P_{s,\lambda}(z) + \sum_{\lambda,ASE}\frac{\sigma_{abs,\lambda}\Gamma_{\lambda,k}}{h\nu_\lambda}P_{ASE,\lambda}(z) \\ W_{3,k}(z) = \sum_{\lambda,s}\frac{\sigma_{ems,\lambda}\Gamma_{\lambda,k}}{h\nu_\lambda}P_{s,\lambda}(z) + \sum_{\lambda,ASE}\frac{\sigma_{ems,\lambda}\Gamma_{\lambda,k}}{h\nu_\lambda}P_{ASE,\lambda}(z) \end{cases} \tag{2.3}$$

where λ stands for the wavelength channels of the signal or the amplified spontaneous emission (ASE), and k refers to the different rings with area A_k. Eq. 2.1 describes the propagation of

the pump power, P_p, the signal, P_s, and the ASE, $P^{\pm}_{ASE}$, in the forward (+) and backward (-) direction. The pump is co-propagating with the signal and the respective background loss of the pump and the signal are α_p and α_s. Also, $\sigma_{abs,p}$ is the absorption cross-section at 980 nm, $\sigma_{ems,\lambda}$ and $\sigma_{abs,\lambda}$ are the emission and absorption cross-sections at the signal or ASE wavelengths. The pump and signal (or ASE) overlaps with each ring are $\Gamma_{p,k}$, and $\Gamma_{\lambda,k}$ respectively. Eq. 2.2 describes the radially resolved population inversion along the fiber. The lower and upper population level densities of a given ring are $n_{1,k}$ and $n_{2,k}$, while $\rho_{Er,k}$ is the erbium concentration of a given doped ring. For the design, $\rho_{Er,k}$ is either 0 or $\rho_{Er,0}$. When simulating experimental results, $\rho_{Er,k}$ will vary from ring to ring. Eq. 2.3 represents the transition rates associated with pump absorption (W_1), signal and ASE absorption (W_2), and signal and ASE stimulated emission (W_3). As usual, h is the Planck constant, ν_p and ν_λ are the pump frequency and signal (or ASE) frequency, and τ is the lifetime of the Er^{3+} upper metastable level.

For the simulations, we consider 31 signal channels uniformly distributed over the C-band (1530 nm to 1560 nm) and 201 ASE channels between 1420 nm and 1620 nm. The spectral resolution of the simulations is therefore 1 nm. At first, we neglect background propagation loss (α_s and α_p are set to 0 dB/m). We use absorption and emission cross-sections measured on an erbium-doped aluminosilicate fiber previously fabricated in our laboratory [113], which are illustrated in Fig. 2.3. The fiber cross-section between radius r = 0 to r = 10 µm is divided into 100 rings. The signal and ASE confinement for each ring, over the whole spectrum of interest (i.e. 1420 nm to 1620 nm with 1 nm resolution), were found by simulating the LP_{01} mode profile with COMSOL. Although not necessary for step-index fibers, this numerical technique is useful when considering variations of the index profile in the cladding and necessary when doing the simulations of the experimentally measured profile in section 2.5 below. The pump overlap for each ring was straightforwardly found by considering that the pump power is uniformly distributed over the fiber cross-section.

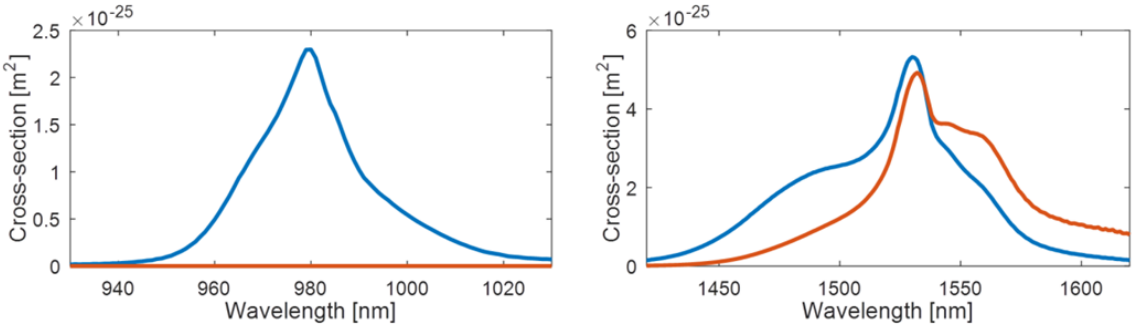

FIGURE 2.3 – Absorption (blue) and emission (orange) cross-sections used in simulations (from [16]).

Our target is to achieve a maximum of 4 dB of gain compression over the C-band when the total input power is varied from -40 dBm (unsaturated amplifier) to 3 dBm (fully loaded

amplifier). This total input power is uniformly distributed over the 31 channels. Considering that 3 dBm corresponds to a fully loaded amplifier (all 31 channels present at its input), the calculated gain compression represents a worst case scenario. If a sub-band is absent from the EDFA input, the amplifier will be less saturated and the gain compression will be lower for the remaining channels, whatever the specific wavelengths of the sub-band channels that are absent. The simulations parameters are summarized in Table 2.1 where $P_{p,in}$ is the input pump power, $P_{s,in,unsat}$ and $P_{s,in,sat}$ are the limits of the total input signal power range used to calculate the gain compression, r_{clad} is the radius of the cladding, n_{core} is the refractive index of the core, n_{doped} is the refractive index of the erbium-doped aluminosilicate region around the core and n_{clad} is the refractive index of the cladding.

Tableau 2.1 – Parameters used in initial simulations, common to all fibers.

Parameter	Value	Unit
$P_{p,in}$	14.5	W
ρ_{Er}	1x10^{25}	ions/m^2
$P_{s,in,sat}$	3 (-11.91 dBm/ch)	dBm
$P_{s,in,unsat}$	-40 (-54.91 dBm/ch)	dBm
$\sigma_{abs,p}$	2.297x10^{-25}	m^{-2}
α_p	0	m^{-1}
α_s	0	m^{-1}
r_{clad}	70	µm
n_{core}	1.4502	-
n_{doped}	1.4460	-
n_{clad}	1.4440	-

For each fiber, we simulated different lengths in order to maximize the minimum gain over the C-band with less than 4 dB of gain compression over the total input power range. The resulting lengths were 0.87 m, 18.2 m and 0.84 m respectively for fibers A, B and C. Fig. 2.4 shows the spectral gain of each fiber calculated with these lengths for the minimum and maximum total input signal power. For each fiber, the maximum gain compression (4 dB) occurs around 1532 nm. The minimum gain, among the 31 channels, for an input power of 3 dBm for fibers A, B and C was respectively 6.8 dB, 17.7 dB and 8.1 dB. With the optimized length, the saturated output power is found by calculating the total signal output power at the 3-dB saturation point of the average amplifier gain. For fibers A, B and C, we find respectively 10.7 dBm, 22.3 dBm and 12.1 dBm. Thus, according to the simulations, Fiber B, with the Er^{3+} located in an annular region of the cladding, is far superior in terms of minimum gain when limiting the gain compression to 4 dB.

2.5 Fiber fabrication and characterization

In order to validate the approach, we fabricated Fiber B using MCVD and solution doping technique. We first deposited a layer of silica sooth using the solution doping technique with

Al_2O_3 and Er_2O_3 to dissolve the Er^{3+} ions in the porous glass [98]. This layer corresponds to the region r = 6.0 – 9.5 µm of the design. This was followed by a second step of MCVD deposition for the fiber core that was made of GeO_2 doped SiO_2 since there was no Er^{3+} doping in this region. Firstly a buffer layer was deposited between r = 4.5 – 6.0 µm with a GeO_2 concentration to match the index of the aluminosilicate glass, then the GeO_2 concentration is increased for the core. In order to break the symmetry of higher-order pump modes, a flat surface was polished on the preform resulting in an optical fiber having a "D"-shaped cross-section [114]. The fiber diameter was 140 µm and a low-index (1.37) polymer with a 205 µm diameter was used to confine the pump power in the cladding.

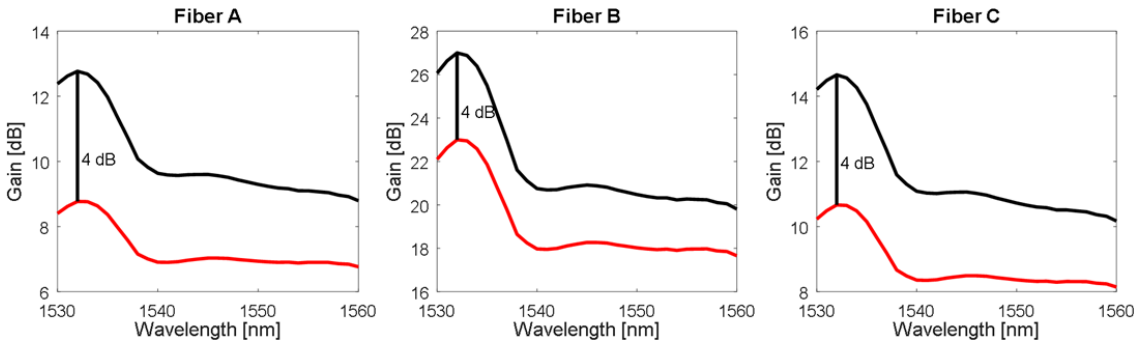

FIGURE 2.4 – Gain as a function of wavelength for total input power of -40 dBm (black) and 3 dBm (red) distributed over 31 channels at the optimum length for each fiber.

2.5.1 Fiber parameters measurements

We measured the resulting refractive index profile of the fiber, at the center of the preform, using a refracted near-field analyzer (EXFO NR-9200HR) at 657.6 nm. The measured refractive profile, neglecting dispersion of the refractive index step, was scaled down to the fiber dimension to compare it to the design in Fig. 2.5(a). We imported this profile into COMSOL in order to calculate the LP_{01} mode confinement in each ring more accurately in subsequent numerical simulations of experimental measurements. The COMSOL simulations also indicated that, although close to cut-off, the LP_{11} mode is guided (at 1530 nm, $n_{eff,LP01} = n_{clad} + 25.0\text{x}10^{-4}$, $n_{eff,LP11} = n_{clad} + 4.67\text{x}10^{-4}$). Fig. 2.6 shows the signal overlap in each ring calculated from the measured refractive index profile and compares the result to the ones of the design at 1550 nm. The fabricated fiber has 53% more signal overlap than the designed one in the 6.0 µm < r < 9.5 µm region ($\Gamma = 0.1345$ compared to $\Gamma = 0.0877$). Using the signal overlap that was calculated from this measurement, numerical simulations were repeated with all other parameters corresponding to the design ones. This leads to an optimal fiber length of 11.1 m and a minimum gain of 16.5 dB for 4 dB of gain compression.

The erbium concentration was measured on the preform as a function of the radial position, using an electron micro-probe analyzer (CAMECA) with a measurement sensitivity of

$\Delta\rho_{Er} = 5\text{x}10^{24}$ ions/m^3, which is close to the doping level of the fiber thereby resulting in a noisy measurement. We performed a fit using a half-Lambertian ($r < 7.4\,\mu m$) and half-Gaussian ($r > 7.4\,\mu m$) profile and used it for the simulations. The asymmetry of this fit allow to consider, in the simulations, the small amount of erbium that was measured above the detection threshold of the CAMECA ($2\text{x}10^{24}$ ions/m^3) in the $r < 6.0\,\mu m$ region. Note that the electron micro-probe analysis showed that a small amount of germanium was present in the erbium-doped region. Both the measured and fitted erbium concentration profiles are compared to the design in Fig. 2.5(b). Note that the obtained erbium ion content is significantly lower than the design with an average concentration of $\rho_{Er} = 3.7\text{x}10^{24}$ ions/m^3 in the $6.0\,\mu m < r < 9.5\,\mu m$ region. Using this averaged concentration in all the doped rings, numerical simulations results in an optimal length of 49.1 m and a minimum gain of 17.6 dB. Using the measured erbium concentration profile directly in the initial simulations leads to an optimal fiber length of 25.5 m and a minimum gain of 14.2 dB. In both cases, all other parameters correspond to the design ones, including the overlap.

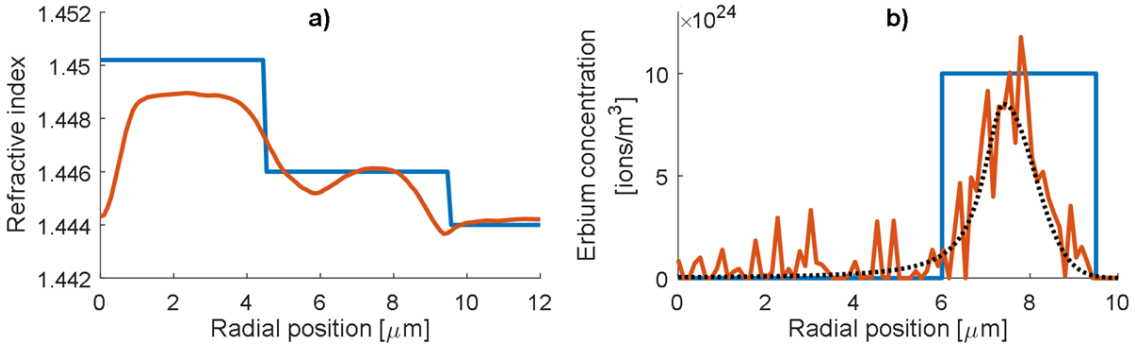

FIGURE 2.5 – For the fabricated Fiber B : a) Designed (blue) and measured (orange) refractive index profile. b) Designed (blue), measured (orange), and fitted (black, dotted) erbium concentration profile.

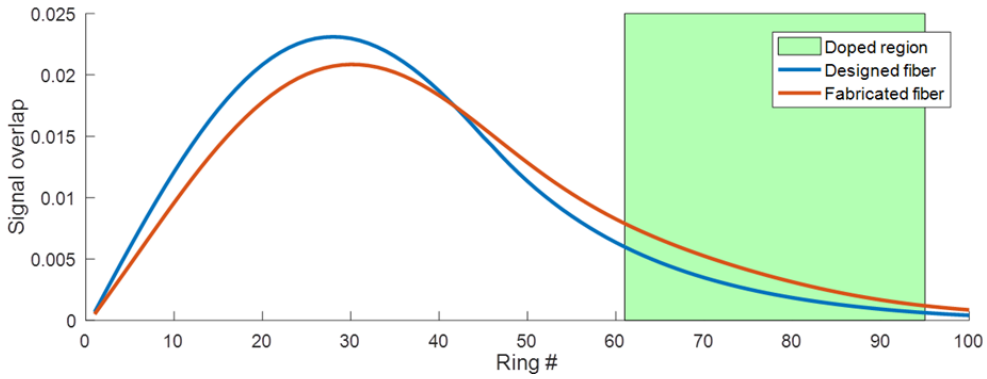

FIGURE 2.6 – Signal overlap of each ring in the designed (blue) and fabricated (orange) fiber.

The pump absorption, when injected in the cladding, was measured using the setup and the procedure shown in Fig. 2.7. The setup consists of an incoherent white-light source followed

by a free-space tunable bandpass filter before being injected into a 2.15 m coreless optical fiber. First, a reference measurement is done at the output of the coreless fiber [Fig. 2.7(a)] to ensure that the power at the output of the coreless fiber is below -40 dBm at each wavelength so that we can assume that the fiber has a very low level of population inversion. The filter has a passband of 1 nm and was tuned with steps of 1 nm from 920 nm to 1020 nm. Afterwards, 9.96 m of the fiber under test (FUT), Fiber B, was added between the coreless fiber and the OSA. The insertion loss in dB/m is determined by dividing the total loss of the FUT by its length. The result is shown on Fig. 2.8.

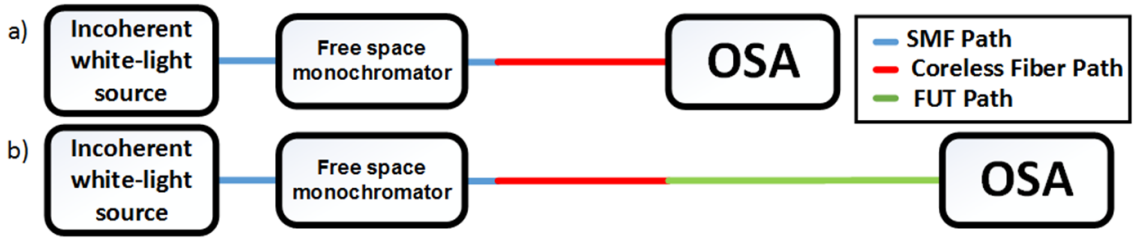

FIGURE 2.7 – Characterization setup used to do spectral measurement of the insertion loss when the light is injected in the cladding a) calibration path and b) measurement of the FUT.

To determine background propagation loss, we use the insertion loss values outside the absorption band of Er^{3+} to interpolate the propagation loss value at 980 nm. The background loss was 0.23 dB/m or 0.053 m^{-1}. Such a high background loss can be caused by either impurities at the outer region of the fiber and scattering of pump light out of the fiber. The absorption of the pump is determined by subtracting the background loss (0.23 dB/m) to the absorption in dB/m at 977 nm (0.294 dB/m). The absorption cross-section of the pump is then calculated with Eq. 2.4-2.6, using the pump overlap with the erbium doping, we find $\sigma_{abs,p} = 2.3\text{x}10^{-25}$ m^2.

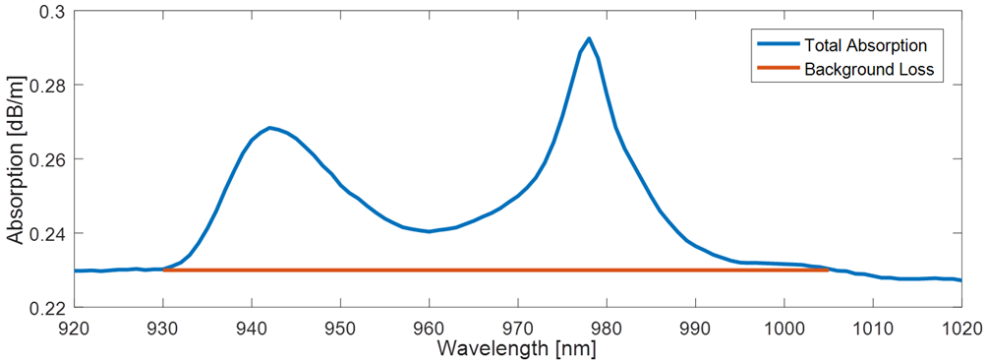

FIGURE 2.8 – Spectral measurement of insertion loss when the light is injected in the cladding of the fabricated Fiber B normalized to fiber length.

The absorption and emission cross-sections at the signal wavelengths were determined using a similar setup as shown in Fig. 2.9. The measurement uses a cut-back technique to determine

signal absorption in the fundamental mode. Absorption and emission cross-sections are then calculated from the spectral absorption result. Once again, a wide-band source with a very low output power is used to ensure a negligible level of population inversion. At first, SMFs are spliced at both ends of the 10.00 m FUT with an active alignment procedure. In order to filter higher-order modes, three loops of 2.2 cm of diameter were made after the first splice. Then, the band pass filter was tuned in steps of 1 nm from 1420 nm to 1620 nm. Finally, a length of 7.90 m of the FUT is cut and the two remaining portions of the FUT are spliced back together resulting in a remaining FUT length of 2.1 m in Fig. 2.9(b). This allows to keep the same splices between the SMF and the FUT. The absorption in dB/m is then found by dividing insertion loss difference by 7.90 m. The result is shown in Fig. 2.10 where it can be observed that the signal propagation background loss is negligible. Also, small oscillations are present on the spectrum, most probably caused by the presence of residual higher-order modes.

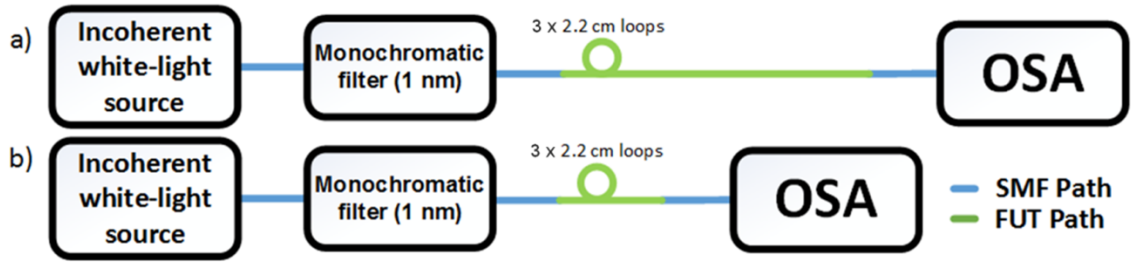

FIGURE 2.9 – Characterization setup used to do spectral measurement of the insertion loss when the light is injected in the core a) calibration path and b) measurement of the FUT.

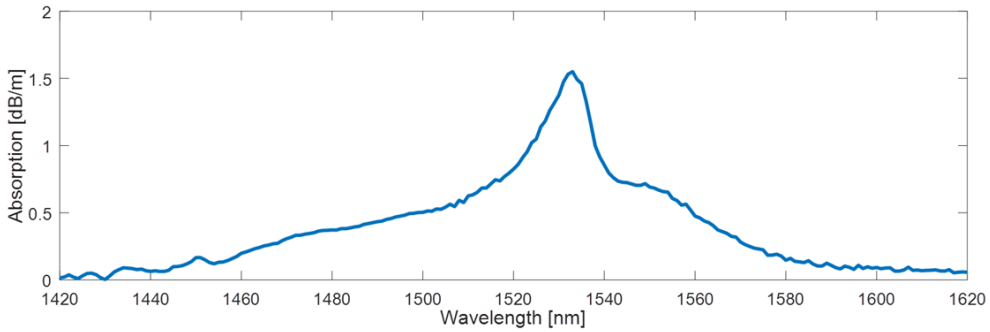

FIGURE 2.10 – Absorption spectrum when light is injected in the core of the fabricated Fiber B.

Then, considering the experimentally determined signal overlap and Er^{3+} doping concentration in each ring, we use the McCumber relation [99] to determine the absorption and emission cross-sections.

$$\sigma_{abs}(\nu)[m^2] = \frac{\alpha[dB/m]}{(10\log_{10} e)\sum_k \rho_{Er,k}[ions/m^3]\Gamma_k} \tag{2.4}$$

$$\sigma_{ems}(\nu) \;=\; \sigma_{abs}(\nu)\cdot e^{(\epsilon - h\nu)/k_B T} \tag{2.5}$$

$$\epsilon = \frac{hc}{1535\text{nm}} \tag{2.6}$$

The resulting cross-section curves, displayed in Fig. 2.11, slightly differ from the curves used for the fiber design. The maximum emission occurs at 1533 nm instead of 1532 nm and a shallow hole appears in the emission cross-section spectrum between 1540 nm and 1546 nm. Those differences could be caused by the presence of germanium in the erbium-doped region [115]. Using these cross-sections in the numerical simulations (with all other parameters fixed corresponding to the design values) leads to an optimal fiber length of 19.6 m and a minimum gain of 14.8 dB.

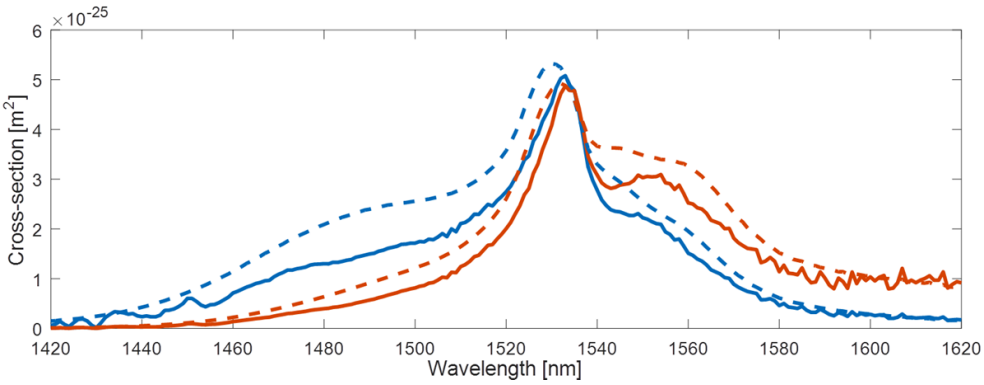

FIGURE 2.11 – Absorption (blue) and emission (orange) cross-sections as a function of wavelength when the signal is injected in the core of the fabricated Fiber B (solid) compared with the cross-sections used for the simulations of the designed fiber (dashed).

2.5.2 Amplifier characterization and validation of the approach

Aiming for a maximum of 4 dB of gain compression when total input signal power varies between -40 dBm and 3 dBm, we used 15 m of the erbium-doped fiber under test (EDFUT), i.e. the fabricated Fiber B with erbium doping in an annular region of the cladding. The gain and noise figure (NF) were measured as a function of wavelength for three different input power values : -40 dBm, -7 dBm and 3 dBm. In the setup shown in Fig. 2.12, the tunable laser #1 is used as a saturating tone at 1550 nm while the tunable laser #2 is used as a low

power tunable wavelength signal (1530 nm – 1560 nm, at least 12 dB lower than $P_{s,in}$). For measurements with $P_{s,in}$ = -40 dBm, no saturating tone is used. Input and output powers were measured on an OSA at the output of the respective input and output isolators. The 25 W 980-nm pump laser is injected in the cladding of the EDFUT. To achieve the injection, a tapered coreless fiber is spliced at the pigtail of the laser source while its tapered section is rolled around the EDFUT [108]. To filter the remaining pump in the cladding at the output of the fiber, a pump dump, consisting of etching cream applied over 5 cm of the EDFUT, is used. The polarization-dependent effects in the EDF were suppressed by using a polarization scrambler. In order to suppress weakly guided higher-order modes, three fiber loops of 2.2 cm diameter were rolled at 0.5 m and 14.5 m of the EDFUT length as shown on Fig. 2.12.

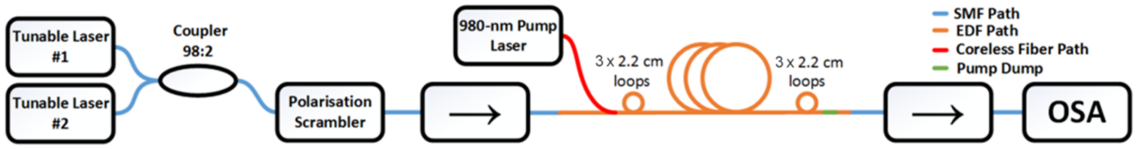

FIGURE 2.12 – Setup used to measure the gain and noise figure of the EDF.

Measured and simulated spectral gain and NF are compared in Fig. 2.13 for the three $P_{s,in}$ values. The simulations assume that 14.5 W of pump power is coupled in the EDFUT cladding (considering loss in the coreless fiber of 3.6 dB/m this translates into a coupling efficiency of 70%).

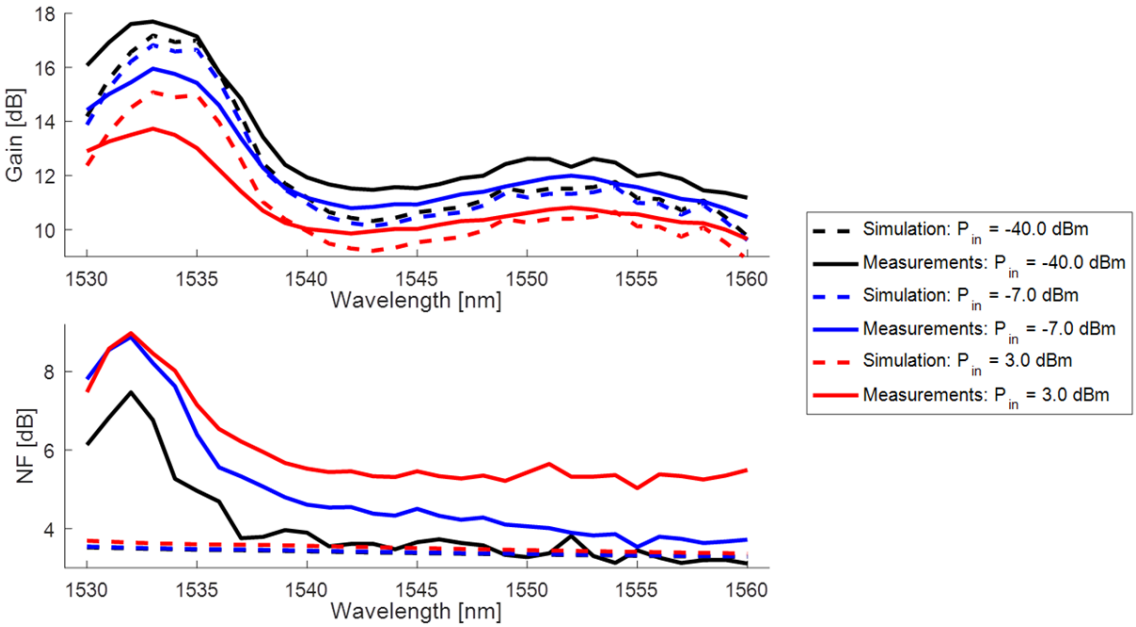

FIGURE 2.13 – Gain (top) and NF (bottom), simulations (dashed) and measurements (solid), as a function of wavelength for different total input power.

Simulations and experiments are in good agreement with a maximum gain difference of 2.0 dB.

Also, in the experiment, the gain compression when $P_{s,in}$ changes from -40 dBm to 3 dBm, was 4.1 dB and occurred at 1532 nm in the experiment, while it was 2.1 dB in the simulations and occurred at 1533 nm with the experimentally measured parameter. According to the simulations with all experimentally determined parameters, the gain compression of 4 dB should occur with a fiber length of 19.9 m and lead to a minimum gain of 10.9 dB with $P_{s,in} = 3$ dBm. Among the factors that could be responsible for this difference between the measured and calculated spectral gain are the presence of residual higher-order modes that are neglected in the model and, also, the fact that the refractive index and erbium doping profiles were measured on a section of the preform but not on the fiber itself. There is a larger difference between the measured and simulated NF, particularly at the shortest wavelengths. Factors that could contribute to this discrepancy include the presence of un-pumped EDFUT sections (before pump coupling and after the pump dump) and the presence of residual higher-order modes, particularly at the shortest wavelengths. Therefore, we believe that the NF peak should be suppressed in future design of annular doped EDFs with singlemode cores. It should be noted that the 4 dB of gain compression, for total input power variations from -40 dBm to 3 dBm, was achieved with a minimum gain of 9.7 dB. Although this result is very far from the 17.7 dB expected from the design, it is still superior to the simulation results of Fiber A (6.8 dB) and C (8.1 dB). This significant difference can be explained by a thinner erbium-doped region, a significantly higher signal overlap and power intensity in the doped region and differences in cross-sections compared to initial expectations. Higher signal overlap in this annular-doped region means higher signal intensity that will lead to saturation and more gain compression. Nevertheless, the good agreement between measurements and simulations using the experimentally determined parameters indicate that refinement of the fiber fabrication technique should lead to the expected performance. It is also important to note that a flat gain spectrum cannot be achieved with unsaturated amplifiers. Thus, this amplifier with low gain compression is designed to be operated with a gain equalization filter.

2.6 Conclusion

Through numerical simulations we compared various erbium doping profiles of cladding-pumped single-core fiber amplifiers to maximize its minimum gain while limiting gain compression to less than 4 dB. The results show that inserting the Er^{3+} in an annular region of the cladding near the core leads to better performance. Compared to designs with uniform erbium doping in the core, the proposed design saturates at higher input signal power due to the small overlap of the signal mode with the annular-doped region. A longer erbium-doped fiber length is required but the minimum gain is significantly increased compared to uniform doping in the core. The approach was validated by fabricating and characterizing a single-core double-cladding fiber with erbium doping in an annular region of the cladding. A low gain compression was achieved but the targeted minimum gain could not be demonstrated with this

fiber. Nonetheless, the measured minimum gain was still better than the simulated values for erbium-doped fibers with uniform doping in the core. Simulations performed with experimentally determined parameters were compared to measurements showing an agreement within 2 dB for the spectral gain, which gives confidence that performance matching more closely the target will be obtained with improvements in fiber fabrication. Some aspects to be refined include the index profile that will have to be modified to ensure single-mode operation over the whole spectral band and the pump background loss that should be reduced. Our results confirm that this type of design would be of interest for multicore EDFAs with reduced gain variations for different input channel reconfigurations.

2.7 Funding

This work is funded by NSERC through a partnership grant with Nokia (RDCPJ 515551-17).

2.8 Acknowledgments

The technical help and insights of Mr. Nicolas Grégoire and Mr. Steeve Morency are acknowledged.

Chapitre 3

Novel fuseless optical fiber side-coupler based on half-taper for cladding-pumped EDFAs

C. Matte-Breton[1], R. Wang[1], Y. Messaddeq[1] et S. LaRochelle[1]

[1]COPL, Université Laval, Québec QC, G1V 0A6, Canada

Présenté à la Optical Fiber Communication Conference (OFC) 2020, paper T3A.2.

Technologie actuellement en processus de brevetage.

3.1 Résumé

Nous présentons une nouvelle méthode de fabrication de coupleurs latéraux à fibre optique qui ne nécessite pas de chauffer les fibres. Une efficacité de couplage moyenne supérieure à 94% a été obtenue pour une puissance de pompe à l'entrée allant de 1,4 W à 20,7 W.

3.2 Abstract

We present a novel method for optical fiber side-coupler fabrication that does not require to heat the fibers. More than 94% of average coupling efficiency is demonstrated for input pump power ranging from 1.4 W to 20.7 W.

3.3 Introduction

Over the next decade, space-division multiplexing (SDM) is expected to be a key technology to increase the capacity in communication networks [77]. For multicore erbium-doped fiber amplifiers (EDFAs) used in SDM networks, cladding pumping is usually preferred over core pumping since it allows using a single low-cost multimode laser diode (LD) as a pump source to amplify multiple cores. Cladding pumping is also beneficial in the case of multimode EDFAs as it leads to a more uniform overlap of the pump intensity with the multiple signal modes, which thereby decreases the differential modal gain. Also note that cladding pumping of SDM EDFAs should ideally be performed by side-coupling since both the input and output fiber facets are usually used to couple the signal from the SDM transmission fiber to the doped core with as little loss as possible. In the past, several methods have been demonstrated to side-couple the output power of a LD into the fiber cladding ; namely, embedded v-grooves ($\eta = 96\%$) [117] or mirrors ($\eta = 80\%$) [118], fused angle-polished fiber ($\eta = 94\%$) [119], fusion of a multimode tapered fiber ($\eta > 96\%$) [120] and fuse-less optical-contact with a multimode tapered fiber ($\eta = 67\%$) [61] (η is the coupling efficiency). Because of their simplicity and their low cost, fused and fuse-less multimode tapered fibers are the most popular methods for SDM EDFAs. However, currently, the fuse-less method does not allow to reach high coupling efficiency, with the latest published results being below 70% [61]. With fusing a tapered fiber, the main issue is that heating of the doped fiber leads to distortion of the refractive index profile, resulting in increased loss and crosstalk between the modes [62; 63]. In this paper, we propose a simple and low-cost method, using a fuse-less multimode tapered fiber, and demonstrate more than 94% of coupling efficiency.

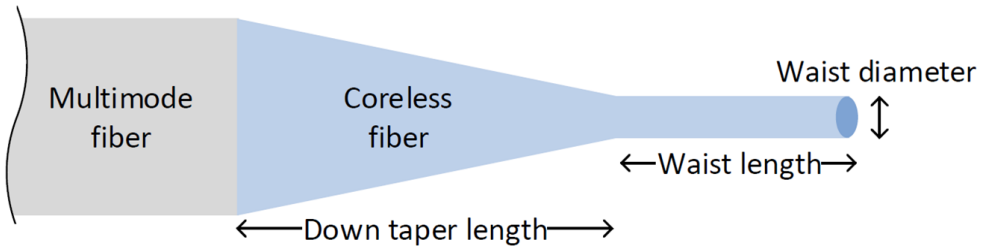

FIGURE 3.1 – Schematic of a half-taper.

3.4 Description of the method

In the proposed method, we first splice a multimode fiber with 105/125 µm of core/cladding diameter to a coreless fiber. We then use a CO_2 laser splicing system (Fujukura LZM-100) to taper the coreless fiber. Then, a blade is used to cut the coreless fiber at the end of the waist region in order to remove the up taper region. For the next steps, we therefore only keep the half-taper shown in Fig. 3.1. The multimode fiber is spliced to the output fiber of a 978-nm

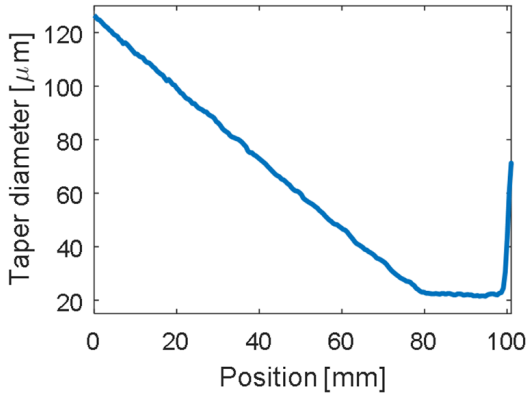

FIGURE 3.2 – Taper profile measurement results.

multimode high power laser diode (the pump source). The receiving fiber, used to quantify the coupling efficiency, is a 125 µm coreless fiber coated with a low-index polymer of the same type that is used in double-clad fibers (n = 1.363) to insure that the pump power is guided in the cladding. The polymer coating of this receiving fiber is mechanically removed over 12 cm to allow optical contact with the half-taper. Finally, the half-taper is put in close proximity to the uncoated region of the receiving fiber and droplets (1-2) of isopropyl alcohol are applied over the whole half-taper. The half taper then spontaneously rolls around the receiving fiber, thanks to surface tension. Even after the liquid has completely dried, the half-taper sticks to the receiving fiber and the coupling efficiency remains stable.

3.5 Couplers characterization

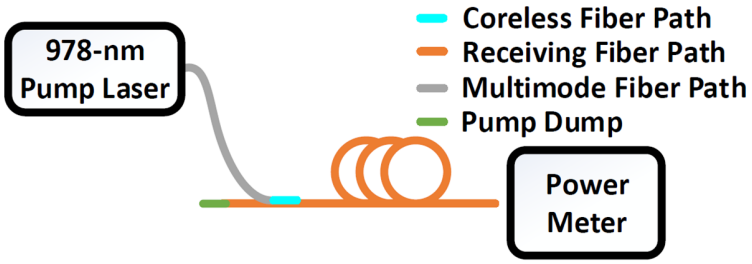

FIGURE 3.3 – Setup used for the characterization of the couplers.

For power efficiency measurement, 13 distinct half-tapers were fabricated with various geometries and a camera was used to measure their tapering profile. An example of a taper profile measurement, before removing the up taper, is shown in Fig. 3.2. Prior to the experiments, the power delivered by the 978-nm pump laser was calibrated by measuring it directly at the output of the multimode fiber for 20 different driving current set points corresponding to an output power range from 1.4 W to 20.7 W. The setup for coupling efficiency measurements is shown in Fig. 3.3. A 1 m length of receiving fiber was used and an index matching gel was

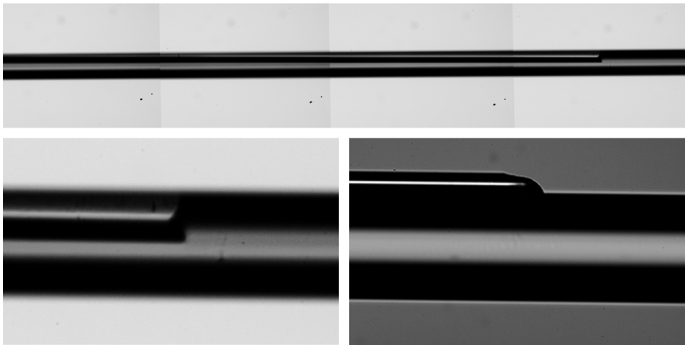

FIGURE 3.4 – Photos of a part of the region where the coreless fiber and the double-cladding fiber are in optical contact.

applied over 4 cm on its unused end (left) in order to eject the power out of the fiber and minimize the impact of reflections on the power measurements. A picture of the region where the coreless fiber and the double-cladding fiber are in optical contact is shown in Fig. 3.4.

Tableau 3.1 – Taper geometry and average coupling efficiency results for the 15 half-taper samples.

Experiment #	Downtaper length [cm]	Waist length [cm]	Waist diameter [µm]	Low-index polymer ?	Average coupling efficiency [%]
1	4.5	4.0	44	No	80
2	4.5	4.0	28	No	77
3	4.5	4.0	15	No	81
4	9.0	1.0	15	No	86
5	7.0	1.0	15	No	88
6	5.0	1.0	15	No	76
7	9.0	1.0	28	No	87
8	7.0	1.0	28	No	82
9	5.0	1.0	28	No	82
10	9.0	1.0	44	No	78
11	7.0	1.0	44	No	66
12	5.0	1.0	44	No	71
13	8.0	2.0	22	No	92
14	7.0	1.0	15	Yes	94
15	8.0	2.0	22	Yes	95

The coupling efficiency was calculated by assuming that all of the power injected into the fiber reaches the power meter without any loss, i.e. it is simply calculated by dividing the measured output power for a given current set point by the power delivered by the 978-nm pump laser for this same set point. Using the method described above, each of the 13 half-tapers was installed on the receiving fiber and their coupling efficiency was measured with the 20 calibrated current set points. The two tapers that gave the best results (#5 and #13) were later re-used for 2 additional experiments, which consisted in using the same method to install

the half-taper but adding a low-index polymer (n = 1.363) over the whole region on which the half-taper and the double-cladding fiber are in optical contact. The details of the taper geometries, as well as the average coupling efficiency over the 20 pump power measurements are shown in Table. 1.

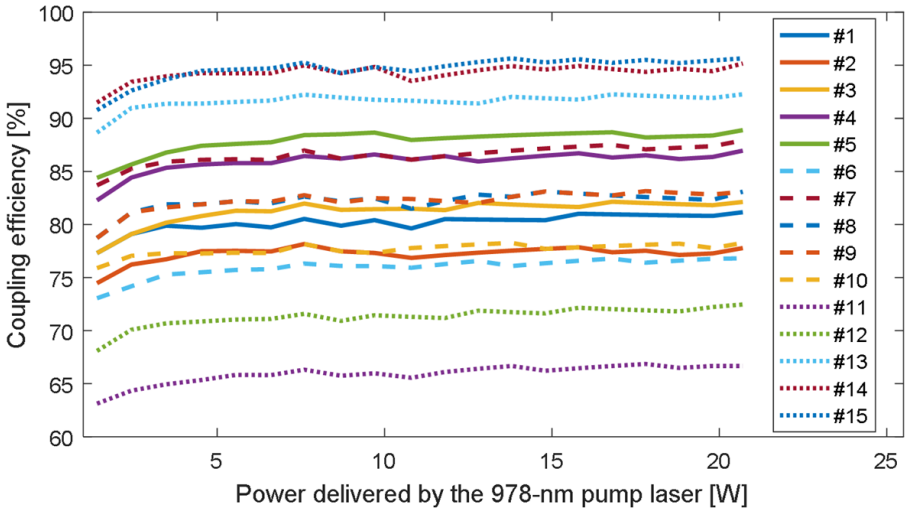

FIGURE 3.5 – Coupling efficiency as a function of power delivered by the 978 nm pump laser for all of the experiments.

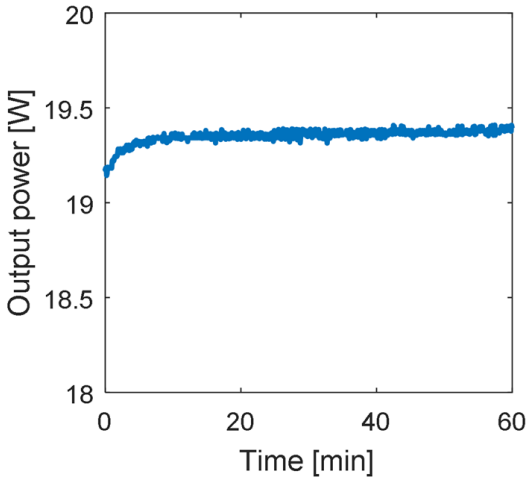

FIGURE 3.6 – Stability of the side-coupler over time.

Considering the limited amount of data, it was not possible to identify optimized values for all parameters. However, by comparing results of experiments #5 vs #14 and #13 vs #15, we see that the use of an overlay of low-index polymer over the optical contact region, clearly allows increasing the coupling efficiency. We also noticed that removing the half-taper from the receiving fiber and replacing it back later, using the same method, always led to coupling efficiency variations of less than 2% from the previous measurements, indicating that the

method has good repeatability. Another trend that can be identified is that the coupling efficiency increases on average by 4% when the power delivered by the 978-nm pump laser is increased from 1.4 W to 20.7 W. This coupling efficiency increase is shown on Fig. 3.5 and could be related to thermal effects increasing the optical contact between the half-taper and the double-cladding fiber. Finally, a coupling efficiency stability test was conducted over one hour and is shown on Fig. 3.6. We also cycled the coupled pump power and did not observe any hysteresis.

3.6 Conclusion

We proposed a novel low-cost and easy to use coupling method to inject high pump power (1.4 W to 20.7 W) in double cladding EDFAs with high efficiency (>94%). This method offers the advantage of not requiring to apply any heat on the receiving fiber, which is a clear benefit for SDM EDFAs where slight geometry distortion can lead to crosstalk between the guided modes and deterioration of the signals.

Chapitre 4

An 8-core erbium-doped fiber with annular doping for low gain compression in cladding-pumped amplifiers

C. Matte-Breton[1], R. Ryf[2], N. K. Fontaine[2], R.-J. Essiambre[2], H. Chen[2], Y. Messaddeq[1], J. C. Alvarado Zacarias[3], R. Amezcua Correa[3], C. Kelly[4] et S. LaRochelle[1]

[1]Centre for Optics, Photonics and Lasers (COPL), U. Laval, Québec, Canada
[2]Nokia Bell Labs, 791 Holmdel-Keyport Rd, Holmdel, NJ, 07733, USA
[3]CREOL, University of Central Florida, Orlando, FL, 32816, USA
[4]Nokia Canada, 600 March Rd, Ottawa, ON, K2K 2T6, Canada

Présenté à la European Conference on Optical Communication (ECOC) 2019, paper W1C.2.

4.1 Résumé

Nous concevons, simulons et caractérisons un EDFA à 8 coeurs pompé par la gaine ayant un profil de dopant annulaire. Une compression du gain inférieure à 1,8 dB et un gain minimum supérieur à 12,2 dB sur la bande C sont démontrés lorsque la puissance d'entrée totale varie entre -23,1 dBm et 1,4 dBm.

4.2 Abstract

We design, simulate and characterize an 8-core cladding-pumped EDFA with annular doping. Gain compression <1.8 dB and minimum gain >12.2 dB over the C-band are demonstrated when the total input power varies between -23.1 dBm and 1.4 dBm.

4.3 Introduction

New modulation format and elastic optical bandwidth are the two main strategies currently used to push the capacity of optical networks to their limits [3]. One of the main issues with elastic optical networks (EONs) is that the output power per channel of erbium doped amplifiers (EDFAs) is affected by its total input load, leading to gain variations when channels are added or removed [121]. To solve this issue, optical-gain-clamping and pump feedback are well known techniques for gain-control of EDFAs under changing input power conditions [121]. With their low gain compression, cladding-pumped EDFAs with annular doping have recently been proposed as a low component count alternative to traditional gain-control systems [101]. In this paper, we demonstrate the first multicore erbium-doped fiber (EDF) with an annular doping region located in the cladding (Fig. 4.1). This fiber was designed specifically to offer low gain compression for applications in EONs. We first characterize the parameters of the fabricated fiber and present measurements of spectral gain (G) and noise figure (NF) when a single core is loaded with input channels. The extracted parameters are fed to a numerical model and simulated gain and NF are compared to experimental results.

4.4 Fiber fabrication and characterization

To achieve low gain compression, the EDFA must operate in an unsaturated regime. This is achieved by placing the region doped with erbium ions (Er^{3+}) in the evanescent tail of the LP_{01} mode field of the signal, i.e. where its intensity is low. Since the Er^{3+} population saturation depends on the local signal intensity, this design allows reaching higher total signal power compared to traditional core doping designs [101]. In the present design, the doped region is located in an annular region of the cladding, at a radial position between r = /5.2 µm and r = /8.0 µm. During fiber fabrication, because aluminium oxide (Al_2O_3) is incorporated in the silica glass to increase the solubility of Er^{3+}, the local refractive index of the doped region is increased. The main challenge in the optimization of this fiber then becomes to design the refractive index profile so that the signal stays strongly confined in the central part of each core, while remaining singlemode. The further the doped region will be from the core, the lower the gain compression will be, but more precision will be required during fabrication to control the mode profile and a longer fiber length will be required.

We modified the fabrication method described in [101] by incorporating an additional SiO_2

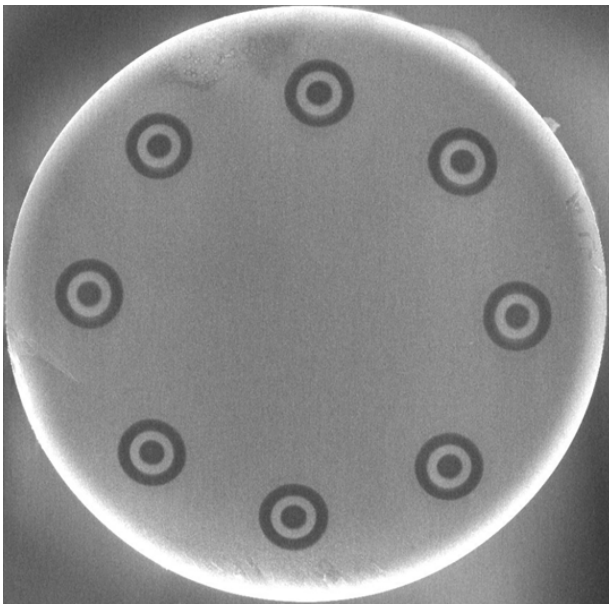

FIGURE 4.1 – Cross-section of the 8-core erbium-doped fiber with annular doping in the cladding and with a core-to-core distance of 38.25 µm.

layer between the core and the doped region. Fig. 4.2 shows the refractive index profile measured on the preform and scaled to the fiber dimension (solid blue), the Er^{3+} concentration profile measured on the preform using an electron micro-probe analyzer (solid green), and the fiber mode simulated from the measured refractive index profile using COMSOL (dashed black). The increase of the local refractive index in the doped region is clearly visible. Also shown is a fit to the Er^{3+} doping profile that is used in the simulations (dashed green).

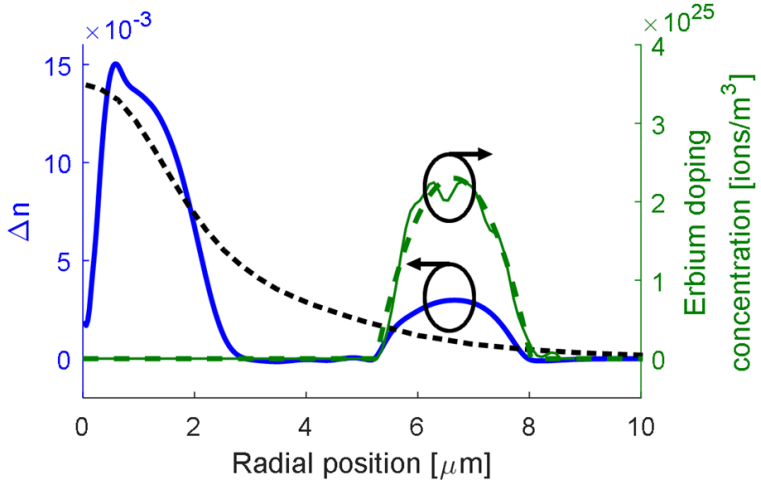

FIGURE 4.2 – Measured refractive index profile Δn (blue), measured (solid green) and fitted (dashed green) Er^{3+} doping concentration profile, and calculated mode profile at 1530 nm (dashed black).

To fabricate the multicore EDFA, the preform was cut in 8 parts of equal lengths and inserted in each of the 8 drilled holes of a silica rod. The optical fiber was drawn with a cladding diameter of 140 µm and coated with a low-index polymer (n = 1.37) for cladding pumping. We characterized the absorption and emission cross-sections of each core from absorption measurements over a short fiber length (see [101] for more details). Due to the small overlap between the signal mode and the Er^{3+} doping, the measured peak absorption at 1532 nm varied between 1.86 and 2.31 dB/m, depending on the core. This variation leads to uncertainty in the calculated absorption cross-sections at 1532 nm that was estimated between 5.96×10^{-25} and 7.39×10^{-25} m^2. The pump absorption cross-section was 1.42×10^{-25} m^2 at 978 nm.

4.5 Numerical model

For the simulations, we used the standard EDFA set of population rate equations and power propagation equations with a radial resolution of 0.1 µm near the cores (up to a radial distance of 10 µm from the center of the cores). We considered pump absorption due to the presence of all cores as in [122]. For this fiber, we also included the impact of Er^{3+} pair-induced quenching [123]. This had to be taken into account because we used a low Al_2O_3 concentration in order to limit the refractive index change in the doped region located in the cladding.

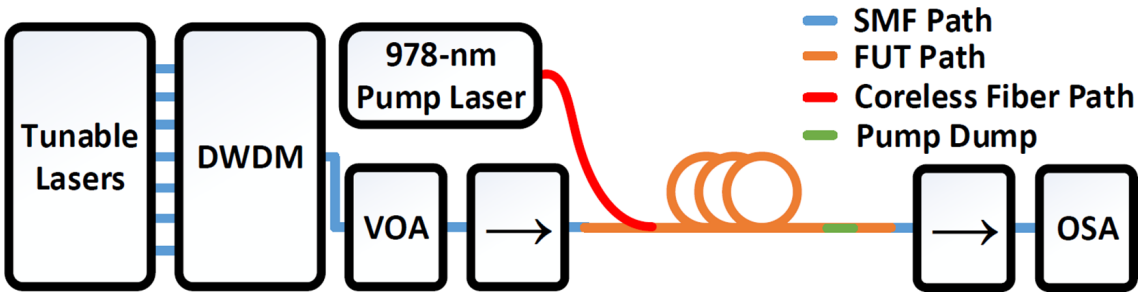

FIGURE 4.3 – Experimental setup used to measure the gain and the noise figure.

4.6 Experimental results

The experimental setup used to measure gain and noise figure is shown in Fig. 4.3. From initial simulations, we estimated that the optimal EDF length was 23 m and used this length for the experimental setup. With active alignment, we spliced SMF pigtails at the input and output of one of the cores of the 8-core fiber. Using a 1300-nm laser source and an optical spectrum analyzer (OSA), we measured a total loss of 1.4 dB, including the two splices and connectors. The output fiber of a 978-nm pigtailed laser diode (105/125 µm) was tapered and rolled around an uncoated part of the 8-core EDF to couple the pump power into its cladding. To emulate multiple channels over the C-band, seven tunable lasers were set to seven wavelengths, evenly distributed over the C-band (1529.55, 1535.05, 1540.55, 1545.33,

1550.13, 1555.75 and 1559.80 nm). All channels had the same power and the variable optical attenuator (VOA) was adjusted to vary the total input signal power of the core under test. After the splice, considering the measured loss, the input power range was between -23.1 dBm and 1.4 dBm. Assuming an 80% coupling efficiency, the injected pump power was set to 8, 12 and 20 W. The pump power coupling efficiency was estimated by cut-back once the characterization was completed. The measured G and NF are shown in Fig. 4.4. In order to help in extracting parameters related to pump loss, we also measured output pump power as a function of input pump power with a large area power meter placed 1.5 cm from the fiber output. We repeated this experiment with different fiber lengths as shown in Fig. 4.5.

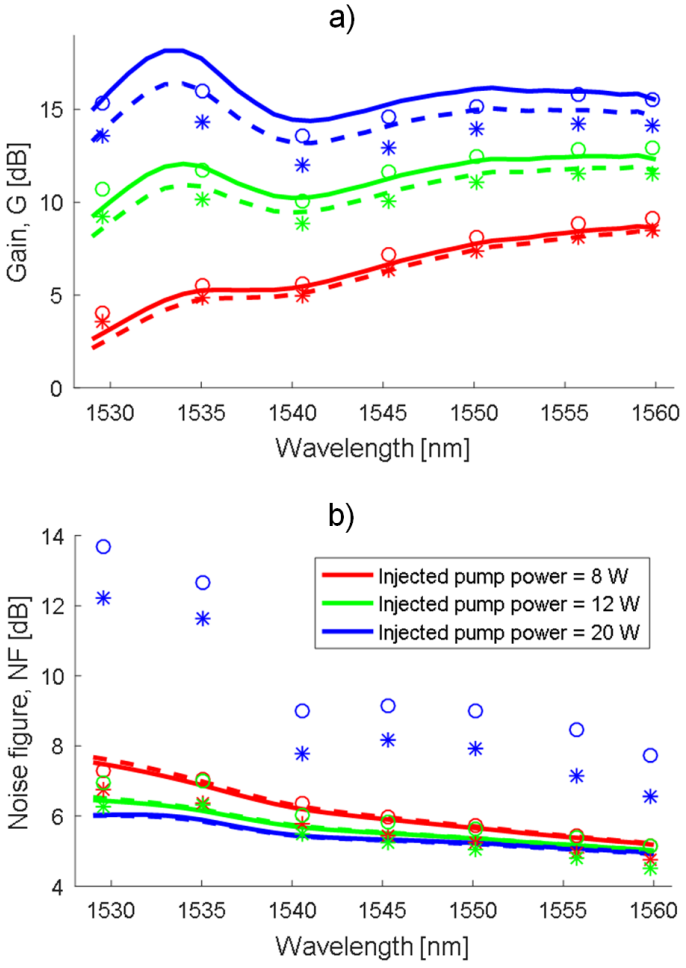

FIGURE 4.4 – Simulation/experimental results for the gain, G (a) and noise figure, NF (b) when one core is loaded with signal input power of -23.1 dBm (solid line/circles) and 1.4 dBm (dashed line/asterisks) for injected pump power of 8 W (red), 12 W (green) and 20 W (blue).

4.7 Simulation results

For the simulations, we used the measured profiles shown in Fig. 4.2 to evaluate the signal and ASE overlap in the EDFA model with radial resolution. We also used the extracted absorption and emission cross-sections (absorption cross-section of 6.30×10^{-25} m^2 at 1532 nm for the core of interest). The fiber length is set to 23 m, the signal input power is swept between -23.1 dBm to 1.4 dBm, and the injected pump power is set to 8, 12 and 20 W. The lifetime of the Er^{3+} upper metastable level is set to 10 ms. In the simulations, the total signal input power is evenly distributed over 32 channels spaced by 1 nm between 1529 and 1560 nm.

Before performing simulations of G and NF, we simulated the experiment shown in Fig. 4.5 (pump transmission without input signal power) in order to extract the pump background loss, α_p, the overlap between the pump and the doping, Γ_p, and the fraction of paired ions, γ_{Er}. For the overlap between the pump and the doped region, rather than uniform pump distribution, we considered that the pump power was slightly (25%) higher in the ring. This was observed using an infrared camera and a 980-nm notch filter to image the fiber output. Since the fraction of paired ions was the only parameters that had a significant impact on the gain measured with 20 W of injected pump power (Fig. 4.4a), it was fitted to $\gamma_{Er} = 18\%$. Then, α_p was adjusted to $\alpha_p = 0.052$ dB/m based on the output pump power experimental results shown in Fig. 4.5. This pump background loss is in agreement to values generally found in the literature. As discussed previously, the high value of the fraction of paired ions can be explained by the low concentration of Al_2O_3 that was used, i.e. 16000 mole ppm, which is only 32 times the Er_2O_3 concentration of 500 mole ppm. Higher aluminium/erbium ratios are usually used to lower the fraction of paired ions, i.e. a ratio of approximately 100 maintains the fraction of paired ions below 6% [124]. In ions pairs, only one of the ions can occupy the excited state leading to decreases in the gain, especially at high pump powers [123]. Ion pairs should thus be minimized but, in the present case, because the Al_2O_3/ Er_2O_3 are introduced in the cladding, there is a trade-off between quenching and index change.

4.8 Discussion

The simulations (lines) are compared to experimental measurements (symbols) of spectral gain in Fig. 4.4a. The results are obtained with one core loaded with signal input power of -23.1 dBm (solid line/circle) and 1.4 dBm (dashed line/asterisk) for three pump power. A gain of 12.2 dB is obtained with a gain compression less than 1.8 dB with total input power up to 1.4 dBm. The spectral gain measurements agree well with simulations results with a maximum gain difference of 1.8 dB. The agreement is also good with the simulated output pump power represented in Fig. 4.5 with a maximum output pump power difference of 0.8 W.

There is an important difference between the measured and simulated NF at 20 W of injected pump power. Note that we spliced a standard single-mode fiber (diameter of 125 m) at an offset

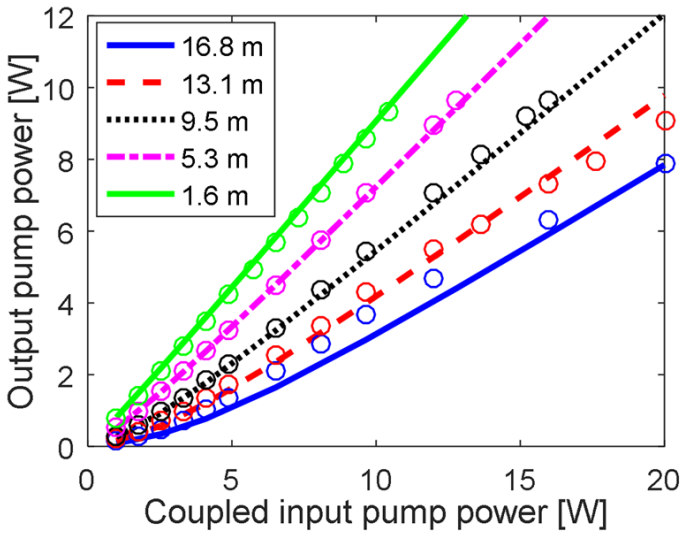

FIGURE 4.5 – Experimental (circles) and simulation (lines) results for the output pump power (without any input signals) when the injected pump power is varied between 1 and 20 W and the fiber length is varied between 1.6 m and 16.8 m.

to the 8-core fiber (diameter of 140 µm). This creates some spurious reflections. The reason for the discrepancy is under investigation ; we think that it could be related to reflections as lasing was sometime observed, or build-up of ASE in the fiber cladding.

4.9 Conclusion

We designed and characterized one core of an 8-core fiber with annular erbium doping. Despite a high fraction of ion pairs due to the low Al_2O_3 concentration, we demonstrate that the approach allows the EDFA to operate in an unsaturated regime over a wide range of input powers. More specifically, we achieved a minimum gain of 12.2 dB, with 1.4 dBm of total input power in the loaded core, and with a maximum gain compression of 1.8 dB over the C-band for input power varying between -23.1 dBm and 1.4 dBm.

4.10 Acknowledgements

This work is supported by NSERC of Canada and Nokia through a partnership grant (RDCPJ5155551-17).

Chapitre 5

Characterization of an aluminophosphosilicate fiber with annular erbium doping for improved performance of cladding-pumped amplifiers

C. Matte-Breton[1], R.-J. Essiambre[2], C. Kelly[3], Y. Messaddeq[1], et S. LaRochelle[1]

[1]Centre for Optics, Photonics and Lasers (COPL), U. Laval, Québec, Canada
[2]Nokia Bell Labs, 791 Holmdel-Keyport Rd, Holmdel, NJ, 07733, USA
[3]Nokia Canada, 600 March Rd, Ottawa, ON, K2K 2T6, Canada

Présenté à la European Conference on Optical Communication (ECOC) 2020, paper Th2A.2.

5.1 Résumé

Une fibre à coeur unique avec profil de dopant annulaire à l'erbium est conçue et investiguée afin d'améliorer les performances des amplificateurs non saturés pompés par la gaine. L'aluminophosphosilicate est utilisé pour réduire le taux de pairage des ions d'erbium et un profil d'indice de réfraction modifié permet d'élargir légèrement le mode, conduisant ainsi à une longueur de fibre plus courte et à un facteur de bruit amélioré.

5.2 Abstract

A single-core fiber with annular erbium doping is investigated to improve the performance of unsaturated cladding-pumped amplifiers. Aluminophosphosilicate reduces the number of ion pairs and a modified refractive index profile slightly enlarges the mode, thus leading to smaller fiber length and improved noise figure.

5.3 Introduction

In elastic optical networks (EONs), channel rerouting often leads to large input power variations in the erbium doped fiber amplifiers (EDFAs) of reconfigurable add-drop multiplexers. Under these conditions, the use of dummy channels or feedback-controlled pumps are necessary in order to maintain a constant gain over the whole wavelength range [121]. In these systems, using integrated multi-core cladding-pumped amplifiers could be advantageous to reduce volume, component count and overall cost compared to multiple single-core EDFAs. In these integrated amplifiers, an alternative strategy to lower gain variations is to operate them in an unsaturated regime [101; 17]. This is enabled by the use of cladding pumping that provides more freedom in the placement of the erbium-doped region. In particular, an annular doped region located in the cladding, where the signal intensity is smaller, lowers gain saturation.

Recently, we demonstrated an eight-core cladding-pumped amplifier designed to decrease the gain variations in EDFAs [17]. The goal is to avoid, or reduce, the requirements of current gain-control techniques. One issue with annular doping is the need for a highly doped, low-index annular region in order to obtain sufficient gain, considering the low signal overlap with the doped region [17]. In highly doped fibers, Al_2O_3 is commonly added to silica to increase rare-earth ion solubility, which unfortunately causes an increase of the refractive index that can lead to the presence of higher order modes. In [17], we thus limited the Al_2O_3 concentration and the estimated fraction of paired ions was 18%. Another issue was a significant degradation of the noise figure (NF) compared to the simulations that was caused by the presence of ASE in the guiding cladding. In this paper, we propose to improve the fiber design by i) using aluminophosphosilicate to lower the refractive index change of the doped region while allowing a high doping concentration with a lower fraction of paired ions [126; 127; 128] ; and ii) tailoring the refractive index profile to decrease the required fiber length and, consequently, the ASE in the cladding. To validate this approach, a single-core fiber with annular doping in the cladding was designed, fabricated and characterized. Its absorption/emission properties are used in numerical simulations and results are compared to measurements of gain and NF with cladding pumping. We show that the fraction of paired ions is significantly reduced and NF is improved.

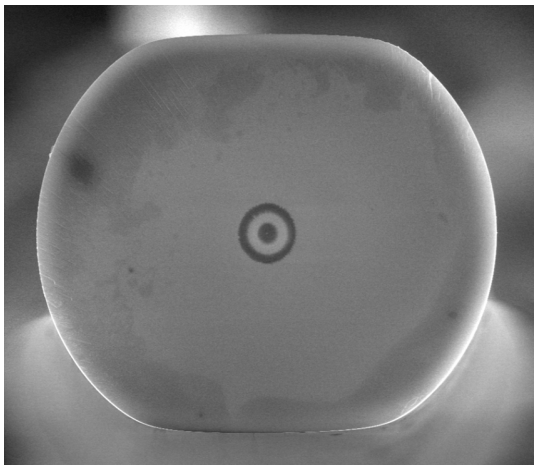

FIGURE 5.1 – Cross-section of the fabricated single-core erbium-doped fiber with annular doping.

5.4 Fiber fabrication and characterization

The preform fabrication method (described in [17]), consisted of using the solution doping method for the doped region in the cladding and the modified chemical vapor deposition method (MCVD) for the core made of germanium-doped SiO_2. In the present case, phosphorus was added to the solution with erbium and aluminium. An electron micro probe analyzer was used on a preform sample to determine the concentration of Al_2O_3, P_2O_5 and Er_2O_3 in the doped region : 23000 ppm, 14000 ppm and 500 ppm, respectively. It is worth noting that the CAMECA measurement results neglect the presence of $AlPO_4$, leading to an overestimation of the concentrations of Al_2O_3 and P_2O_5 which are actually indicative of the total concentration of aluminium and phosphorus elements in the glass matrix. In our previous work [17], these were respectively 16000 ppm, 0 ppm and 500 ppm. The addition of phosphorus allows to increase the concentration of aluminium without the detrimental effects of an increase in the refractive index [126; 127; 128]. The preform is polished on two sides to obtain a double-D shaped fiber (cladding diameters 105.8/122.5 µm) shown in Fig. 5.1. The fiber is drawn with a low-index polymer coating to allow cladding pumping.

The refractive index profile of the preform was measured using a refracted near-field analyzer (NR-9200HR, EXFO) at 657.6 nm. Knowing the diameter ratio of the preform and fiber, we calculated the mode profile at 1530 nm using COMSOL. The refractive index and mode profiles are presented in Fig. 5.2 that compares this new single-core fiber to one core of the 8-core fiber in [17]. Due to the phosphorus, the refractive index change of the doped region is lower, although the aluminium concentration is 1.44 times higher. Also, the core Δn was decreased to slightly increase the mode radius and the overlap with the doped region. This leads to higher gain and allows to reduce the fiber length, which decreases the amount of ASE in the cladding at the fiber output. The absorption cross-sections were measured by cutback

using a filtered supercontinuum laser source (1350 nm to 1700 nm) ; the emission cross-sections were calculated using McCumber's equation.

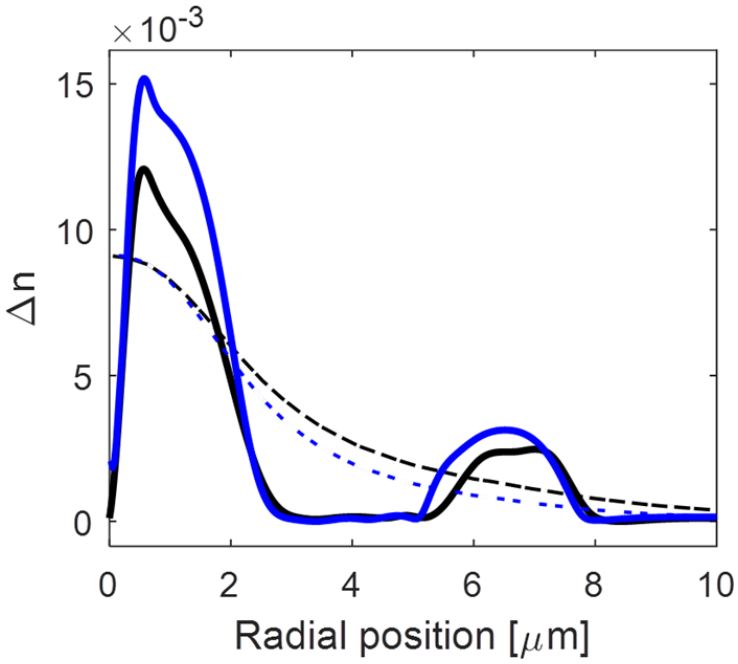

FIGURE 5.2 – Measured refractive index profile Δn (solid) and calculated mode profile (dotted) of the proposed single-core EDF (black) and of one core the 8-core fiber in [17] (blue).

5.5 Numerical model

The absorption and emission cross-sections, the mode profile, and the erbium doping concentration profile were fed into the numerical model described in [17] (considering that only a single-core is present). The pump power distribution was assumed to be uniform over the cladding.

5.6 Experimental results

The spectral gain and NF, and the output pump power were measured as in [17]. To couple the pump power into the fiber cladding, we used the half-taper method described in [116]. For the gain measurement, the experiment was first conducted with an EDF length of 15.9 m and a total input signal power of -23.0 dBm to 1.5 dBm, distributed over 8 channels between 1528.8 nm and 1563.9 nm. Then, 2.9 m of fiber was removed and the experiment was repeated with 13.0 m of fiber length. The internal gain and NF results are shown in Fig. 5.4 for the two fiber lengths, the two total input signal power and three pump powers (8.5 W, 12.7 W, and 21.1 W). The measured input and output splice loss was 0.7 dB. Then, without touching the half-taper pump coupler, we cut the EDF to 12.9 m, 10.1 m, 7.0 m, 4.1 m and 0.5 m to

measure the output pump power in the cladding with a free-space power meter (Fig. 5.3). The coupled input power was assumed to be equal to the output pump power measured after 0.5 m (pump coupling efficiency ≈ 85%).

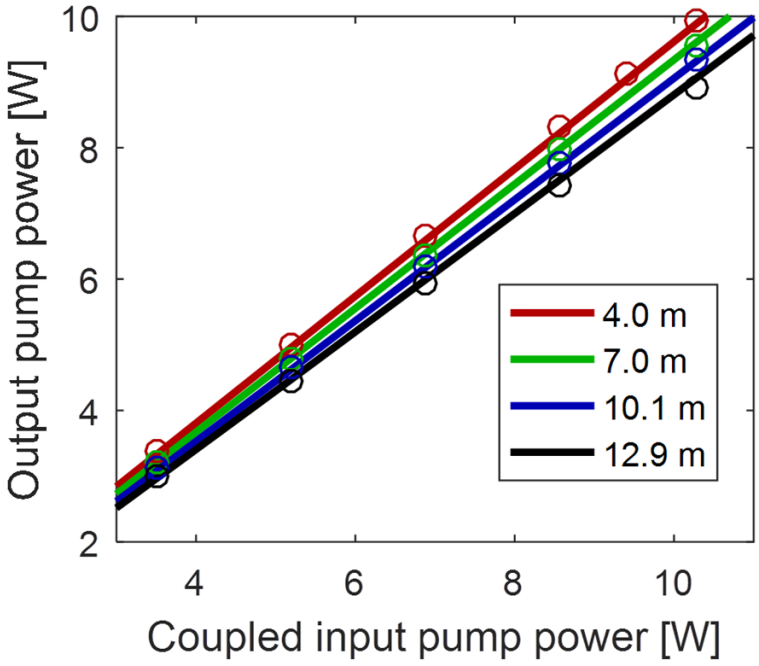

FIGURE 5.3 – Output pump power measured (circles) and simulated (lines) (without any input signals) as a function of input pump power for various fiber lengths.

5.7 Numerical simulation results and discussion

The simulations consider 36 channels uniformly distributed from 1529 nm to 1564 nm and the experimentally measured fiber lengths, coupled pump powers and total input signal powers. The pump background loss was estimated to be 0.028 dB/m by optimizing the fit between the simulations and the results in Fig. 5.3. A fraction of paired ions of 5% was determined by optimizing the fit of the simulations to the spectral gain measurement in Fig. 5.4, which is an important improvement with respect to 18% in [17] for similar erbium concentration. This can be explained by the combination of aluminium and phosphorus which has been linked [126; 127] to the formation of $AlPO_4$ that has a structure and a Δn similar to SiO_2.

Experiments and simulations are in good agreement with differences $<$1.0 dB for NF and $<$3.0 dB for gain. In [17], significant NF disagreement between experimental results and simulation results were observed and were associated with the presence of ASE in the cladding (NF $>$ 7 dB when the pump power is 20 W). This disagreement is not observed in the present case where NF difference between measurements and simulations $<$1 dB is observed even at the high pump power of 21.1 W (see Fig. 5.4). This improvement is mainly due to the lower

core Δn that leads to a slightly larger mode and increased overlap with the doped ring. This in turn results in a shorter length of fiber being required to reach a given minimum gain over the C-Band. According to simulations, with this new fiber, the same gain compression as in [17] (<1.8 dB) would be achieved under the same scenario : 8 cores sharing 20 W of injected pump power, one core under load with an input power range of -23.1 dBm to 1.4 dBm. This scenario provided a minimum gain of 12.2 dB over the 1530 nm to 1560 nm spectral region. Thus, the higher gain compression shown in Fig. 5.4 results from the larger spectral region and a higher minimum gain. This paper demonstrates that the main issues previously encountered with annular doping can be addressed by careful optimization of the fiber design ; both material and waveguide. We think that annular doping can be highly beneficial for many applications that require cladding-pumped amplifiers with low gain compression.

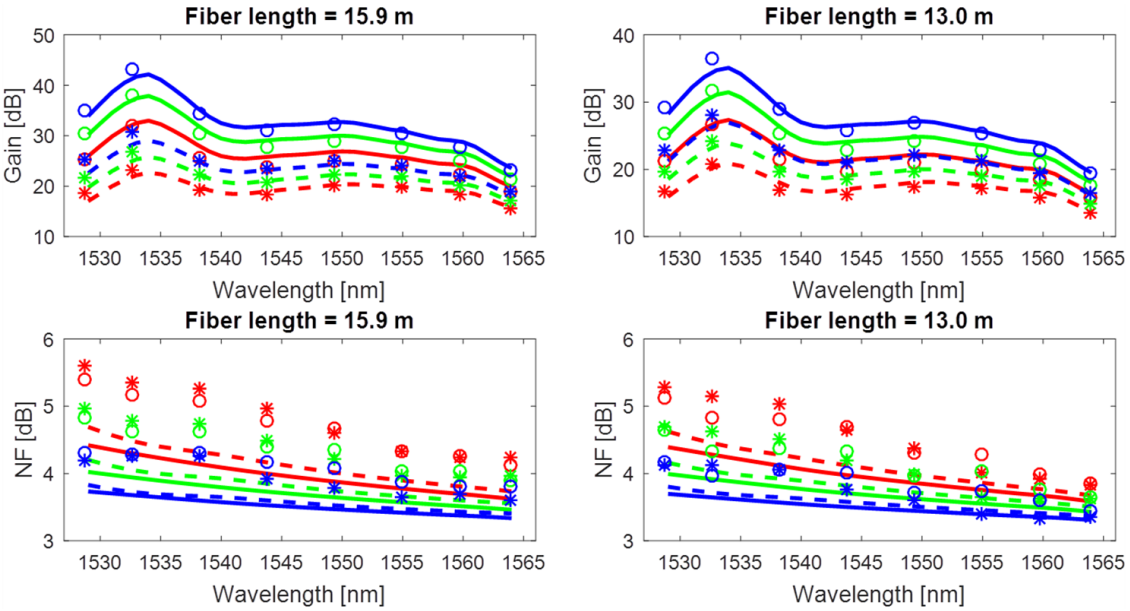

FIGURE 5.4 – Simulation/experimental results for the gain and NF when the doped fiber length is 15.9 m and 13.0 m, the core is loaded with signal input power of -23.1 dBm (solid line/circle) and 1.4 dBm (dashed line/asterisk) for injected pump power of 8.5 W (red), 12.7 W (green) and 21.1 W (blue).

5.8 Conclusion

We fabricated and characterized a double-cladding single-core EDFA with aluminophosphosilicate in an annular-doped region and a refractive index profile designed to reduce the NF degradations caused by ASE in the cladding. Through simulations and experiments, we show that the fraction of paired ions was significantly reduced and the excess NF caused by ASE in the cladding was reduced from >7 dB to <1 dB.

5.9 Acknowledgements

This work is supported by NSERC and Nokia through a partnership grant (RDCPJ5155551-17).

Chapitre 6

Multicore Cladding-Pumped Fiber Amplifier with Annular Erbium Doping for Low Gain Compression

C. Matte-Breton[1], R.-J. Essiambre[2], C. Kelly[3], Y. Messaddeq[1], et S. LaRochelle[1]

[1]Centre for Optics, Photonics and Lasers (COPL), U. Laval, Québec, Canada
[2]Nokia Bell Labs, 791 Holmdel-Keyport Rd, Holmdel, NJ, 07733, USA
[3]Nokia Canada, 600 March Rd, Ottawa, ON, K2K 2T6, Canada

Publié dans IEEE Journal of Lightwave Technology.

6.1 Résumé

Nous rapportons la caractérisation d'une fibre multicoeur pompée par la gaine avec un dopage annulaire à l'erbium visant l'obtention d'une faible compression du gain sur la bande C (1528,8 nm à 1563,9 nm). La fibre vise à minimiser les effets de saturation en plaçant le dopage à l'erbium dans la gaine, où l'intensité du signal est plus faible. Le défi d'assurer une solubilité adéquate des ions erbium dans la gaine, sans augmenter indûment son indice de réfraction, a été relevé en utilisant de l'aluminophosphosilicate dans la région dopée. Avant d'assembler l'amplificateur à huit coeurs, avec fan-in et fan-out, nous devions déterminer la longueur de fibre optimale permettant d'atteindre l'objectif de compression du gain lorsque les huit coeurs sont chargés, pour une puissance de pompe donnée injectée dans la gaine. Nous avons ainsi effectué une caractérisation expérimentale approfondie d'un seul coeur. Cela a permis de déterminer tous les paramètres de la fibre qui sont requis pour effectuer des simulations numériques et prédire les performances de l'amplificateur à fibre multicoeur dans un

scénario pour lequel tous les coeurs sont chargés. Pour la première fois, ces résultats numériques sont comparés aux résultats expérimentaux d'un amplificateur multicoeur pompé par la gaine, ayant un dopage à l'erbium dans la gaine et dont tous les coeurs sont chargé. Nous discutons des performances de l'amplificateur en termes de compression du gain lorsque la puissance du signal à l'entrée change, comme ce serait le cas dans les réseaux de communication reconfigurables. Nous examinons également les variations de gain entre les coeurs et la sensibilité du design aux variations de la géométrie et du matériau causées par le processus de fabrication. Les résultats montrent qu'une réduction significative de la compression du gain des amplificateurs multicoeurs pompés par la gaine peut être obtenue avec un design utilisant la géométrie de dopant en anneau proposée, bien qu'une amélioration de l'uniformité de fabrication des coeurs soit nécessaire pour être viable dans le cadre d'applications pratiques. Enfin, nous discutons de l'intérêt de ce design de fibre dopée à l'erbium dans une perspective d'amélioration de l'efficacité de conversion de puissance (PCE) dans les amplificateurs pompés par gaine.

6.2 Abstract

We report the characterization of a cladding-pumped multicore fiber with annular erbium doping for low gain compression over the C-band (1528.8 nm to 1563.9 nm). The fiber aims to minimize saturation effects by placing the erbium doping in the cladding where the signal intensity is lower. The challenge of ensuring adequate erbium ion solubility in the cladding, without unduly raising its refractive index, was answered by using aluminophosphosilicate for the doped region. Before assembling the eight-core amplifier with fan-in and fan-out, we needed to determine the optimum fiber length to meet the gain compression target when the eight cores are loaded, for a given pump power injected in the cladding. We thus performed a thorough experimental characterization of a single core. This allowed the determination of all the relevant fiber parameters needed to do numerical simulations and predict the multicore fiber amplifier performance under the fully loaded scenario. For the first time, these numerical results are compared to the experimental results of a fully loaded multicore amplifier with cladding pumping and erbium doping in the cladding. We discuss the amplifier performance in terms of gain compression when the input power signal is varied, as would be the case in dynamic optical networks. We also examine the core-to-core gain variations and the sensitivity of the design to fabrication variations. Results show that significant reduction in gain compression of multicore cladding-pumped amplifiers can be achieved with the proposed annular doping design in the cladding, although improvement in the fabrication uniformity of the core will be required for practical applications. Lastly, we discuss how this erbium doped fiber design can also lead to improved power conversion efficiency (PCE) in cladding-pumped amplifiers.

6.3 Introduction

During the last decade, spatial multiplexing has been investigated by many research groups as a means to improve capacity of communication networks by using multiple independent cores per fiber [130; 131; 132; 133; 134], multiple modes per core [135; 136; 137; 138; 139], a combination of both [140; 141] or a coupled-core structure [142; 143]. In erbium-doped fiber amplifiers (EDFAs), one of the promising improvements allowed by spatial multiplexing is to decrease system complexity by using only one high-power and low-cost multimode laser diode as a pump source to amplify multiple cores sharing the same cladding [144; 13; 145; 58; 108].

However, cladding-pumped multicore fiber amplifiers come with several challenges due to the low pump intensity caused by the large cladding surface area. In fact, this low pump intensity, compared to the high intensity of the amplified signal in the core, leads to lower saturation power compared to core-pumped EDFAs [62; 146]. Lower saturation power causes higher gain variations for a given range of input signal power variations, which is especially critical in reconfigurable network nodes where routing wavelength bands can lead to large variations of input signal power. Due to the high number of optical paths that need to be amplified at these nodes, the multicore technology could be beneficial for this application if the gain compression problem could be solved. Furthermore, in single-core EDFAs and core-pumped multicore EDFAs, it is possible to adjust the pump power to maintain a desired gain (and gain shape) as the signal power changes. In a multicore design using a single pump for cladding-pumping, the flexibility of independent pump power adjustment in each core is lost. Therefore, the amplifiers would ideally be operated in the unsaturated regime in order to maintain a constant gain profile (matched to the gain-flattening filter (GFF) design) as the signal power per core changes.

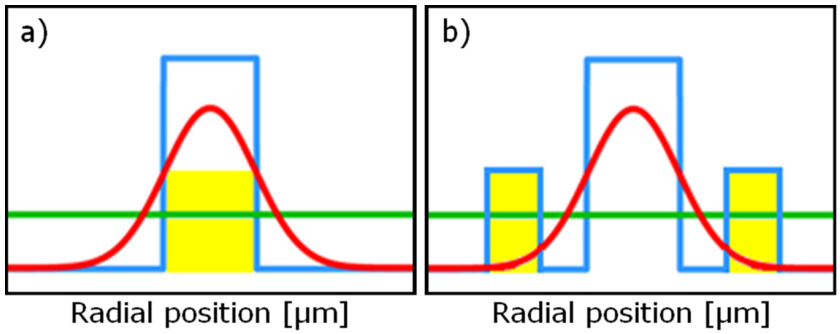

FIGURE 6.1 – Schematic representation of the refractive index profile (blue), the signal intensity (red), the pump intensity (green) and the doped region (yellow) for a cladding-pumped EDFA using a) core doping or b) annular doping.

In cladding-pumped amplifiers, fibers with annular erbium doping profiles can allow decreasing the signal intensity in the doped region while keeping the same pump intensity [101; 17; 125]. This results from the careful design of the doping profile so that it only interacts with the

evanescent region of the mode field (as shown in Fig. 6.1), The first attempt at using annular doping in a multicore fiber [17] suffered from high amplified spontaneous emission (ASE) in the cladding, due to the presence of cladding modes and the long fiber length required by the low overlap of LP_{01} mode with the doped region. Also, the pumping efficiency was compromised by the high level of erbium clustering. The high clustering was due to the low concentration of Al_2O_3 used in the doped region during the preform fabrication. This concentration was maintained low by design, in order to limit the refractive index change, Δn, in the doped region and thus prevent higher order core modes from being guided [17]. Recently, the design has been improved by using aluminophosphosilicate in the doped region so as to maintain a low Δn despite the higher Al_2O_3 concentration, and by reducing the radius of the doped ring to prevent high ASE in the cladding. This design was validated by fabricating a single-core fiber with annular erbium doping and the results were reported in [125]. Using the same core design, a multicore fiber was fabricated. Characterization results, with one loaded core, and a simulation based investigation to estimate the gain compression in a fully loaded scenario were presented in [147].

The paper is structured as follows. We first give details on the fabrication and characterization of the multicore fiber in Section 6.4. We present the chemical analysis of the doped region, the refractive index profile, the spectral distribution of the pump source, the pump absorption and the in-band absorption spectrum. From these measurements, we determine the erbium doping concentration profile, the mode overlap and the absorption and emission cross-sections between 1420 nm and 1620 nm. Then, in Section 6.5, we performed exhaustive characterization of one of the cores by splicing singlemode fibers at its input and output to estimate all the additional fiber parameters required to perform numerical simulations. In particular, the coupled pump power and propagation loss in the cladding and the fraction of erbium ion pairs. In Section 6.6, with all parameters having now been experimentally characterized, we performed numerical simulations to determine the required fiber length to meet the gain compression target when the eight cores are loaded. In Section 6.7, we demonstrate, for the first time, characterization results of a fully loaded 8-core cladding-pumped amplifier with erbium doping located in rings embedded in the cladding surrounding the cores. The new multicore fiber, shown in Fig. 6.2, was connected with input/output fan-in/fan-out so that the core-to-core gain (G) and noise figure (NF) variations could be characterized under a fully loaded configuration representative of a dense wavelength division multiplexing (DWDM) scenario. Finally, in Section 6.8, we analyze the sensitivity of this design to refractive index profile variations through numerical simulations.

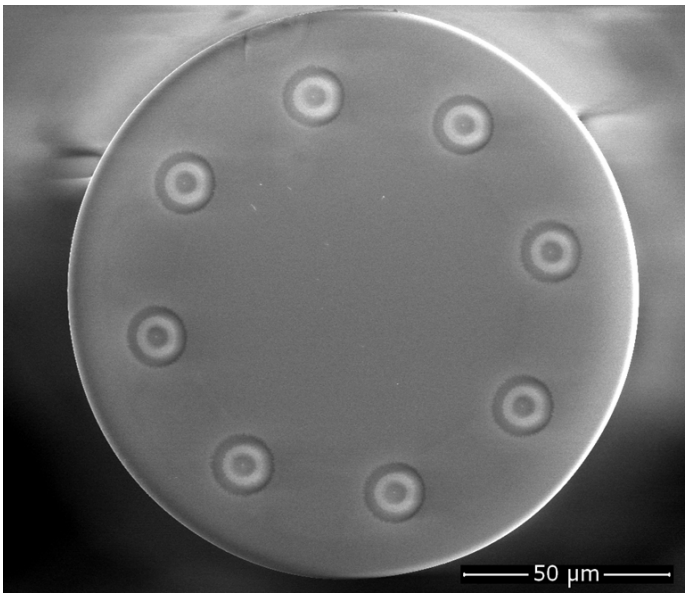

FIGURE 6.2 – Cross section of the multicore erbium-doped fiber with annular doping.

6.4 Fabrication process and determination of the fiber parameters

In this section, we present the detailed process used to fabricate the multicore fiber with annular doping and measure the erbium doping concentration profile, the mode overlap and the absorption and emission cross-sections between 1420 nm and 1620 nm that will be used to simulate the gain and NF performances of the fiber.

The multicore erbium-doped fiber (EDF), shown in Fig. 6.2, was made from a single-core preform cut into eight equal parts and assembled into a multicore preform with the stack-and-draw technique [148; 149]. The single core preform was fabricated by first using the solution doping technique [150] for the doped region, i.e. using an aluminium-phosphorus-erbium solution in the porous silica glass. The process was done in two steps, with two successive sooth deposition and solution doping, to make the annular doped region thicker. Then, using modified chemical vapor deposition (MCVD) [151], a silica layer and the central part of the core, made of GeO_2 doped SiO_2, was added.

The refractive index profile was measured, with a refracted near-field analyzer (EXFO NF-9200HR at 657.6 nm), at 21 longitudinal positions over the 50 cm preform. The extremities were discarded to only keep the 30 cm of the preform over which the refractive index was the most uniform. The average of all refractive index profile measurements, taken on the part of the preform that was not discarded, is shown in Fig. 6.3. To determine the erbium doping profile, a 5 mm slice of the single core preform was cut to perform a chemical analysis with an electron micro-probe analyzer (CAMECA). The measurement sensitivity is

$\Delta\rho_{Er}$ = 5x10^{24} ions/m^3. As shown in Fig. 6.3, the peak erbium concentration is located at a radial position of 5.9 µm. At this radial position, the measured molar concentration of Al_2O_3, P_2O_5 and Er_2O_3 is 26400 ppm, 13600 ppm and 540 ppm. It is worth noting that the CAMECA measurement results neglect the presence of $AlPO_4$, leading to an overestimation of the concentrations of Al_2O_3 and P_2O_5 which are actually indicative of the total concentration of aluminium and phosphorus elements in the glass matrix.

In Fig. 6.3, the radial position, with respect to the center of one of the cores, was determined by scaling down the measured profile by a factor of 182x, which corresponds to the ratio of the multicore preform diameter to the fiber diameter. The final fiber diameter was 140 µm and a low-index polymer was used for the double-cladding in order to achieve cladding pumping with low pump background loss. The resulting refractive index profile was used in COMSOL to determine the LP_{01} mode profile (shown in Fig. 6.3).

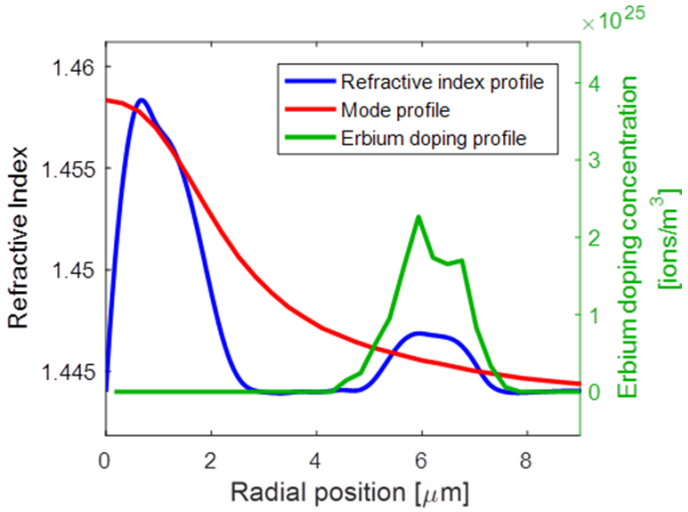

FIGURE 6.3 – Refractive index profile (blue), erbium doping profile (green) and calculated LP_{01} mode field profile (red) of the fabricated fiber cores.

To determine the absorption and emission cross-sections, a supercontinuum laser source was filtered with a free space 1200-1700 nm bandpass filter and coupled in one of the fiber cores with a free space injection setup. To ensure that the injected signal was guided by the core and not by the cladding, the fiber coating was removed over 5 cm near the input and 5 cm near the output of the fiber under test and a refractive index matching gel was applied over these regions to scatter the light guided by the cladding outside of the fiber. A bare fiber adapter was used to connect the fiber output to an OSA. Then, the free space injection was optimized by active alignment with the aim to maximize the measured output power at 1650 nm. The output was measured before and after a cutback, with an original fiber length L_1 of 5.0 m and cut length L_2 of 1.9 m. Due to the short fiber length and small overlap between the doped region and signal mode, we estimate that the supercontinuum output power $<$ 30 dBm/nm

was low enough to keep the level of inversion close to 0. The resulting absorption coefficient, $\alpha_{(\lambda)}$, is shown in Fig. 6.4. The measured peak absorption is 2.6 dB/m at 1532.5 nm. Then, the absorption and emission cross-sections σ_{abs} and σ_{ems} are determined by using Eq. 6.4 of Section 6.10. The resulting cross-sections are shown in Fig. 6.5.

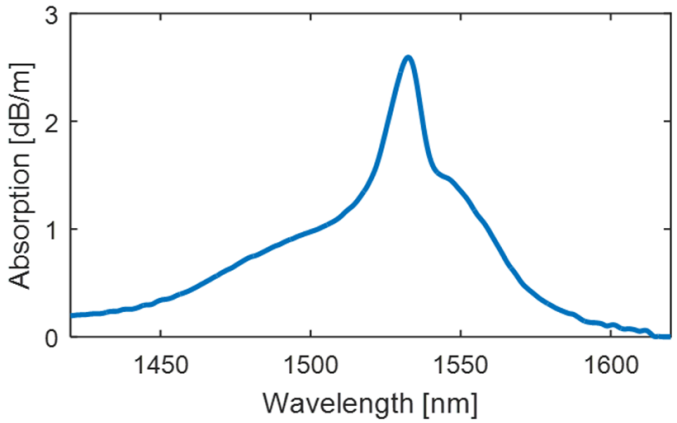

FIGURE 6.4 – Absorption coefficient spectrum when the light is injected in one of the cores of the multicore fiber with annular doping.

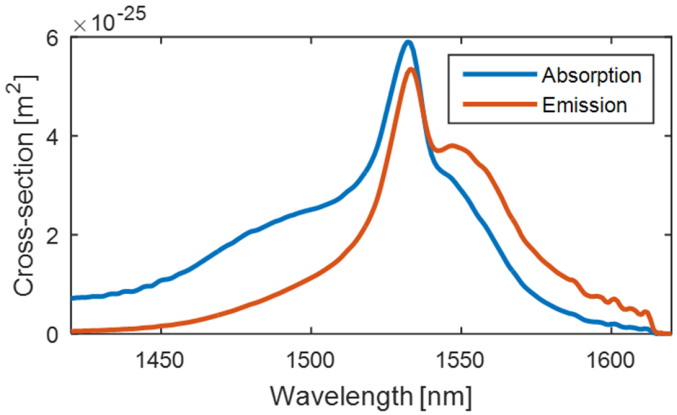

FIGURE 6.5 – Absorption and emission cross-sections as a function of wavelength of the multicore fiber with annular doping.

The absorption in the pump region was determined by using a supercontinuum laser source, filtered with a free-space 800 nm-1300 nm bandpass filter, injected into a passive multimode fiber (MMF). The MMF was first spliced to a tapered coreless fiber [116]. Then, the coreless fiber was rolled around the multicore fiber with the half-taper method [116] in order to couple the power into the cladding of the fiber. A bare fiber adapter was used at the output of the fiber to measure the output spectrum with an OSA. The measurement was first made with a fiber length of 20.0 m. Then, a cutback was done, and the measurement was repeated with a fiber length of 1.43 m. The difference between the measured spectra allowed to determine the absorption spectrum in dB/m (shown in Fig. 6.6). For this measurement, we assume that the

ratio of captured power by the OSA to total output power in the 140 µm fiber is the same in both measurements, before and after the cutback.

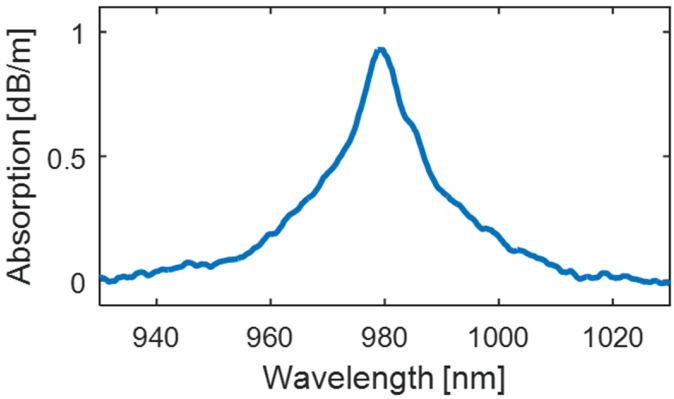

FIGURE 6.6 – Absorption spectrum when light is injected in the cladding of the multicore fiber with annular doping.

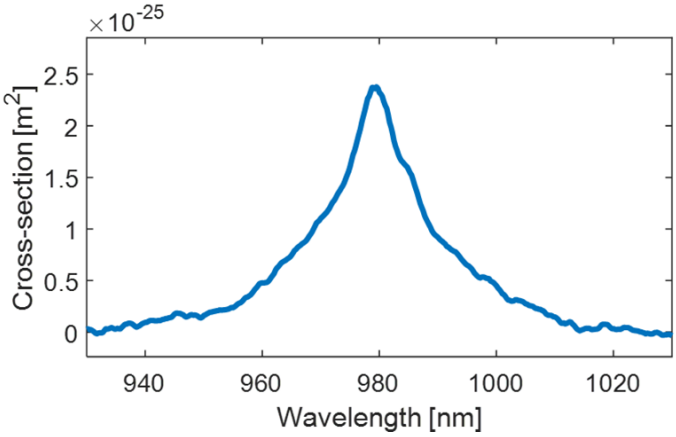

FIGURE 6.7 – Absorption cross-section used in the simulations.

Finally, the output spectrum of the 976-nm source (±4 nm according to the specification sheet) was measured with an OSA, by directing the pump source output in free-space to a black screen (power monitor) and capturing a fraction of the scattered power with the MMF (105/125 µm). The spectra, shown in Fig. 6.8, show significant variation as the pump current (power) is increased. The measured spectra will be considered in the simulations to determine the pump absorption taking into account these wavelength variations.

6.5 Gain and NF : single core characterization

In this section, we measure the gain and NF performances of the multicore fiber when only one core is loaded with input signal power and the output pump power when none of the cores is loaded. The goal is to extract the coupled pump power and propagation loss in the

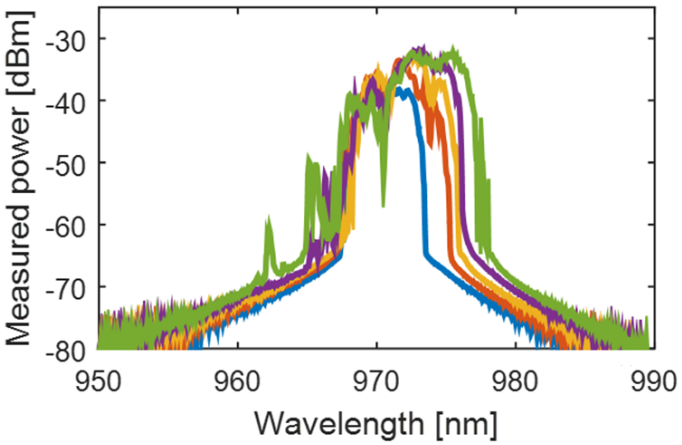

FIGURE 6.8 – Spectral content of the pump source used for the characterization of the multicore fiber with annular doping when the input current is set to 2.92 A (blue), 4.74 A (orange), 6.56 A (yellow), 8.38 A (violet) and 10.20 A (green).

cladding and the fraction of erbium ion pairs that will be used to simulate the gain and NF performances of the fiber.

To determine the gain and NF of the fiber, the setup shown in Fig. 6.9 was used. The tunable lasers and DWDM allow to generate a flat comb source that emulates eight channels distributed uniformly over the spectrum of interest (1528.8 nm, 1532.7 nm, 1539.2 nm, 1543.7 nm, 1549.3 nm, 1554.9 nm, 1559.8 nm and 1563.9 nm) and the variable optical attenuator (VOA) controls the input signal power. One of the cores of the fiber under test (FUT), which is the multicore fiber with annular doping, is spliced to commercial single mode fibers (SMFs) at both ends with an active alignment using a 1550 nm source. Using a 1550 nm source for the alignment is possible with cores having an annular doping geometry due to the low absorption resulting from the small overlap between the LP_{01} mode and the doped region. During fusion splicing, a low temperature was maintained by doing several short duration electrical arcs to limit mechanical distortion of the fibers. The FUT was uncoated over 15 cm near the input splice to make an unfused half-taper pump combiner with the half-taper method [116]. A pump dump was made by uncoating the FUT over 5 cm near the output splice and then applying a high index polymer. The polymer was cured and placed between two metal groves to allow for passive cooling.

The initial length of the FUT was 19.4 m. After measuring the gain and NF for various pump powers at this fiber length (FL), the fiber was cut back to 16.8 m and 14.2 m. The output splice and pump dump steps were repeated as described previously before measuring the gain and NF at these new fiber lengths (FL).

Afterwards, the fiber was cut to 11.1 m, 8.0 m, 5.0 m, 3.0 m, 2.01 m, 1.05 m, 0.68 m and 0.44 m and the setup shown in Fig. 6.10 was used to measure the output pump power. A

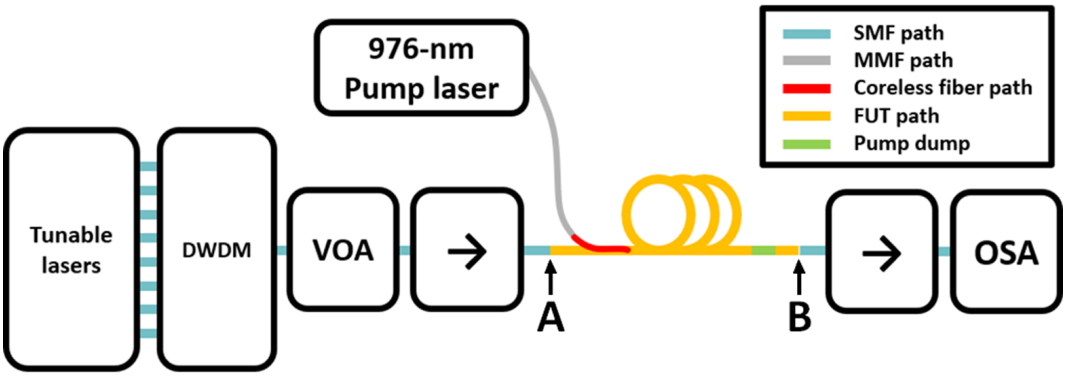

FIGURE 6.9 – Setup used to characterize the gain and NF of one of the cores on the multicore fiber with annular doping.

pump dump was applied over 2 cm, near the input splice, to minimize pump reflections. A high power (max 30 W) free space power meter (PM) calibrated at 976 nm was used for this measurement. The measured output pump power is shown in Fig. 6.11.

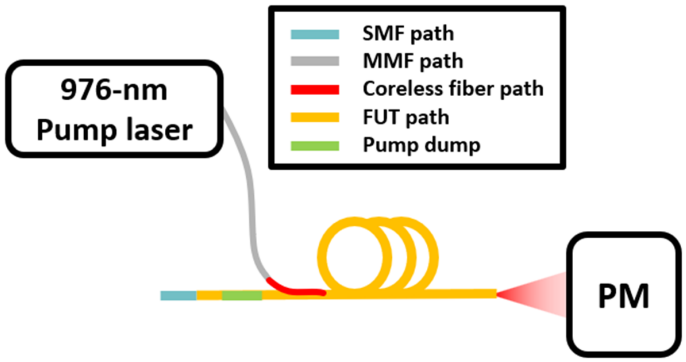

FIGURE 6.10 – Setup used to measure the output pump power (cladding pumping) when none of the cores are loaded.

The measured internal gain and NF for the fiber lengths of 14.2 m, 16.8 m, and 19.4 m are shown in Fig. 6.12 and Fig. 6.13. The measured insertion loss was 1.2 dB between the two APC connectors located at the output of the first isolator (A in Fig. 6.8) and the input of the second isolator (B in Fig. 6.8), leading to an estimated splice loss of 0.6 dB between the SMF and the FUT. This could be caused, in part, by mode mismatch and the necessity to maintain a low temperature during fusion splicing to prevent mechanical distortions. The theoretical minimal transmission loss between the mode profile shown in Fig. 6.3 and an ideal gaussian with a mode-field diameter (MFD) of 10.4 µm is 0.4 dB.

In Fig. 6.11, Fig. 6.12 and Fig. 6.13, the measurement results are compared with simulations to validate the simulation parameters used in the numerical model. Some of the model parameters could not be measured directly and were swept to find the best fit. The injected pump power (5.2 W, 10.1 W, 14.9 W, 19.5 W and 24.0 W for the respective currents of 2.92 A, 4.74

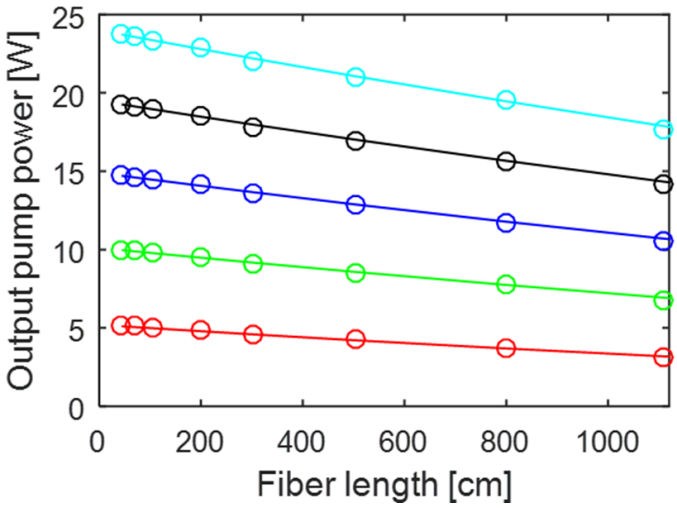

FIGURE 6.11 – Measured output pump power (cladding pumping) when none of the cores is loaded and the input current is set to 2.92 A (red), 4.74 A (green), 6.56 A (blue), 8.38 A (black) and 10.20 A (cyan).

A, 6.56 A, 8.38 A and 10.20 A) and pump background loss (0.012 m^{-1}) were adjusted by minimizing the maximum difference between measured and simulated output pump power results in Fig. 6.11. Note that we need to consider the ASE building up inside the unloaded cores in the simulations. When measured with an OTDR at 1310 nm, the background loss in the cladding was 0.010±0.001 m^{-1}, which is in good agreement with the value of the loss parameter extracted from the fit. We prefer to use the latter one in our simulations because, firstly, the OTDR measurement is performed at a different wavelength than the pump wavelength, and, secondly, the OTDR measurement is done by injection at the fiber end facet, which is likely to excite a different set of modes than the ones excited by pump injection on the side of the fiber. The fraction of paired ions γ_{Er} and the pump absorption, which considers the wavelength dependency of the pump source, were adjusted by minimizing the maximum difference between measured and simulated gain in Fig. 6.12. Note that the simulations assume that the input signal power is uniformly distributed over 36 channels between 1529 nm and 1564 nm.

Since the fraction of paired ions and pump absorption have a small impact on the output power results and since the pump background loss has a small impact on the gain results, we iteratively repeated each fit until all of the parameters have converged to a stable value. The final simulation results, represented by the curves in Fig. 6.11, Fig. 6.12 and Fig. 6.13, were all obtained with the same values for the injected pump power, pump background loss, fraction of paired ions and pump absorption.

When assuming uniform pump power intensity over the fiber cladding, converting the absorption spectrum of Fig. 6.6 to a cross-section spectrum with Eq. 6.4 leads to a peak cross-section, at 978 nm, of 3.2x10^{-25} m^2. However, to obtain an optimal fit, that minimizes the maximum

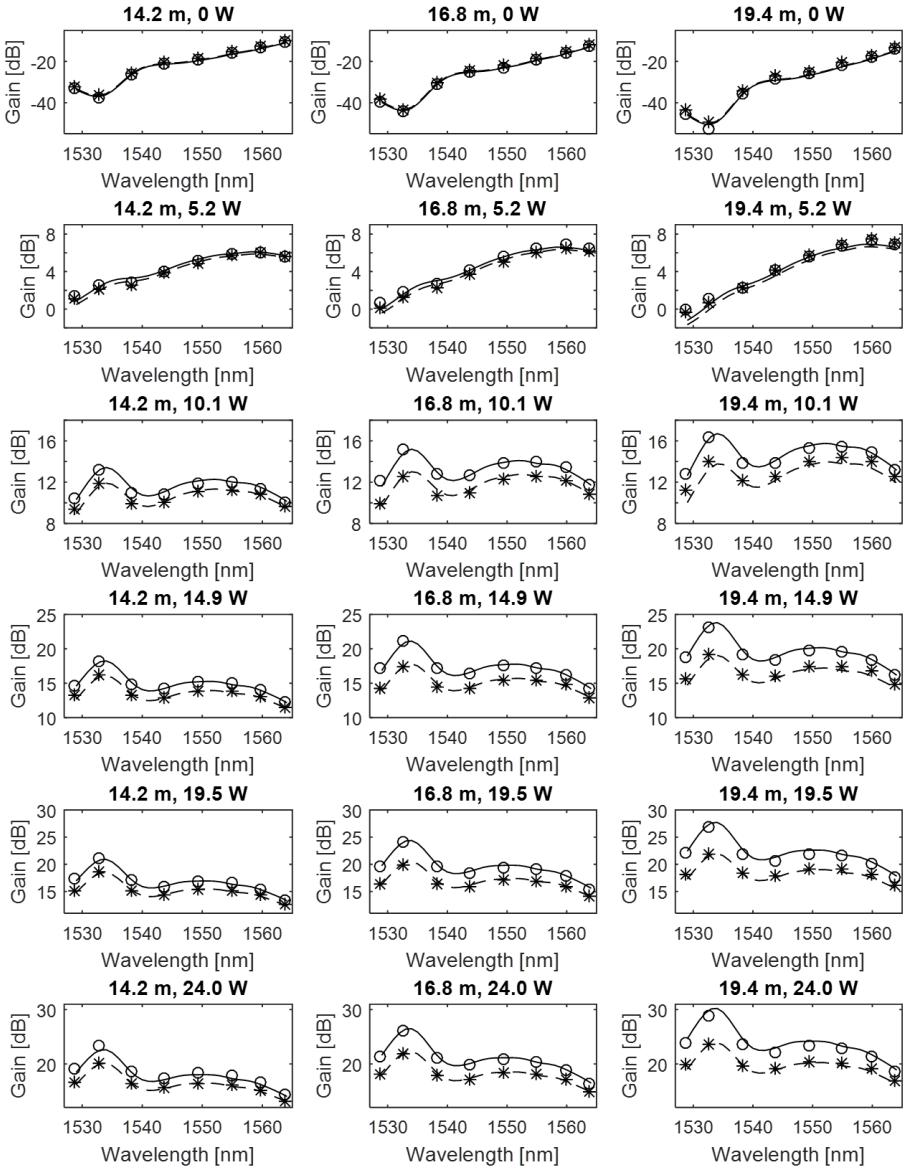

FIGURE 6.12 – Measurement (circles and asterisks) and simulation results (solid and dashed lines) for the internal gain of one of the eight cores when the seven other cores are not loaded for a fiber length of 14.2 m, 16.8 m and 19.4 m, and injected pump power of 0 W, 5.2 W, 10.1 W, 14.9 W, 19.5 W and 24.0 W. Results are shown for input signal power of -23.1 dBm (circles and solid lines) and 1.4 dBm (asterisks and dashed lines) in the loaded core.

difference between measured and simulated gain results in Fig. 6.12, the pump absorption measured in Section 6.4 had to be multiplied by a factor of 0.74. The calculated peak absorption cross-section is then estimated to be $2.4\text{x}10^{-25}$ m^2, as shown in Fig. 6.7, which is similar to values found in the literature [152; 153]. Additionally, the optimum fit was obtained when the fraction of paired ions was set to 7%. Since the pump absorption results from the overlap of all cladding modes with all the doped rings, this discrepancy could partly be due

to the assumption of uniform pump power over the cladding, the measurement sensitivity of $\Delta\rho_{Er} = 5\text{x}10^{24}$ ions/m^3 on the erbium doping concentration or the assumption of uniform erbium doping profile radially and longitudinally.

Figure 6.13 shows a good agreement between the simulated and measured NF with the exception of the experimentally measured NF with a length of 16.8 m. In this case, the higher value is most probably caused by a lower quality of output splice (in the single core characterization an off-axis splice is performed), which can lead to more feedback and coupling from the ASE cladding modes to the spliced SMF core.

In order to estimate the accuracy of the extracted parameter values for the fraction of paired ions and the pump background loss, we examined the sensitivity of the fit by varying one parameter and keeping other parameters of the model constant. Firstly, we investigated the accuracy of the fit for the fraction of paired ions by sweeping this parameter between 0% and 15% in order to determine the range for which the root mean square error (RMSE) between the simulation results and the 288 data points of experimentally measured gain, in dB, shown in Fig. 6.12, is lower than 1.0 dB. Our analysis showed that the RMSE is lower than 1.0 dB when the fraction of paired ions is between 5% and 9%. We then set the fraction of paired ions back to 7% and swept the value of pump background loss between 0.000 m^{-1} and 0.020 m^{-1} to determine the range for which the RMSE between the simulation results and the 40 data points of experimentally measured output pump power, in W, shown in Fig. 6.11 is lower than 0.2 W. Our analysis showed that the RMSE is lower than 0.2 W when the pump background loss is between 0.010 m^{-1} and 0.015 m^{-1}. Thus, we believe that the extracted fraction of paired ions and the extracted value of pump background loss are accurate within the above-mentioned intervals. Most importantly, the goal of extracting these parameters is to simulate the amplifier with sufficient precision so that the fiber length can be adequately determined under given input power conditions. Table 6.1 summarizes the experimentally determined parameters, which will be considered in the simulations.

6.6 Gain and NF : multicore prediction

In this section, we used the fiber parameters that were measured and validated in Section 6.4 and Section 6.5, to determine the required fiber length to meet the gain compression target of 6.9 dB when the total input signal power per core varies from -23.1 dBm to 1.4 dBm, simultaneously in all eight cores, and when the injected pump power is 24.0 W. According to our simulations results, a fiber length of 19.8 m is the optimum length, a longer fiber can provide higher gain with higher gain compression, whereas a shorter fiber meets the gain compression criteria but does not maximize the gain. When the input power varies between -23.1 dBm and 1.4 dBm, simulations show that this multicore amplifier should have a minimum gain of 16.4 dB, a maximum NF of 4.2 dB and a maximum gain compression of 6.9 dB according

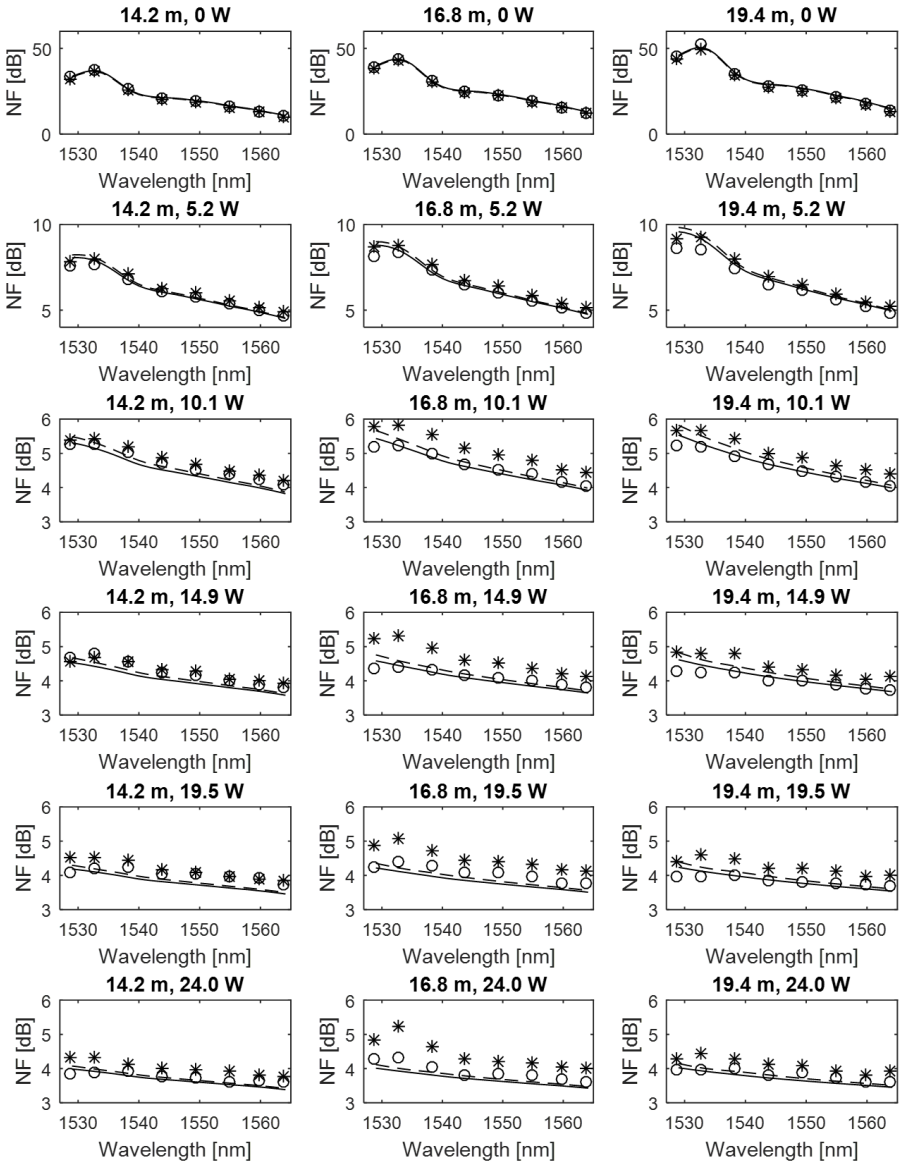

FIGURE 6.13 – Measurement (circles and asterisks) and simulation results (solid and dashed lines) for the internal NF of one of the eight cores when the seven other cores are not loaded for a fiber length of 14.2 m, 16.8 m and 19.4 m, and injected pump power of 0 W, 5.2 W, 10.1 W, 14.9 W, 19.5 W and 24.0 W. Results are shown for input signal power of -23.1 dBm (circles and solid lines) and 1.4 dBm (asterisks and dashed lines) in the loaded core.

to the simulations. The simulation results are shown in Fig. 6.14 and will also be compared with experimental results in Fig. 6.19 and Fig. 6.20.

Tableau 6.1 – Summary of the parameters used in the simulations

Symbol	Parameter	Value
r_{clad}	Cladding radius	70 µm
$\Gamma_{s,(\lambda,k)}$ $\Gamma_{ASE,(\lambda,k)}$	Overlap between each individual ring and the signal and ASE	Determined with COMSOL, using the refractive index profile in Fig. 6.3
$\Gamma_{p,(k)}$	Overlap between each individual ring and the pump	A_k/A_{clad}
$\sigma_{abs,s,(\lambda)}$ $\sigma_{ems,s,(\lambda)}$ $\sigma_{abs,ASE,(\lambda)}$ $\sigma_{ems,ASE,(\lambda)}$	Absorption and emission cross-sections for the signal and ASE	Fig. 6.5
$\sigma_{abs,p,(\lambda)}$	Absorption cross-section for the pump	Fig. 6.7
α_s α_{ASE}	Signal and ASE background loss	Negligible due to the short fiber length used
α_p	Pump background loss	0.012 m^{-1} (0.052 dB/m)
$\rho_{Er,(k)}$	Erbium doping concentration	Fig. 6.3
γ_{Er}	Percentage of paired ions	7%
τ_{Er}	Lifetime of the Er^{3+} upper level	10.4 ms
λ_p	Pump source wavelength	Fig. 6.8

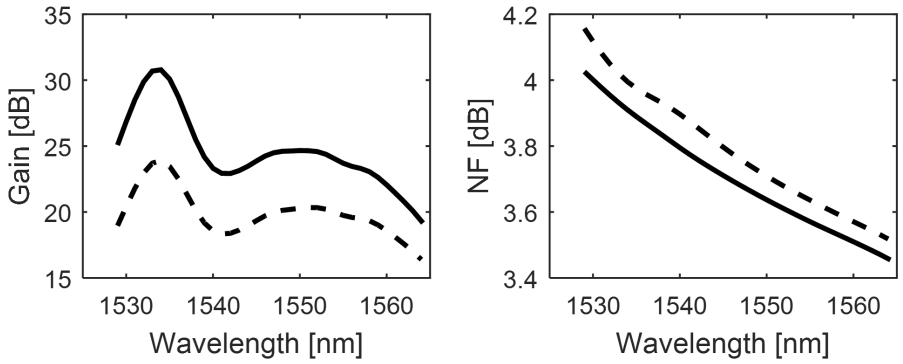

FIGURE 6.14 – Simulation results for the internal gain (left) and internal NF (right) of one of the eight cores when the seven other cores are loaded with the same input power for a fiber length of 19.8 m, an injected pump power of 24.0 W and input signal power of -23.1 dBm (solid lines) and 1.4 dBm (dashed lines) in all the cores.

6.7 Gain and NF : eight cores loaded results

In this section, we investigate the core-to-core variations of the fabricated multicore fiber which is a crucial factor to consider for practical applications.

For the eight cores loaded measurements, a custom tapered-fiber-based fan-in/fan-out (Chiral Photonics) was spliced to the 8-core fiber. The insertion loss was measured in each branch at 1650 nm and 1300 nm and the splice loss in each branch was estimated by taking the average

between of those two measurements. For cores #1 to #8, the insertion loss was 2.4 dB, 2.6 dB, 1.6 dB, 1.4 dB, 1.7 dB, 1.9 dB, 1.6 dB and 2.2 dB, from the fan-in inputs to the fan-out outputs. We assumed that half of the insertion loss was caused by the input splice and the other half was due to the output splice.

To measure the internal gain and NF, the setup shown in Fig. 6.15 was used. The signal power was measured at the output of each branch of the 1x8 coupler to pair the 1x8 coupler channels that have the lowest power with the fan-in/fan-out branches that have the lowest insertion loss. Therefore, when the amplifier was under the low signal power configuration, the signal input power for cores #1 to #8 was -23.3 dBm, -23.5 dBm, -23.3 dBm, -23.1 dBm, -22.9 dBm, -22.9 dBm, -22.9 dBm and -23.3 dBm. Under the high signal power configuration, the signal input power for cores #1 to #8 was 1.3 dBm, 1.1 dBm, 1.3 dBm, 1.5 dBm, 1.7 dBm, 1.7 dBm, 1.7 dBm and 1.3 dBm.

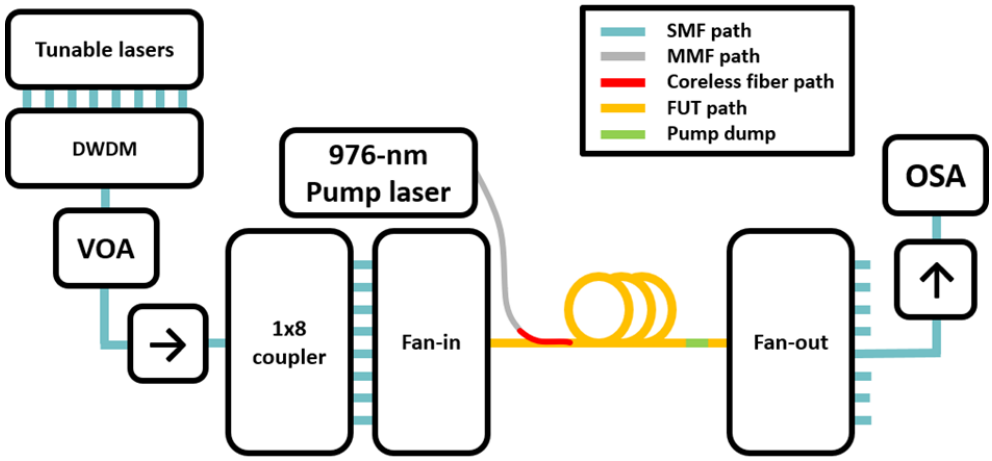

FIGURE 6.15 – Setup used to characterize the gain and NF of each of the cores when the multicore fiber with annular doping is fully loaded.

The input current of the pump source was set to 10.20 A, which did correspond to 24.0 W of injected pump power in the cladding in the single core characterization (section 6.5). In this experiment, the actual injected pump power could not be measured directly with the fan-in/fan-out. Thus, for the simulations, we will assume that the same coupling efficiency was reached during the eight loaded cores characterization than in the previous experiment (section 6.5).

The internal gain, NF and gain compression measurement results are shown in Fig. 6.16, Fig. 6.17 and Fig. 6.18. A significant gain difference can be observed in the case of core #8 (red), which could be caused by longitudinal variations on the refractive index profile over the preform used to fabricate the fiber. In fact, annular doping designs are very sensitive to variations of the core Δn (central region). Such variations can slightly modify the signal mode field diameter, which has a significant impact on the overlap between the signal mode and the

doped region. For core #8, a lower Δn could have caused an increase in the MFD compared to cores #1 to #7, which would explain the gain difference shown in Fig. 6.16. Among all the results, the minimum gain was 15.3 dB and the maximum NF was 5.4 dB.

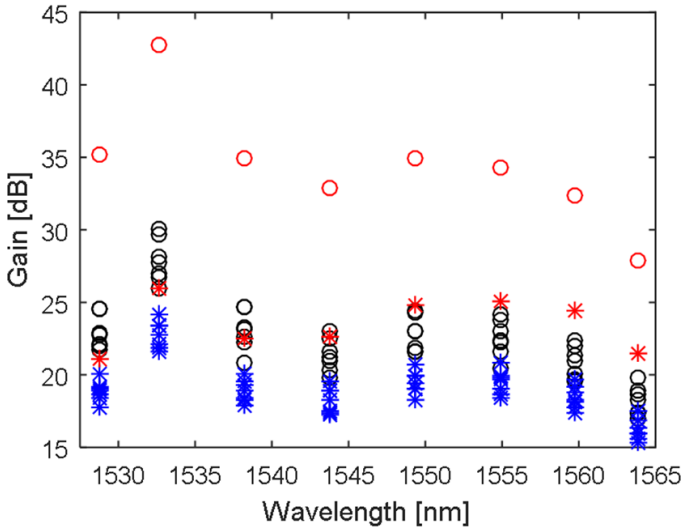

FIGURE 6.16 – Measurement results for the internal gain of each of the eight cores (#1 to #7 in black and blue, #8 in red) when all cores are loaded with an input signal power of -23.2±0.3 dBm (circles, black or red) and 1.4±0.3 dBm (asterisks, blue or red) for a 19.8 m fiber length and an injected pump power of 24.0 W.

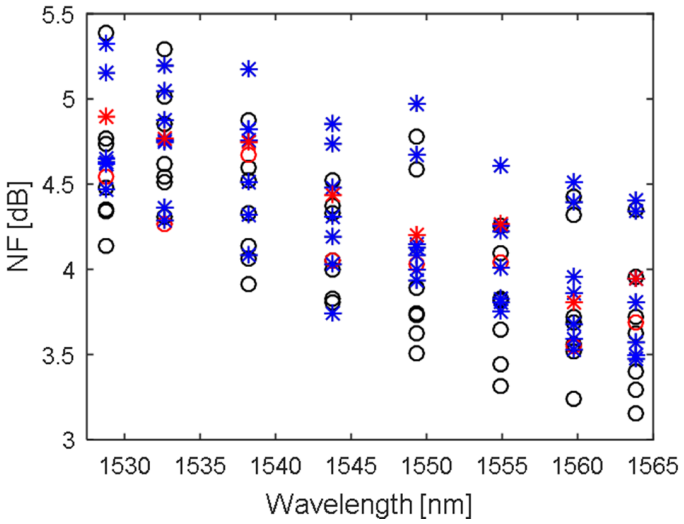

FIGURE 6.17 – Measurement results for the internal NF of each of the eight cores (#1 to #7 in black and blue, #8 in red) when all the cores are loaded with an input signal power of -23.2±0.3 dBm (circles, black or red) and 1.4±0.3 dBm (asterisks, blue or red) for a fiber length of 19.8 m and an estimated injected pump power of 24.0 W.

In Fig. 6.19 and Fig. 6.20, we discarded the results of core #8 to compare the gain and NF measurement results from cores #1 to #7 with the simulation-based performance predictions

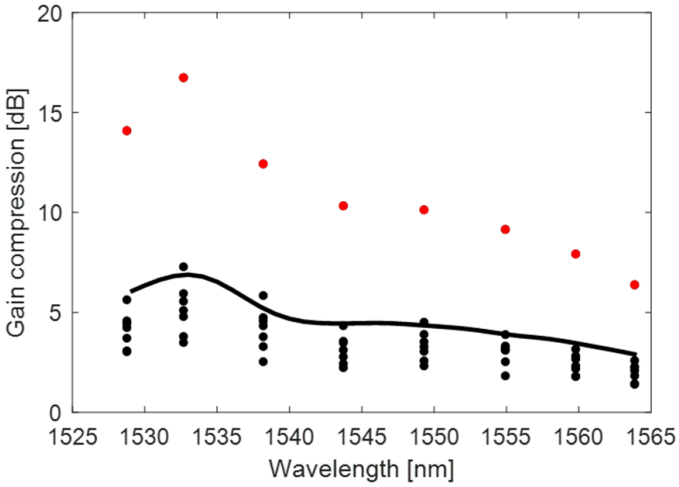

FIGURE 6.18 – Measurement (dots) and simulation (line) results for the gain compression of each of the eight cores (#1 to #7 in black, #8 in red) when all the cores input signal power increases from -23.2±0.3 dBm to 1.4±0.3 dBm for a fiber length of 19.8 m and an estimated injected pump power of 24.0 W.

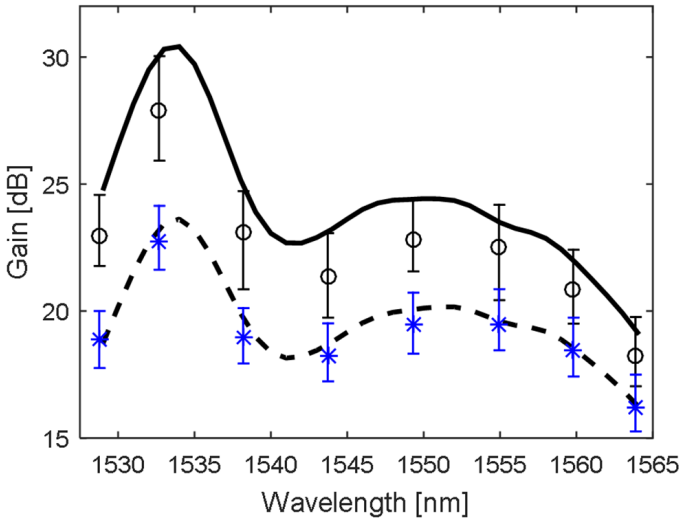

FIGURE 6.19 – Measurement (circles and asterisks with error bars) and simulation (solid and dashed lines) results for the internal gain of cores #1 to #7 when all the cores are loaded with an input signal power of -23.2±0.3 dBm (black circles and solid line) and 1.4±0.3 dBm (blue asterisks and dashed line) for a fiber length of 19.8 m and an estimated injected pump power of 24.0 W.

shown in Fig. 6.14, which used the previously determined fiber parameters extracted in Section 6.4 and Section 6.5. The error bars indicate the minimum and maximum measured values and the circles and asterisks indicate the average of all the measured values, in dB, for the seven remaining cores. The lower than expected gain results could be caused by a lower pump coupling efficiency into the cladding of the fiber compared to the single core characterization results.

Since no marker was used to visually distinguish cores, the exact core correspondence between the single core results and the eight loaded cores results is unknown. The higher NF observed in Fig. 6.20 can also be observed with the single core characterization results in Fig. 6.13 and could be explained by the presence of ASE guided inside the cladding [17]. The results indicate that the maximum core-to-core gain variation is 4.1 dB between core #4 and core #6, at 1532.7 nm, when all eight cores are in the unsaturated condition (P_s = 23.2±0.3 dBm).

Finally, it is worth mentioning that, when removing the signal power in cores #2 to #8, the maximum absolute gain variation in core #1 was smaller than 0.3 dB over all the channels (max[$|\Delta G(\lambda_s)|$] < 0.3 dB). This indicates that the inter-core cross-gain modulation is small compared to the other gain compression effects in the fiber.

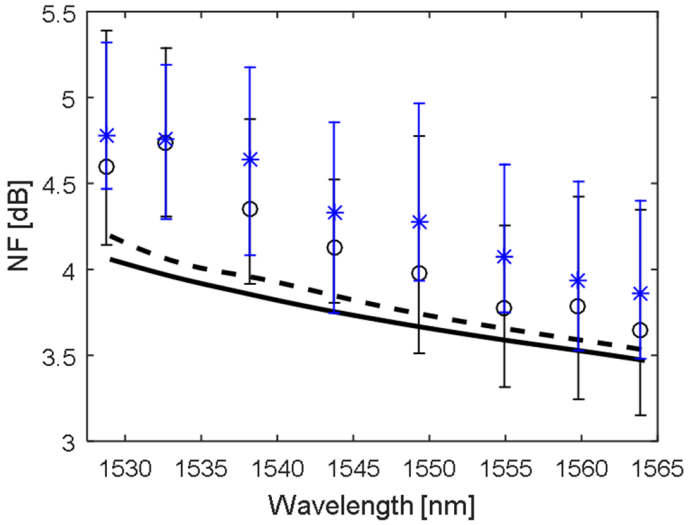

FIGURE 6.20 – Measurement (circles and asterisks with error bars) and simulation (solid and dashed lines) results for the internal NF of cores #1 to #7 when all the cores are loaded with an input signal power of -23.2±0.3 dBm (black circles and solid line) and 1.4±0.3 dBm (blue asterisks and dashed line) for a fiber length of 19.8 m and an estimated injected pump power of 24.0 W.

6.8 Gain sensitivity to refractive index profile variations analysis

The main factor that could have contributed to the significant gain difference in core #8 is the Δn of the central part of the core. Assuming that all other parameters are kept constant, we determined that decreasing the Δn within the 3 µm radius central region of the core by 14% allowed increasing the mode overlap with the doped region as shown in Fig. 6.21, leading to the simulation and experimental gain agreement shown of Fig. 6.22 for core #8. These results show the sensitivity of the gain of fibers with annular doping to the refractive index profile variations.

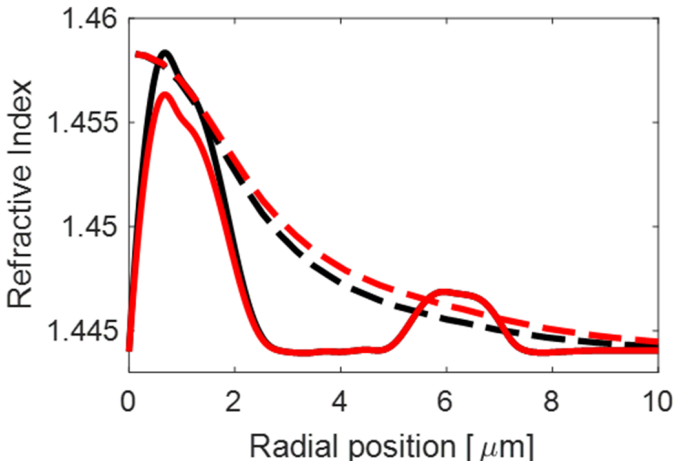

FIGURE 6.21 – Refractive index profile (solid lines) and calculated LP_{01} mode field profile (dashed lines) of the fabricated fiber cores with (red) and without (black) applying a -14% Δn adjustment on the central region of the core.

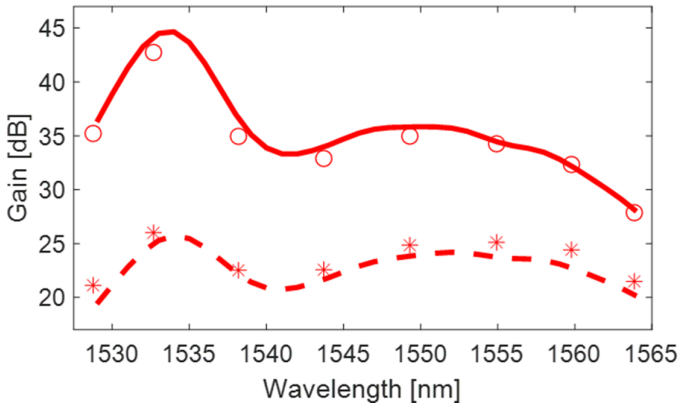

FIGURE 6.22 – Measurement (circles and asterisks) and simulation (solid and dashed lines) results for the internal gain of core #8 when all the cores are loaded with an input signal power of -23.2±0.3 dBm (circles and solid line) and 1.4±0.3 dBm (asterisks and dashed line) for a fiber length of 19.8 m and an estimated injected pump power of 24.0 W when a 14% Δn adjustment is applied on the central region of the core when calculating the signal mode profile used in the simulations with COMSOL.

To further validate this hypothesis, we also compared the absorption measurements for all the cores when the pump source is turned off (0 W of injected pump power) with simulation results under the same conditions. The results are shown on Fig. 6.23. The absorption for core #8 could not be determined experimentally at 1528.8 nm and 1532.7 nm because of the noise floor of the OSA.

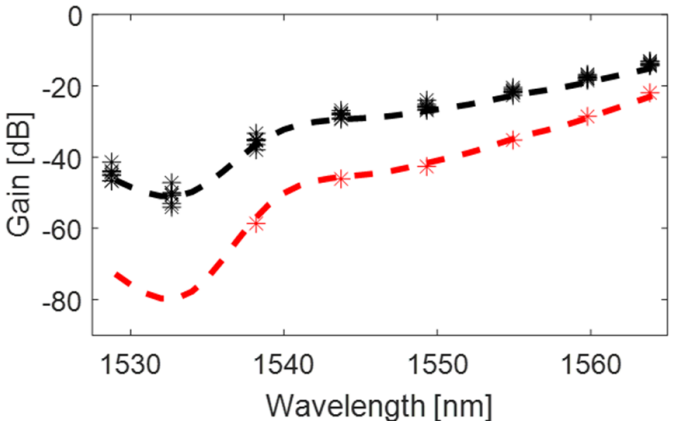

FIGURE 6.23 – Measurement (asterisks) and simulation (dashed lines) results for the internal gain of cores #1 to #7 (black) and core #8 (red) when all the cores are loaded with an input signal power of 1.4±0.3 dBm for a fiber length of 19.8 m and an injected pump power of 0 W assuming a 14% Δn adjustment applied on the central region of the core #8 when calculating the signal mode profile used in the simulations with COMSOL.

6.9 Conclusion

Despite significant core-to-core gain variations due to the sensitivity of the signal mode overlap with respect to refractive index profile variations, the results indicate that annular doping designs are a promising technique to achieve low gain compression in cladding-pumped multicore fibers. The refractive index profile could be improved through further process development as this fiber was fabricated in-house from a single preform. For example, with core #4, a minimum gain of 15.6 dB, a maximum NF of 5.0 dB and a maximum gain compression of only 3.8 dB was achieved for input signal power that varies between -23.1 dBm and 1.5 dBm. Therefore, with future improvement to the fiber fabrication technique to reduce core-to-core gain variations, we believe that doped fibers with annular doping are very promising for terrestrial applications requiring low gain compression. Furthermore, according to our simulations in Section 6.11, annular doping could also be advantageously exploited to improve the PCE in cladding-pumped amplifiers.

6.10 Appendix I

The model used for the numerical simulations is based on the standard radially resolved two-level model for EDFAs with the power propagation and population rate equations presented in [154; 155; 156], to which we add the terms describing erbium ion pairs [123]. The fiber cross section is divided into rings with a 0.1 µm thickness that cover the 0 µm – 8.0 µm region (80 rings).

In Eq. 6.1-6.3, P_p, P_s and P_{ASE} are the pump, signal and ASE power, $\sigma_{abs,p}$, $\sigma_{abs,s}$ and $\sigma_{abs,ASE}$

are the pump, signal and ASE absorption cross-sections, $\sigma_{ems,s}$ and $\sigma_{ems,ASE}$ are the signal and ASE emission cross-sections, Γ_p, Γ_s and Γ_{ASE} are the overlap between each individual ring and the pump, signal and ASE modes, ν_p, ν_s and ν_{ASE} are the frequencies associated with each pump, signal and ASE channels and α_p, α_s and α_{ASE} is the pump, signal and ASE background loss. Presence of indices m, λ_i or k are indicators of a core, wavelength or radial dependency, respectively. Also, A_k is the area of each individual ring, h is Planck constant, γ_{Er} is the percentage of paired ions, τ_{Er} is the lifetime of the Er^{3+} upper level $^4I_{13/2}$ and ρ_{Er} is the erbium concentration. W_{13}, W_{12} and W_{21} are the $^4I_{15/2} \rightarrow {}^4I_{11/2}$, $^4I_{15/2} \rightarrow {}^4I_{13/2}$ and $^4I_{13/2} \rightarrow {}^4I_{15/2}$ transition rates. This model assumes instantaneous transfer from $^4I_{11/2}$ to $^4I_{13/2}$, so that the population level densities are n_1, n_2 and 0 for $^4I_{15/2}$, $^4I_{13/2}$ and $^4I_{11/2}$. Finally, n_2^s and n_2^p represent the densities of single and paired erbium ions in the Er^{3+} upper level $^4I_{13/2}$.

The absorption and emission cross-sections σ_{abs} and σ_{ems} are determined by McCumber relations [157; 99]. In Eq. 6.4, $\alpha_{(\lambda_i)}$ is the absorption spectrum, $\rho_{Er,(k)}$ is the doping concentration in ring k, $\Gamma_{(\lambda,k)}$ is the wavelength dependent power confinement in ring k, k_B is Boltzmann's constant, h is Planck's constant, T is the temperature and ϵ the temperature-dependent excitation energy.

$$
\begin{cases}
\frac{\mathrm{d}P_p(z)}{\mathrm{d}z} = -\left(\sum_{m=1}^{M}\sum_{k=1}^{K}\sigma_{abs,p}n_{1,(m,k)}(z)\Gamma_{p,(k)}\right)P_p(z) - \alpha_p P_p(z) \\
\frac{\mathrm{d}P_{s,(m,\lambda_i)}(z)}{\mathrm{d}z} = \left(\sum_{k=1}^{K}\sigma_{ems,s,(\lambda_i,k)}n_{2,(m,k)}(z)\Gamma_{s,(\lambda_i,k)} - \sum_{k=1}^{K}\sigma_{abs,s,(\lambda_i,k)}n_{1,(m,k)}(z)\Gamma_{s,(\lambda_i,k)}\right)P_{s,(m,\lambda_i)}(z) \\
\qquad -\alpha_s P_{s,(m,\lambda_i)}(z) \\
\frac{\mathrm{d}P^{\pm}_{ASE,(m,\lambda_i)}(z)}{\mathrm{d}z} = \left(\sum_{k=1}^{K}\sigma_{ems,ASE,(\lambda_i,k)}n_{2,(m,k)}(z)\Gamma_{ASE,(\lambda_i,k)}\right)2h\nu_{ASE,(\lambda_i)}\Delta\nu_{ASE,(\lambda_i)} - \alpha_{ASE}P^{\pm}_{ASE,(m,\lambda_i)} \\
+\left(\sum_{k=1}^{K}\sigma_{ems,ASE,(\lambda_i,k)}n_{2,(m,k)}(z)\Gamma_{ASE,(\lambda_i,k)} - \sum_{k=1}^{K}\sigma_{abs,ASE,(\lambda_i,k)}n_{1,(m,k)}(z)\Gamma_{ASE,(\lambda_i,k)}\right)P^{\pm}_{ASE,(m,\lambda_i)}(z)
\end{cases}
\tag{6.1}
$$

$$
\begin{cases}
n^s_{2,(m,k)}(z) = \frac{W_{13,(k)}(z)+W_{12,(m,k)}(z)}{W_{13,(k)}(z)+W_{12,(m,k)}(z)+W_{21,(m,k)}(z)+\frac{A_k}{\tau_{Er}}}\left(\rho_{Er,(k)}(z)\cdot(1-2\gamma_{Er})\right) \\
n^p_{2,(m,k)}(z) = \frac{W_{13,(k)}(z)+W_{12,(m,k)}(z)}{2\left(W_{13,(k)}(z)+W_{12,(m,k)}(z)\right)+W_{21,(m,k)}(z)+\frac{A_k}{\tau_{Er}}}\left(\rho_{Er,(k)}(z)\cdot(2\gamma_{Er})\right) \\
n_{2,(m,k)}(z) = n^s_{2,(m,k)}(z) + n^p_{2,(m,k)}(z) \\
\rho_{Er,(k)}(z) = n_{1,(m,k)}(z) + n_{2,(m,k)}(z)
\end{cases}
\tag{6.2}
$$

$$\begin{cases} W_{13,(k)}(z) = \frac{\sigma_{abs,p,(k)}\Gamma_{p,(k)}}{h\nu_p} P_p(z) \\ W_{12,(m,k)}(z) = \sum_i \frac{\sigma_{abs,s,(\lambda_i,k)}\Gamma_{s,(\lambda_i,k)}}{h\nu_{s,(\lambda_i)}} P_{s,(m,\lambda_i)}(z) + \sum_i \frac{\sigma_{abs,ASE,(\lambda_i,k)}\Gamma_{ASE,(\lambda_i,k)}}{h\nu_{ASE,(\lambda_i)}} P_{ASE,(m,\lambda_i)}(z) \\ W_{21,(m,k)}(z) = \sum_i \frac{\sigma_{ems,s,(\lambda_i,k)}\Gamma_{s,(\lambda_i,k)}}{h\nu_{s,(\lambda_i)}} P_{s,(m,\lambda_i)}(z) + \sum_i \frac{\sigma_{ems,ASE,(\lambda_i,k)}\Gamma_{ASE,(\lambda_i,k)}}{h\nu_{ASE,(\lambda_i)}} P_{ASE,(m,\lambda_i)}(z) \end{cases} \tag{6.3}$$

$$\begin{cases} \sigma_{abs,(\lambda_i)}[m^2] = \frac{\alpha_{\lambda_i}[dB/m]}{(10\log_{10} e)\sum_k \rho_{Er,(k)}[ions/m^3]\Gamma_{\lambda_i,k}} \\ \sigma_{ems,(\lambda_i)}[m^2] = \sigma_{abs,(\lambda_i)}[m^2] e^{(\epsilon - hc/\lambda_i)/k_B T} \\ \epsilon = \frac{hc}{1537.5nm} \end{cases} \tag{6.4}$$

6.11 Appendix II

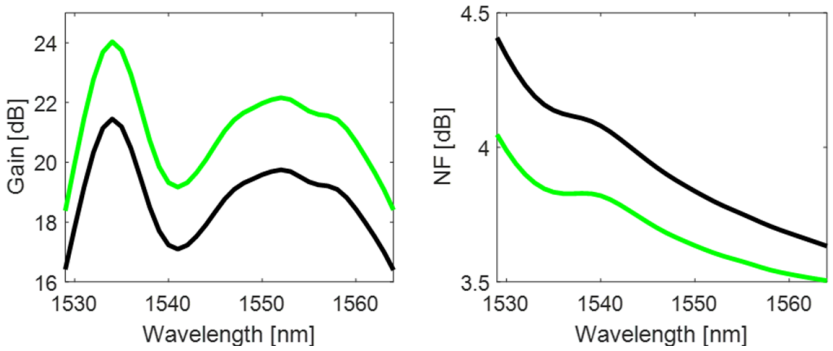

FIGURE 6.24 – Simulation results for the internal gain (left) and internal NF (right) when the pump source wavelength is 973 nm (black) and 978 nm (green). Each of the eight cores is loaded with 5.0 dBm of input power, injected pump power is 24.0 W and the fiber length is 23.1 m (black) and 26.0 m (green).

The higher saturation power that can be reached with cladding-pumped fibers with annular doping could also allow to increase the PCE compared to core-doped cladding-pumped fibers. To validate this, we fixed the input power to 5.0 dBm per core and swept the fiber length to obtain the same gain for the channels located at both ends of the spectral range of interest. The resulting minimum gain and PCE were 16.4 dB and 8.2% and the required fiber length was 23.1 m. Then, instead of considering the pump source that we characterized and presented in Fig. 6.8, we repeated the numerical simulations by considering an ideal pump source that would be centered on the erbium absorption peak of this fiber (≈978 nm). Under these conditions,

the required fiber length now becomes 26.0 m and the resulting minimum gain and PCE are 18.4 dB and 14.0%. Fig. 6.24 shows the gain and NF profiles for both of these scenarios. To our best knowledge, the current record for PCE in full C-band cladding-pumped amplifiers is 10.2%, achieved with a coupled-core configuration with 12 cores and a cladding diameter of 90 µm [158]. These results suggest that a properly engineered annular doping design could improve the PCE in cladding-pumped amplifiers.

6.12 Acknowledgment

The authors are grateful to N. Grégoire, S. Morency, P. Larochelle, S. Levasseur and N. Landry for their help regarding the fiber fabrication and characterization. The authors would also like to thank N. K. Fontaine, R. Ryf and H. Chen for multiple advice and insights throughout the duration of the project. This work was supported by NSERC and Nokia through a partnership grant (RDCPJ5155551-17).

Chapitre 7

Concentric layers with heterogeneous doping for cladding-pumped L-band fiber amplifiers

C. Matte-Breton[1], L. Wang[2], F. Maes[2], Y. Messaddeq[1], et S. LaRochelle[1]

[1]COPL, Université Laval, Québec QC, G1V 0A6, Canada
[2]Huawei Technologies Canada, 2475 Boul. Laurier, suite 100, Québec QC, G1T 2X3, Canada

Présenté à la conférence Photonics West 2022. [159]

7.1 Résumé

Le pompage par la gaine dans les amplificateurs optiques a récemment suscité un intérêt croissant dans le contexte des amplificateurs multicoeurs. L'utilisation de fibres multicoeurs dopées à l'erbium (EDF) peut réduire la complexité des sous-systèmes d'amplification car elle permet le pompage avec une seule diode laser multimode de haute puissance pour plusieurs canaux d'amplification parallèles dans la gaine d'une seule et même fibre. En raison de la plus faible intensité de pompage dans les amplificateurs pompés par la gaine, une inversion de population élevée est plus difficile à réaliser par rapport aux amplificateurs pompés par le coeur, ce qui favorise les applications en bande L plutôt qu'en bande C. Les différents designs d'amplificateurs à fibre pompée par gaine qui ont été proposés pour amplifier la bande L ont tendance à utiliser soit un dopage homogène à l'erbium, soit un co-dopage homogène à l'erbium-ytterbium dans le coeur. Dans cet article, nous démontrons qu'une combinaison soigneusement conçue de couches dopées à l'erbium (Er) et de couches co-dopées à l'erbium-ytterbium (Er/Yb) dans un seul coeur (couches concentriques hétérogènes de dopage) peut améliorer l'efficacité de conversion de puissance (PCE) par rapport aux designs utilisant un

dopage homogène.

L'idée principale derrière cette investigation est d'utiliser ce degré de liberté supplémentaire dans le cadre du design afin de mieux contrôler l'inversion de la population des ions d'erbium le long de la fibre, ce qui aide à minimiser l'émission spontanée amplifiée et augmente ainsi la PCE. Grâce à des simulations numériques, nous comparons la PCE et le facteur de bruit (NF) de quatre types de géométries de dopant homogènes dans le coeur (Er annulaire, Er/Yb annulaire, Er central et Er/Yb central) avec des designs utilisant des couches concentriques hétérogènes de dopant. Pour tous les scénarios, la géométrie de dopant et la longueur des fibres sont soigneusement optimisées afin de maximiser le PCE. La puissance du signal à l'entrée, la puissance de la pompe à l'entrée, la direction de propagation de la pompe, le profil d'indice de réfraction et les autres paramètres non liés au dopage sont maintenus constants pour tous les scénarios.

7.2 Abstract

Cladding pumping in optical amplifiers has recently seen rising interest in the context of multi-core amplifiers. The use of multicore erbium-doped fibers (EDFs) can decrease the complexity of amplifier subsystems since it allows pumping with a single high-power multimode laser diode for multiple parallel amplification channels in the same fiber cladding. Due to the lower pump intensity in cladding-pumped amplifiers, high population inversion is harder to achieve compared to core-pumped amplifiers, which favors L-Band applications over C-Band applications. The various designs of cladding-pumped fiber amplifiers that have been proposed to amplify the L-Band tend to use either homogeneous erbium doping or homogeneous erbium/ytterbium co-doping in the core. In this paper, we demonstrate that a carefully engineered combination of erbium (Er) doped layers and erbium-ytterbium (Er/Yb) co-doped layers in a single core (concentric layers with heterogeneous doping) can improve the power conversion efficiency (PCE) compared to homogeneous doping designs.

The main idea behind this investigation is to use this additional degree of freedom in the design to better control the erbium ion population inversion along the fiber, which helps to minimize the amplified spontaneous emission and thus increases the PCE. Through numerical simulations, we compare the PCE and noise figure (NF) of four types of homogeneous doping geometries in the core (annular Er, annular Er/Yb, central Er and central Er/Yb) with a design based on concentric layers with heterogeneous doping. For all the scenarios, the doping geometry and fiber length are carefully optimized to maximize the PCE. The input signal power, input pump power, pump propagating direction, refractive index profile and other not-doping-related parameters are kept constant for all the scenarios.

7.3 Introduction

Cladding pumping is a promising way to decrease complexity in communication networks because it allows replacing multiple independent singlecore erbium-doped fiber amplifiers (EDFAs) by a single multicore erbium-doped fiber amplifier (MC-EDFA) that requires only a single multimode laser diode pump source [144; 13; 145; 58; 108]. However, when pump power is distributed over the cladding, a much higher total pump power is required to reach the same pump intensity over the doped region [62; 146; 101]. For this approach to become economically viable for C-band applications, comparatively to the multiple independent singlecore EDFAs solution, the lower saturation output power and the lower PCE caused by this lower pump intensity, which also leads to degradation of the NF, must be overcome. In C-band amplifiers, ring doping has been proposed as a means to decrease saturation effects in cladding-pumped EDFAs because it allows to place erbium ions in a region of the fiber where the signal intensity is low [101].

Instead of fighting the saturation of cladding-pumped amplifiers, as required for their use in the C-band, cladding pumping can be advantageously used in applications where high saturation is required. For example, cladding pumping has been investigated for L-band amplifiers [58; 160; 161], an application where a lower inversion level of the Er population is needed. L-band amplifiers are therefore inherently more compatible with cladding pumping than C-band amplifiers.

However, to our best knowledge, the optimization of the doping type and geometry for cladding-pumped L-band fiber amplifiers has not yet been investigated in details. In this paper, we compare the performances of the six core types shown in Fig. 7.1. Core types A and B use Er doping only, core types C and D use Er/Yb co-doping only and core types E and F consider heterogeneous designs where concentric layers of Er doping and Er/Yb co-doping are placed in the same core.

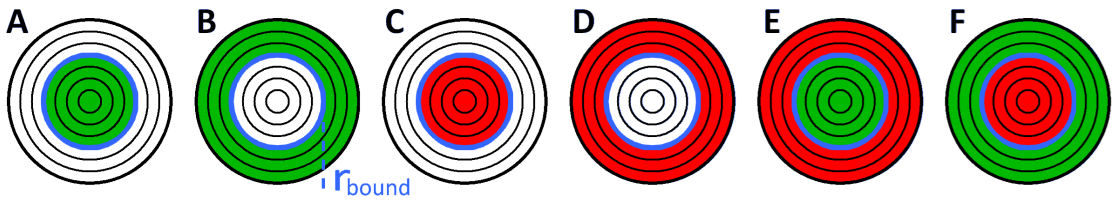

FIGURE 7.1 – Schematic representation of the six core types considered. Green regions correspond to Er doping and red regions correspond to Er/Yb co-doping. Schematics A, B, C and D represent fibers with homogeneously doped region (either Er or Er/Yb), and schematics E and F are fibers with heterogeneous doping. The cores are divided in two regions with a boundary of radius r_{bound} (blue) that is varied in the numerical simulations.

Due to the important costs related to fiber fabrication, this paper uses a numerical model to compare the different fiber types. In fact, these simulation results aim to determine the

optimized doping geometry of a cladding-pumped L-band amplifier, with maximized PCE, compatible with fabrication constraints. In this respect, we only consider designs in which the core is separated in two concentric regions, rather than more complex doping profiles.

7.4 Numerical model

We developed a numerical model that calculates the gain and noise figure of EDFAs and Er/Yb co-doped fiber amplifiers (EYDFAs). The model considers Er/Yb co-doping with the energy level diagram illustrated in Fig. 7.2. We use the rate equations presented in Ref. [162] with the added assumption that the upconversion of the erbium ions and the energy back-transfer from erbium to ytterbium can be neglected. The model assumes an azimuthal symmetry but provides radial resolution of the doping concentrations and inversion levels. In the simulations, the fiber core is divided in discrete annular regions, such as in Ref. [75], called radial elements. The model includes erbium and ytterbium ASE. When simulating EDFAs, the ytterbium doping concentration is simply set to 0. The model also considers the overlap $\Gamma_{s,k}$ between the signal mode and each radial element k.

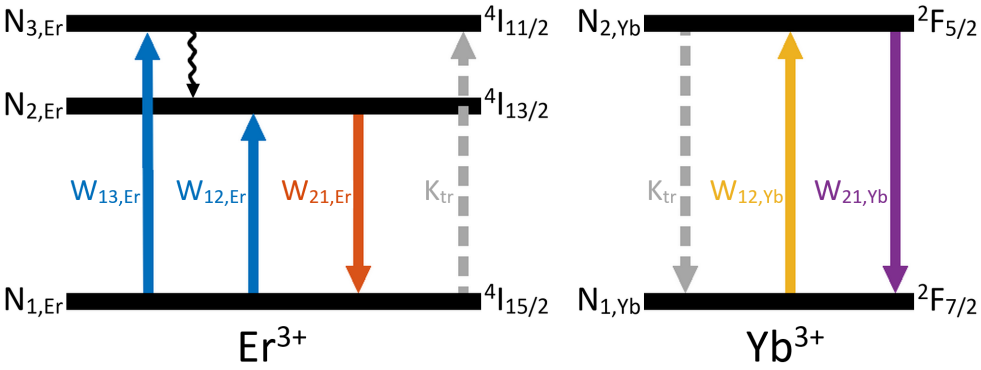

FIGURE 7.2 – Simplified energy level diagram of the Er^{3+} :Yb^{3+} system in oxide glasses. $W_{13,Er}$, $W_{12,Er}$ and $W_{21,Er}$ are the transition rates between the energy levels of the erbium ions, $W_{12,Yb}$ and $W_{21,Yb}$ are the transition rates between the energy levels of the ytterbium ions and K_{tr} is the transition rate from the ytterbium ions to the erbium ions.

7.5 Fiber parameters

For each core type shown in Fig. 7.1, the simulations will consider an ideal step-index fiber with a core radius of $r_{core} = 3.5\,\mu m$ and a Δn of 10×10^{-3}. The signal mode intensity profile is computed with COMSOL and shown in Fig. 7.3. The core is divided into 35 radial elements of 0.1 µm, which are each assumed to overlap with the pump power by a factor of A_k/A_{clad} where A_k is the ring area and A_{clad} is the area of the fiber cladding that has a diameter of 125 µm.

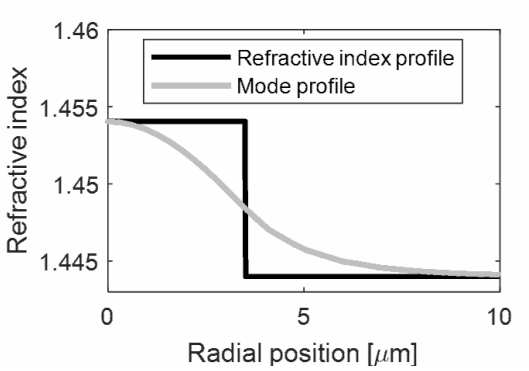

FIGURE 7.3 – Refractive index profile (black) and signal mode intensity profile (a.u., grey) considered in the simulations.

The erbium and ytterbium absorption ($\sigma_{Er,abs}$, $\sigma_{Yb,abs}$) and emission ($\sigma_{Er,ems}$, $\sigma_{Yb,ems}$) cross-sections are shown in Fig. 7.4. The erbium cross-sections were measured on an erbium doped aluminophosphosilicate fiber made in-house and the ytterbium cross-sections were extracted from the datasheet of a commercial Er/Yb fiber made by CorActive (DCF-EY-6/128). The erbium absorption and emission cross-sections are assumed to be the same whether or not ytterbium ions are present.

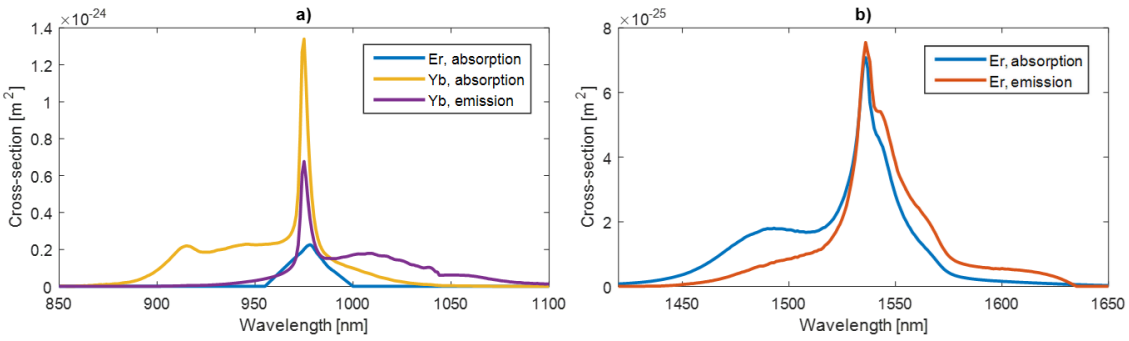

FIGURE 7.4 – Erbium and ytterbium absorption and emission cross-sections considered in the simulations. The absorption cross-sections over the pump wavelength bands are shown in a), and the emission and absorption cross-section over the signal wavelength band are shown in b).

Each core type shown in Fig. 7.1 is divided into two distinct regions r = 0 µm to r = r_{bound} and r = r_{bound} to r = r_{core}. In Fig. 7.1, the delimitation at r = r_{bound} is represented by a blue circle. In the red regions (Er/Yb), the ytterbium doping concentration ρ_{Yb} is set to 34.0×10^{25} ions/m^3 and the erbium doping concentration ρ_{Er} is set to 2.0×10^{25} ions/m^3. In the green region (Er only), the ytterbium doping concentration is set to 0 ions/m^3 and the erbium doping concentration is again set to 2.0×10^{25} ions/m^3. Finally, in the white regions (no doping), the ytterbium doping concentration is set to 0 ions/m^3 and the erbium doping concentration is also set to 0 ions/m^3.

In the simulations, the cladding pump wavelength λ_p is set to 980 nm for core types A and B, which is where the peak absorption of the erbium is located. For core types C, D, E and F, however, a lower wavelength of 915 nm is used due to the very high ytterbium absorption near 980 nm, which would lead to a very quick depletion of the pump over a fiber length that would not allow for an optimal L-band amplification of the signal.

The total signal power P_s is set to 5.0 dBm and is assumed to be distributed uniformly over 44 channels between 1575 nm and 1618 nm (λ_s), which corresponds to a resolution of one channel per nm. Also, the pump power P_p is set to 3.0 W and is assumed to be injected inside the cladding, uniformly distributed over the cladding area and propagating in the same direction as the signal. Also, the lifetime of the Er^{3+} and Yb^{3+} upper metastable levels τ_{Er} and τ_{Yb} are set to 10.4 ms and 1.5 ms and the energy-transfer rate from ytterbium to erbium, K_{tr}, is set to 1×10^{-22} m^3/s. The pump and signal background loss, α_p and α_s, are set to 0.009 m^{-1} and 0.001 m^{-1} respectively. The parameters used for the simulations are summarized in Table 7.1.

7.6 Simulation results

In the numerical simulations, for each of the six core types, r_{bound} is swept from 0.0 µm to 3.5 µm with steps of 0.1 µm. For each value of r_{bound}, the fiber length L is swept and the value that minimizes the gain difference of the 1579 nm and 1618 nm channels is selected. The condition of equal gain between these two wavelengths is used to identify the length required to have an average inversion condition that provides a flat gain over the spectrum of interest. The amplifier performance is then evaluated at this fiber length. The achieved minimum gain and noise figure as a function of the radius of the boundary between the two regions are shown in Fig. 7.5 and Fig. 7.6 for each core type, at the optimal fiber length. It is worth noting that we only plot the results for the values of r_{bound} for which it is possible to reach a gain difference <0.1 dB between the 1579 nm and 1618 nm channels with a fiber length between 1 m and 100 m.

The simulation results indicate that a fiber length longer than 100 m would be required to obtain a flat gain for fiber types A, B, C and D when $r_{bound} < 1.1$ µm, $r_{bound} > 2.7$ µm, $r_{bound} < 1.4$ µm and $r_{bound} > 2.7$ µm, respectively. For core types E and F, which correspond to the heterogeneous designs, a flat gain could simply never be reached, no matter the fiber length, when $r_{bound} > 2.5$ µm and $r_{bound} < 1.7$ µm, respectively, due to the high amount of unexcited erbium ions in the erbium-doped region compared to the amount of excited erbium ions in the Er/Yb co-doped region, which does not allow sufficient average inversion of the erbium ions inside the fiber to obtain a flat gain. Another interesting behaviour that can only be observed for core type E, when r_{bound} is equal to 2.4 µm or 2.5 µm, is the dramatic increase of NF (up to 8.2 dB at $r_{bound} = 2.5$ µm). This effect is caused by the fact that, again, the amount of unexcited ions in the erbium-doped region is too high to allow any significant

Tableau 7.1 – Summary of the parameters used in the simulations

Symbol	Parameter	Value
L	Fiber length	Swept : [1.00, 100.00] m
r_{bound}	Radius of the boundary between two regions with different doping types	Swept : [0.0, 3.5] µm
r_{clad}	Radius of the cladding	62.5 µm
$\Gamma_{s,k}$	Overlap between the signal mode and each radial element k	Fig. 7.3
$\Gamma_{p,k}$	Overlap between the pump power and each radial element k	A_k/A_{clad}
$\sigma_{Er,abs}, \sigma_{Er,ems}$	Absorption and emission cross-sections of the erbium ions	Fig. 7.4
$\sigma_{Yb,abs}, \sigma_{Yb,ems}$	Absorption and emission cross-sections of the ytterbium ions	Fig. 7.4
r_{core}	Radius of the core	3.5 µm
P_p	Input pump power	3.0 W
P_s	Input signal power	5.0 dBm
ρ_{Er}	Erbium doping concentration	2.0×10^{25} ions/m^3
ρ_{Yb}	Ytterbium doping concentration	34.0×10^{25} ions/m^3
λ_p	Pump wavelength	A and B : 980 nm C, D, E and F : 915 nm
λ_s	Signal wavelength	1575 nm – 1618 nm
K_{tr}	Transition rate from the ytterbium ions to the erbium ions	1×10^{-22} m^3/s
τ_{Er}	Lifetime of the Er^{3+} upper metastable level	10.4 ms
τ_{Yb}	Lifetime of the Yb^{3+} upper metastable level	1.5 ms
α_p	Pump background loss	0.009 m^{-1}
α_s	Signal background loss	0.001 m^{-1}

amplification over the first few meters of the fiber. However, since our model considers Er ASE guided in the fundamental mode of the core, both in C and L bands, this ASE builds up over the first few meters of the fiber until it is high enough to excite a significant amount of erbium ions located in the central region of the core. Therefore, a flat gain can be reached but this whole behaviour leads to higher ASE in the L-band compared to geometries where $r_{bound} \leq 2.3\,\mu m$.

Fig. 7.5 allows to conclude that, under the conditions specified previously, the optimal core design, assuming a homogeneous doping design (core types A, B, C or D) is core type C with $r_{bound} = 2.2\,\mu m$. This core design would allow to reach a minimum gain of 19.0 dB and a PCE of 8.3%. With a heterogeneous doping design (core types E and F), the optimal geometry is achieved with core type F and a boundary radius of $r_{bound} = 2.1\,\mu m$. This core design would allow to reach a minimum gain of 19.8 dB and a PCE of 10.0%, which is a

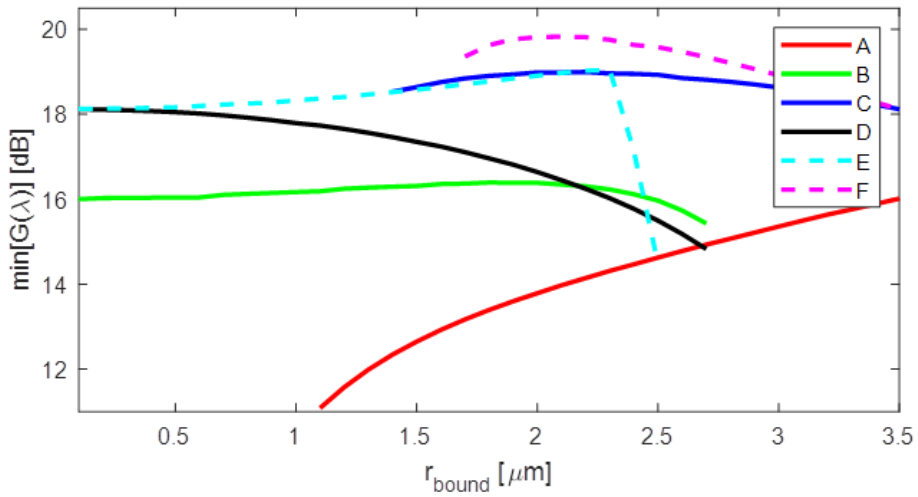

FIGURE 7.5 – Minimum gain over the spectral region of interest (1575 nm – 1618 nm) as a function of r_{bound} at the optimal fiber length for each doping profile under consideration. Fibers with only one type of doping (profile A-D) are shown by solid lines and fibers with heterogeneous doped regions (E-F) are shown by dashed lines.

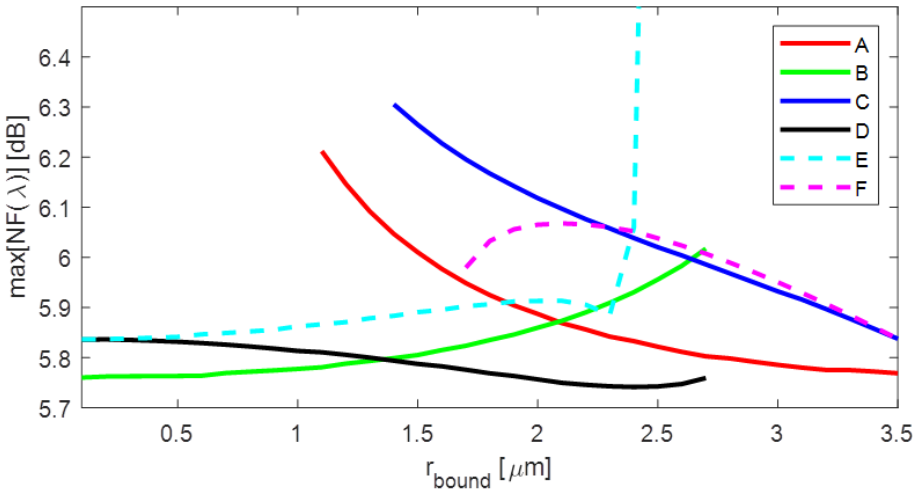

FIGURE 7.6 – Noise figure over the spectral region of interest (1575 nm – 1618 nm) as a function of r_{bound} at the optimal fiber length for each doping profile under consideration. Fibers with only one type of doping (core types A-D) are shown by solid lines and fibers with heterogeneous doped regions (E-F) are shown by dashed lines.

significant improvement compared to the optimal homogeneous design. For all core types, the PCE obtained for the optimal design (r_{bound} and L) are compared in Table 7.2.

The gain and NF spectrum for the best optimized homogeneous (type C) and heterogeneous (type F) designs are shown in Fig. 7.7. In Fig. 7.8, we trace the population inversion level as a

Tableau 7.2 – PCE for each core type when the optimal boundary radius and fiber length are used

Category	Core type	Minimum gain	PCE under optimal conditions	Noise figure at minimum gain
Homogeneous	A	16.0 dB	4.1%	5.8 dB
	B	16.4 dB	4.5%	5.8 dB
	C	19.0 dB	8.3%	6.1 dB
	D	18.1 dB	6.7%	5.8 dB
Heterogeneous	E	19.0 dB	8.4%	5.9 dB
	F	19.8 dB	10.0%	6.1 dB

function of the longitudinal position for each of the 35 individual radial elements for these two fibers, type C (blue) and type F (pink). This means that the blue trace is the superimposition of 22 lines, one for each radial element where doping is present. While the inversion level of the optimized fiber with a core type C seems to be quite uniform radially, the radial elements of the optimized fiber with a core type F can be divided into two distinct groups. The 21 inner radial elements, that contain ytterbium ions (from r = 0 to r = r_{bound} = 2.1 µm), have a significantly higher inversion level than the 14 outer radial elements which only contain erbium ions. In these amplifiers, the inversion level peak that can be observed at 5.3 m (core type F) and 8.6 m (core type C) in Fig. 7.8 is responsible for the local generation of a significant amount of ASE in the C-band which depletes the available pump power in the fiber. The higher PCE in fiber F is caused by the effect of the erbium ions located in the outer radial elements which act as a filter that locally absorbs ASE, thus recycling the pump power.

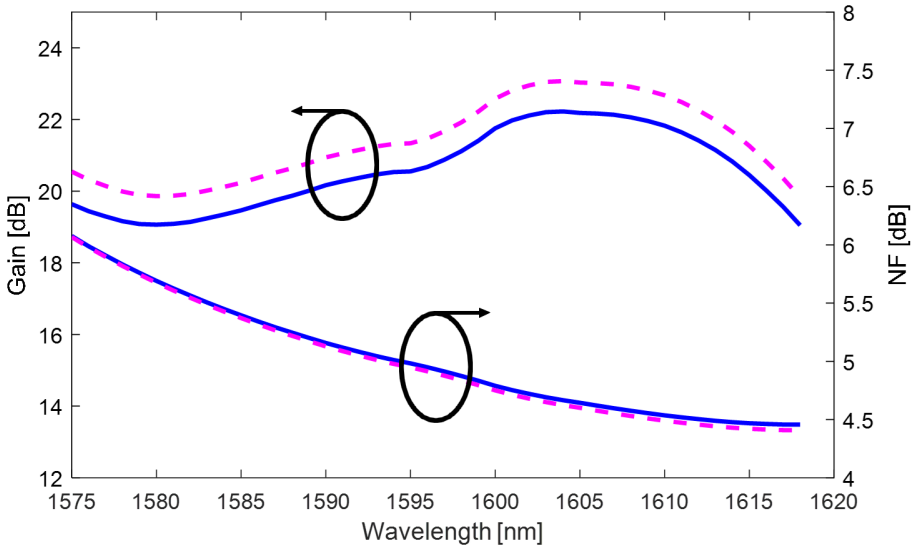

FIGURE 7.7 – Gain and NF spectrum for core types C (blue solid lines) and F (pink dashed lines) when r_{bound} and L are optimized to reach the highest possible minimum gain in the 1575 nm to 1618 nm spectral region.

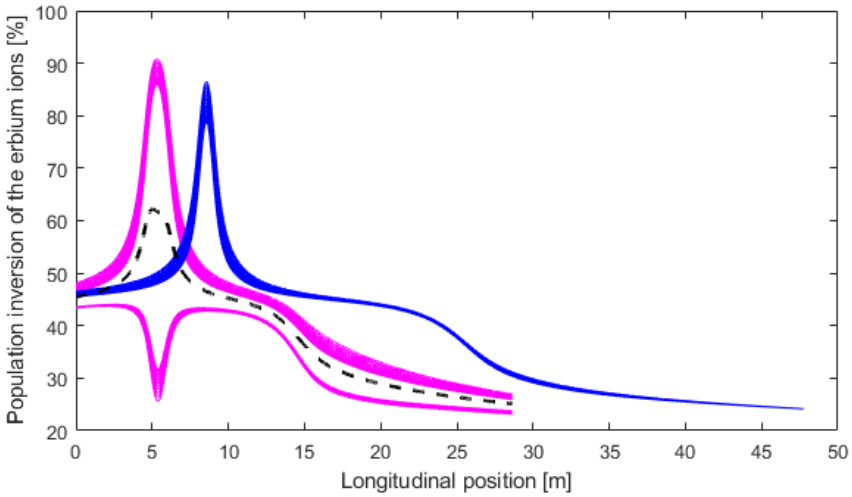

FIGURE 7.8 – Population inversion of the erbium ions as a function of the radial position for core types C (blue) and F (pink) when r_{bound} and L are optimized to reach the highest possible minimum gain in the 1575 nm to 1618 nm spectral region. The weighted average of the population inversion in core type F (black dashed line) is calculated using the overlap between the signal mode and each radial element k divided by the total overlap inside the core as a weight.

7.7 Conclusion

We proposed and showed, through numerical simulations, that using a heterogeneous doping design increases the PCE in cladding-pumped L-band amplifiers. In the specific conditions considered in this paper, heterogeneous doping design allows to increase the PCE to 10.0%, compared to 8.3% with the best homogeneous design. It is worth noting that the input signal power of 5 dBm is relatively high but corresponds to a typical requirement for the last stage of a multi-stage amplifier. This improvement can be explained by a region doped only with erbium ions that is present all along the fiber and that is pumped only through absorption of the C-band ASE. This region then contributes to L-band amplification, thus limiting the loss of available pump power due to ASE.

7.8 Acknowledgement

We would like to thank CorActive for the ytterbium cross-section data.

Chapitre 8

Large area Bragg grating for pump recycling in cladding-pumped multicore erbium-doped fiber amplifiers

C. Matte-Breton, L. Talbot, Y. Messaddeq, M. Bernier et S. LaRochelle

COPL, Université Laval, Québec QC, G1V 0A6, Canada

Publié dans Optics Express, Vol. **30**, no. 11, 17824-17835 (2022). [163]

8.1 Résumé

Nous démontrons pour la première fois qu'un réseau de Bragg peut être inscrit sur une grande surface à l'intérieur de la gaine d'une fibre amplificatrice multicoeur dopée à l'erbium pour augmenter l'efficacité de conversion de puissance en recyclant la puissance de la pompe à la sortie. Nos résultats indiquent qu'un réseau de Bragg couvrant ∼25% de la surface de la gaine permet de recycler 19% de la puissance de pompe à la sortie, menant ainsi à une augmentation relative de la PCE de 16% pour une puissance de pompe en entrée de 10,6 W dans le cas particulier de une fibre dopée à l'erbium à huit coeurs, d'une longueur de 20,3 m, et ayant un coeur chargé avec une puissance du signal à l'entrée de 1,5 dBm.

8.2 Abstract

We demonstrate for the first time that a Bragg grating can be written over a large area inside the cladding of a multicore erbium-doped fiber amplifier to increase the power conversion efficiency (PCE) by recycling the output pump power. Our results indicate that a Bragg grating covering ∼25% of the cladding area allows to recycle 19% of the output pump power which leads to a relative increase of the PCE by 16% for an input pump power of 10.6 W in the specific case of an eight-core erbium-doped fiber with a length of 20.3 m and one core loaded with an input signal power of 1.5 dBm.

8.3 Introduction

Cladding-pumped multicore erbium-doped fiber amplifiers (CP-MC-EDFAs) are a promising technology for cost-reduction in optical communication networks since they simultaneously provide gain to multiple cores, sharing the same cladding, with a single low-cost multimode pump laser diode having a high electrical to optical conversion efficiency. However, one of the main drawbacks for cladding pumping is the lower pump intensity in the doped core, compared to core pumping, due to the total pump power being distributed over the whole cladding area of the fiber. This lower pump intensity results in lower saturation output power that limit gain and bandwidth of CP-MC-EDFAs for C-band amplifiers. Consequently, high pump power must be used to maintain the inversion level of the erbium ions over the whole fiber length which leads to a high amount of unabsorbed output pump power. Therefore, achieving high power conversion efficiency (PCE), from the pump to the signal, can be challenging in cladding-pumped amplifiers in comparison to core-pumped ones.

To mitigate this drawback, higher core density [164], decreased cladding area [109], erbium-ytterbium co-doping [147] and an annular doping geometry [101] have all been proposed. Pump recycling has also been investigated and has been demonstrated in CP-MC-EDFAs by using a side-coupled pump collector [165], cascaded side-coupled pump collectors [166] or turbo cladding pumping with free space optics [73]. All these methods consist in using one or multiple pump collectors at the fiber output, and passive fiber loops, to route the pump power back to the input of the active fiber, recycling as much as 55.2% of the residual pump power [73]. The main drawbacks of these methods are the increased complexity due to the additional components and the corresponding additional input and output signal loss.

Another promising technology for pump recycling is to use inner-cladding Bragg gratings (ICBGs), which are all-fiber reflectors written directly in the cladding of cladding-pumped erbium doped fibers to reflect the pump. ICBGs have been previously used to recycle the unabsorbed pump light of single-core cladding-pumped high-power fiber lasers [167; 74]. For example, an ICBG with an effective reflectivity of 58% was inscribed at the end of a 29 W erbium-doped fiber laser emitting at 1.6 µm, which allowed to significantly increase the laser

efficiency [168]. This Bragg grating component only reflects light at the pump wavelength while letting through the laser light propagating inside the fiber core. The ICBGs also have the advantages of being able to handle high power, do not require additional components and leave the fiber tip free of any constraints. Therefore, increasing the PCE with such a component is a promising approach to shorten the required length of active fiber in fiber lasers and decrease the required pump power for amplifier systems. To our knowledge, ICBGs have not yet been investigated in the context of CP-MC-EDFAs that are currently being considered to increase spatial density in optical communication networks [61].

This paper aims to compare the PCE of a CP-MC-EDFA with and without an ICBG. To achieve this goal, in section 8.4, we first write such a grating covering ∼25% of the cladding area of a double-cladding 8-core fiber with annular doping, which was initially designed for low gain compression [129]. Then, in section 8.5, the internal gain and noise figure (NF) are measured experimentally with and without an ICBG and the resulting PCE is determined. Finally, in section 8.6, the experimental results are compared with simulations to estimate the effective percentage of reflected output pump power in the presence of ICBG. We find that the pump effective reflectivity reaches 19%, resulting in a PCE increase of 16%.

8.4 ICBG inscription

In this paper, the CP-MC-EDFA is based on the 8-core fiber extensively described in [129]. Each core, single mode in the C-band and undoped, is surrounded by an annular erbium-doped region located in the cladding. This design mitigates saturation effects since only the low intensity evanescent tail of the guided signal mode interacts with the doped region. Aluminophosphosilicate is used in the doped region of the cladding to reduce the refractive index change while limiting the percentage of paired ions [129]. The pure-silica cladding, surrounded by a low refractive index fluoroacrylate coating, has a NA of 0.46 and a diameter of 140 µm that make it viable for cladding pumping. The cores are placed along a ring with a radius of 2.3 µm and the distance between two cores is 38 µm as shown in Figure 8.1. In [129], a MC-CP-EDFA was assembled with this fiber. With a fiber length of 19.8 m and 24.0 W of pump injected in the cladding, the amplifier provided a gain >15.3 dB and a noise figure <5.4 dB over the C-band with all the cores loaded with 1.4±0.3 dBm. Under these conditions, it is estimated that 12.8 W of unused pump power exit the fiber at the amplifier output.

The ICBG was obtained by photo-inscribing a periodic refractive index modulation inside the fiber cladding. As pure silica is not photosensitive to standard UV illumination, we relied on the femtosecond laser inscription [169]. To this end, we used the setup shown in Figure 1 of reference [168], except for the capillary around the fiber that was not present in our case, and employed a Ti-Sapphire regenerative amplifier system (Astrella, Coherent Inc.) that emits 800 nm pulses at a repetition rate of 1 kHz. The laser beam was then frequency doubled

to 400 nm [170] using a BBO crystal (EKSMA optics, BBO 1502). The beam, which has a diameter of 11 mm, was afterwards sent through the fiber cladding [170] with an acylindrical lens having a 10 mm focal length. This allowed to reach sufficient light intensity inside the glass to induce a refractive index change by multiphotons absorption [171]. The interference pattern required to inscribe a periodic refractive index modulation was generated thanks to the use of the phase mask-scanning technique [172; 173]. An in-house fabricated phase mask, having a central period of 677.5 nm, was placed between the acylindrical lens and the fiber. It created an interference pattern in the spatial region where the diffracted ± 1 orders of the femtosecond beam overlapped with a period corresponding to half of that of the phase mask. Given the Bragg equation and the fiber's cladding refractive index, it inscribed an ICBG with a reflection peak centered at 981 nm. Such wavelength was chosen given the availability of a wavelength-stabilized laser diode emitting at that wavelength (BWT, model K981AN1RN-90.00W) which was used as the pump source for the CP-MC-EDFA. This wavelength is also close to the 979 nm peak absorption wavelength of the multicore fiber [129]. The phase mask was chosen with a period chirp rate of 1.2 nm/cm across its length of 3.5 cm. Given the highly multimode propagation of the pump light inside the cladding, a chirped ICBG is needed to cover a range of different effective refractive indices. In the present case, the ICBG covers effective refractive indices from 1.4432 to 1.4527, at the pump wavelength given the chirp rate of the phase mask and the 3.7 cm grating length. This chirp rate was chosen given the availability of this phase mask and because it was shown to optimize the reflectivity of ICBGs in a previous experiment, but with a different fiber-laser system [167]. In the future, optimizing the chirp rate for the specific NA of the fiber cladding and pump injection conditions, as described later, should increase the effective ICBG reflectivity.

Given the non-linear nature of photo-induced index change process in pure silica by fs writing at 400 nm, and the short focal length of the acylindrical lens, refractive index modifications occur only in the close vicinity of the laser beam focus. When focused at the center of the fiber, the beam induces a refractive index modulation over a depth of about 10 µm and a height of about 1 µm. Therefore, in order to increase the transverse area covered by the ICBG, and ultimately its reflectivity, the beam had to be scanned over the fiber cladding cross-section. To this end, the acylindrical lens of the writing setup was placed on a 2D piezoelectric stage allowing to move the focal point of the femtosecond beam. The piezoelectric actuator moving the height of the lens, was driven at a 1 Hz frequency with a peak-to-peak amplitude of 100 µm, while the other actuator moving the focus depth was driven at 0.133 Hz over the same amplitude. These different frequencies were chosen to focus pulses over the largest possible fraction of the fiber transverse area.

To write a grating of a few cm long, we used the phase mask scanning technique that consists in moving both the laser beam and the acylindrical lens along the fiber axis using a motorized translation stage, while the fiber and the phase mask remained still. During the 30-minute

inscription process, the beam was scanned over a fiber length of 2.6 cm that was stripped of its coating beforehand. This led to a 3.7 cm long ICBG when taking into account the 11 mm inscription beam diameter. Such a slow longitudinal scanning speed allowed to send multiple pulses at each grating position in the fiber cross-section so as to increase the refractive index modification. We used an average laser power of 190 mW, with a pulsewidth of 40 fs and a repetition rate of 1 kHz. Then, the short fiber segment containing the grating was thermally annealed at 475°C for 10 minutes with an oven as a standard procedure to reduce the photoinduced absorption losses. Finally, it was recoated with the same low-index polymer that was used during fiber drawing.

The cross-section of an ICBG inscribed in the 8-core fiber under the same conditions as the one tested with the amplifier is shown in Fig. 8.1. The grating only covers about ∼25% of the cladding area, which was determined by manually defining the grating and cladding areas in Fig. 8.1 and using an image processing software afterwards to count the number of pixels for each region. The area of ∼25% limits the maximum achievable ICBG reflectivity and means that the grating has a different effective reflectivity for each mode depending on their spatial overlap. The modes with higher n_{eff}, which are mainly confined into the center of the cladding, and thus less absorbed by the doped regions, are also likely to experience a stronger reflectivity. Furthermore, the ICBG cross-section has a conical shape due to the curvature of the fiber cladding. Given the large number of pump cladding modes, which includes both even and odd modes, this grating asymmetry can be helpful to reflect odd modes. As the laser beam is scanned perpendicularly to the fiber axis during the inscription process, the beam is refracted at different angles depending on its instantaneous height on the cladding that introduces a lensing effect. Also, noting that the writing process is a nonlinear phenomenon, regions where the focusing effect are the highest exhibit a stronger refractive index modulation as can be observed on the right of the ICBG in Fig. 8.1. This effect limits the maximum reachable ICBG area since these hot spots could induce signal losses if they overlapped a core. In the future, it could be circumvented by inserting the fiber inside a hollow capillary with an inner diameter slightly larger than the fiber cladding diameter and a significantly larger outer diameter, that has been shown to improve grating uniformity and increase the scanning area [168] or by using a different beam scanning technique [174], allowing to significantly increase the grating area and reflectivity.

The transmission spectrum of the ICBG is shown in Fig. 8.2. It was measured by injecting the light of a supercontinuum laser source (Koheras, NKT Photonics) inside a 1 m long fiber segment containing the grating and by using a bare fiber adapter to connect the output to an OSA. The power spectrum was measured before and after the ICBG inscription. It is worth noting that the free space optical input of the OSA has a NA of 0.105, which is significantly lower than the NA of the fiber cladding (0.46). Therefore, the transmittance shown in Fig. 8.2 only applies to the lower order cladding modes. An insertion loss of -3.7 dB is observed at

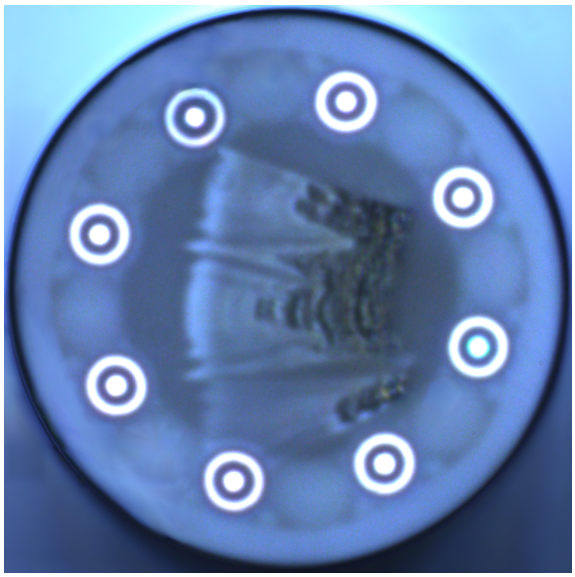

FIGURE 8.1 – Cross section of the 8-core fiber with an inner-cladding Bragg grating. It was measured with a phase-contrast microscope. The inscription laser beam is incident from the left.

981 nm from which we can deduce a maximum peak reflectivity of 57%. The transmittance above 0 dB observed near 950 nm and 1000 nm is due to the noise of the supercontinuum laser source used for this measurement. While no significant losses were measured for wavelengths outside of the Bragg resonance, it is possible that a fraction of this measured insertion loss could also be caused by coupling of the 981 nm light to some radiative modes, which was confirmed by observing the fiber with an infrared viewer.

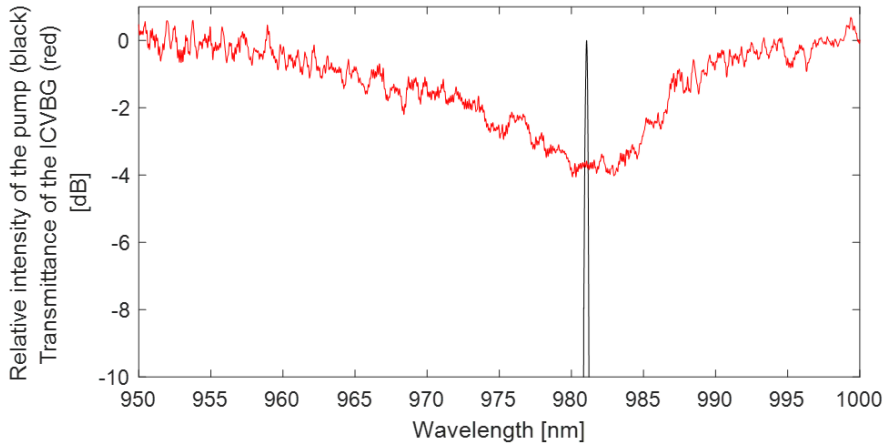

FIGURE 8.2 – Normalized spectral intensity of the 981-nm wavelength-controlled pump source for an output pump power of 10.0 W (black) and transmission spectrum of an ICBG written with the phase mask used for this investigation (red).

8.5 Gain and NF measurement results

In this section, we aim to determine the internal gain, NF and PCE of the CP-MC-EDFA in two distinct configurations : i) when an ICBG is used to recycle the pump power and ii) when the pump power is not recycled. To determine the internal gain and NF with and without the ICBG, we first did the measurements with an ICBG, for a doped fiber length of 20.3 m, as shown in Fig. 8.3. Then, we removed the last 0.7 m of doped fiber near the output, between points B and C in Fig. 8.3, which included the ICBG, and made a new output splice and pump dump to, afterwards, repeat the measurements without the ICBG with a doped fiber length of now 19.6 m. The total signal power was uniformly distributed over eight spectral channels generated by eight tunable lasers centered at 1528.8 nm, 1532.7 nm, 1539.2 nm, 1543.7 nm, 1549.3 nm, 1554.9 nm, 1559.8 nm and 1563.9 nm. For these measurements, only one of the cores was loaded with signal power. To identify the same core that was used for the single core characterization reported for this fiber in [129], the absorption at 1530 nm was measured in each of the 8 cores of the fiber under test (FUT). Using the same core was important considering that some of the parameters used in the simulations, namely the concentration of paired ions, could have core-to-core variations and were only measured in this core. Then, using an active alignment system, single-mode fibers (SMFs) were spliced to both ends of the FUT into the selected core and a total loss of 2.4 dB was measured between point A and B in Fig. 8.3a using a 1300 nm tunable laser. The variable optical attenuator (VOA) was then adjusted so that the total signal power at the input of the active fiber, when considering 1.2 dB of loss per SMF-FUT splice, was 1.5 dBm. Also, the pump power was coupled into the cladding of the FUT with an unfused half-taper [116] made by splicing a 105/125 µm fiber to a coreless pure-silica fiber that was tapered to obtain a downtaper length of 8.0 cm and a waist length of 2.5 cm. The pump coupling region is located 10 cm after the input splice. The achieved coupling efficiency was 93%±1% with the 981 nm wavelength-stabilized pump diode mentioned previously (BWT). To avoid damaging the isolators, cladding pump strippers were made at both ends of the FUT by applying high index polymer over 3 cm at the input and output of the fiber, directly next to the splices. It is also worth noting that the ICBG was located 55 cm before the output splice. The total fiber length for the FUT was 20.3 m. The gain and NF were measured when a current of 0.0 A, 1.3 A, 1.4 A, 1.5 A, 1.6 A, 1.7 A, 1.8 A, 1.9 A and 2.0 A was applied to the pump laser diode. Below, we show that these currents correspond to a coupled pump power of 0 W, 5.2 W, 5.9 W, 6.6 W, 7.4 W, 8.2 W, 9.0 W, 9.7 W and 10.6 W. The spectral gain and noise figure (NF) measurement results are shown in Fig. 8.4 and 8.5 (red circles).

After measuring the gain and NF with the setup configuration of Fig. 8.3, we cut the FUT 10 cm before the output splice, measured the output pump power with a free-space power meter, then cut the FUT 10 cm before the ICBG, for a new fiber length of 19.6 m and measured the output pump power again. The results, shown in Fig. 8.6, indicate that the transmittance

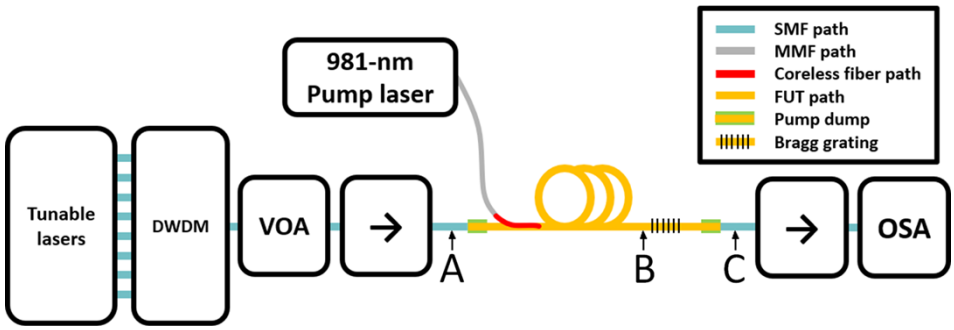

FIGURE 8.3 – Setup configuration used to measure the gain and NF with and without an ICBG.

of the ICBG at the pump wavelength is 40% on average, which is good agreement with the -3.7 dB observed at 981 nm in Fig. 8.2. We then made a new splice using an active alignment and the same splice recipe as previously, as well as a new pump dump right before the splice. To ensure a proper comparison, the input splice, VOA, and half-taper pump coupler were left untouched. The insertion loss at 1300 nm was measured again and, was also 2.4 dB for this configuration, indicating that the ICBG did not cause any significant degradation of the core signal. The gain and NF were then measured again for the same pump laser diode current setpoints. The results are also shown in Fig. 8.4 and 8.5 (black circles).

When all gain and NF measurements were completed, the FUT was cut 1.0 m after the pump coupler and we measured the exiting pump power with a free-space power meter. The input pump power was then estimated from these results, by multiplying the measured pump power by 1.012 to account for the pump background loss of 0.012 m^{-1} or 0.052 dB/m over 1.0 m of fiber length. This measurement allowed us to determine that the pump laser diode current setpoints used for the gain and NF measurements correspond to coupled pump power of 0 W, 5.2 W, 5.9 W, 6.6 W, 7.4 W, 8.2 W, 9.0 W, 9.7 W and 10.6 W.

Finally, the measured coupled pump power, input signal power and gain were used to calculate the PCE with and without an ICBG. The resulting PCE as a function of input pump power is shown in Fig. 8.7. Such low PCE can be explained by the fact that only one core was used, and the fiber length was not optimized. Nevertheless, the PCE is 23% higher in the configuration for which an ICBG was used compared to the configuration for which the pump was not recycled, when the input pump power was set to 10.6 W. It is however worth noting that a longer fiber length of 20.3 m, instead of 19.6 m, was used in the configuration with the ICBG. This aspect will be discussed in more details in the next section.

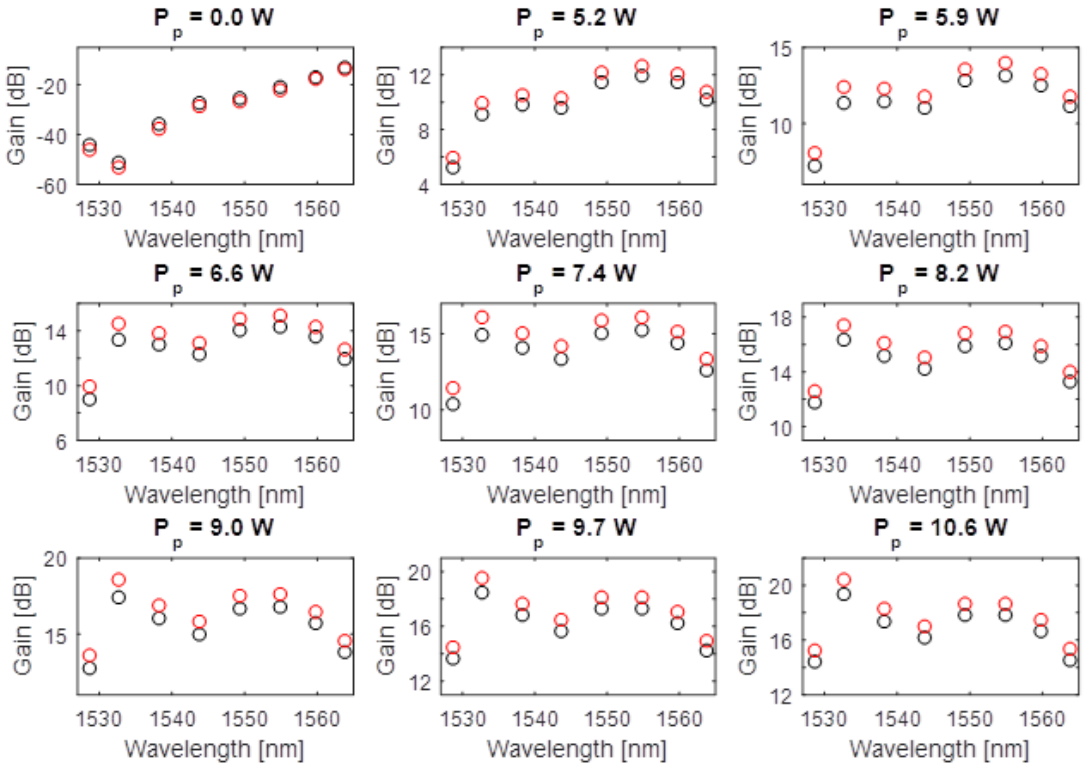

FIGURE 8.4 – Gain measurement results for a total input signal power of 1.5 dBm, and various input pump power ranging from 0 W to 10.6 W when i) an ICBG is used to recycle the output pump power (red) with a fiber length of 20.3 m and ii) when the pump is not recycled (black) with a fiber length of 19.6 m.

8.6 Simulation results and discussion

In this section, we first estimate the effective reflectivity of the ICBG by fitting spectral gain and NF simulations to the measurement results. We then determine the relative increase of the PCE caused by the ICBG for a fixed fiber length.

For the simulations, we first used the model and parameters determined in [129], namely, a pump background loss of 0.012 m^{-1}, a paired ions concentration of 7% and a pump absorption cross-section of 2.2×10^{-25} m^2 at 981 nm (for the latter see Fig. 8.7 of [129]). To have a better spectral resolution in the simulations, we consider 37 signal channels between 1528 nm and 1564 nm, for a resolution of 1 nm, and a total input signal power of 1.5 dBm. For the spectral gain, a good agreement was obtained between the simulation results and the experimental measurements without an ICBG with a root mean square error (RMSE) of 0.6 dB.

We then modified the model to also consider a contra-propagating pump power, uniformly distributed over the cladding, with an initial power equal to the output pump power of the co-propagating pump power times an effective reflectivity R. In the simulations, we assumed the pump power to be coupled into the fiber at the longitudinal position z = 0 m and to be

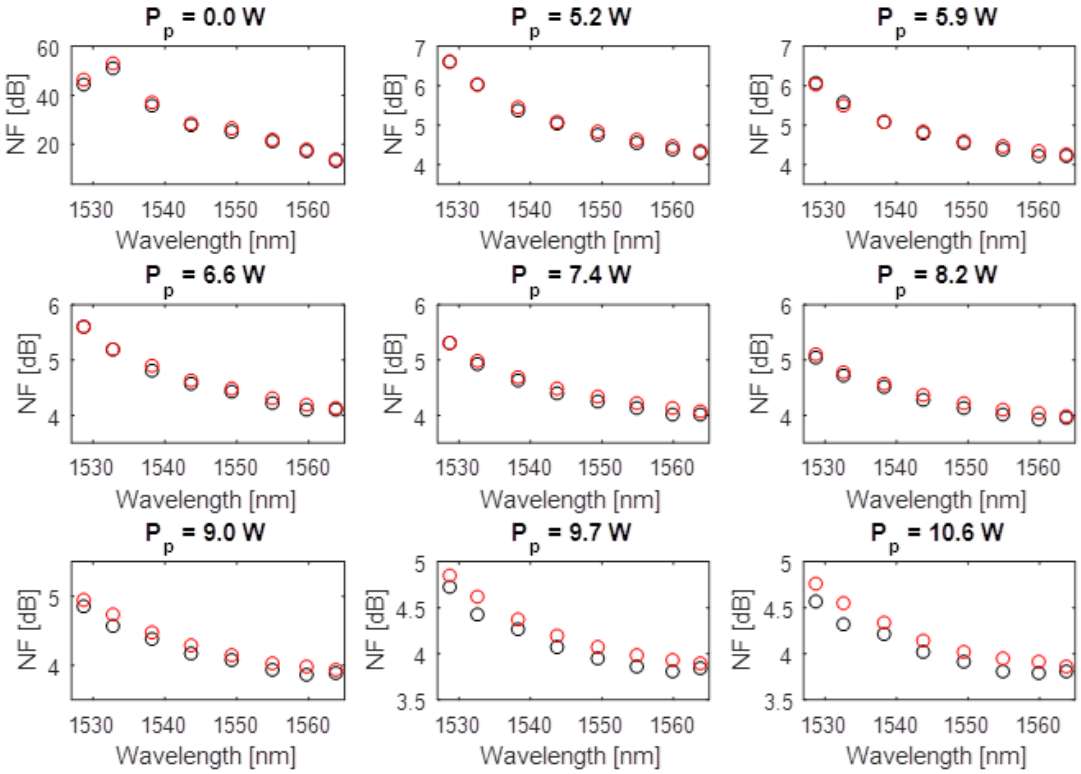

FIGURE 8.5 – NF measurement results for a total input signal power of 1.5 dBm, and various input pump power ranging from 0 W to 10.6 W when i) an ICBG is used to recycle the output pump power (red) with a fiber length of 20.3 m and ii) when the pump is not recycled (black) with a fiber length of 19.6 m.

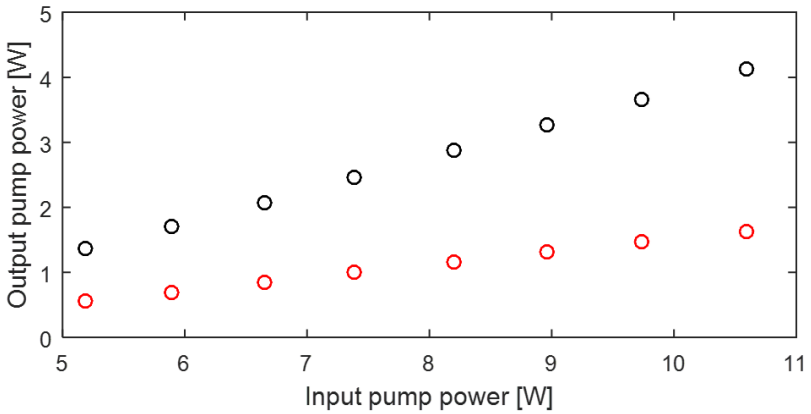

FIGURE 8.6 – Measurement results for the output pump power as a function of the input pump power (without an input signal) for a fiber length of 19.6 m without ICBG (black) and a fiber length of 20.2 m with an ICBG (red).

reflected by the ICBG at the output of the active fiber, z = 20.3 m.

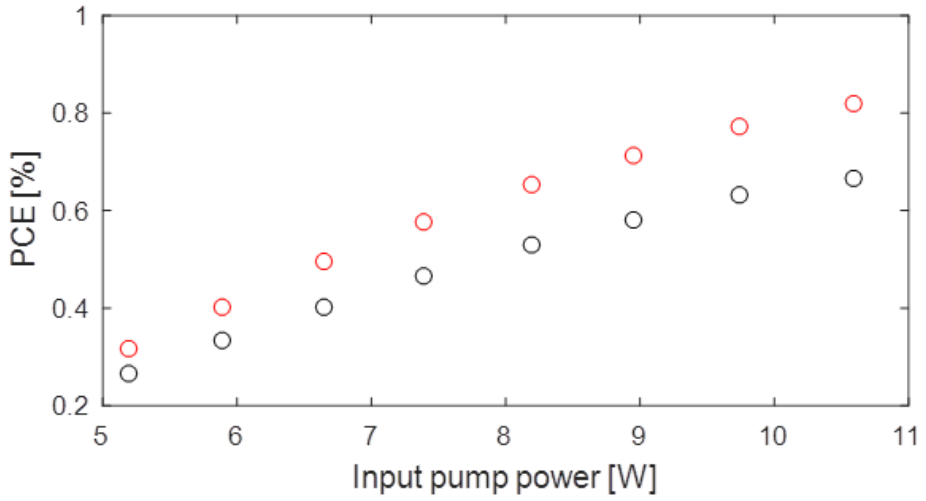

FIGURE 8.7 – PCE as a function of input pump power for an input signal power of 1.5 dBm when an ICBG is used to recycle the output pump power with a fiber length of 20.3 m (red) and when the pump is not recycled with a fiber length of 19.6 m (black).

Then, to estimate the effective reflectivity R of the ICBG, we computed the RMSE between the 72 data points of the measured gain with or without the ICBG (shown in Fig. 8.4) and the corresponding simulated gain results for given values of R. The RMSE is plotted as a function of the effective reflectivity in Fig. 8.8. As expected, when there is no ICBG and the fiber length is set to 19.6 m (black), the fit is optimal for an effective reflectivity of 0%. When an ICBG is present in the fiber cladding for pump recycling, and considering a fiber length of 20.3 m (red), the fit is optimal for an effective reflectivity of 19%.

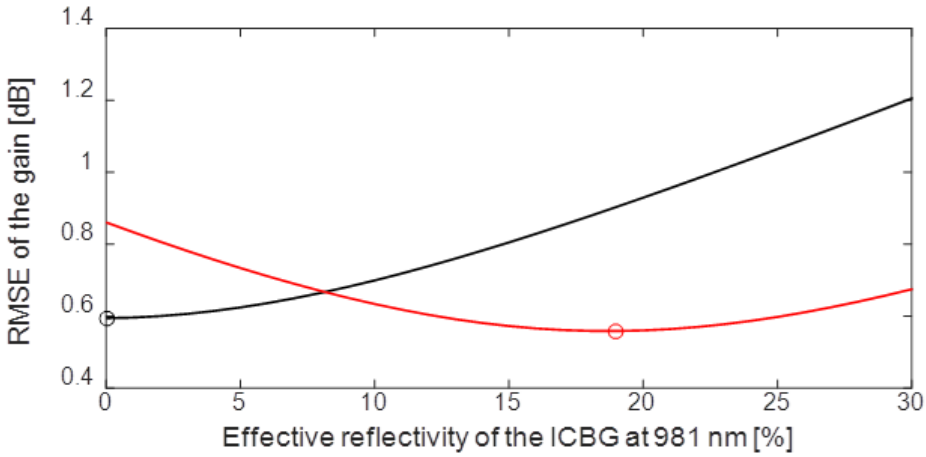

FIGURE 8.8 – RMSE between the simulated and measured gain as a function of the ICBG effective reflectivity when an ICBG is used to recycle the output pump power and considering a fiber length of 20.3 m (red). For comparison, the RMSE between the simulated and measured gain is also shown when there is no ICBG and considering a fiber length of 19.6 m (black). The circles indicate the optimal fit.

In Fig. 8.9 and 8.10, the simulation results obtained when using the previously determined effective reflectivity (0% when the pump is not recycled and 19% when the ICBG is used for pump recycling) are compared with the gain and NF measurements for the various pump powers reported in section 8.5.

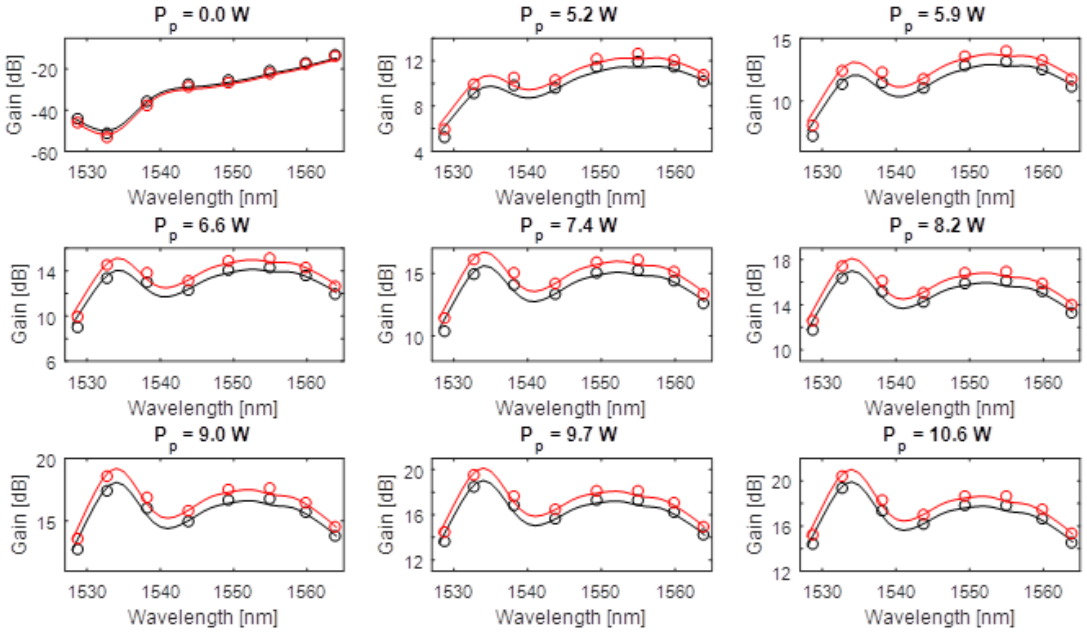

FIGURE 8.9 – Gain measurement (circles) and simulations (lines) for a total input signal power of 1.5 dBm, and various input pump power ranging from 0 W to 10.6 W, when i) an ICBG is used to recycle the output pump power (red) with a fiber length of 20.3 m and assuming $R = 19\%$ for the simulations ; and ii) when the pump is not recycled (black) with a fiber length of 19.6 m and assuming $R = 0\%$ for the simulations.

The experimental results shown in Fig. 8.7 indicate a 23% increase in the PCE when $P_p = 10.6$ W. These results were however obtained with slightly different conditions for the fiber length. According to our simulations and using the fiber parameters described above, when no ICBG is used, for input signal power of 1.5 dBm and input pump power of 10.6 W, increasing the fiber length from 19.6 m to 20.3 m increases the PCE by 6%. Thus, the actual PCE increase that is caused by the recycled pump, and not the fiber length, is actually $(1.23/1.06 - 1) = 16\%$. An increase of 16% for the PCE when only recycling 19% of the output pump power, which corresponds to 19% of ∼780 mW, can be explained by the fact that the last meters of the fiber have a lower average inversion level. Therefore, increasing the pump power over this part of the active fiber has a more significant positive impact on the performance than recycling the pump power by reinjecting it at the input of the fiber.

Considering the same 981 nm pump wavelength and coupled pump power of 10.6 W, we now use simulations to estimate the PCE that would be obtained if the input signal power was set to 1.5 dBm per core in all eight cores and if the fiber length was adjusted to maximize

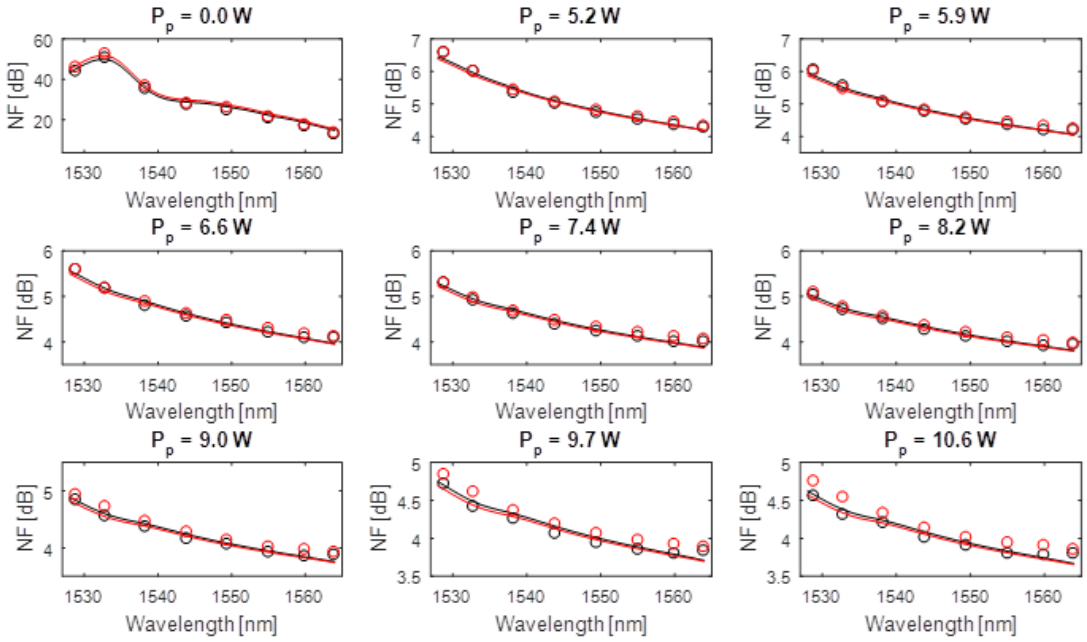

FIGURE 8.10 – NF measurement (circles) and simulations (lines) for a total input signal power of 1.5 dBm, and various input pump power ranging from 0 W to 10.6 W, when i) an ICBG is used to recycle the output pump power (red) with a fiber length of 20.3 m and assuming $R = 19\%$ for the simulations ; and ii) when the pump is not recycled (black) with a fiber length of 19.6 m and assuming $R = 0\%$ for the simulations.

the PCE for various values of effective reflectivity R, between 0% and 100%. The results are shown in Fig. 8.11 and indicate that an ideal ICBG could theoretically lead to an increase of the PCE by 52%, from 7.9% to 12.0%. Also, the optimal fiber length was 30.8 m for $R = 0\%$ and 27.3 m for $R = 100\%$, indicating that pump recycling also allows decreasing the required fiber length. Lastly, we note that the 8-core fiber with annular doping used in this study was designed to achieve low gain compression in multi-core amplifiers designed for dynamic network. Considering that more pump power would be reflected under the low input signal power conditions, compared to high input signal power conditions, recycling the pump may not be beneficial to the gain compression performance. Nonetheless, the results clearly show the benefits in terms of PCE that are obtained by the introduction of ICBG for pump recycling and this technique could easily be implemented to more standard CP-MC-EDFA designs with uniform doping in the core.

8.7 Conclusion

In summary, we were able to demonstrate, for the first time of our knowledge, pump recycling with a Bragg grating inscribed in the cladding of a CP-MC-EDFA. The technique uses readily available Bragg grating writing technology and presents a low complexity solution to imple-

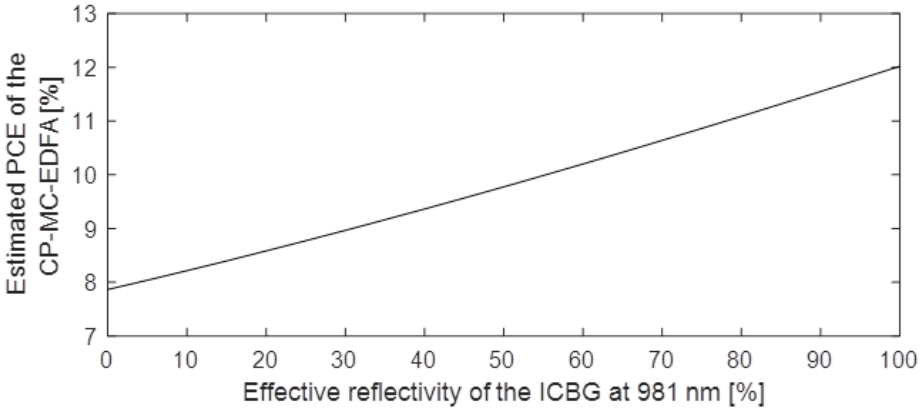

FIGURE 8.11 – Calculated PCE for a fully loaded CP-MC-EDFA as a function of the effective reflectivity of the ICBG at 981 nm. The 8 cores are loaded with an input signal power of 1.5 dBm per core, the pump wavelength is 981 nm, the coupled pump power is 10.6 W and the fiber length is adjusted for each value of R to maximize the PCE.

ment pump recycling. According to our simulations, the effective reflectivity of the ICBG was 19%, which led to a relative increase of 16% for the PCE. These results are very promising considering that significant pump power is typically lost at the output of CP-EDFAs given that high pump intensity is required for the signal to be properly amplified. In this paper, although we achieved a pump recycling ratio of only 19%, compared to the record of 55.2% achieved with turbo cladding pumping [73], the proposed method has the advantage of not requiring any additional component and, therefore, has the potential of becoming a scalable and economically viable solution for pump recycling provided that techniques to decrease the inscription time and to increase the ICBG efficiency can be developed. Currently only ∼25% of the cladding area covered by the ICBG and, therefore, improvement in the grating effective reflectivity is expected as the writing technique is refined to increase the grating area and uniformity. Considering the high electrical to optical conversion efficiency of low-cost multimode laser diode used with cladding pumping, using ICBGs for pump recycling might be the very last step required to make cladding pumping more economically viable than core pumping in communication networks.

Chapitre 9

Applications des fibres optiques amplificatrices pompées par la gaine pour les futurs réseaux de communication

9.1 Résumé

Ce chapitre a pour objectif de discuter des résultats présentés dans cette thèse afin de tirer une conclusion sur la viabilité des fibres optiques amplificatrices pompées par la gaine pour deux applications distinctes des réseaux de communication.

Dans un premier temps, les spécifications présentées en introduction seront comparées aux résultats de caractérisation de la fibre conçue et présentée au chapitre 6 afin de conclure sur l'intérêt des fibres optiques amplificatrices multicoeurs pompées par la gaine dans les réseaux reconfigurables et des principaux éléments à améliorer.

Dans un second temps, les résultats des chapitres 7 et 8 seront utilisés afin de discuter de l'intérêt des fibres optiques amplificatrices pompées par la gaine pour amplifier la bande L avec une efficacité énergétique élevée.

9.2 Fibres optiques amplificatrices pompées par la gaine pour les réseaux reconfigurables

Les analyses menées aux chapitres 1 à 5 ont permis de converger vers le design présenté au chapitre 6, conçu spécifiquement pour répondre aux exigences des réseaux reconfigurables. Dans le tableau 9.1, les requis des réseaux reconfigurables sont comparés aux performances

réelles de la fibre présentées au chapitre 6 afin de tirer une conclusion sur la viabilité des fibres optiques amplificatrices à coeurs multiples pompées par la gaine et ayant une géométrie de dopant en anneau dans les réseaux reconfigurables.

Tableau 9.1 – Comparaison entre la performance requise et la performance mesurée de l'amplificateur optique testé au laboratoire

Paramètre	Requise	Mesurée
Nombre de coeurs	8	8
Plage de puissance du signal à l'entrée	-23.1 dBm à 1.4 dBm	-23.2±0.3 dBm à 1.4±0.3 dBm
Plage spectrale couverte	1529 nm à 1565 nm	1528.8 nm à 1563.9 nm
Gain	>17 dB	>15.3 dB
Facteur de bruit	<5 dB	<5.4 dB
Compression du gain	<5 dB	<16.8 dB ou <7.3 dB si on néglige le coeur #8
Méthode de couplage de la pompe	Par la gaine, avec une seule diode laser multimode	Par la gaine, avec une seule diode laser multimode

Or, si on considère uniquement la performance du coeur #4, on obtient plutôt les résultats présentés au tableau 9.2.

Tableau 9.2 – Comparaison entre la performance requise et la performance mesurée du coeur #4 de l'amplificateur optique testé au laboratoire

Paramètre	Requise	Mesurée
Plage de puissance du signal à l'entrée	-23.1 dBm à 1.4 dBm	-23.1 dBm à 1.5 dBm
Plage spectrale couverte	1529 nm à 1565 nm	1528.8 nm à 1563.9 nm
Gain	>17 dB	>15.6 dB
Facteur de bruit	<5 dB	<5.0 dB
Compression du gain	<5 dB	<3.8 dB
Méthode de couplage de la pompe	Par la gaine, avec une seule diode laser multimode	Par la gaine, avec une seule diode laser multimode

Bien que les requis initiaux n'aient pas été atteints, en se penchant sur le coeur #4 uniquement, on remarque que la compression du gain mesurée (3.8 dB) est nettement inférieure à la compression requise (5.0 dB). On peut donc en conclure qu'il y aurait une certaine marge de manoeuvre possible au niveau du design afin d'augmenter le gain minimum légèrement, en rapprochant l'anneau d'ions actifs de la partie centrale du coeur. Une telle modification aurait pour effet d'augmenter le gain ainsi que la compression du gain, sans toutefois modifier la longueur de fibre de façon significative, maintenant ainsi l'ASE dans la gaine au même niveau.

Néanmoins, des efforts additionnels de recherche et de développement seraient requis pour que

cette technologie puisse être utilisée dans les réseaux reconfigurables. En particulier, l'uniformité des coeurs et la sensibilité du design à l'uniformité des coeurs devraient être améliorées considérablement. Une piste de solution pourrait être d'augmenter le nombre de couches utilisées pendant le processus MCVD et pendant l'étape de dopage par solution afin d'améliorer la précision radiale sur la géométrie du coeur. Autrement, l'utilisation de la méthode MCVD-chelate [175] pourrait être explorée afin d'améliorer le contrôle de l'épaisseur de l'anneau d'ions actifs, par rapport à la méthode du dopage par solution, lors du processus de fabrication.

Le co-dopage à l'ytterbium n'a pas été utilisé pour cette application dans le cadre de cette thèse puisque l'objectif était de couvrir la bande C en entier. Or, dans la littérature scientifique, une fibre amplificatrice multicoeur pompée par la gaine et avec co-dopage a l'ytterbium a récemment été démontrée pour les réseaux reconfigurables [176]. Bien qu'elle ne permette pas d'amplifier les longueurs d'onde inférieures à 1535 nm, ses performances et sa PCE sont nettement supérieures à celles obtenues dans le cadre de cette thèse puisque l'ytterbium permet d'atteindre un niveau d'inversion élevé des ions d'erbium, malgré la faible intensité de la pompe.

Un enjeu additionnel relié à un tel design d'amplificateur intégré pompé par la gaine réside dans l'impossibilité de contrôler la pompe de façon indépendante pour chacun des coeurs afin d'ajuster la courbe de gain au nombre de canaux présents. Or, puisque les amplificateurs optiques comportent souvent deux étages, un tel amplificateur pourrait néanmoins être utilisé pour le premier étage, en combinaison avec des fibres amplificatrices pompées par le coeur dans le deuxième étage. Autrement, le contrôle de la pompe peut être assuré par des amplificateurs pompés par le coeur situés plus loin dans le lien de communication.

Malgré ces nombreux défis, le pompage par la gaine a l'avantage de permettre l'utilisation d'une seule fibre amplificatrice, d'une seule source pompe multimode abordable et d'un seul coupleur de pompe, consistant en une simple fibre de silice pure cônique, pour amplifier plusieurs canaux spatiaux. Les gains économiques potentiels à ce niveau sont donc significatifs.

Bref, les performances obtenues dans le cadre de ces travaux de doctorat sont prometteuses et consistuent en une nette amélioration par rapport à l'état de l'art au début du projet. Bien que des améliorations soient encore nécessaires avant une implémentation commerciale fructueuse, les fibres amplificatrices pompées par la gaine pourraient permettre de diminuer significativement les coûts dans les réseaux reconfigurables du futur.

9.3 Fibres optiques amplificatrices pompées par la gaine pour amplifier la bande L

Alors qu'il a été démontré que l'efficacité energétique du pompage par la gaine pouvait être supérieure à celle du pompage par le coeur dans la bande C [10] vue l'efficacité de conver-

sion électrique vers optique élevée des diodes laser multimodes, une autre étude récente s'est penchée sur l'efficacité energétique du pompage par la gaine dans la bande L [177].

Dans cet article, deux fibres amplificatrices, l'une conçue pour le pompage par le coeur et l'autre pour le pompage par la gaine, sont comparées à titre de médium de gain pour un booster stage dans un amplificateur couvrant la plage spectrale de 1575 nm à 1626 nm. Dans le cas de la fibre A, conçue pour le pompage par le coeur, une source de pompage à mode unique centrée à 976 nm est utilisée. Quant à elle, la fibre B a été conçue pour le pompage par la gaine et a donc été co-dopée à l'ytterbium, en plus d'avoir un polymère guidant permettant le guidage de la puissance pompe injectée dans la gaine. La fibre B est pompée avec une source multimode centrée à 915 nm coutant environ 10% du prix de la source à mode unique utilisée pour le pompage par le coeur.

En utilisant chacune de ces fibres et méthodes de pompage dans l'amplificateur au booster stage, la puissance du signal a été variée entre -1 dBm et 20 dBm tout en ajustant la puissance de la pompe afin de maintenir un gain constant. Pour chaque valeur de puissance du signal à l'entrée, la consommation électrique a été mesurée. Cette analyse a permis de déterminer que, sous ces conditions expérimentales, le pompage par la gaine permettait d'obtenir une consommation électrique plus faible que le pompage par le coeur, à condition que la puissance du signal à l'entrée soit supérieure à 11 dBm.

Bien qu'il s'agisse d'une application nichée, il est intéressant de constater que, sous certains scénarios, le pompage par la gaine peut permettre l'obtention de performances similaires au pompage par le coeur tout en coûtant une fraction du coût en terme de composants et en permettant une consommation énergétique plus faible. De plus, dans ce cas-ci, la fibre amplificatrice ne contenait qu'un seul coeur.

À la lumière de ces résultats, et en considérant que, tel que démontré au chapitre 7, l'utilisation de couches concentriques hétérogènes de dopants permettrait d'augmenter la PCE davantage dans une fibre amplificatrice pompée par la gaine pour la bande L, les fibres amplificatrices pompées par la gaine pourraient permettre de diminuer significativement les coûts dans les amplificateurs pour la bande L du futur. Additionellement, le recyclage de la pompe à l'aide d'un réseau de Bragg intra-gaine, tel que celui démontré au chapitre 8, permettrait aussi d'améliorer la PCE des fibres amplificatrices pompées par la gaine. Enfin, il pourrait être intéressant d'investiguer la consommation énergétique d'une fibre amplificatrice intégrée multicoeur pour la bande L afin de la comparer à celle de plusieurs fibres amplificatrices distinctes pompées par le coeur.

Vu ces nombreuses pistes d'amélioration, il serait intéressant de poursuivre l'investigation en concevant une fibre amplificatrice multicoeur, ayant des couches hétérogènes de dopant et utilisant un réseau de Bragg intra-gaine afin de la caractériser en laboratoire.

Conclusion

L'objectif de cette thèse était d'investiguer l'intérêt des fibres amplificatrices pompées par la gaine pour les réseaux de communication. Actuellement, le pompage par le coeur, une technologie qui a l'avantage d'être simple d'utilisation et mature tout en permettant un recouvrement important entre la pompe et les ions d'erbium, est largement répandu dans les réseaux de communications optiques. Or, par rapport au pompage par le coeur, le pompage par la gaine a pour principaux avantages de permettre 1) l'amplification de plusieurs canaux spatiaux intégrés dans une même fibre et ; 2) l'utilisation d'une source laser multimode abordable et ayant une efficacité de conversion électrique vers optique élevée. Or, dans les noeuds des réseaux reconfigurables, des nombreux canaux spatiaux doivent être amplifiés à un même endroit. Cette application pourrait donc bénéficier d'une intégration des multiples canaux spatiaux dans une même fibre. En contrepartie, le pompage par la gaine a une limitation inhérente, soit une faible intensité locale de pompe ainsi qu'un faible recouvrement avec la région dopée, puisque la puissance de la pompe est répartie sur toute la surface de la gaine, ce qui augmente les effets de saturation du signal.

En considérant cette contrainte majeure, et en sachant que le co-dopage à l'ytterbium dans les EDFAs permet un taux d'absorption de la pompe plus élevé, la première investigation, présentée au chapitre 1, a consisté à utiliser des simulations numériques validées par des résultats expérimentaux afin de déterminer dans quelles circonstances le co-dopage à l'ytterbium était préférable au dopage à l'erbium seul dans les EDFAs pour la bande C. Cette investigation a permis de conclure que l'utilisation du co-dopage à l'ytterbium peut permettre l'obtention d'un gain minimum plus élevé que le dopage à l'erbium seul sur la bande C dans les fibres amplificatrices pompées par la gaine lorsque la plage spectrale amplifiée ne couvre pas les longueurs d'ondes inférieures à 1535 nm ou encore lorsque des conditions de forte saturation sont requises. Puisque les réseaux reconfigurables nécessitent d'amplifier la bande C en entier, il a été conclu qu'il serait préférable de s'en tenir à l'erbium seul dans le cadre de la conception d'un amplificateur intégré qui viendrait s'insérer dans les réseaux reconfigurables actuels.

Une idée alternative visant à limiter les effets de saturation causés par la faible intensité de puissance de la pompe, inhérent au pompage par la gaine, consiste à placer les ions d'erbium dans la gaine autour des coeurs afin qu'ils interagissent avec la région évanescente du mode,

là où l'intensité locale du signal est plus faible. Pour vérifier cette théorie, au chapitre 2, des simulations numériques validées par des résultats expérimentaux ont permis de conclure que, pour une fibre amplificatrice dopée à l'erbium pompée par la gaine, la géométrie de distribution des ions actifs en anneau autour du coeur permet l'obtention d'un gain minimum plus élevé pour une compression du gain fixée à 4 dB dans la bande C lorsque la puissance totale du signal à l'entrée varie entre -40 dBm et 3 dBm, comparativement à la géométrie de distribution des ions actifs qui couvre uniquement le coeur ou encore celle qui couvre le coeur ainsi qu'une région en périphérie du coeur.

Outre la composition de la matrice de verre et la distribution des ions actifs, un élément critique visant l'amélioration des performances des amplificateurs à fibre amplificatrice pompée par la gaine est la méthode de couplage latéral de la puissance pompe. Dans cette perspective, au chapitre 3, une nouvelle méthode de couplage latéral de la gaine permettant d'atteindre une efficacité de couplage supérieure à 94% a été présentée. Cette méthode offre l'avantage de ne pas nécessiter de chauffer la fibre réceptrice, ce qui est avantageux pour les EDFAs multiplexés spatialement pour lesquels une légère distorsion de géométrie peut conduire à une diaphonie entre les modes guidés et une détérioration des signaux. De plus, cette méthode est simple à réaliser et peu coûteuse. Cette méthode de couplage latéral de la pompe a donc été utilisée pour les expériences subséquentes.

Ayant précédemment identifié que l'erbium seul (chapitre 1), avec distribution des ions actifs dans la gaine autour du coeur (chapitre 2) était l'approche à prioriser pour un design de fibre amplificatrice pour les réseaux reconfigurables, les chapitres 4 à 6 présentent l'optimisation de la géométrie du coeur afin d'atteindre les performances énoncées dans l'introduction de cette thèse, à l'aide d'un processus itératif de conception, fabrication et caractérisation de fibres amplificatrices.

Au chapitre 4, une première fibre à coeurs multiples utilisant une géométrie de distribution des ions actifs en anneau autour de chacun des coeurs a été présentée. Les résultats de caractérisation permettent d'identifier deux problèmes majeurs relatifs à ce premier design :

— Premièrement, la faible concentration d'Al_2O_3 utilisée afin de maintenir un Δn suffisamment bas dans l'anneau, pour éviter l'obtention d'un coeur multimode, mène à un haut taux de pairage des ions d'erbium ;

— Deuxièmement, une combinaison de plusieurs facteurs mène à l'obtention d'un niveau important d'ASE dans la gaine, qui a pour effet d'augmenter le facteur de bruit : la surface totale élevée de la gaine occupée par des ions d'erbium, l'utilisation d'un polymère guidant pour confiner les modes de pompe à l'intérieur de la gaine et la nécessité d'utiliser une grande longueur de fibre vu le faible recouvrement entre le mode fondamental guidé par chacun des coeurs et les ions d'erbium.

Au chapitre 5, un nouveau design de coeur a été validé en fabriquant une fibre à coeur unique

dopée à l'erbium avec une géométrie en anneau et en la caractérisant expérimentalement. Par rapport au design précédent, les deux principales modifications apportées sont les suivantes :

— Premièrement, du P_2O_5 a été introduit dans la région active avec le Al_2O_3 afin d'obtenir du $AlPO_4$ qui a pour effet de limiter le taux de pairage des ions d'erbium sans toutefois augmenter le Δn ;

— Deuxièmement, la position de l'anneau d'erbium a été rapproché du coeur afin de diminuer la longueur de fibre requise dans le but de limiter le niveau d'ASE dans la gaine.

Au chapitre 6, une fibre à huit coeurs utilisant le design de coeur présenté au chapitre 5 a été fabriquée et caractérisée. Pour la première fois sur une fibre multicoeur utilisant un profil de distribution d'erbium en anneau, un fan-in/fan-out a été utilisé afin d'injecter du signal dans tous les coeurs en parallèle et de mesurer les variations coeur à coeur de gain. Ce chapitre a permis de conclure que les designs utilisant une géométrie de distribution des ions d'erbium en anneau ont des performances particulièrement sensibles aux variations dans le profil d'indice de réfraction. Néanmoins, l'un des coeurs caractérisés permet l'obtention d'un gain minimum de 15.6 dB et d'une compression du gain de seulement 3.8 dB lorsque la puissance du signal à l'entrée varie entre -23.1 dBm et 1.5 dBm, des résultats prometteurs qui permettent de confirmer l'intérêt de ce type de design de fibre amplificatrice multicoeur pour les noeuds des réseaux reconfigurables.

Outre les noeuds des réseaux reconfigurables, une application qui a été investigué dans le cadre de cette thèse est l'utilisation du pompage par la gaine pour amplifier la bande L avec une PCE élevée et en utilisant une source laser multimode abordable et ayant une efficacité de conversion électrique vers optique élevée à titre de source de pompage. En effet, tel que présenté au chapitre 1, le co-dopage à l'ytterbium permet d'augmenter la PCE, dans les EDFAs utilisant le pompage par la gaine, mais a aussi pour effet de modifier la forme du spectre d'émission, de sorte que la bande C ne soit pas couverte en entier. Cet effet n'est cependant pas nuisible pour une amplification dans la bande L, qui nécessite d'ailleurs un niveau d'inversion moyen des ions d'erbium plus bas que dans la bande C, soit une caractéristique compatible avec la faible intensité de la pompe inhérente au pompage par la gaine. Dans cette perspective, le chapitre 7 vise à augmenter davantage la PCE d'une fibre amplificatrice à coeur simple pour la bande L en utilisant des couches concentriques hétérogènes de dopants. Ce chapitre permet de conclure que l'utilisation de couches concentriques hétérogènes de dopants dans les fibres amplificatrices pour la bande L pompées par la gaine permet d'augmenter l'efficacité de conversion de puissance par rapport aux designs qui utilisent uniquement de l'erbium seul ou un co-dopage à l'erbium-ytterbium. En effet, alors que la région co-dopée avec de l'ytterbium absorbe la pompe à 915 nm, la région dopée à l'erbium seul agit quant à elle en tant que filtre pour l'ASE, menant ainsi à une augmentation de la PCE.

Ensuite, que ce soit pour les fibres multicoeurs ou pour un amplificateur à coeur unique dans

la bande L, la PCE des EDFAs pompées par la gaine peut être augmentée en recyclant la pompe résiduelle à la sortie de la fibre. Au chapitre 8, le recyclage de la pompe à l'aide d'un ICBG dans une fibre amplificatrice multicoeur a été démontrée pour la première fois. En effet, dans ce chapitre, une augmentation relative du PCE de 16% a pu être démontrée en inscrivant simplement un ICBG couvrant environ 25% de la gaine sur quelques cm près de la sortie de la fibre, et ce, sans nécessiter l'insertion de composants coûteux et complexes induisant des pertes au signal tel que dans les méthodes alternatives de recyclage de la pompe.

Finalement, à la lumière de ces résultats et des récents résultats présentés par d'autres chercheurs dans la littérature scientifique, le chapitre 9 consiste en une discussion qui vient proposer deux applications distinctes pour lesquelles le pompage par la gaine a effectivement le potentiel de permettre l'obtention de meilleures performances que le pompage par le coeur : 1) l'amplification dans les noeuds des réseaux reconfigurables et ; 2) l'amplification dans la bande L avec une efficacité de conversion de la puissance élevée. Bien que des investigations additionnelles seraient requises afin de définir plus précisément les performances maximales qui pourraient être obtenues, les résultats obtenus dans le cadre de cette thèse ont permis de faire avancer les connaissances relatives au design de fibres amplificatrices pour ces deux applications. Néanmoins, pour que les fibres amplificatrices pompées par la gaine avec profil de dopant actif en anneau soient viables dans les réseaux reconfigurables, des efforts additionnels devront être déployés afin de minimiser les variations de gain entre les coeurs. Alternativement, lorsque les longueurs d'onde inférieures à 1535 nm ne doivent pas impérativement être amplifiées, le co-dopage à l'ytterbium peut être utilisé et ne requiert pas d'utiliser une géométrie en anneau vu le haut niveau d'inversion des ions d'erbium que permettent les ions d'ytterbium malgré la faible intensité local de la pompe. Dans le cas des fibres amplificatrices pompées par la gaine pour la bande L, elles permettent L'obtention d'une efficacité énergétique aux fibres pompées par le coeur lorsque la puissance du signal à l'entrée est supérieure à 11 dBm. Or, cette efficacité pourrait être améliorée davantage en utilisant des couches concentriques hétérogènes de dopants ainsi qu'en inscrivant un réseau de Bragg intra-gaine. Il serait donc judicieux de poursuivre l'analyse en fabriquant une telle fibre afin de la caractériser expérimentalement pour enfin valider les résultats de simulation et définir les principales contraintes de fabrication relatives à ce type de fibre.

Liste des publications

P.1 Brevet

1. **C. Matte-Breton**, S. Duval, S. LaRochelle, R. Vallée et M. Bernier, "METHOD OF COUPLING OPTICAL FIBERS, AND OPTICAL COUPLER", WO2021030911A1, Février 2021.

P.2 Journaux

1. **C. Matte-Breton**, L. Talbot, Y. Messaddeq, M. Bernier, et S. LaRochelle, "Large area Bragg grating for pump recycling in cladding-pumped multicore erbium-doped fiber amplifiers," Opt. Express, (Mai 2022).
2. **C. Matte-Breton**, R.-J. Essiambre, C. Kelly, Y. Messaddeq, et S. LaRochelle, "Multicore Cladding-Pumped Fiber Amplifier with Annular Erbium Doping for Low Gain Compression," IEEE/OSA J. Lightwave Technol., (Janvier 2022).
3. **C. Matte-Breton**, R. Ryf, N. K. Fontaine, R.-J. Essiambre, H. Chen, C. Kelly, Y. Messaddeq, et S. LaRochelle, "Modeling and Characterization of Cladding-Pumped Erbium-Ytterbium Co-doped Fibers for Amplification in Communication Systems," IEEE/OSA J. Lightwave Technol., vol. 38, no.7, pp.1936-1944, (Décembre 2019).
4. **C. Matte-Breton**, H. Chen, N. K. Fontaine, R. Ryf, R.-J. Essiambre, C. Kelly, C. Jin, Y. Messaddeq, et S. LaRochelle, "Demonstration of an Erbium-Doped Fiber with Annular Doping for Low Gain Compression in Cladding Pumped Amplifiers," Opt. Express, vol.26, no.20, pp. 26633-45 (Octobre 2018).

P.3 Conférences

1. **C. Matte-Breton**, L. Wang, F. Maes, Y. Messaddeq et S. LaRochelle, "Concentric Layers with Heterogeneous Doping for Cladding-Pumped L-Band Fiber Amplifiers," Photonics West conference (PW 2022), paper 12028-11, Janvier 2022.

2. S. LaRochelle, **C. Matte-Breton**, C. Kelly et R.-J. Essiambre, "Cladding-pumped multicore amplifiers with ring doping," Optical Fiber Communications conference (OFC'2021), invited paper, paper M3D.1, San Francisco, USA, Juin 2021.
3. **C. Matte-Breton**, R.-J. Essiambre, C. Kelly, Y. Messaddeq et S. LaRochelle, "Characterization of an Aluminophosphosilicate Fiber with Annular Erbium Doping for Improved Performance of Cladding-Pumped Amplifiers," the 46th European conference on optical communications (ECOC'2020), paper Th2A-1, Bruxelles, Belgique, Décembre 2020.
4. S. LaRochelle et **C. Matte-Breton**, "Design of Fibers with Erbium-Ring-Doping in the Cladding for Spatially Integrated Optical Amplifiers," invited paper, OSA Advanced Photonics Congress, Photonic Networks and Devices (NETWORKS'2020), paper NeW2B.2, Montréal, Canada, Juillet 2020.
5. **C. Matte-Breton**, R. Wang, Y. Messaddeq et S. LaRochelle, "Novel Fuseless Optical Fiber Side-Coupler based on Half-Taper for Cladding Pumped EDFAs," Optical Fiber Communications conference (OFC'2020), paper T3A.2, San Diego, USA, Mars 2020.
6. **C. Matte-Breton**, R. Ryf, N. K. Fontaine, R.-J. Essiambre, H. Chen, Y. Messaddeq, J. C. Alvarado Zacarias, R. Amezcua Correa, C. Kelly et S. LaRochelle, "An 8-core Erbium-doped fiber with annular doping for low gain compression in cladding-pumped amplifiers," 45th European conference on optical communications (ECOC'2019), paper W.1.C.2, Dublin, Ireland, Septembre 2019.
7. J. C. Alvarado-Zacarias, **C. Matte-Breton**, R. Ryf, N. K. Fontaine, H. Chen, S. Wittek, H. Sakuma, T. Ohtsuka, T. Hayashi, T. Hasegawa, S. LaRochelle et R. Amezcua-Correa, "Characterization of Coupled-Core Fiber Amplifiers Using Swept-Wavelength Interferometer," Optical Fiber Communications conference (OFC'2019), paper Th1B.6, San Diego, USA, Mars 2019.
8. **C. Matte-Breton**, H. Chen, N. Fontaine, R. Ryf, R.-J. Essiambre, Y. Messaddeq et S. LaRochelle, "Analysis of Inter-core Cross-gain Modulation in Cladding Pumped Multi-core Fiber Amplifiers," the 44th European conference on optical communications (ECOC'2018), paper We2.4 Italy, Rome, Septembre 2018.
9. S. LaRochelle, C. Jin, **C. Matte-Breton** et Y. Messaddeq, "Cladding Pumped Multicore Fiber Amplifiers for Space Division Multiplexing," invited paper 2018 IEEE Canadian Conference on Electrical Computer Engineering (CCECE), Quebec, Canada, Mai 2018. DOI : 10.1109/CCECE.2018.8447740 IEEE Women in Engineering best paper award of the CCECE'2018 conference (IEEE Canada).
10. **C. Matte-Breton**, H. Chen, N. Fontaine, R. Ryf, R-J. Essiambre, Y. Messaddeq et S. LaRochelle, "Cladding Pumped EDFAs with Annular Erbium Doping," Conference on Lasers and Electro Optics (CLEO'2018), paper JTH2A.133, San José, USA, Mai 2018.

Bibliographie

[1] H. Takeshita, M. Sato, Y. Inada, E. L. T. de Gabory, and Y. Nakamura, "Past, current and future technologies for optical submarine cables," in *2019 IEEE/ACM Workshop on Photonics-Optics Technology Oriented Networking, Information and Computing Systems (PHOTONICS)*. IEEE, 2019, pp. 36–42.

[2] W. I. Way, P. N. Ji, and A. N. Patel, "Wavelength contention-free via optical bypass within a colorless and directionless roadm," *Journal of Optical Communications and Networking*, vol. 5, no. 10, pp. A220–A229, 2013.

[3] O. Gerstel, M. Jinno, A. Lord, and S. B. Yoo, "Elastic optical networking : A new dawn for the optical layer ?" *IEEE communications Magazine*, vol. 50, no. 2, pp. s12–s20, 2012.

[4] N. K. Fontaine, "Components and devices for space-division multiplexed systems," in *2015 IEEE Photonics Conference (IPC)*. IEEE, 2015, pp. 317–318.

[5] S. Jain, N. K. Thipparapu, P. Barua, and J. K. Sahu, "Cladding-pumped Er/Yb-doped multi-element fiber amplifier for wideband applications," *IEEE Photonics Technology Letters*, vol. 27, no. 4, pp. 356–358, 2014.

[6] M. Wada, T. Sakamoto, S. Aozasa, T. Mori, T. Yamamoto, and K. Nakajima, "Two-LP-mode six-core cladding pumped EDFA with high pump power density," *Journal of Lightwave Technology*, vol. 36, no. 2, pp. 331–335, 2018.

[7] C. Castro, S. Jain, E. De Man, Y. Jung, J. Hayes, S. Calabro, K. Pulverer, M. Bohn, S.-u. Alam, D. J. Richardson *et al.*, "100-Gb/s transmission over a 2520-km integrated MCF system using cladding-pumped amplifiers," *IEEE Photonics Technology Letters*, vol. 29, no. 14, pp. 1187–1190, 2017.

[8] H. Ono, K. Takenaga, K. Ichii, S. Matsuo, T. Takahashi, H. Masuda, and M. Yamada, "12-core double-clad Er/Yb-doped fiber amplifier employing free-space coupling pump/signal combiner module," in *39th European Conference and Exhibition on Optical Communication (ECOC 2013)*. IET, 2013, pp. 1–3.

[9] T. Sakamoto, M. Wada, S. Aozasa, R. Imada, T. Yamamoto, and K. Nakajima, "Characteristics of randomly coupled 12-core erbium-doped fiber amplifier," *Journal of Lightwave Technology*, vol. 39, no. 4, pp. 1186–1193, 2020.

[10] G. Mélin, R. Kerampran, A. Monteville, S. Bordais, T. Robin, D. Landais, A. Lebreton, Y. Jaouën, and T. Taunay, "Power efficient all-fiberized 12-core erbium/ytterbium doped optical amplifier," in *Optical Fiber Communication Conference*. Optical Society of America, 2020, pp. M4C–2.

[11] S. Takasaka, K. Maeda, K. Kawasaki, K. Yoshioka, H. Oshio, R. Sugizaki, H. Takahashi, T. Tsuritani, and M. Shiino, "Edf length dependence of amplification characteristics of cladding pumped 19-core EDFA," in *Optical Fiber Communication Conference*. Optical Society of America, 2018, pp. Th1K–2.

[12] S. Jain, T. Mizuno, Y. Jung, Q. Kang, J. R. Hayes, M. N. Petrovich, G. Bai, H. Ono, K. Shibahara, A. Sano *et al.*, "32-core inline multicore fiber amplifier for dense space division multiplexed transmissionsystems," in *ECOC 2016-Post Deadline Paper; 42nd European Conference on Optical Communication*. VDE, 2016, pp. 1–3.

[13] K. Abedin, T. Taunay, M. Fishteyn, D. DiGiovanni, V. Supradeepa, J. Fini, M. Yan, B. Zhu, E. Monberg, and F. Dimarcello, "Cladding-pumped erbium-doped multicore fiber amplifier," *Optics express*, vol. 20, no. 18, pp. 20 191–20 200, 2012.

[14] K. S. Abedin, J. M. Fini, T. F. Thierry, B. Zhu, M. F. Yan, L. Bansal, F. V. Dimarcello, E. M. Monberg, and D. J. DiGiovanni, "Seven-core erbium-doped double-clad fiber amplifier pumped simultaneously by side-coupled multimode fiber," *Optics Letters*, vol. 39, no. 4, pp. 993–996, 2014.

[15] H. Takeshita, K. Matsumoto, H. Noguchi, and E. L. T. de Gabory, "Optical amplification efficiency improvement of multicore EDFA by using turbo cladding pumping scheme," in *2020 IEEE Photonics Society Summer Topicals Meeting Series (SUM)*. IEEE, 2020, pp. 1–2.

[16] C. Matte-Breton, H. Chen, N. Fontaine, R. Ryf, R. Essiambre, Y. Messaddeq, and S. LaRochelle, "Cladding pumped EDFAs with annular erbium doping," in *CLEO : QELS_Fundamental Science*. Optical Society of America, 2018, pp. JTh2A–133.

[17] C. Matte-Breton, R. Ryf, N. K. Fontaine, R.-J. Essiambre, H. Chen, Y. Messaddeq, J. C. A. Zacarias, R. A. Correa, C. Kelly, and S. LaRochelle, "An 8-core erbium-doped fiber with annular doping for low gain compression in cladding-pumped amplifiers," in *45th European Conference on Optical Communication (ECOC 2019)*. IET, 2019, pp. 1–3.

[18] D. L. Williams, "Light and the evolution of vision," *Eye*, vol. 30, no. 2, pp. 173–178, 2016.

[19] D.-E. Nilsson, "Eye evolution : a question of genetic promiscuity," *Current opinion in neurobiology*, vol. 14, no. 4, pp. 407–414, 2004.

[20] M. F. Land and D.-E. Nilsson, *Animal eyes*. Oxford University Press, 2012.

[21] G. G. Rosenthal and M. J. Ryan, "Visual and acoustic communication in non-human animals : a comparison," *Journal of biosciences*, vol. 25, no. 3, pp. 285–290, 2000.

[22] "Internet growth statistics 1995 to 2021 - the global village online." [Online]. Available : https://www.internetworldstats.com/emarketing.htm

[23] E. Agrell, M. Karlsson, A. Chraplyvy, D. J. Richardson, P. M. Krummrich, P. Winzer, K. Roberts, J. K. Fischer, S. J. Savory, B. J. Eggleton *et al.*, "Roadmap of optical communications," *Journal of Optics*, vol. 18, no. 6, p. 063002, 2016.

[24] J. Brown, "Report of advances in microwave theory and techniques in great britain-1959," *IRE Transactions on Microwave Theory and Techniques*, vol. 8, no. 4, pp. 382–386, 1960.

[25] Y. Tamura, H. Sakuma, K. Morita, M. Suzuki, Y. Yamamoto, K. Shimada, Y. Honma, K. Sohma, T. Fujii, and T. Hasegawa, "Lowest-ever 0.1419-db/km loss optical fiber," in *Optical Fiber Communication Conference*. Optical Society of America, 2017, pp. Th5D–1.

[26] G. Rademacher, B. J. Puttnam, R. S. Luís, J. Sakaguchi, W. Klaus, T. A. Eriksson, Y. Awaji, T. Hayashi, T. Nagashima, T. Nakanishi *et al.*, "10.66 peta-bit/s transmission over a 38-core-three-mode fiber," in *Optical Fiber Communication Conference*. Optical Society of America, 2020, pp. Th3H–1.

[27] N. A. Olsson, "Lightwave systems with optical amplifiers," *Journal of Lightwave Technology*, vol. 7, no. 7, pp. 1071–1082, 1989.

[28] S. Xu, J. B. Khurgin, I. Vurgaftman, and J. R. Meyer, "Reducing crosstalk and signal distortion in wavelength-division multiplexing by increasing carrier lifetimes in semiconductor optical amplifiers," *Journal of Lightwave technology*, vol. 21, no. 6, pp. 1474–1485, 2003.

[29] M. Tachibana, R. Laming, P. Morkel, and D. Payne, "Erbium-doped fiber amplifier with flattened gain spectrum," *IEEE Photonics Technology Letters*, vol. 3, no. 2, pp. 118–120, 1991.

[30] [Online]. Available : https://www.submarinecablemap.com/

[31] T. A. Strasser and J. L. Wagener, "Wavelength-selective switches for roadm applications," *IEEE journal of selected topics in quantum electronics*, vol. 16, no. 5, pp. 1150–1157, 2010.

[32] M. D. Feuer, D. C. Kilper, and S. L. Woodward, "Roadms and their system applications," in *Optical Fiber Telecommunications VB*. Elsevier, 2008, pp. 293–343.

[33] E. B. Basch, R. Egorov, S. Gringeri, and S. Elby, "Architectural tradeoffs for reconfigurable dense wavelength-division multiplexing systems," *IEEE Journal of selected topics in quantum electronics*, vol. 12, no. 4, pp. 615–626, 2006.

[34] T. Li, "The impact of optical amplifiers on long-distance lightwave telecommunications," *Proceedings of the IEEE*, vol. 81, no. 11, pp. 1568–1579, 1993.

[35] S. L. Hansen, P. Thorsen, K. Dybdal, and S. B. Andreasen, "Gain tilt of erbium-doped fiber amplifiers due to signal-induced inversion locking," *IEEE photonics technology letters*, vol. 5, no. 4, pp. 409–411, 1993.

[36] F. Shehadeh, R. Vodhanel, C. Gibbons, and M. Ali, "Comparison of gain control techniques to stabilize EDFAs for WDM networks," in *Optical Fiber Communications, OFC*. IEEE, 1996, pp. 190–191.

[37] A. Srivastava, Y. Sun, J. Zyskind, J. Sulhoff, C. Wolf, and R. Tkach, "Fast gain control in an erbium-doped fiber amplifier," in *Optical Amplifiers and Their Applications*. Optical Society of America, 1996, p. PP4.

[38] K. Ishii, J. Kurumida, and S. Namiki, "Experimental investigation of gain offset behavior of feedforward-controlled WDM AGC EDFA under various dynamic wavelength allocations," *IEEE Photonics Journal*, vol. 8, no. 1, pp. 1–13, 2016.

[39] K. Ishii, J. Kurumida, K. Tanizawa, S. Namiki, N. Sato, K. Ota, Y. Oikawa, and N. Shiga, "Suppression of transients in an EDFA chain using feed-forward pump control and a high-speed voa," in *OFC/NFOEC*. IEEE, 2012, pp. 1–3.

[40] B.-H. Choi, S. S. Lee, C.-B. Kim, and J. Ko, "Automatic gain flattening control and automatic gain control using an all optical method in an optical amplifier," in *COIN-NGNCON 2006-The Joint International Conference on Optical Internet and Next Generation Network*. IEEE, 2006, pp. 148–150.

[41] C.-H. Yeh, K.-H. Lai, C.-C. Lee, and S. Chi, "Simultaneously gain-flattening and gain-clamping technique for erbium-doped fiber amplifiers by backward injection of a fabry–perot laser light," *Japanese journal of applied physics*, vol. 43, no. 7R, p. 4238, 2004.

[42] S. H. Yun, B. W. Lee, H. K. Kim, and B. Y. Kim, "Dynamic erbium-doped fiber amplifier based on active gain flattening with fiber acoustooptic tunable filters," *IEEE photonics technology letters*, vol. 11, no. 10, pp. 1229–1231, 1999.

[43] B. Offrein, F. Horst, G. Bona, R. Germann, H. Salemink, and R. Beyeler, "Adaptive gain equalizer in high-index-contrast sion technology," *IEEE photonics technology letters*, vol. 12, no. 5, pp. 504–506, 2000.

[44] S. Li, K. Chiang, and W. Gambling, "Gain flattening of an erbium-doped fiber amplifier using a high-birefringence fiber loop mirror," *IEEE Photonics Technology Letters*, vol. 13, no. 9, pp. 942–944, 2001.

[45] Z. Lu, P. Lin, and C. Grover, "A dynamically gain-flattened erbium-doped fiber amplifier," *Microwave and Optical Technology Letters*, vol. 39, no. 1, pp. 8–11, 2003.

[46] D. C. Kilper and C. A. White, "Amplifier issues for physical layer network control," in *Optically Amplified WDM Networks*. Elsevier, 2011, pp. 221–251.

[47] B. J. Puttnam, B. C. Thomsen, A. Lopez, and P. Bayvel, "Experimental investigation of optically gain-clamped EDFAs in dynamic optical-burst-switched networks," *Journal of Optical Networking*, vol. 7, no. 2, pp. 151–159, 2008.

[48] P. J. Winzer, "Making spatial multiplexing a reality," *Nature Photonics*, vol. 8, no. 5, pp. 345–348, 2014.

[49] P. J. Winzer, "Capacity scaling through spatial parallelism : From subsea cables to short-reach optical links," in *Optical Fiber Communication Conference*. Optical Society of America, 2021, pp. M2A–5.

[50] W. Klaus, B. J. Puttnam, R. S. Luis, J. Sakaguchi, J.-M. D. Mendinueta, Y. Awaji, and N. Wada, "Advanced space division multiplexing technologies for optical networks," *Journal of Optical Communications and Networking*, vol. 9, no. 4, pp. C1–C11, 2017.

[51] J. Rivas-Moscoso, B. Shariati, A. Mastropaolo, D. Klonidis, and I. Tomkos, "Cost benefit quantification of SDM network implementations based on spatially integrated network elements," in *ECOC 2016 ; 42nd European Conference on Optical Communication*. VDE, 2016, pp. 1–3.

[52] Y. Mimura, Y. Tsuchida, K. Maeda, R. Miyabe, K. Aiso, H. Matsuura, and R. Sugizaki, "Batch multicore amplification with cladding-pumped multicore EDF," in *European Conference and Exhibition on Optical Communication*. Optical Society of America, 2012, pp. Tu–4.

[53] H. Chen, C. Jin, B. Huang, N. K. Fontaine, R. Ryf, K. Shang, N. Grégoire, S. Morency, R.-J. Essiambre, G. Li *et al.*, "Integrated cladding-pumped multicore few-mode erbium-doped fibre amplifier for space-division-multiplexed communications," *Nature Photonics*, vol. 10, no. 8, pp. 529–533, 2016.

[54] P. M. Krummrich, "Optical amplification and optical filter based signal processing for cost and energy efficient spatial multiplexing," *Optics express*, vol. 19, no. 17, pp. 16 636–16 652, 2011.

[55] C. Jin, B. Huang, K. Shang, H. Chen, R. Ryf, R. Essiambre, N. K. Fontaine, G. Li, L. Wang, Y. Messaddeq *et al.*, "Efficient annular cladding amplifier with six, three-mode cores," in *2015 European Conference on Optical Communication (ECOC)*. IEEE, 2015, pp. 1–3.

[56] S. Jain, T. Sakamoto, Y. Jung, I. A. Davidson, P. Barua, J. R. Hayes, K. Shibahara, T. Mizuno, Y. Miyamoto, K. Nakajima *et al.*, "High spatial density 6-mode 7-core fibre amplifier for C-band operation," in *2020 European Conference on Optical Communications (ECOC)*. IEEE, 2020, pp. 1–3.

[57] S. Takasaka, K. Maeda, R. Sugizaki, and Y. Arashitani, "Output power increase of cladding pumped 7-core EDFA by using mie scattering," in *2020 European Conference on Optical Communications (ECOC)*. IEEE, 2020, pp. 1–4.

[58] B. J. Puttnam, G. Rademacher, R. S. Luís, T. A. Eriksson, W. Klaus, Y. Awaji, N. Wada, K. Maeda, S. Takasaka, and R. Sugizaki, "High data-rate and long distance MCF transmission with 19-core c+ l band cladding-pumped EDFA," *Journal of Lightwave Technology*, vol. 38, no. 1, pp. 123–130, 2020.

[59] Z. S. Eznaveh, N. K. Fontaine, H. Chen, J. A. Lopez, J. A. Zacarias, B. Huang, A. A. Correa, C. Gonnet, P. Sillard, G. Li *et al.*, "Ultra-low dmg multimode EDFA," in *2017 Optical Fiber Communications Conference and Exhibition (OFC)*. IEEE, 2017, pp. 1–3.

[60] Q. Kang, E.-L. Lim, F. P. Y. Jung, C. Baskiotis, S.-u. Alam, and D. J. Richardson, "Minimizing differential modal gain in cladding-pumped EDFAs supporting four and six mode groups," *Optics express*, vol. 22, no. 18, pp. 21 499–21 507, 2014.

[61] K. S. Abedin, J. M. Fini, T. F. Thierry, V. Supradeepa, B. Zhu, M. F. Yan, L. Bansal, E. M. Monberg, and D. J. DiGiovanni, "Multicore erbium doped fiber amplifiers for space division multiplexing systems," *Journal of Lightwave Technology*, vol. 32, no. 16, pp. 2800–2808, 2014.

[62] Y. Tsuchida, K. Maeda, K. Watanabe, K. Takeshima, T. Sasa, T. Saito, S. Takasaka, Y. Kawaguchi, T. Tsuritani, and R. Sugizaki, "Cladding pumped seven-core EDFA using

an absorption-enhanced erbium doped fibre," in *ECOC 2016 ; 42nd European Conference on Optical Communication*. VDE, 2016, pp. 1–3.

[63] K. Takeshima, T. Tsuritani, Y. Tsuchida, K. Maeda, T. Saito, K. Watanabe, T. Sasa, K. Imamura, R. Sugizaki, K. Igarashi *et al.*, "51.1-tbit/s MCF transmission over 2520 km using cladding-pumped seven-core EDFAs," *Journal of Lightwave Technology*, vol. 34, no. 2, pp. 761–767, 2016.

[64] Y. Sun, J. Sulhoff, A. Srivastava, A. Abramov, T. Strasser, P. Wysocki, J. Pedrazzani, J. Judkins, R. Espindola, C. Wolf *et al.*, "A gain-flattened ultra wide band EDFA for high capacity WDM optical communications systems," in *24th European Conference on Optical Communication. ECOC'98 (IEEE Cat. No. 98TH8398)*, vol. 1. IEEE, 1998, pp. 53–54.

[65] H. Ono, Y. Miyamoto, T. Mizuno, and M. Yamada, "Gain control in multi-core erbium-doped fiber amplifier with cladding and core hybrid pumping," *Journal of Lightwave Technology*, vol. 37, no. 13, pp. 3365–3372, 2019.

[66] J. L. Zyskind, J. A. Nagel, and H. D. Kidorf, "Erbium-doped fiber amplifiers for optical communications," *Optical Fiber Telecommunications IIIB*, pp. 13–68, 1997.

[67] Y. Jeong, S. Yoo, C. A. Codemard, J. Nilsson, J. K. Sahu, D. N. Payne, R. Horley, P. Turner, L. Hickey, A. Harker *et al.*, "Erbium : ytterbium codoped large-core fiber laser with 297-w continuous-wave output power," *IEEE Journal of Selected Topics in Quantum Electronics*, vol. 13, no. 3, pp. 573–579, 2007.

[68] W. Loh, B. Samson, L. Dong, G. Cowle, and K. Hsu, "High performance single frequency fiber grating-based erbium : ytterbium-codoped fiber lasers," *Journal of lightwave technology*, vol. 16, no. 1, p. 114, 1998.

[69] J. Townsend, W. Barnes, and S. Crubb, "Yb^{3+} sensitised Er^{3+} doped silica optical fibre with ultra high transfer efficiency and gain," *MRS Online Proceedings Library (OPL)*, vol. 244, 1991.

[70] V. Gapontsev, S. Matitsin, A. Isineev, and V. Kravchenko, "Erbium glass lasers and their applications," *Optics & Laser Technology*, vol. 14, no. 4, pp. 189–196, 1982.

[71] J. Nilsson, J. Minelly, R. Paschotta, A. Tropper, and D. Hanna, "Ring-doped cladding-pumped single-mode three-level fiber laser," *Optics Letters*, vol. 23, no. 5, pp. 355–357, 1998.

[72] P. Bousselet, C. Simonneau, C. Moreau, L. Provost, P. Lambelet, X. Rejeaunier, F. Leplingard, L. Gasca, and D. Bayart, "+33 dBm output power from a full C-band cladding diode-pumped EDFA," in *2002 28TH European Conference on Optical Communication*, vol. 5. IEEE, 2002, pp. 1–2.

[73] H. Takeshita, K. Matsumoto, S. Yanagimachi, and E. L. T. de Gabory, "Configurations of pump injection and reinjection for improved amplification efficiency of turbo cladding pumped MC-EDFA," *Journal of Lightwave Technology*, vol. 38, no. 11, pp. 2922–2929, 2020.

[74] S. Baek, D. B. Soh, Y. Jeong, J. K. Sahu, J. Nilsson, and B. Lee, "A cladding-pumped fiber laser with pump-reflecting inner-cladding Bragg grating," *IEEE Photonics Technology Letters*, vol. 16, no. 2, pp. 407–409, 2004.

[75] C. Matte-Breton, R. Ryf, N. K. Fontaine, R.-J. Essiambre, H. Chen, C. Kelly, Y. Messaddeq, and S. LaRochelle, "Modeling and characterization of cladding-pumped erbium-ytterbium co-doped fibers for amplification in communication systems," *Journal of Lightwave Technology*, vol. 38, no. 7, pp. 1936–1944, 2019.

[76] R.-J. Essiambre, G. Kramer, P. J. Winzer, G. J. Foschini, and B. Goebel, "Capacity limits of optical fiber networks," *Journal of Lightwave Technology*, vol. 28, no. 4, pp. 662–701, 2010.

[77] D. J. Richardson, J. M. Fini, and L. E. Nelson, "Space-division multiplexing in optical fibres," *Nature photonics*, vol. 7, no. 5, pp. 354–362, 2013.

[78] K. Takeshima, T. Tsuritani, Y. Tsuchida, K. Maeda, T. Saito, K. Watanabe, T. Sasa, K. Imamura, R. Sugizaki, K. Igarashi *et al.*, "51.1-tbit/s MCF transmission over 2,520 km using cladding pumped 7-core EDFAs," in *Optical Fiber Communication Conference*. Optical Society of America, 2015, pp. W3G–1.

[79] P. M. Krummrich and S. Akhtari, "Selection of energy optimized pump concepts for multi core and multi mode erbium doped fiber amplifiers," *Optics express*, vol. 22, no. 24, pp. 30 267–30 280, 2014.

[80] M. Nooruzzaman, S. Jain, Y. Jung, S.-u. Alam, D. J. Richardson, Y. Miyamoto, and T. Morioka, "Power consumption in multi-core fibre networks," in *2017 European Conference on Optical Communication (ECOC)*. IEEE, 2017, pp. 1–3.

[81] E. Artem'ev, A. Murzin, Y. K. Fedorov *et al.*, "Some characteristics of population inversion of the 4i13/2 level of erbium ions in ytterbium–erbium glasses," *Soviet Journal of Quantum Electronics*, vol. 11, no. 9, p. 1266, 1981.

[82] B.-C. Hwang, S. Jiang, T. Luo, J. Watson, G. Sorbello, and N. Peyghambarian, "Cooperative upconversion and energy transfer of new high Er^{3+}-and Yb^{3+}–Er^{3+}-doped phosphate glasses," *JOSA B*, vol. 17, no. 5, pp. 833–839, 2000.

[83] S. Taccheo, G. Sorbello, S. Longhi, and P. Laporta, "Measurement of the energy transfer and upconversion constants in Er–Yb-doped phosphate glass," *Optical and quantum electronics*, vol. 31, no. 3, pp. 249–262, 1999.

[84] S. Grubb, W. Humer, R. Cannon, T. Windhorn, S. Vendetta, K. Sweeney, P. Leilabady, W. Barnes, K. Jedrzejewski, and J. Townsend, "+21 dBm erbium power amplifier pumped by a diode-pumped nd : Yag laser," *IEEE photonics technology letters*, vol. 4, no. 6, pp. 553–555, 1992.

[85] E. Yahel and A. Hardy, "Efficiency optimization of high-power, Er^{3+}–Yb^{3+}-codoped fiber amplifiers for wavelength-division-multiplexing applications," *JOSA B*, vol. 20, no. 6, pp. 1189–1197, 2003.

[86] G. G. Vienne, J. E. Caplen, L. Dong, J. D. Minelly, J. Nilsson, and D. N. Payne, "Fabrication and characterization of Yb^{3+} : Er^{3+} phosphosilicate fibers for lasers," *Journal of lightwave technology*, vol. 16, no. 11, p. 1990, 1998.

[87] G. C. Valley, "Modeling cladding-pumped Er/Yb fiber amplifiers," *Optical Fiber Technology*, vol. 7, no. 1, pp. 21–44, 2001.

[88] G. Vienne, W. Brocklesby, R. Brown, Z. Chen, J. Minelly, J. Roman, and D. Payne, "Role of aluminum in ytterbium–erbium codoped phosphoaluminosilicate optical fibers," *Optical Fiber Technology*, vol. 2, no. 4, pp. 387–393, 1996.

[89] P. Laporta, S. Taccheo, S. Longhi, O. Svelto, and C. Svelto, "Erbium–ytterbium microlasers : optical properties and lasing characteristics," *Optical Materials*, vol. 11, no. 2-3, pp. 269–288, 1999.

[90] C. Strohhöfer and A. Polman, "Absorption and emission spectroscopy in Er^{3+}–Yb^{3+} doped aluminum oxide waveguides," *Optical Materials*, vol. 21, no. 4, pp. 705–712, 2003.

[91] J. Philipps, T. Töpfer, H. Ebendorff-Heidepriem, D. Ehrt, and R. Sauerbrey, "Spectroscopic and lasing properties of Er^{3+} : Yb^{3+}-doped fluoride phosphate glasses," *Applied Physics B*, vol. 72, no. 4, pp. 399–405, 2001.

[92] N. Park, P. Wysocki, R. Pedrazzani, S. Grubb, D. DiGiovanni, and K. Walker, "High-power Er-Yb-doped fiber amplifier with multichannel gain flatness within 0.2 db over 14 nm," *IEEE Photonics Technology Letters*, vol. 8, no. 9, pp. 1148–1150, 1996.

[93] Y. Jaouën, J.-P. Bouzinac, J.-M. Delavaux, C. Chabran, and M. Le Flohic, "Generation of four-wave mixing products inside WDM c-band 1 w Er^{3+}/Yb^{3+} amplifier," *Electronics Letters*, vol. 36, no. 3, pp. 233–235, 2000.

[94] C. Castro, S. Jain, E. De Man, Y. Jung, J. Hayes, S. Calabro, K. Pulverer, M. Bohn, S.-u. Alam, D. J. Richardson *et al.*, "15x200 Gbit/s 16-QAM SDM transmission over an integrated 7-core cladding-pumped repeatered multicore link in a recirculating loop," *Journal of Lightwave Technology*, vol. 36, no. 2, pp. 349–354, 2018.

[95] J. Nilsson, P. Scheer, and B. Jaskorzynska, "Modeling and optimization of short Yb^{3+}-sensitized Er^{3+}-doped fiber amplifiers," *IEEE photonics technology letters*, vol. 6, no. 3, pp. 383–385, 1994.

[96] P. Peterka, J. Kanka, M. Karasek, P. Honzatko, and F. Abdelmalek, "Characterization and modeling of Er/Yb-codoped fibers," in *Photonics, Devices, and Systems*, vol. 4016. International Society for Optics and Photonics, 1999, pp. 282–287.

[97] C. Lester, A. Bjarklev, T. Rasmussen, and P. G. Dinesen, "Modeling of Yb^{3+}-sensitized Er^{3+}-doped silica waveguide amplifiers," *Journal of lightwave technology*, vol. 13, no. 5, pp. 740–743, 1995.

[98] B. J. Ainslie, "A review of the fabrication and properties of erbium-doped fibers for optical amplifiers," *Journal of Lightwave Technology*, vol. 9, no. 2, pp. 220–227, 1991.

[99] D. McCumber, "Einstein relations connecting broadband emission and absorption spectra," *Physical Review*, vol. 136, no. 4A, p. A954, 1964.

[100] H. Takeshita, K. Matsumoto, S. Yanagimachi, and E. L. T. de Gabory, "Improvement of the pump recycling ratio of turbo cladding pumped MC-EDFA with paired spatial pump combiner and splitter," in *Optical Fiber Communication Conference*. Optical Society of America, 2019, pp. Th1B–2.

[101] C. Matte-Breton, H. Chen, N. K. Fontaine, R. Ryf, R.-J. Essiambre, C. Kelly, C. Jin, Y. Messaddeq, and S. LaRochelle, "Demonstration of an erbium-doped fiber with annular doping for low gain compression in cladding-pumped amplifiers," *Optics express*, vol. 26, no. 20, pp. 26 633–26 645, 2018.

[102] R.-J. Essiambre and R. W. Tkach, "Capacity trends and limits of optical communication networks," *Proceedings of the IEEE*, vol. 100, no. 5, pp. 1035–1055, 2012.

[103] P. J. Winzer, "Scaling optical networking technologies for next generation SDM," in *2018 Optical Fiber Communications Conference and Exposition (OFC)*. IEEE, 2018, pp. 1–57.

[104] D. Soma, Y. Wakayama, S. Beppu, S. Sumita, T. Tsuritani, T. Hayashi, T. Nagashima, M. Suzuki, M. Yoshida, K. Kasai *et al.*, "10.16-Peta-B/s dense SDM/WDM transmission over 6-mode 19-core fiber across the c+ l band," *Journal of Lightwave Technology*, vol. 36, no. 6, pp. 1362–1368, 2018.

[105] T. Mizuno and Y. Miyamoto, "High-capacity dense space division multiplexing transmission," *Optical Fiber Technology*, vol. 35, pp. 108–117, 2017.

[106] K. S. Abedin, M. F. Yan, T. F. Taunay, B. Zhu, E. M. Monberg, and D. J. DiGiovanni, "State-of-the-art multicore fiber amplifiers for space division multiplexing," *Optical Fiber Technology*, vol. 35, pp. 64–71, 2017.

[107] Y. Sakamaki, T. Kawai, M. Fukutoku, T. Kataoka, and K. Suzuki, "Experimental demonstration of arrayed optical amplifiers with a shared pump laser for realizing colorless, directionless, contentionless roadm," *Optics express*, vol. 20, no. 26, pp. B131–B140, 2012.

[108] H. Chen, N. K. Fontaine, R. Ryf, C. Jin, B. Huang, K. Shang, R.-J. Essiambre, L. Wang, T. Hayashi, T. Nagashima *et al.*, "Demonstration of cladding-pumped six-core erbium-doped fiber amplifier," *Journal of Lightwave Technology*, vol. 34, no. 8, pp. 1654–1660, 2016.

[109] C. Jin, B. Ung, Y. Messaddeq, and S. LaRochelle, "Annular-cladding erbium doped multicore fiber for SDM amplification," *Optics express*, vol. 23, no. 23, pp. 29 647–29 659, 2015.

[110] Z. Várallyay and J. Jasapara, "Comparison of amplification in large area fibers using cladding-pump and fundamental-mode core-pump schemes," *Optics express*, vol. 17, no. 20, pp. 17 242–17 252, 2009.

[111] Q. Kang, E.-L. Lim, Y. Jung, J. K. Sahu, F. Poletti, C. Baskiotis, S.-u. Alam, and D. J. Richardson, "Accurate modal gain control in a multimode erbium doped fiber amplifier incorporating ring doping and a simple LP_{01} pump configuration," *Optics Express*, vol. 20, no. 19, pp. 20 835–20 843, 2012.

[112] C. Jin, B. Ung, Y. Messaddeq, and S. LaRochelle, "Tailored modal gain in a multi-mode erbium-doped fiber amplifier based on engineered ring doping profiles," in *Photonics North 2013*, vol. 8915. International Society for Optics and Photonics, 2013, p. 89150A.

[113] L. Gagné-Godbout, "Modélisation, fabrication et caractérisation d'un amplificateur à fibre optique à sept cœurs dopés à l'erbium," Ph.D. dissertation, Université Laval, 2014.

[114] H. Zellmer, A. Tünnermann, H. Welling, and V. Reichel, "Double-clad fiber laser with 30 w output power," in *Optical Amplifiers and Their Applications*. Optical Society of America, 1997, p. FAW18.

[115] B. Pedersen, A. Bjarklev, J. H. Povlsen, K. Dybdal, and C. C. Larsen, "The design of erbium-doped fiber amplifiers," *Journal of lightwave technology*, vol. 9, no. 9, pp. 1105–1112, 1991.

[116] C. Matte-Breton, R. Wang, Y. Messaddeq, and S. LaRochelle, "Novel fuseless optical fiber side-coupler based on half-taper for cladding pumped EDFAs," in *Optical Fiber Communication Conference*. Optical Society of America, 2020, pp. T3A–2.

[117] D. Ripin and L. Goldberg, "High efficiency side-coupling of light into optical fibres using imbedded v-grooves," *Electronics Letters*, vol. 31, no. 25, pp. 2204–2205, 1995.

[118] J. P. Koplow, S. W. Moore, and D. A. Kliner, "A new method for side pumping of double-clad fiber sources," *IEEE Journal of Quantum Electronics*, vol. 39, no. 4, pp. 529–540, 2003.

[119] Q. Xiao, P. Yan, Y. Wang, J. Hao, X. Zhang, and M. Gong, "Fused angle-polished multi-points side-pumping coupler for monolithic fiber lasers and amplifiers," *Optics Communications*, vol. 285, no. 8, pp. 2137–2143, 2012.

[120] Q. Xiao, P. Yan, H. Ren, X. Chen, and M. Gong, "A side-pump coupler with refractive index valley configuration for fiber lasers and amplifiers," *Journal of lightwave technology*, vol. 31, no. 16, pp. 3015–3022, 2013.

[121] D. H. Richards, J. L. Jackel, and M. A. Ali, "A theoretical investigation of dynamic all-optical automatic gain control in multichannel EDFA's and EDFA cascades," *IEEE Journal of Selected Topics in Quantum Electronics*, vol. 3, no. 4, pp. 1027–1036, 1997.

[122] C. Matte-Breton, H. Chen, N. K. Fontaine, R. Ryf, R.-J. Essiambre, Y. Messaddeq, and S. La Rochelle, "Analysis of inter-core cross-gain modulation in cladding pumped multi-core fiber amplifiers," in *2018 European Conference on Optical Communication (ECOC)*. IEEE, 2018, pp. 1–3.

[123] E. Delevaque, T. Georges, M. Monerie, P. Lamouler, and J.-F. Bayon, "Modeling of pair-induced quenching in erbium-doped silicate fibers," *IEEE Photonics Technology Letters*, vol. 5, no. 1, pp. 73–75, 1993.

[124] J. L. Wagener, M. J. Digonnet, P. F. Wysocki, and H. J. Shaw, "Effect of composition on clustering in Er-doped fiber lasers," in *Fiber Laser Sources and Amplifiers V*, vol. 2073. International Society for Optics and Photonics, 1994, pp. 14–19.

[125] C. Matte-Breton, R.-J. Essiambre, C. Kelly, Y. Messaddeq, and S. LaRochelle, "Characterization of an aluminophosphosilicate fiber with annular erbium doping for improved performance of cladding-pumped amplifiers," in *2020 European Conference on Optical Communications (ECOC)*. IEEE, 2020, pp. 1–3.

[126] M.-P. Lord, L. Talbot, O. Boily, T. Boilard, G. Gariépy, S. Grelet, P. Paradis, V. Boulanger, N. Grégoire, S. Morency *et al.*, "Erbium-doped aluminophosphosilicate all-fiber laser operating at 1584 nm," *Optics express*, vol. 28, no. 3, pp. 3378–3387, 2020.

[127] D. J. DiGiovanni, J. B. MacChesney, and T. Kometani, "Structure and properties of silica containing aluminum and phosphorus near the $AlPO_4$ join," *Journal of Non-Crystalline Solids*, vol. 113, no. 1, pp. 58–64, 1989.

[128] M. Likhachev, S. Aleshkina, A. Shubin, M. Bubnov, E. Dianov, D. Lipatov, and A. Guryanov, "Large-mode-area highly Yb-doped photodarkening-free Al_2O_3-P_2O_5-SiO_2-based fiber," in *The European Conference on Lasers and Electro-Optics*. Optical Society of America, 2011, p. CJ_P24.

[129] C. Matte-Breton, R.-J. Essiambre, C. Kelly, Y. Massadeq, and S. Larochelle, "Multicore cladding-pumped fiber amplifier with annular erbium doping for low gain compression," *Journal of Lightwave Technology*, 2022.

[130] B. J. Puttnam, R. S. Luís, E. Agrell, G. Rademacher, J. Sakaguchi, W. Klaus, G. M. Saridis, Y. Awaji, and N. Wada, "High capacity transmission systems using homogeneous multi-core fibers," *Journal of Lightwave Technology*, vol. 35, no. 6, pp. 1157–1167, 2017.

[131] K. Imamura, K. Mukasa, and T. Yagi, "Effective space division multiplexing by multi-core fibers," in *36th European Conference and Exhibition on Optical Communication*. IEEE, 2010, pp. 1–3.

[132] H. Takara, A. Sano, T. Kobayashi, H. Kubota, H. Kawakami, A. Matsuura, Y. Miyamoto, Y. Abe, H. Ono, K. Shikama *et al.*, "1.01-Pb/s (12 SDM/222 WDM/456 Gb/s) crosstalk-managed transmission with 91.4-b/s/hz aggregate spectral efficiency," in *European Conference and Exhibition on Optical Communication*. Optical Society of America, 2012, pp. Th–3.

[133] K. Igarashi, T. Tsuritani, I. Morita, and M. Suzuki, "Ultra-long-haul high-capacity super-Nyquist-WDM transmission experiment using multi-core fibers," *Journal of lightwave technology*, vol. 33, no. 5, pp. 1027–1036, 2015.

[134] J. Sakaguchi, B. J. Puttnam, W. Klaus, Y. Awaji, N. Wada, A. Kanno, T. Kawanishi, K. Imamura, H. Inaba, K. Mukasa *et al.*, "305 tb/s space division multiplexed transmission using homogeneous 19-core fiber," *Journal of Lightwave Technology*, vol. 31, no. 4, pp. 554–562, 2012.

[135] R. Ryf, S. Randel, A. H. Gnauck, C. Bolle, A. Sierra, S. Mumtaz, M. Esmaeelpour, E. C. Burrows, R.-J. Essiambre, P. J. Winzer *et al.*, "Mode-division multiplexing over 96 km of few-mode fiber using coherent 6×6 mimo processing," *Journal of Lightwave technology*, vol. 30, no. 4, pp. 521–531, 2011.

[136] V. Sleiffer, Y. Jung, V. Veljanovski, R. Van Uden, M. Kuschnerov, H. Chen, B. Inan, L. G. Nielsen, Y. Sun, D. J. Richardson *et al.*, "73.7 tb/s (96 x 3 x 256-Gb/s) mode-division-multiplexed dp-16QAM transmission with inline MM-EDFA," *Optics Express*, vol. 20, no. 26, pp. B428–B438, 2012.

[137] E. Ip, M.-J. Li, K. Bennett, Y.-K. Huang, A. Tanaka, A. Korolev, K. Koreshkov, W. Wood, E. Mateo, J. Hu *et al.*, "146$\lambda \times 6 \times$ 19-Gbaud wavelength-and mode-division

multiplexed transmission over 10× 50-km spans of few-mode fiber with a gain-equalized few-mode EDFA," *Journal of Lightwave Technology*, vol. 32, no. 4, pp. 790–797, 2013.

[138] R. Ryf, N. K. Fontaine, S. Wittek, K. Choutagunta, M. Mazur, H. Chen, J. C. Alvarado-Zacarias, R. Amezcua-Correa, M. Capuzzo, R. Kopf *et al.*, "High-spectral-efficiency mode-multiplexed transmission over graded-index multimode fiber," in *2018 European Conference on Optical Communication (ECOC)*. IEEE, 2018, pp. 1–3.

[139] B. Ung, P. Vaity, L. Wang, Y. Messaddeq, L. Rusch, and S. LaRochelle, "Few-mode fiber with inverse-parabolic graded-index profile for transmission of oam-carrying modes," *optics express*, vol. 22, no. 15, pp. 18 044–18 055, 2014.

[140] T. Mizuno, T. Kobayashi, H. Takara, A. Sano, H. Kawakami, T. Nakagawa, Y. Miyamoto, Y. Abe, T. Goh, M. Oguma *et al.*, "12-core× 3-mode dense space division multiplexed transmission over 40 km employing multi-carrier signals with parallel mimo equalization," in *Optical Fiber Communication Conference*. Optical Society of America, 2014, pp. Th5B–2.

[141] K. Shibahara, D. Lee, T. Kobayashi, T. Mizuno, H. Takara, A. Sano, H. Kawakami, Y. Miyamoto, H. Ono, M. Oguma *et al.*, "Dense SDM (12-core × 3-mode) transmission over 527 km with 33.2-ns mode-dispersion employing low-complexity parallel mimo frequency-domain equalization," *Journal of Lightwave Technology*, vol. 34, no. 1, pp. 196–204, 2016.

[142] R. Ryf, J. C. Alvarado-Zacarias, S. Wittek, N. K. Fontaine, R.-J. Essiambre, H. Chen, R. Amezcua-Correa, H. Sakuma, T. Hayashi, and T. Hasegawa, "Coupled-core transmission over 7-core fiber," in *Optical Fiber Communication Conference*. Optical Society of America, 2019, pp. Th4B–3.

[143] R. Ryf, J. C. Alvarado, B. Huang, J. Antonio-Lopez, S. H. Chang, N. K. Fontaine, H. Chen, R.-J. Essiambre, E. Burrows, R. Amezcua-Correa *et al.*, "Long-distance transmission over coupled-core multicore fiber," in *ECOC 2016-Post Deadline Paper; 42nd European Conference on Optical Communication*. VDE, 2016, pp. 1–3.

[144] M. Wada, T. Sakamoto, T. Yamamoto, S. Aozasa, S. Nozoe, Y. Sagae, K. Tsujikawa, and K. Nakajima, "Cladding pumped randomly coupled 12-core erbium-doped fiber amplifier with low mode-dependent gain," *Journal of lightwave technology*, vol. 36, no. 5, pp. 1220–1225, 2018.

[145] S. Jain, T. Mizuno, Y. Jung, A. Isoda, K. Shibahara, J. R. Hayes, Y. Sasaki, K. Takenaga, Y. Miyamoto, S. Alam *et al.*, "Improved cladding-pumped 32-core multicore fiber amplifier," in *2017 European Conference on Optical Communication (ECOC)*. IEEE, 2017, pp. 1–3.

[146] E. L. T. de Gabory, H. Takeshita, K. Matsumoto, and S. Yanagimachi, "Reduction in power consumption in multi-core amplifier," in *Optical Fiber Communication Conference*. Optical Society of America, 2019, pp. Th1B–1.

[147] S. LaRochelle, C. Matte-Breton, C. Kelly, and R. Essiambre, "Cladding-pumped multicore amplifiers with ring doping," in *Optical Fiber Communication Conference*. Optical Society of America, 2021, pp. M3D–1.

[148] A. Samir, L. Perpar, and B. Batagelj, "Fabrication of a single-mode seven-core optical fiber using the stack-and-draw procedure," in *2016 International Workshop on Fiber Optics in Access Network (FOAN)*. IEEE, 2016, pp. 1–4.

[149] E. Chillcce, C. M. d. B. Cordeiro, L. Barbosa, and C. B. Cruz, "Tellurite photonic crystal fiber made by a stack-and-draw technique," *Journal of Non-Crystalline Solids*, vol. 352, no. 32-35, pp. 3423–3428, 2006.

[150] J. Townsend, S. Poole, and D. Payne, "Solution-doping technique for fabrication of rare-earth-doped optical fibres," *Electronics letters*, vol. 23, no. 7, pp. 329–331, 1987.

[151] K. Walker, F. Geyling, and S. Nagel, "Thermophoretic deposition of small particles in the modified chemical vapor deposition (MCVD) process," *Journal of the American Ceramic Society*, vol. 63, no. 9-10, pp. 552–558, 1980.

[152] R. S. Quimby and W. J. Miniscalco, "Excited state absorption at 980 nm in erbium-doped silica glass," in *Optical Amplifiers and Their Applications*. Optical Society of America, 1992, p. WE3.

[153] Q. He, F. Wang, Z. Lin, C. Shao, M. Wang, S. Wang, C. Yu, and L. Hu, "Temperature dependence of spectral and laser properties of Er^{3+}/Al^{3+} co-doped aluminosilicate fiber," *Chinese Optics Letters*, vol. 17, no. 10, p. 101401, 2019.

[154] C. R. Giles and E. Desurvire, "Modeling erbium-doped fiber amplifiers," *Journal of lightwave technology*, vol. 9, no. 2, pp. 271–283, 1991.

[155] P. M. Becker, A. A. Olsson, and J. R. Simpson, *Erbium-doped fiber amplifiers : fundamentals and technology*. Elsevier, 1999.

[156] C. Jin, "Spatially integrated erbium-doped fiber amplifiers enabling space-division multiplexing," Ph.D. dissertation, Université Laval, 2016.

[157] W. J. Miniscalco and R. S. Quimby, "General procedure for the analysis of Er^{3+} cross sections," *Optics letters*, vol. 16, no. 4, pp. 258–260, 1991.

[158] M. Wada, T. Sakamoto, S. Aozasa, R. Imada, T. Yamamoto, and K. Nakajima, "Full C-band and power efficient coupled-multi-core fiber amplifier," in *Optical Fiber Communication Conference*. Optical Society of America, 2020, pp. M4C–3.

[159] C. Matte-Breton, L. Wang, F. Maes, Y. Messaddeq, and S. LaRochelle, "Concentric layers with heterogeneous doping for cladding-pumped L-band fiber amplifiers," in *Photonics West Conference (PW)*. SPIE, 2022, pp. 1–8.

[160] C. Codemard, D. B. S. Soh, K. Ylä-Jarkko, J. Sahu, M. Laroche, and J. Nilsson, "Cladding-pumped L-band phosphosilicate erbium-ytterbium co-doped fiber amplifier," in *Optical Amplifiers and Their Applications*. Optical Society of America, 2003, p. TuC2.

[161] Y. Tsuchida, K. Maeda, K. Watanabe, T. Saito, S. Takasaka, M. Tadakuma, R. Sugizaki, H. Ogoshi, K. Doi, H. Matsuura *et al.*, "Cladding-pumped L-band multicore EDFA with reduced power consumption," in *2014 IEEE Photonics Society Summer Topical Meeting Series*. IEEE, 2014, pp. 148–149.

[162] M. Achtenhagen, R. J. Beeson, F. Pan, B. Nyman, and A. Hardy, "Gain and noise in ytterbium-sensitized erbium-doped fiber amplifiers : measurements and simulations," *Journal of lightwave technology*, vol. 19, no. 10, p. 1521, 2001.

[163] C. Matte-Breton, L. Talbot, Y. Messaddeq, M. Bernier, and S. LaRochelle, "Large area bragg grating for pump recycling in cladding-pumped multicore erbium-doped fiber amplifiers," *Optics Express*, vol. 30, no. 11, pp. 17 824–17 835, 2022.

[164] S. Takasaka, K. Maeda, K. Kawasaki, K. Yoshioka, H. Oshio, R. Sugizaki, Y. Kawaguchi, H. Takahashi, T. Tsuritani, and M. Shiino, "Increase of cladding pump power efficiency by a 19-core erbium doped fibre amplifier," in *2017 European Conference on Optical Communication (ECOC)*. IEEE, 2017, pp. 1–3.

[165] S. Takasaka, K. Maeda, K. Kawasaki, K. Yoshioka, R. Sugizaki, and M. Tsukamoto, "Cladding pump recycling device for 19-core EDFA," in *Optical Fiber Communication Conference*. Optical Society of America, 2019, pp. Th3D–7.

[166] K. Maeda, S. Takasaka, K. Kawasaki, K. Yoshioka, R. Sugizaki, and M. Tsukamoto, "Cladding pump recycling using cascaded pump collectors in 7-core EDFA," in *45th European Conference on Optical Communication (ECOC 2019)*. IET, 2019, pp. 1–4.

[167] L. Talbot, P. Paradis, and M. Bernier, "All-fiber laser pump reflector based on a femtosecond-written inner cladding Bragg grating," *Optics Letters*, vol. 44, no. 20, pp. 5033–5036, 2019.

[168] L. Talbot, L.-C. Michaud, V. Boulanger, P. Paradis, and M. Bernier, "Inner-cladding pump reflector based on chirped volume Bragg gratings," in *Components and Packaging for Laser Systems VI*, vol. 11261. International Society for Optics and Photonics, 2020, p. 112610R.

[169] S. J. Mihailov, C. W. Smelser, D. Grobnic, R. B. Walker, P. Lu, H. Ding, and J. Unruh, "Bragg gratings written in all-SiO_2 and Ge-doped core fibers with 800-nm femtosecond radiation and a phase mask," *Journal of Lightwave Technology*, vol. 22, no. 1, p. 94, 2004.

[170] M. Bernier, R. Vallée, B. Morasse, C. Desrosiers, A. Saliminia, and Y. Sheng, "Ytterbium fiber laser based on first-order fiber Bragg gratings written with 400nm femtosecond pulses and a phase-mask," *Optics express*, vol. 17, no. 21, pp. 18 887–18 893, 2009.

[171] K. M. Davis, K. Miura, N. Sugimoto, and K. Hirao, "Writing waveguides in glass with a femtosecond laser," *Optics letters*, vol. 21, no. 21, pp. 1729–1731, 1996.

[172] J. Thomas, E. Wikszak, T. Clausnitzer, U. Fuchs, U. Zeitner, S. Nolte, and A. Tünnermann, "Inscription of fiber Bragg gratings with femtosecond pulses using a phase mask scanning technique," *Applied Physics A*, vol. 86, no. 2, pp. 153–157, 2007.

[173] S. J. Mihailov, D. Grobnic, C. W. Smelser, P. Lu, R. B. Walker, and H. Ding, "Bragg grating inscription in various optical fibers with femtosecond infrared lasers and a phase mask," *Optical Materials Express*, vol. 1, no. 4, pp. 754–765, 2011.

[174] L. Talbot, S. Pelletier-Ouellet, F. Trépanier, and M. Bernier, "Wavelength stabilization of high-power laser diodes using Bragg gratings inscribed in their highly multimode fiber pigtails," *Optics Letters*, vol. 47, no. 3, pp. 633–636, 2022.

[175] K. Anuar, S. Muhd-Yasin, M. Zulkifli, S. Hanif, A. Yusoff, S. Aljamimi, H. T. Zubair, Z. Yusoff, H. Abdul-Rashid, and N. Tamchek, "Er_2O_3-Al_2O_3 doped silica preform prepared by MCVD-chelate vapor phase delivery technique," in *Advanced Materials Research*, vol. 896. Trans Tech Publ, 2014, pp. 219–224.

[176] E. Pincemin, J. Jauffrit, P.-Y. Disez, Y. Loussouarn, C. Le Bouëtté, R. Kerampran, S. Bordais, G. Melin, T. Taunay, Y. Jaouën *et al.*, "12-core erbium/ytterbium-doped fiber amplifier for 200G/400G long-haul, metro-regional, DCI transmission applications with ROADM," in *2021 European Conference on Optical Communication (ECOC)*. IEEE, 2021, pp. 1–4.

[177] L. Wand, M. Sharma, F. Maes, S. Jalilpiran, F. Durak, Y. Messaddeq, S. LaRochelle, and Z. Jiang, "Low cost solution for super L-band fiber amplifier based on single-mode and multi-mode hybrid pumping scheme," in *2022 Optical Fiber Communications Conference and Exhibition (OFC)*. IEEE, 2022, pp. 1–3.